T.R.
GEBZE TECHNICAL UNIVERSITY
GRADUATE SCHOOL OF NATURAL AND APPLIED SCIENCES

SEISMIC PERFORMANCE OF STEEL MOMENT FRAMES WITH GRAVITY-ONLY FRAMES

GAMZE KARAKAŞ
A THESIS SUBMITTED FOR THE DEGREE OF
MASTER OF SCIENCE
DEPARTMENT OF CIVIL ENGINEERING
EARTHQUAKE AND STRUCTURAL ENGINEERING PROGRAM

GEBZE
2021

T.R.

GEBZE TECHNICAL UNIVERSITY

GRADUATE SCHOOL OF NATURAL AND APPLIED SCIENCES

SEISMIC PERFORMANCE OF STEEL MOMENT FRAMES WITH GRAVITY-ONLY FRAMES

GAMZE KARAKAŞ

A THESIS SUBMITTED FOR THE DEGREE OF

MASTER OF SCIENCE

DEPARTMENT OF CIVIL ENGINEERING

EARTHQUAKE AND STRUCTURAL ENGINEERING PROGRAM

THESIS SUPERVISOR

PROF. DR. BÜLENT AKBAŞ

GEBZE

2021

T.C.
GEBZE TEKNİK ÜNİVERSİTESİ
FEN BİLİMLERİ ENSTİTÜSÜ

DÜŞEY YÜK TAŞIYICI ÇERÇEVELER İLE ÇELİK MOMENT ÇERÇEVELERİN SİSMİK PERFORMANSI

GAMZE KARAKAŞ
YÜKSEK LİSANS TEZİ
İNŞAAT MÜHENDİSLİĞİ ANABİLİM DALI
DEPREM VE YAPI MÜHENDİSLİĞİ PROGRAMI

DANIŞMANI
PROF. DR. BÜLENT AKBAŞ

GEBZE
2021

GEBZE TEKNİK ÜNİVERSİTESİ	**YÜKSEK LİSANS JÜRİ ONAY FORMU**

GTÜ Fen Bilimleri Enstitüsü Yönetim Kurulu'nun 01/07/2021 tarih ve 2021/30 sayılı kararıyla oluşturulan jüri tarafından 14/07/2021 tarihinde tez savunma sınavı yapılan Gamze KARAKAŞ'ın tez çalışması İnşaat Mühendisliği Anabilim Dalı Deprem ve Yapı Mühendisliği Programında YÜKSEK LİSANS tezi olarak kabul edilmiştir.

JÜRİ

ÜYE
(TEZ DANIŞMANI) : PROF. DR. BÜLENT AKBAŞ

ÜYE : PROF. DR. BİLGE DORAN

ÜYE : DR. ÖĞR. ÜYESİ ONUR ŞEKER

ONAY

Gebze Teknik Üniversitesi Fen Bilimleri Enstitüsü Yönetim Kurulu'nun

...../...../…… tarih ve ……/…..... sayılı kararı.

SUMMARY

Special Moment Resisting Frames (SMRF) are systems that provide lateral resistance against strong ground motions through transferring forces by bending and shearing in steel structures. Most large inelastic deformations are supplied with yields occurring at the beam ends thanks to plastic hinges. However, the contribution of gravity load-carrying systems designed in inner spans to lateral strength and rigidity is often overlooked. If it is not taken into consideration that the connections in the Gravity Frames (GFs), which are designed with shear tab connection and accepted to not transfer moment, can reach up to 20% to 50% of the plastic bending capacity of the beams, the seismic performance of the structures is underestimated. For this reason, 5 and 10 story GFs are not included, 10% of the stiffness of gravity beams are taken into account and GFs meet 10% of lateral loads with the help of infinite stiffness link elements are represented by 3 models to examine the interaction between GFs and SMRFs and to evaluate seismic performance. Nonlinear Incremental Dynamic Analysis was applied to all models. For each model and each earthquake record, the maximum drift ratio, top story displacements, base shear forces, capacity curves, and drift ratio distribution occurring along the floors in the buildings against the increased earthquake intensities were examined according to the specifications. As a result of the analysis, it was observed that the GFs in second and third cases mentioned above increased the capacity by 9% and 17% compared to the bare moment frame, respectively.

Key Words: Special Moment Frame, Gravity-Only Frame, Incremental Dynamic Analysis, Seismic Performance.

ÖZET

Çelik yapılarda, sismik kuvvetlerin eğilme ve kesme yoluyla aktarılarak güçlü yer hareketlerine karşı yanal direnç sağlayan sistemler özel çelik moment çerçevelerdir. Plastik mafsallar sayesinde kiriş uçlarında oluşan akmalar ile büyük elastik olmayan deformasyonların çoğu karşılanmış olur. Fakat iç açıklıklarda tasarlanan düşey yük taşıyıcı sistemlerin yanal dayanım ve rijitliğe katkısı çoğunlukla göz ardı edilmektedir. Basit bağlantı ile tasarlanan ve moment aktarmadığı kabul edilen düşey yük taşıyıcı çerçevelerdeki bağlantıların, kirişlerin plastik eğilme kapasitesinin %20 ile %50'sine kadar ulaşabildiği göz önüne alınmadığı taktirde yapıların sismik performansı eksik değerlendirilmiş olur. Bu nedenle, bu çalışmada 5 ve 10 katlı olmak üzere düşey yük taşıyıcı çerçevelerin dahil edilmediği, düşey yük taşıyıcı kirişlerinin rijitliklerinin %10'unun dikkate alındığı ve düşey yük çerçevelerin link elemanlar yardımıyla yanal yüklerin %10'unu karşıladığı üç durum 3 adet model ile temsil edilerek, düşey yük taşıyıcı çerçeveler ile moment çerçeveler arasındaki etkileşimi inceleyebilmek ve sismik performansı değerlendirebilmek amaçlanmıştır. Tüm modellere doğrusal olmayan Artımsal Dinamik Analizler uygulanmıştır. Her bir model ve her bir deprem kaydı için arttırılan deprem yoğunluklarına karşılık maksimum ötelenme oranları, en üst kat yer değiştirmeleri, taban kesme kuvvetleri, kapasite eğrileri ve yapılarda kat boyunca meydana gelen ötelenme oranlarının dağılımları yönetmelik sınırlarına göre incelenmiştir. Analiz sonucunda yukarıda bahsedilen ikinci ve üçüncü durumlardaki düşey yük taşıyıcı sistemlerin, sırasıyla yalnızca moment çerçeveye göre kapasiteyi %9 ve %17 arttırdığı gözlemlenmiştir.

Anahtar Kelimeler: Özel Moment Çerçeve, Düşey Yük Taşıyıcı Çerçeve, Artımsal Dinamik Analiz, Sismik Performans.

ACKNOWLEDGMENT

First of all, I would like to express my deep and sincere gratitude to my supervisor, Prof. Dr. Bülent AKBAŞ, whose valuable knowledge and experience I have benefited from in my graduate education and studies and who guided me in the formation of this study. It has been a great honor for me to be his student.

I would also like to express my appreciation to the jury members; Prof. Dr. Bilge DORAN and Assoc. Prof. Dr. Onur ŞEKER for their valuable time and criticism.

Also, I would like to thank to my engineer friends for did not spare their support during my working period.

I would like to express my deepest gratitude to my dear parents Nurcan KARAKAŞ and Zafer KARAKAŞ with me their love and sacrifices throughout my entire life.

Finally, a special thanks to my beloved boyfriend Cem Ali ÇELİK for his love, support, encouragement, patience, and help at every step of my academic life.

CONTENTS

	Page
SUMMARY	v
ÖZET	vi
ACKNOWLEDGMENT	vii
CONTENTS	viii
SYMBOLS and ABBREVIATIONS LIST	xi
LIST of FIGURES	xvii
LIST of TABLES	xxviii
1. INTRODUCTION	1
1.1. Scope and Objectives of the Thesis	1
1.2. Methodology	2
1.3. Seismic Performance of Steel Frames	2
1.3.1. General Informations	2
1.3.2. Previous Studies	11
2. STRUCTURAL MODELS	19
3. DESIGN REQUIREMENTS	22
3.1. Load Analyses	22
3.1.1. Dead Loads and Live Loads	22
3.1.2. Earthquake Loads	22
3.1.3. Design Spectrum	24
3.1.4. Structural Parameters	24
3.2. Special Moment Frame (SMF) Design	25
3.2.1. Seismic Base Shear	25
3.2.2. Numerical Model	27
3.2.3. Story Drift Requirement	29
3.2.4. Second Order Effects	30
3.2.5. Full Penetration Welded Joint	31
3.2.5.1. Probable Maximum Moment at Plastic Hinge	32
3.2.5.2. Required Shear Strength of The Connection	33
3.2.6. Strong Column-Weak Beam Requirement	34

3.2.7. Stability Analysis 36
3.2.7.1. Lateral Stiffnes Reduction 37
3.2.7.2. Notional Loads 37
3.2.7.3. Determination of Stiffness Reduction 39
3.2.8. Strength Requirement 39
3.2.8.1. Design of Seismic SMRF Columns 39
3.2.8.2. Design of Seismic SMRF Beams 42
3.2.8.3. Design of Non-Seismic GF Members 42
3.2.9. Member Requirement 42
3.3. Special Concentrically Braced Frame (SCBF) Design 43
3.3.1. Seismic Base Shear 43
3.3.2. Braces Design 44
3.3.3. Design of Beams in The Braced Bays 46
3.3.4. Design of Column 49
3.3.4.1. Tension and Compression Forces That Occur In Columns 49
3.3.4.2. Calculation of Gravity Loads 50
3.3.4.3. Applicable Column Selection 51
3.3.5. Story Drift Requirement 51
4. NONLINEAR DYNAMIC TIME HISTORY ANALYSES 52
4.1. Nonlinear Models 52
4.1.1. Nonlinear Modeling of Moment Frame Element Connections 54
4.1.2. Nonlinear Modeling of Gravity Frame Element Connections 58
4.2. Earthquake Ground Motions in The Time History 67
5. INCREMENTAL DYNAMIC ANALYSES 75
5.1. IDA For 5-Story Building Models 77
5.1.1. Düzce_8166 Earthquake 77
5.1.2. Park Field_4132 Earthquake 83
5.1.3. L'Aquila_4481 Earthquake 88
5.1.4. Kobe_1111 Earthquake 94
5.1.5. New Zealand_587 Earthquake 99
5.1.6. Morgan Hill_451 Earthquake 105
5.1.7. Chuetsu_4840 Earthquake 110
5.2. IDA For 10-Story Building Models 116

5.2.1. Düzce_8166 Earthquake 116
5.2.2. Park Field_4132 Earthquake 122
5.2.3. L'Aquila_4481 Earthquake 129
5.2.4. Kobe_1111 Earthquake 136
5.2.5. New Zealand_587 Earthquake 143
5.2.6. Morgan Hill_451 Earthquake 150
5.2.7. Chuetsu_4840 Earthquake 157
5.3. Average of Results Obtained with IDA 164
5.3.1. Results for 5-Story Buildings 165
5.3.2. Results for 10-Story Buildings 174
6. RESULTS and SUGGESTIONS 183
6.1. Numerical Results 183
6.2. Theoretical Results and Suggestions 184

REFERENCES 187
BIOGRAPHY 189
APPENDICES 190

SYMBOLS and ABBREVIATIONS LIST

Symbols and Abbreviations		Descriptions
α	:	ASD/LRFD force level adjustment factor
α	:	The height of the compression slab zone
β_{tE}	:	Equivalent base shear amplification coefficient
β_{II}	:	Second order amplification coefficient
γ_E	:	Multiplier determined according to irregularity
Ω_0	:	Overstrength coefficient
λ	:	The empirical coefficient used to limit the relative story drifts
λ_{hd}	:	Cross-section boundary condition for elements with high ductility
κ	:	The coefficient used differently for reinforced concrete and steel load-bearing systems in the definition of permissible relative story drifts
δ	:	Deflection, [cm]
δ_i	:	Effective relative story drift for the column or shear walls at the i^{th} floor of the building for the earthquake direction, [m]
$\delta_{i,max}$	:	The maximum value of the effective relative story drifts in the floor at the i^{th} floor of the building for the earthquake direction, [m]
Δ	:	Total elastic and plastic displacement, [m]
Δ_i	:	Horizontal displacement difference between consecutive floors, [m]
Δ_y	:	Displacement at yield point, [m]
θ	:	Angle between braced and floor, degrees
θ	:	Total elastic and plastic rotation of elements
θ_y	:	The rotation at yield point
$\theta_{II,i}$	:	Second order indicator value defined for each i^{th} floor in the earthquake direction

$\theta_{II,max}$	:	The maximum second order indicator value defined in the earthquake direction
τ_b	:	Stiffness reduction parameter
$\emptyset_c$	:	Resistance factor for compression
$\emptyset_v$	:	Resistance factor for shear
A_g	:	Gross cross-sectional area, [mm^2]
A_w	:	Area of web, the overall depth times the web thickness, [mm^2]
C_b	:	Lateral-torsional buckling modification factor for nonuniform moment diagrams
C_{EPB}	:	The expected post-buckling brace strength, [kN]
C_{ET}	:	The expected brace strength in compression, [kN]
C_h	:	The empirical coefficient used in the second order calculation
C_{pr}	:	Factor to account for peak connection strength
C_t	:	The coefficient used in the empirical natural vibration period calculation
C_v	:	Web shear coefficient
CP	:	Collapse Prevention performance level
D	:	Overstrength factor
DD-2	:	Earthquake ground motion level with 10% probability of exceedance in 50 years (recurrence period of 475 years)
E	:	Modulus of elasticity of steel, [mm^3]
$E_d^{(H)}$	:	Horizontal earthquake effect based on the design
$E_d^{(Z)}$	:	Vertical earthquake effect based on the design
$F_{b,DL}$	:	Forces on the braces created by dead loads, [kN]
$F_{b,LL}$	:	Forces on the braces created by live loads, [kN]
$F_{b,QE}$	:	Forces on the braces created by earthquake loads, [kN]
F_{cr}	:	Flexural buckling stress, [MPa]
F_e	:	Elastic buckling stress, [MPa]
F_s	:	Factor to adjust spectral acceleration in the short-period range for site class

F_u	:	Seismic loads due to expected brace capacity acting on beams, [MPa]
F_y	:	Minimum yield strength of steel, [MPa]
F_1	:	Factor to adjust spectral acceleration at 1 s for site class
G	:	Dead Load, [kN]
H_n	:	Building height, [m]
I	:	Building importance coefficient
I	:	Moment of inertia in the plane of bending, [mm^4]
IO	:	Immediate Occupancy performance level
K	:	Effective length factor
K_{eff}	:	Effective stiffness
L	:	Length of span, [mm]
L_b		Length between points that are either braced against lateral displacement of compression flange or braced against twist of the cross section, [mm]
L_c	:	Length of column, [mm]
L_p	:	Lateral unsupported boundary length for the yield boundary state, [mm]
L_r	:	Limit length in non-elastic lateral torsional buckling, [mm]
LS	:	Life Safety perofrmance level
M_c	:	Design axial flexural strength, [kN-m]
M_n	:	Nominal flexural strength, [kN-m]
M_r	:	Required flexural strength, [kN-m]
M_p	:	Plastic bending moment strength, [kN-m]
MPa	:	Mega Pascal
M_{pr}	:	The probable maximum moment at the plastic hinge, [kN-m]
M_{uv}	:	Additional moment due to shear amplification from the locaion of the plastic hinge to the column centerline, [kN-m]
M_{u-}	:	Negative ultimate moment, [kN-m]
M_{u+}	:	Positive ultimate moment, [kN-m]
M_{y-}	:	Negative yielding moment, [kN-m]
M_{y+}	:	Positive yielding moment, [kN-m]
N_i	:	Horizontal load acting on the floor, [kN]

NG	:	Notional dead Load, [kN]
NQ	:	Notional live load, [kN]
NQ_r	:	Notional roof live load, [kN]
P_c	:	Design axial compressive strength, [kN]
$P_{C,L}$	:	Tension forces that ocur in column, [kN]
$P_{C,R}$	:	Compression forces that ocur in column, [kN]
P_n	:	Characteristic axial compressive strength, [kN]
PR	:	Partially rigid
P_r	:	Required axial strength, [kN]
P_{uc}	:	Required axial compressive strength, [kN]
Q	:	Live load, [kN]
Q_r	:	Roof live load, [kN]
R	:	Response modification coefficient
$R_a\ (T)$	:	Earthquake load reduction coefficient
R_y	:	Ratio of the expected yield stress to the specified minimum yield stress
S	:	Nominal snow load, [kN]
$S_{ae}\ (T)$	:	Horizontal elastic design spectral acceleration [g]
$S_{aR}\ (T)$	:	Reduced design spectral acceleration [g]
S_{DS}	:	Design short-period spectral response acceleration parameter
S_{D1}	:	Design spectral response acceleration parameter at a one-second period
SF	:	Scale factor
S_S	:	Spectral response acceleration parameter at short periods
S_1	:	Spectral response acceleration parameter at a one-second period
T	:	Natural vibration period [s]
T_A, T_B	:	Horizontal elastic design spectrum corner periods [s]
T_{ET}	:	The expected brace strength in tension, [kN]
T_L	:	The long-period transition parameter [s]
T_{pA}	:	Empirical fundamental natural period of vibration [s]
V_i	:	Reduced floor shear force at the i^{th} floor in the direction of the earthquake, [kN]

V_d	:	Shear force calculated under the effect of gravity load with the load combination (1.2G+0.5Q+0.2S) at the possible plastic hinge points at the beam ends, [kN]
V_n	:	Characteristic shear force strength, [kN]
$(V_s)_{30}$	:	The shear wave velocities of the soils, [m/s]
V_t	:	Total earthquake load [kN]
V_{tE}	:	Design shear force resulting from earthquake effects, [kN]
V_{uc}	:	Required shear strength of beam and beam web-to-column connection, [kN]
Y_i	:	Total vertical load acting on the floor at each floor level
W_e	:	Elastic section modülüs, [mm^3]
W_p	:	Plastic section modülüs, [mm^3]
b	:	Width of member, [mm]
b_{eff}	:	Effective bay of beam, [mm]
d_c	:	Depth of column, [mm]
d_{st}	:	Depth of connection plate's, [mm]
d_1	:	Depth of concrete deck, [mm]
f_c', f_{cu}	:	Characteristic compressive strength, [MPa]
g	:	Acceleration of gravity, [g=9.81 m/s^2]
h	:	Height of element, [mm]
h_i	:	Story height, [mm]
h_r	:	Slab rib depth, [mm]
h_s	:	Shear stud height, [mm]
i	:	Radius of gyration, [mm]
kN	:	Kilonewton
l_h	:	The distance of the plastic hinge from the column face, [mm]
l_n	:	Distance between plastic hinge locations, [mm]
m	:	Meter
m_t	:	Total mass, [t]
rad	:	Radian
s	:	Second
s_r	:	Slab rib spacing, [mm]
t_c	:	Slab depth, [mm]

t_f	:	Thickness of flange, [mm]
t_{st}	:	Thickness of connection plate's, [mm]
t_w	:	Thickness of web [mm]
u_i	:	For any column or shearwall in the seismic direction, the reduced displacement at the ith floor [m]
w_k	:	Total weight at kth floor, [kN]
w_{rb}	:	Rib width bottom, [mm]
w_{rt}	:	Rib width top, [mm]
AISC	:	American Institute of Steel Construction
ASCE	:	American Society of Civil Engineering
ATC	:	Applied Technology Council
ACMR	:	Adjusted Collapse Margin Ratio
FEMA	:	Federal Emergency Management Agency
GF	:	Gravity Frame
GTÜ	:	Gebze Technical University
IDA	:	Incremental Dynamic Analysis
LFRS	:	Lateral Force Resisting System
LRFD	:	Load and Resistance Factor Design
MF	:	Moment Frame
NGA	:	National Geospatial-Intelligence Agency
PEER	:	Pacific Earthquake Engineering Research Center
RF	:	Reference Frame
SAC	:	Symposium on Applied Computing
SCBF	:	Special Concentrically Braced Frame
SMRF	:	Special Moment Resisting Frame
SDCCSS	:	Specification for Design, Calculation and Construction of Steel Structure
TBEC	:	Turkish Building Earthquake Code
USA	:	United States of America

LIST of FIGURES

Figure No:		Page
1.1:	Examples of beam-to-column welded connections damaged by the Hyogo-ken Nanbu (Kobe, Japan) earthquake: a) fracture at the lower beam flange, b) fracture in column-to-diaphragm welded connections, c) close-up view of fractured welds along box-column plate.	4
1.2:	Steel frame including frame system.	5
1.3:	Steel frame including moment-resisting frame.	5
1.4:	Moment resisting frame with high ductility.	6
1.5:	Gravity frame with shear tab (simple) connection.	8
1.6:	Moment-rotation curve for shear tab connection with the slab.	10
1.7:	Comparison of moment versus rotation response for specimens with and without slab.	12
1.8:	Moment-rotation model.	13
1.9:	Moment-rotation model of GF with composite slab.	14
1.10:	Moment-rotation characterization curve.	15
1.11:	Numerical model and moment-rotation relationship for gravity beam-column connections.	17
1.12:	Fragility curves: a) For the moment frame only, b) For the moment frame with gravity frames.	18
2.1:	5-story frame plan view.	19
2.2:	5-story elevations.	20
2.3:	10-story frame plan view.	21
2.4:	10-story frame elevations.	21
3.1:	Elastic design spectrum function.	24
3.2:	Full penetration welded connection detail.	31
3.3:	Shear force at the beam and web-to-column connection.	33
3.4:	Computing the required shear strength.	34
3.5:	Shear and moment forces at the joint indicated by a circle.	35
3.6:	Sum of moments in beams.	36
3.7:	Notional load.	38

3.8:	Axial force-moment interaction curve.	40
3.9:	Load distribution.	44
3.10:	Point gravity loads.	44
3.11:	Forces caused by dead and live loads on the braces.	45
3.12:	Illustration of T_{ET}, C_{EB} and C_{EPB} strengths to be used in the two structural analysis cases.	47
3.13:	General view of cases.	48
3.14:	Tension and compression in 1st floor column as per Case I.	49
3.15:	Load areas of SCBF columns.	50
4.1:	Generalized force-deformation relation for steel elements.	54
4.2:	Moment frame column plastic hinge definition.	56
4.3:	Moment frame beam plastic hinge definition.	57
4.4:	Beam hinges location.	57
4.5:	Assigning hinges to moment frame members.	58
4.6:	Connection models: a) Bare steel shear tab connection model, b) Composite steel shear tab connection model.	59
4.7:	Beam-to-column connection models in GFs.	60
4.8:	Moment-rotation relation of IPE O 400 for Set-1 models.	61
4.9:	Moment-rotation relation of IPE O 450 for Set-1 models.	62
4.10:	Typical GF shear tab connection detail.	63
4.11:	Filled deck properties.	64
4.12:	Moment-rotation relationship for Set-2 models.	64
4.13:	Moment-rotation models for Set-1 and Set-2.	65
4.14:	Spring elements.	65
4.15:	View of link elements in elevation.	66
4.16:	View of link elements in plan.	66
4.17:	Elastic design spectrum function.	68
4.18:	Scaled response spectrums for 5 story RF.	69
4.19:	Scaled response spectrums for 5 story Set-1.	70
4.20:	Scaled response spectrums for 5 story Set-2.	71
4.21:	Scaled response spectrums for 10 story RF.	72
4.22:	Scaled response spectrums for 10 story Set-1.	73
4.23:	Scaled response spectrums for 10 story Set-2.	74

5.1:	Hingings and plastic rotation demands of 5-story RFs under the Düzce earthquake.	78
5.2:	Hingings and plastic rotation demands of 5-story Set-1 under the Düzce earthquake.	78
5.3:	Hingings and plastic rotation demands of 5-story Set-2 under the Düzce earthquake.	79
5.4:	Max drift ratios of 5-story models under Düzce earthquake acceleration intensities.	79
5.5:	Max top displacements of 5-story models under Düzce earthquake acceleration intensities.	80
5.6:	Max base shears of 5-story models under Düzce earthquake acceleration intensities.	80
5.7:	Capacity curves of 5-story models under Düzce earthquake acceleration intensities.	81
5.8:	Hinging and plastic rotation demands of 5-story models at Sa=1.50g under the Düzce earthquake.	82
5.9:	Drift ratio distributions along 5-story models' height at Sa=1.50g under the Düzce earthquake.	82
5.10:	Hingings and plastic rotation demands of 5-story RFs under the Park Field earthquake.	83
5.11:	Hingings and plastic rotation demands of 5-story Set-1 under the Park Field earthquake.	84
5.12:	Hingings and plastic rotation demands of 5-story Set-2 under the Park Field earthquake.	84
5.13:	Max drift ratios of 5-story models under Park Field earthquake acceleration intensities.	85
5.14:	Max top displacements of 5-story models under Park Field earthquake acceleration intensities.	85
5.15:	Max base shears of 5-story models under Park Field earthquake acceleration intensities.	86
5.16:	Capacity curves of 5-story models under Park Field earthquake acceleration intensities.	86

5.17:	Hinging and plastic rotation demands of 5-story models at Sa=1.60g under the Park Field earthquake.	87
5.18:	Drift ratio distributions along 5-story models' height at Sa=1.60g under the Park Field earthquake.	88
5.19:	Hingings and plastic rotation demands of 5-story RFs under the L'Aquila earthquake.	89
5.20:	Hingings and plastic rotation demands of 5-story Set-1 under the L'Aquila earthquake.	89
5.21:	Hingings and plastic rotation demands of 5-story Set-2 under the L'Aquila earthquake.	90
5.22:	Max drift ratios of 5-story models under L'Aquila earthquake acceleration intensities.	90
5.23:	Max top displacements of 5-story models under L'Aquila earthquake acceleration intensities.	91
5.24:	Max base shears of 5-story models under L'Aquila earthquake acceleration intensities.	91
5.25:	Capacity curves of 5-story models under L'Aquila earthquake acceleration intensities.	92
5.26:	Hinging and plastic rotation demands of 5-story models at Sa=1.10g under the L'Aquila earthquake.	93
5.27:	Drift ratio distributions along 5-story models' height at Sa=1.10g under the L'Aquila earthquake.	93
5.28:	Hingings and plastic rotation demands of 5-story RFs under the Kobe earthquake.	94
5.29:	Hingings and plastic rotation demands of 5-story Set-1 under the Kobe earthquake.	95
5.30:	Hingings and plastic rotation demands of 5-story Set-2 under the Kobe earthquake.	95
5.31:	Max drift ratios of 5-story models under Kobe earthquake acceleration intensities.	96
5.32:	Max top displacements of 5-story models under Kobe earthquake acceleration intensities.	96

5.33:	Max base shears of 5-story models under Kobe earthquake acceleration intensities.	97
5.34:	Capacity curves of 5-story models under Kobe earthquake acceleration intensities.	97
5.35:	Hinging and plastic rotation demands of 5-story models at Sa=0.70g under the Kobe earthquake.	98
5.36:	Drift ratio distributions along 5-story models' heightt at Sa=0.70g under the Kobe earthquake.	99
5.37:	Hingings and plastic rotation demands of 5-story RFs under the New Zealand earthquake.	100
5.38:	Hingings and plastic rotation demands of 5-story Set-1 under the New Zealand earthquake.	100
5.39:	Hingings and plastic rotation demands of 5-story Set-2 under the New Zealand earthquake.	101
5.40:	Max drift ratios of 5-story models under New Zealand earthquake acceleration intensities.	101
5.41:	Max top displacements of 5-story models under New Zealand earthquake acceleration intensities.	102
5.42:	Max base shears of 5-story models under New Zealand earthquake acceleration intensities.	102
5.43:	Capacity curves of 5-story models under New Zealand earthquake acceleration intensities.	103
5.44:	Hinging and plastic rotation demands of 5-story models at Sa=0.95g under the New Zealand earthquake.	104
5.45:	Drift ratio distributions along 5-story models' height at Sa=0.95g under the New Zealand earthquake.	104
5.46:	Hingings and plastic rotation demands of 5-story RFs under the Morgan Hill earthquake.	105
5.47:	Hingings and plastic rotation demands of 5-story Set-1 under the Morgan Hill earthquake.	106
5.48:	Hingings and plastic rotation demands of 5-story Set-2 under the Morgan Hill earthquake.	106

5.49:	Max drift ratios of 5-story models under Morgan Hill earthquake acceleration intensities.	107
5.50:	Max top displacements of 5-story models under Morgan Hill earthquake acceleration intensities.	107
5.51:	Max base shears of 5-story models under Morgan Hill earthquake acceleration intensities.	108
5.52:	Capacity curves of 5-story models under Morgan Hill earthquake acceleration intensities.	108
5.53:	Hinging and plastic rotation demands of 5-story models at Sa=0.85g under the Morgan Hill earthquake.	109
5.54:	Drift ratio distributions along 5-story models' height at Sa=0.85g under the Morgan Hill earthquake.	110
5.55:	Hingings and plastic rotation demands of 5-story RFs under the Chuetsu earthquake.	111
5.56:	Hingings and plastic rotation demands of 5-story Set-1 under the Chuetsu earthquake.	111
5.57:	Hingings and plastic rotation demands of 5-story Set-2 under the Chuetsu earthquake.	112
5.58:	Max drift ratios of 5-story models under Chuetsu earthquake acceleration intensities.	112
5.59:	Max top displacements of 5-story models under Chuetsu earthquake acceleration intensities.	113
5.60:	Max base shears of 5-story models under Chuetsu earthquake acceleration intensities.	113
5.61:	Capacity curves of 5-story models under Chuetsu earthquake acceleration intensities.	114
5.62:	Hinging and plastic rotation demands of 5-story models at Sa=1.55g under the Chuetsu earthquake.	115
5.63:	Drift ratio distributions along 5-story models' height at Sa=1.55g under the Chuetsu earthquake.	115
5.64:	Hingings and plastic rotation demands of 10-story RFs under the Düzce earthquake.	116

5.65:	Hingings and plastic rotation demands of 10-story Set-1 under the Düzce earthquake.	117
5.66:	Hingings and plastic rotation demands of 10-story Set-2 under the Düzce earthquake.	118
5.67:	Max drift ratios of 10-story models under Düzce earthquake acceleration intensities.	119
5.68:	Max top displacements of 10-story models under Düzce earthquake acceleration intensities.	119
5.69:	Max base shears of 10-story models under Düzce earthquake acceleration intensities.	120
5.70:	Capacity curves of 10-story models under Düzce earthquake acceleration intensities.	120
5.71:	Hinging and plastic rotation demands of 10-story models at Sa=0.60g under the Düzce earthquake.	121
5.72:	Drift ratio distributions along 10-story models' height at Sa=0.60g under the Düzce earthquake.	122
5.73:	Hingings and plastic rotation demands of 10-story RFs under the Park Field earthquake.	123
5.74:	Hingings and plastic rotation demands of 10-story Set-1 under the Park Field earthquake.	124
5.75:	Hingings and plastic rotation demands of 10-story Set-2 under the Park Field earthquake.	125
5.76:	Max drift ratios of 10-story models under Park Field earthquake acceleration intensities.	126
5.77:	Max top displacements of 10-story models under Park Field earthquake acceleration intensities.	126
5.78:	Max base shears of 10-story models under Park Field earthquake acceleration intensities.	127
5.79:	Capacity curves of 10-story models under Park Field earthquake acceleration intensities.	127
5.80:	Hinging and plastic rotation demands of 10-story models at Sa=0.70g under the Park Field earthquake.	128

5.81:	Drift ratio distributions along 10-story models' height at Sa=0.70g under the Park Field earthquake.	129
5.82:	Hingings and plastic rotation demands of 10-story RFs under the L'Aquila earthquake.	130
5.83:	Hingings and plastic rotation demands of 10-story Set-1 under the L'Aquila earthquake.	131
5.84:	Hingings and plastic rotation demands of 10-story Set-2 under the L'Aquila earthquake.	132
5.85:	Max drift ratios of 10-story models under L'Aquila earthquake acceleration intensities.	133
5.86:	Max top displacements of 10-story models under L'Aquila earthquake acceleration intensities.	133
5.87:	Max base shears of 10-story models under L'Aquila earthquake acceleration intensities.	134
5.88:	Capacity curves of 10-story models under L'Aquila earthquake acceleration intensities.	134
5.89:	Hinging and plastic rotation demands of 10-story models at Sa=0.40g under the L'Aquila earthquake.	135
5.90:	Drift ratio distributions along 10-story models' height at Sa=0.40g under the L'Aquila earthquake.	136
5.91:	Hingings and plastic rotation demands of 10-story RFs under the Kobe earthquake.	137
5.92:	Hingings and plastic rotation demands of 10-story Set-1 under the Kobe earthquake.	138
5.93:	Hingings and plastic rotation demands of 10-story Set-2 under the Kobe earthquake.	139
5.94:	Max drift ratios of 10-story models under Kobe earthquake acceleration intensities.	140
5.95:	Max top displacements of 10-story models under Kobe earthquake acceleration intensities.	140
5.96:	Max base shears of 10-story models under Kobe earthquake acceleration intensities.	141

5.97:	Capacity curves of 10-story models under Kobe earthquake acceleration intensities.	141
5.98:	Hinging and plastic rotation demands of 10-story models at Sa=0.60g under the Kobe earthquake.	142
5.99:	Drift ratio distributions along 10-story models' height at Sa=0.60g under the Kobe earthquake.	143
5.100:	Hingings and plastic rotation demands of 10-story RFs under the New Zealamd earthquake.	144
5.101:	Hingings and plastic rotation demands of 10-story Set-1 under the New Zealamd earthquake.	145
5.102:	Hingings and plastic rotation demands of 10-story Set-2 under the New Zealamd earthquake.	146
5.103:	Max drift ratios of 10-story models under New Zealand earthquake acceleration intensities.	147
5.104:	Max top displacements of 10-story models under New Zealand earthquake acceleration intensities.	147
5.105:	Max base shears of 10-story models under New Zealand earthquake acceleration intensities.	148
5.106:	Capacity curves of 10-story models under New Zealand earthquake acceleration intensities.	148
5.107:	Hinging and plastic rotation demands of 10-story models at Sa=0.60g under the New Zealand earthquake.	149
5.108:	Drift ratio distributions along 10-story models' height at Sa=0.60g under the New Zealand earthquake.	150
5.109:	Hingings and plastic rotation demands of 10-story RFs under the Morgan Hill earthquake.	151
5.110:	Hingings and plastic rotation demands of 10-story Set-1 under the Morgan Hill earthquake.	152
5.111:	Hingings and plastic rotation demands of 10-story Set-2 under the Morgan Hill earthquake.	153
5.112:	Max drift ratios of 10-story models under Morgan Hill earthquake acceleration intensities.	154

5.113: Max top displacements of 10-story models under Morgan Hill earthquake acceleration intensities. 154
5.114: Max base shears of 10-story models under Morgan Hill earthquake acceleration intensities. 155
5.115: Capacity curves of 10-story models under Morgan Hill earthquake acceleration intensities. 155
5.116: Hinging and plastic rotation demands of 10-story models at Sa=0.70g under the Morgan Hill earthquake. 156
5.117: Drift ratio distributions along 10-story models' height at Sa=0.70g under the Morgan Hill earthquake. 157
5.118: Hingings and plastic rotation demands of 10-story RFs under the Chuetsu earthquake. 158
5.119: Hingings and plastic rotation demands of 10-story Set-1 under the Chuetsu earthquake. 159
5.120: Hingings and plastic rotation demands of 10-story Set-2 under the Chuetsu earthquake. 160
5.121: Max drift ratios of 10-story models under Chuetsu earthquake acceleration intensities. 161
5.122: Max top displacements of 10-story models under Chuetsu earthquake acceleration intensities. 161
5.123: Max base shears of 10-story models under Chuetsu earthquake acceleration intensities. 162
5.124: Capacity curves of 10-story models under Chuetsu earthquake acceleration intensities. 162
5.125: Hinging and plastic rotation demands of 10-story models at Sa=0.45g under the Chuetsu earthquake. 163
5.126: Drift ratio distributions along 10-story models' height at Sa=0.45g under the Chuetsu earthquake. 164
5.127: The average of the max drift ratios of the 5-story RF model. 165
5.128: The average of the max drift ratios of the 5-story Set-1 model. 165
5.129: The average of the max drift ratios of the 5-story Set-2 model. 166
5.130: Averages of max drift ratios for the 5-story models. 166
5.131: The average of the top displacements of the 5-story RF model. 167

5.132: The average of the top displacements of the 5-story Set-1 model. 167
5.133: The average of the top displacements of the 5-story Set-2 model. 168
5.134: Averages of top displacements for the 5-story models. 168
5.135: The average of the max base shears of the 5-story RF model. 169
5.136: The average of the max base shears of the 5-story Set-1 model. 169
5.137: The average of the max base shears of the 5-story Set-2 model. 170
5.138: Averages of max base shears for the 5-story models. 170
5.139: The average of the capacity curves of the 5-story RF model. 171
5.140: The average of the capacity curves of the 5-story Set-1 model. 171
5.141: The average of the capacity curves of the 5-story Set-2 model. 172
5.142: Averages of capacity curves for the 5-story models. 172
5.143: Average drift ratio distributions of 5-story models at Sa=1.00 g. 173
5.144: The average of the story drift ratios of the 10-story RF model. 174
5.145: The average of the story drift ratios of the 10-story Set-1 model. 174
5.146: The average of the story drift ratios of the 10-story Set-2 model. 175
5.147: Averages of max drift ratios for the 10-story models. 175
5.148: The average of the top displacements of the 10-story RF model. 176
5.149: The average of the displacements of the 10-story Set-1 model. 176
5.150: The average of the displacements of the 10-story Set-2 model. 177
5.151: Averages of top displacements for the 10-story models. 177
5.152: The average of the max base shears of the 10-story RF model. 178
5.153: The average of the max base shears of the 10-story Set-1 model. 178
5.154: The average of the max base shears of the 10-story Set-2 model. 179
5.155: Averages of max base shears for the 10-story models. 179
5.156: The average of the capacity curves of the 10-story RF model. 180
5.157: The average of the capacity curves of the 10-story Set- model 1. 180
5.158: The average of the capacity curves of the 10-story Set-2 model. 181
5.159: Averages of capacity curves obtained for 10-story models. 181
5.160: Average drift ratio distribution of 10-story models at Sa=0.50 g. 182

LIST of TABLES

Table No:		Page
3.1:	Dead loads.	22
3.2:	Site-specific information.	23
3.3:	Structural parameters for 5-story building.	24
3.4:	Structural parameters.	25
3.5:	Application limits of full penetration welded connection details.	32
3.6:	Load combinations including notional load effects.	38
4.1:	Modeling parameters and acceptance criteria.	55
4.2:	Modeling parameters and acceptance criteria.	55
4.3:	Sections of Set-2 models of 5 and 10 story buildings.	59
4.4:	Earthquake parameters and scale factors for 5-story RF.	69
4.5:	Earthquake parameters and scale factors for 5-story Set-1.	70
4.6:	Earthquake parameters and scale factors for 5-story Set-2.	71
4.7:	Earthquake parameters and scale factors for 10-story RF.	72
4.8:	Earthquake parameters and scale factors for 10-story Set-1.	73
4.9:	Earthquake parameters and scale factors for 10-story Set-2.	74
5.1:	SFs for 5-story models under the Düzce earthquake.	77
5.2:	Responses of 5-story models under Düzce earthquake.	81
5.3:	SFs for 5-story models under the Park Field earthquake.	83
5.4:	Responses of 5-story models under Park Field earthquake.	87
5.5:	SFs for 5-story models under the L'Aquila earthquake.	88
5.6:	Responses of 5-story models under L'Aquila earthquake.	92
5.7:	SFs for 5-story models under the Kobe earthquake.	94
5.8:	Responses of 5-story models under Kobe earthquake.	98
5.9:	SFs for 5-story models under the New Zealand earthquake.	99
5.10:	Responses of 5-story models under New Zealand earthquake.	103
5.11:	SFs for 5-story models under the Morgan Hill earthquake.	105
5.12:	Responses of 5-story models under Morgan Hill earthquake.	109
5.13:	SFs for 5-story models under the Chuetsu earthquake.	110
5.14:	Responses of 5-story models under Chuetsu earthquake.	114
5.15:	SFs for 10-story models under the Düzce earthquake.	116

5.16: Responses of 10-story models under Düzce earthquake. 121
5.17: SFs for 10-story models under the Park Field earthquake. 122
5.18: Responses of 10-story models under Park Field earthquake. 128
5.19: SFs for 10-story models under the L'Aquila earthquake. 129
5.20: Responses of 10-story models under L'Aquila earthquake. 135
5.21: SFs for 10-story models under the Kobe earthquake. 136
5.22: Responses of 10-story models under Kobe earthquake. 142
5.23: SFs for 10-story models under the New Zealand earthquake. 143
5.24: Responses of 10-story models under New Zealand earthquake. 149
5.25: SFs for 10-story models under the Morgan Hill earthquake. 150
5.26: Responses of 10-story models under Morgan Hill earthquake. 156
5.27: SFs for 10-story models under the Chuetsu earthquake. 157
5.28: Responses of 10-story models under Chuetsu earthquake. 163
6.1: Fundamental periods of 5 and 10-story models. 183
6.2: Sa corresponding to max drift ratio limit for 5 and 10-story models. 183
6.3: Sa corresponding to displacement limits for 5 and 10-story models. 183
6.4: Max base shear forces for 5 and 10-story models. 184
6.5: Max plastic rotation demands for 5 and 10-story models. 184

1. INTRODUCTION

1.1 Scope and Objectives of the Thesis

The violent earth motion shakings that have occurred since the existence of the world have damaged or caused millions of structures to collapse. On the other hand, to be less affected by these earthquakes that occur day by day, human beings have tended to design the structures in a way that will show non-linear behavior, will take damage in a controlled manner, and survive without collapse. In line with this purpose lateral load-bearing systems such as Special Moment Resisting Frame (SMRF) and Special Concentrically Braced Frame (SCBF) are used in steel structures to absorb the energies of incoming severe ground motions.

SMRFs are Lateral Force Resisting Systems (LFRS) against seismic force expected to provide high ductility. When the building is subjected to a strong ground motion, the beams and columns in the moment frame (MF) are connected by moment transfer connections (rigid or semi-rigid) so that lateral forces can be transferred by bending and shear. MFs are seismically designed in such a way that yielding occurs at the beam ends through the formation of plastic hinges and large inelastic deformations occur. Thus, seismic lateral forces are absorbed without deteriorating the stability of the structure.

In addition, due to the high labor costs of SMRFs in steel structures and to save time, gravity load-carrying systems are used in the frames in the internal spans. These systems are only carried gravity loads and only gravity-loaded combinations are considered during the analysis phase. In these frames, whose lateral load carrying capacity is neglected and is responsible to carry gravity loads even under earthquake-induced displacements, the simple connection type (pinned) with freedom of rotation is used for beam-column connections.

The purpose of this thesis is to examine the interaction between MFs and gravity frames (GFs) in low-rise and medium-rise story steel structures designed following the Turkish Building Earthquake Code (TBEC-2018) [1] and Specification for Structural Steel Buildings (AISC 360-10) [2] design requirements and to investigate the contribution of GFs to the inelastic seismic response of moment frames.

1.2 Methodology

In this study, six different steel structure models in total, 5 and 10 floors called "Reference Frame (RF)", "Set-1" and "Set-2", containing both gravity frame and moment frames, were designed according to the specification rules. While the RF represents the analytical model in which GFs are not included in the model, the case where 10% of the plastic rotational stiffness of beams is taken into account in the connections of Set-1 GFs, and Set-2 represents the model in which both composite slab effects and GFs carry 10% of the lateral loads with the help of link elements with infinite stiffness. While the nonlinear behavior model defined in TBEC-2018 was used for beam-column connections in moment frames, infinite stiffness link elements are used for beam-column connections of GFs in Set-1 and Set-2 models. These structures were modeled using the structural analysis software ETABS-2016 [3]. To examine the interaction between MFs and GFs and to evaluate seismic performance, nonlinear Incremental Dynamic Analysis (IDA) has been performed for 5 and 10-story steel buildings designed with current design specifications that are subjected to design-level earthquake ground motions. Within the scope of this analysis, 7 earthquake records determined according to TBEC-2018 conditions were applied to the buildings. For each model and each earthquake record, the maximum drift ratio, top story displacements, base shear forces, capacity curves, plastic rotations, and drift ratio distributions occurring along the floors in the buildings against the increased earthquake intensities were examined according to the specifications. The contribution of GFs to seismic performance has been revealed by comparing the obtained results between RF, Set-1, and Set-2 in 5-story and 10-story buildings.

1.3 Seismic Performance of Steel Frames

1.3.1 General Informations

Moment resistant frames applied in steel buildings are one of the widely used lateral load-bearing systems to resist seismic loads. Looking at the history of steel moment frames, its history dates back to the late 1880s, with the start of building multi-story structures in Chicago and New York City. The 12-story Home Insurance

Building in Chicago, the first building in the world to use steel frames, is known as "skeleton construction". While the steel frames that started to be used in those years were designed to carry gravity loads only, stiff claddings were used to resist lateral loads and it was thought to be sufficient. This design approach lasted until the 1906 San Francisco earthquake. Thanks to empirical evidence that high-rise buildings remained intact after this earthquake occurred and moment frames survived without part of any frontispiece, engineers of the period were convinced that moment frames resisted earthquakes. In the next stage, over the decades, the knowledge gained about steel structures and moment frames has changed and improved. However, with the occurrence of the 1994 Northridge (Los Angeles) earthquake in the United States and the 1995 Hyogo-ken Nanbu (Kobe) earthquake in Japan, the steel moment frames could not show a ductile performance as engineers expected. Although some of the structures subjected to the effects of earthquakes managed to survive without collapse, it was observed that serious brittle failures occurred in the rigid joint areas of the moment frame beam-columns, especially in the flange welds, beam flanges, column flanges, and webs. Some of the damages that occurred after these earthquakes are shown in Figure 1.1 [4]. After this situation, engineers of the period realized that they had incomplete knowledge about the behavior of moment frames and carried out many comprehensive analytical and theoretical studies to better understand the factors that contributed to the seismic performance of these systems, for good or bad, and these historical earthquakes caused serious changes in steel structure regulations. [4]. One of the results of the extensive studies carried out is that the gravity load-bearing systems designed with moment frames increase the expected overstrength in the structure and provide a secondary reserve capacity.

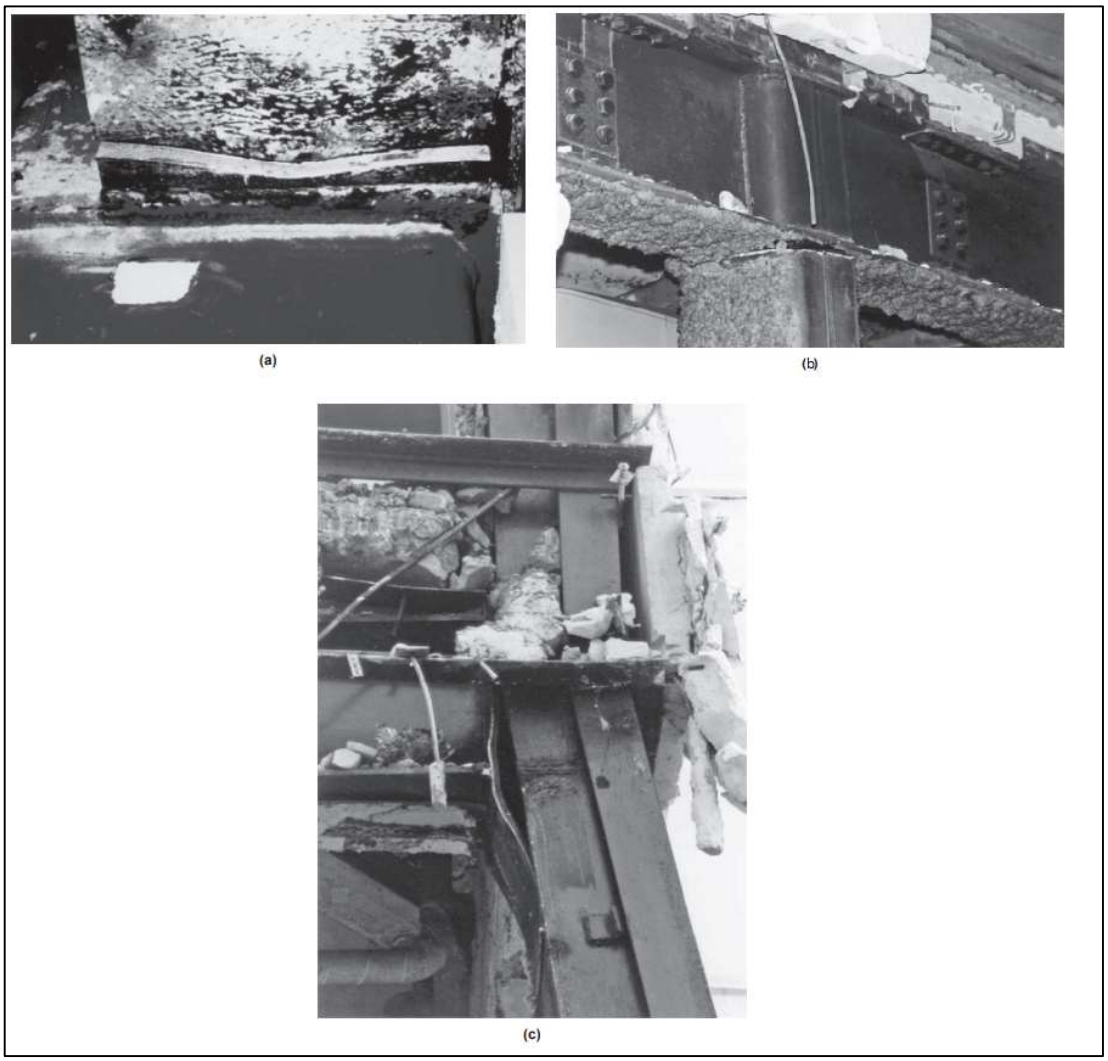


Figure 1.1: Examples of beam-to-column welded connections damaged by the Hyogo-ken Nanbu (Kobe, Japan) earthquake: a) fracture at the lower beam flange, b) fracture in column-to-diaphragm welded connections, c) close-up view of fractured welds along box-column plate.

Resistance to lateral seismic forces in moment frames is provided by the rigid frame movement formed by the rigid connection of columns and beams, which are frame elements. In other words, the horizontal movement of the moment frame arises from the bending moments and shear forces occurring in the columns and beams. For this reason, moment-resisting frames provide the lateral stiffness of the entire frame by showing strength against bending in elements such as beams, columns, and joints forming the frame. From this point of view, some of the most important advantages of moment frames and the reasons for their popular use are, no supporting elements that prevent the openings that provide maximum flexibility in terms of architecture, the

desired ductile behavior can be met with economic cross-sections and it provides convenience in terms of design.

Structure examples including frame system and moment-resisting frames are given in Figure 1.2 [5] and Figure 1.3 [6].



Figure 1.2: Steel frame including frame system.



Figure 1.3: Steel frame including moment-resisting frame.

In the seismic design code of AISC 341-16 [7], moment resisting steel frame systems are examined in three parts in terms of ductility. The first of these is "Frames with Limited Ductility Level", frames that can meet inelastic deformations at a limited level. Second, " Frames with Medium Ductility Level " are frames designed to resist inelastic deformations at a medium level. The last one, "Frames of Highly Ductility Level" used in this study, are steel moment-resisting frames designed at a level that can meet large inelastic deformations. Frames designed with high ductility level within the scope of the regulation are special moment frames and since they have high ductile properties, they increase the damping ratio and reduce the rigidity of the structure by allowing inelastic deformations such as the yielding of steel material, the occurrence of plastic hinges at the beam end regions, the formation of limited local buckling. Since these systems have a flexible structure, they oscillate over longer periods and are therefore subjected to lower seismic forces. At the same time, since the largest earthquake load reduction coefficient is applied for SMRF in the existing building codes for design earthquake forces, the design is made by considering the lowest lateral design forces.

In Figure 1.4, deformation shape and connection details of the moment frame with high ductility level under lateral seismic forces are shown.

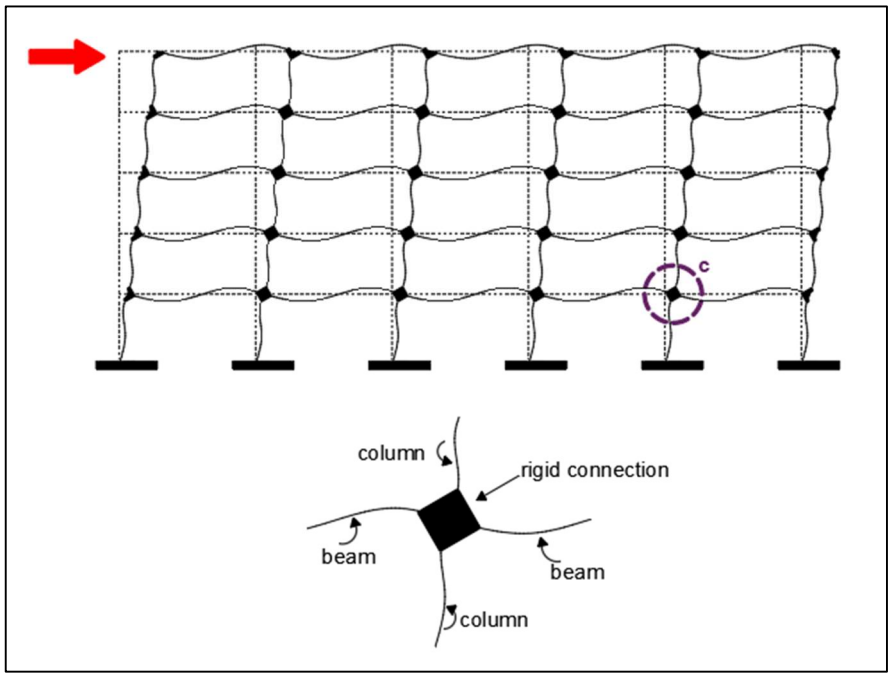


Figure 1.4: Moment resisting frame with high ductility.

To ensure maximum ductile behavior in SMRFs, plastic hinges should occur at all beam-ends along with the height of the structure and a sway plastic mechanism should be formed, but in the meantime, when the frames are subjected to seismic lateral loads, their lateral deflections must have enough strength to ensure that they do not exceed the regulation drifts.

As a performance target in the design provisions included in the 'Regulation on Buildings to be Built in Disaster Areas', which was published in 1998 and still in effect, and also in the 'Recommended Lateral Force Requirements and Commentary', it is necessary to ensure that no structural and non-structural elements are damaged during mild ground motions, damage to structural and non-structural elements during moderate ground motions are repairable, and in severe earthquakes, the structures must be prevented from collapsing partially or completely and preventing loss of life [8]. Permanent damage causes a non-ductile behavior in the structures, a decrease in the rigidity of the structure, and an increase in the fundamental vibration period. The degree of permanent damage to buildings as a result of seismic lateral forces and the magnitude of seismic forces to occur in buildings are inversely proportional to each other. Therefore, the more the structure is damaged, the fewer seismic forces formed within the structure. For this reason, in the current design regulations, moment frame systems are allowed to be designed with a limited degree of permanent damage. For the occurrence of damage in special moment resisting frames, the yield of steel material and the absorption of energy by the occurrence of plastic hinges near the joint areas of the beams are offered, however, due to the high ductility of the moment frames and the fragility of the steel structure elements, large lateral deflections together with local and global buckling can occur under lateral seismic loads. In SMRFs, damage to the beam-column joint areas due to buckling is undesirable behavior. Since the buckling and fracturing of the structural elements in the joint areas is a brittle behavior, it significantly reduces the rigidity and strength of the system in terms of carrying the gravity loads in the system after the effect of lateral seismic forces. For this reason, it should be designed in a way that prevents the connections from being damaged prematurely under nonlinear cyclic movements.

Damage to the joint areas of the frame elements is provided by limiting the plastic rotation motions of the connections. Plastic rotation estimates are obtained as a result of nonlinear analysis and the results obtained differ according to the modeling assumptions, the use of different ground motion records, and the amount of plastic

energy emitted by beam, column, panel regions. General expectations regarding plastic rotation demand for moment frames are based on observations from past analytical studies. Before the Northridge earthquake, the expected maximum plastic rotations in beams alone (in the absence of panel zone deformations) were expected to be 0.02 rad (Popov and Tsai 1989, Tsai and Popov 1988), while in some studies it was determined to be 0.025 rad (Roeder et al., 1989) [8]. After the earthquake, the plastic rotation capacity for the new structures was determined as 0.03 rad, while it was updated as 0.025 rad for the post-earthquake modification [4].

To prove the adequacy of the rigid connections used for the beam-column joints of special moment frames, certain conditions are set in the current regulations. According to the AISC 358-16 [9] regulation, in frames with high ductility levels, the moment capacity of the connection at a total rotation angle of 0.04 rad should not fall below 80% of the plastic moment capacity of the beam. In the TBEC-2018 regulation, this situation must be proved by experimental or analytical methods with the capacity to provide at least 0.04 rad relative story drift angle (relative story drift/story height) for moment transfer frame beam-column connections.

Gravity frames, known as gravity load carriers, are designed to be positioned inner part of the buildings. For these systems, in many design regulations are expected to carry only gravitational loads only, even under earthquake-induced displacements, considering only combinations of gravity loads. It is assumed that they cannot show any resistance against seismic lateral forces and for this reason, simple (shear) connections are used for beam-column connections in gravity systems. It is assumed that these connections are free to rotate and do not transmit moments.

In Figure 1.5, the typical gravity frame system and shear tab connection used in beam-column joints in this frame system are shown.

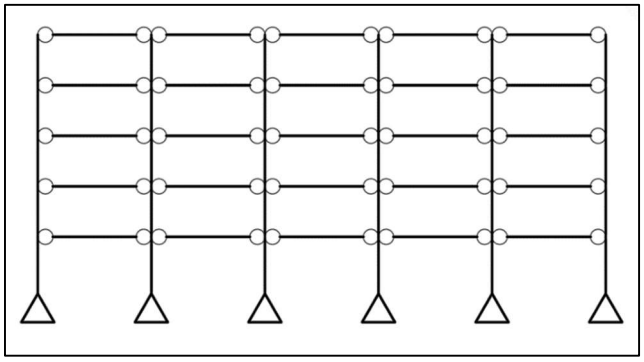


Figure 1.5: Gravity frame with shear tab connection.

The lateral seismic performance of gravity systems has been handled differently in many regulations published until today. For example, in Annex F of the FEMA P-695 [10] regulation used to evaluate the failure performance of structures states that gravity frames do not need to be included in the analysis in terms of their contribution to lateral seismic performance, but it is still stated that it is up to the engineer's request. The PEER / ATC 72-1 [11] report from previous studies stated that gravity systems can benefit lateral stability at large displacements, leaving it to the engineer's choice whether to include them in the analysis like in P-695. In the ASCE 41-13 [12] regulation, which is still in effect today, it is stated that gravity systems, which are seen as secondary components in nonlinear static and nonlinear dynamic analysis stages, should be included in the analysis assuming that they are a backup system that prevents structural collapse in case of failure of moment frame connections.

To evaluate the contribution of gravity frames in the interior to the performance of the structure under lateral seismic forces, shear tab connections in beams and gravity columns are modeled with zero-length link elements with infinite rigidity and idealized as semi-rigid joints and the contribution of these frames to inelastic behavior through their connection is examined. When composite concrete floor slabs are included in the analysis together with gravity systems, it is known that greater rotational motions can be made under higher moment forces and increase the seismic capacity reserve of the structure.

According to the Specification for Design, Calculation, and Construction of Steel Structures (SDCCSS-2016) [13] Section 13, the amount of rotation of the pinned connections should be compatible with the end rotation of the beams, and limited inelastic deformations are allowed in the connections to accommodate between the beam end rotations and the rotation of the connections. The rotational capacity of the semi-rigid connections, including the composite slab effects, varies between 0.035-0.065 rad when local yields and torsions at the webs occur in the gravity system columns. When the composite concrete floor fails, the semi-rigid connection can reach 0.01-0.045 rad values without collapse. They can rotate up to 0.03 rad in case of the yield of gravity beam bottom flange or fracture of bolts [14].

In Figure 1.6, the approximate moment-rotation curvature model is given for the semi-rigid shear tab connection including the effects of composite concrete slabs [15].

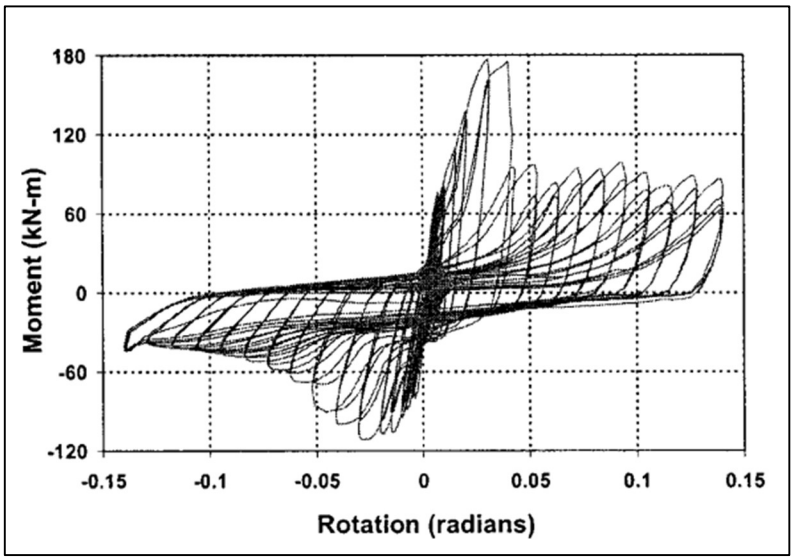


Figure 1.6: Moment-rotation curve for shear tab connection with the slab.

If it is mentioned about the earthquake regulations applied in Turkey and developed and changed over the years, the 2007 earthquake regulation [16] is not much different from the earthquake regulation published in 1997 [17], except for minor changes. Although 20 years have passed, the 2007 regulation did not include the gains from new scientific studies and new design principles. In addition, since there are some incomplete, inaccurate, and difficult to understand sections within the scope of the regulation, its draft was published in 2016 and the original earthquake regulation was published in 2018. The design of the steel carrier systems was made with the calculation rules in TBEC-2018 [1], considering the loads predicted in TS 498 [18]. At this stage, as required by the regulation, while designing, attention has been paid to the strength, stability, and rigidity of the structural elements and connections to be able to fulfill the tasks expected from them during the entire life of the structure under a certain safety. In addition, the TS 648 "Calculation and Construction Rules for Steel Structures" standard published in 1980 about steel structures in Turkey has lost its currency against the developments in the world in the calculation methods and materials field and its applicability has almost come to an end. As a result of the experiences and researches obtained after the 1999 earthquake, it was decided that the regulations should be changed. Therefore, it made more sense to rely on a strong regulation rather than developing the regulation and to comply with the Turkish Earthquake Regulation, the translation of the draft text of AISC 360-16 [19], which was arranged by the AISC "American Institute of Steel Construction" organization in

the USA, regarding steel structures has been developed. The new regulation called "Specification for Design, Calculation, and Construction of Steel Structures", which takes into account the Design Principles According to the Carrying Capacity Principles entered into force in 2016. In this study, the dimensioning of the steel structure elements was made by using the load combinations including the earthquake effect in the Load and Resistance Factor Design (LRFD) method based on Section 5.3 of SDCCSS.

1.3.2 Previous Studies

Liu and Astaneh-Asl (2000) conducted researches to determine whether simple connections used in beam-column joints of gravity frames together with floor slab additives can show lateral resistance against seismic loads. In this study, eight full-scale two series cyclic tests were conducted on floor slabs and shear connections to determine the strength, rigidity, and ductility of shear connections under cyclic loading. The authors mentioned that when positive results are obtained, shear connections can be used more actively in reinforcing damaged steel frames and in new constructions with slabs [20].

The first of the two series of tests, Series A, consists of designs based on current practice, while the second Series B is for the improvement of existing details and performance of past standard details according to the experimental results of the first series. For the test specimens to be subjected to cyclic testing, a test setup was generated in a way that both lateral load and gravity loads can be applied and by using the boundary conditions that will be closest to the theoretical structures. The lateral load was gradually increased until distortion occurred in the specimens due to inter-story drifts, or typically to the limit of 0.15 radians. Gravity loads were determined as 25% of live loads according to ATC-33 philosophy. As a result of the cyclic tests performed, it was observed that the pin connections in the bare steel specimens without slab for two different specimens had approximately 15% and 20% of the plastic moment capacity (M_P) of the beam and also was behaved very ductile by making a maximum -0.14 rad rotation until the collapse moment. Then the floor slabs were added to the specimens and the tests were repeated and the shear tab connection was obtained as approximately 30% and 45% of the beam plastic moment capacity. As it can be seen in Figure 1.7, composite motions lost their effects with the formation of

local out-of-plane deformations and cracks at approximately 0.04 rad rotation and behaved like bare shear tab connections [20].

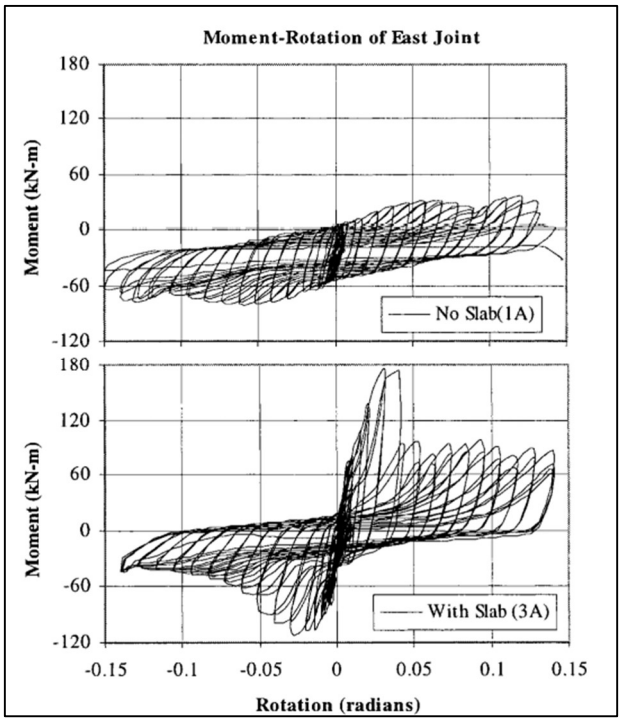


Figure 1.7: Comparison of moment versus rotation response for specimens with and without slab.

This study demonstrated that the simple connections used in gravity frames have significant moment capacities both by themselves and with floor slabs and are an important position for seismic performance evaluation of steel-framed buildings [20].

Liu and Astaneh-Asl (2004), in another study they conducted, investigated the moment-rotation capacities of these connections under cyclic tests, as they provided lateral stability to the structures by moving composite together with the floor slab and prevent them from collapsing during the 1994 Northridge Earthquake [15].

In the tests, a total of 13 specimens were examined considering various situations such as the number of bolts, being connected to the column web (weak axis), is connected to the column flange (strong axis), with and without floor slabs, with and without additional slab reinforcement. Unlike the typical shear tab connection details, some of these specimens were designed and tested according to pre-1980s shear tab connection details. The connections are subjected to lateral loading by gradually increasing them until they fail or make interstory of 0.15 rad according to the SAC-1997 protocol. The inclusion of floor slabs in typical shear tab connections has been

found to increase the maximum positive bending moment capacities of the connections from 15-20% of the plastic moment capacity of the beam to 30-60% levels. When this ratio was examined for pre-1980s shear tabs, it was found that the plastic moment value increased from 26% to 36% as most of the deformations occurred in the beam web and bolt holes rather than connections. Figure 1.8 is used to create moment-rotation models of shear tab connections with and without slab [15].

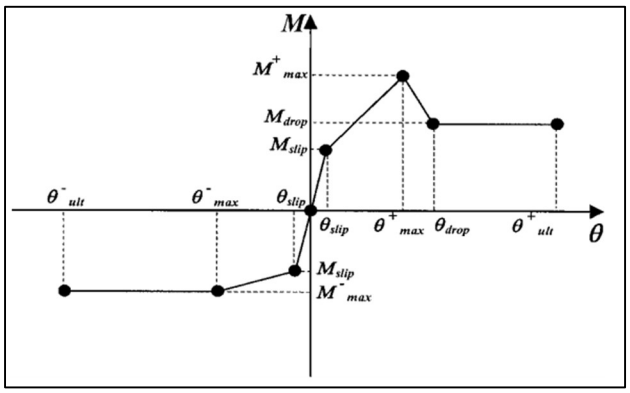


Figure 1.8: Moment-rotation model.

The backbone curves of the typical shear tab connections showed that the slip moment and initial rotational stiffness were related to the maximum positive moment. At the same time, these curves showed that the slip moment is typically equal to 25% of the maximum positive moment. For typical bare steel connections, the slip moment was observed at 50-60% of the maximum positive moment. As a result, it was concluded that the shear tab connections, that make the composite motion with the slab, contribute to the lateral load resistance to to an extent that cannot be ignored [15].

Wen, Akbas, and Shen (2013) studied the moment-rotation relationship of shear tab connections in steel structures. In this study, it was assumed that shear tab connections move composite together with the concrete slab to provide strength reserve capacity and structural redundancy. The cyclic responses were examined by performing physical tests on the shear tab connections. Then, finite element models and a non-ductile concentrically braced frame structural model with gravity frame with and without floor slab was created and these situations were compared [21].

In the test results, when the gravity beams make approximately 0.10 rad rotation, the moment capacity of bare steel shear tab connections is approximately 20-30% of the plastic moment capacity of the beams, while it was found that the shear tab

connections showing composite effects with the floor slab approximately doubled the moment capacity until the slab crushed over 0.04 rad rotation. The behavior of the shear tab connected models with and without concrete slab effects were examined and it was observed that while the non-included connection models have the same moment-rotation behavior under positive and negative moments, non-symmetrical behaviors occur under positive and negative moments in the models in which the slabs are included. The unsymmetrical multi-linear model for composite steel shear tab connections in which concrete slabs are included is shown in Figure 1.9.a). The normal stress distributions for yield moment and ultimate moment in the positive direction including composite slab effects are given in Figure 1.9.b) and Figure 1.9.c) [21].

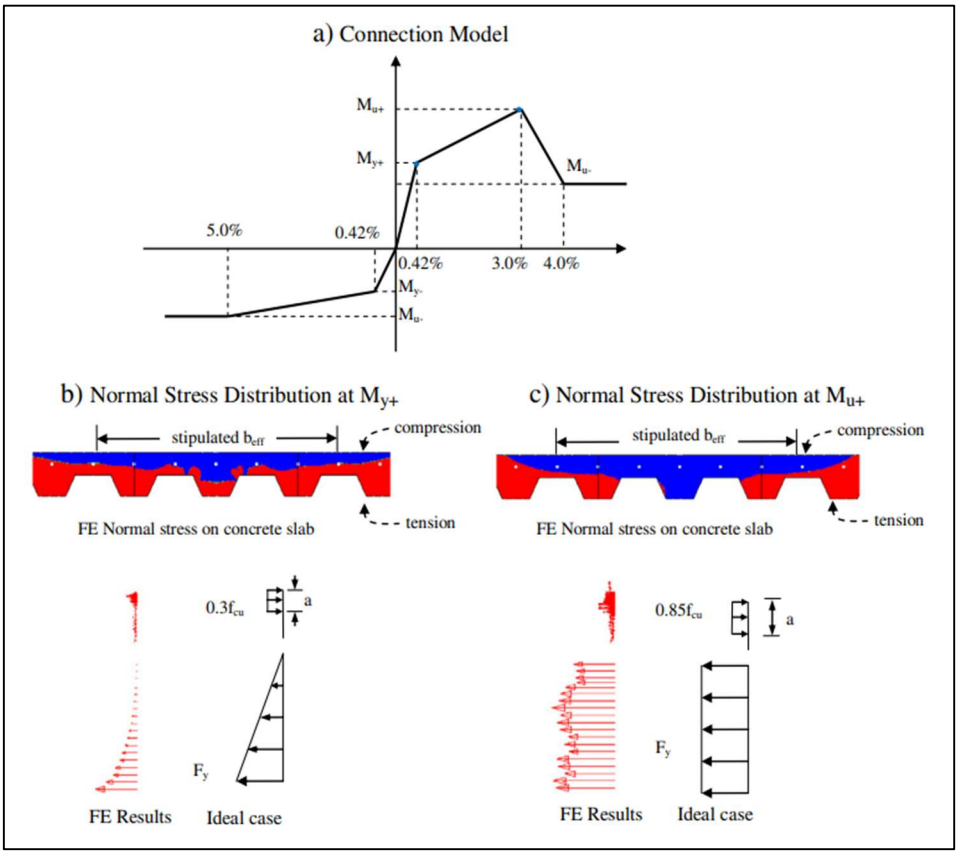


Figure 1.9: Moment-rotation model of GF with composite slab.

According to the results obtained by the authors, it has been observed that steel shear connections have significant flexural strength and ductility in large lateral drifts and gravity frames using these connections increases the seismic performance and stability of non-ductile CBFs and delay collapse [21].

Flores, Finley, Charney, and Lopez-Garcia (2014) investigated the effect of special moment frames of gravity frames on collapse performance. For this purpose, the authors studied on the contribution of beam-column connections to the stiffness and strength of gravity frames, the location of splices in gravity columns, and the inelastic deformation capacities of gravity columns. The sample prototype 2, 4, and 8-story buildings used in this study were taken from the ATC 76-1 project, which uses the FEMA P-695 methodology to evaluate the probability of SMF systems collapse and was designed according to ASCE / SEI 7-05 requirements. By incorporating gravity systems into these models, the buildings have been re-analyzed and compared with their original state [22].

Nonlinear links were used to obtain the cyclic behavior of the partially restrained (PR) connections used in the beam-column connections of gravity frames, and the hysteretic behavior in ASCE 41-13 was used for dynamic analysis (Figure 1.10) [22]. The minimum strengths required to prevent PR connections from reaching 0.005 rad rotation under gravity loads are determined as 0, 35, 50, 70%.

In the incremental dynamic analysis (IDA) performed by subjecting 44 different far-field to ground motion, it is accepted that the stability is disrupted when the elastic slope of the IDA curve is less than or equal to 20% or when the global drift reaches 0.1. The collapse margin ratio (CMR) was examined to see the contribution of gravity frames in the analysis results.

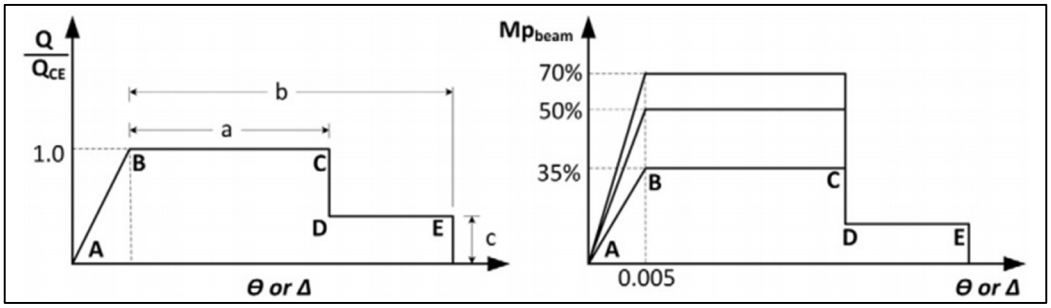


Figure 1.10: Moment-rotation characterization curve.

In the analysis results, it was observed that the CMR increased from 2.15 to 2.80 when the capacity of the connections in the two-story structure was designed to be 70% of the plastic bending moment capacity of the beams. In the four-story building, when designed according to 0% and 35%, CMR increased by 8% and 45%, respectively. Finally, for an eight-story building, when the strength of the PR

connection is 0%, the CMR increases from 1.48 to 1.85, and the collapse probability increases from 8.51% to 2.93.

In this study, it was concluded that PR connections increased overstrength and CMR, especially in low-rise structures, due to their strength, and also gravity frames with these connections are included in the system increase the collapse capacity compared according to FEMA P-695 [22].

In the study conducted by Zorlu (2018), the contribution of gravity frames to the seismic performance of special moment resisting frames were examined on low-rise and medium-rise buildings [23].

In this research, the case where gravity frames are not included in the system (Case A), the case where the semi-rigid connections are formed by considering 10% of the rotational stiffness of the composite slabs and 20% of the plastic moment capacity of the gravity beams (Case B) and finally, 3 models, including the case in which gravity frames are included in the system (Case C), have been examined. After the design of shear connections with link elements in Case B and Case C models, the fundamental period which was 1.14 s for the 4-story structure in Case A decreased to 1.12 s and 1.09 s in Case B and C, respectively. Likewise, building periods for the 9-story buildings were obtained as 2.44 s, 2.40 s, and 2.33 s for Case A, B, and C, respectively. For the beam-column connections in the moment frame, the nonlinear behavior model in ASCE 41-13 is used.

Finally, incremental dynamic analysis is applied to all models and maximum drift ratios, top displacements, base shears, and hinges corresponding to the scale factor are graphed. While the 4-story building reached the 4.7% design drift ratio calculated as a result of the analysis at 1.15g, the 9-story building reached at 0.75g. It was concluded that the responses of Case B where composite slab effects and Case C, where both the slab effects and the contribution of gravity frames to the performance are taken into account, are 7% and 15% higher than the bare moment frames, respectively. As a result of this study, it was concluded that gravity frames improve the general performance of steel structures, especially if they are taken into account together with composite slabs [23].

Seker (2019) investigated the contributions of lateral strength and stiffness to the seismic performance of special moment frames from gravity systems formed by simple connections in the nonlinear time domain, using the incremental dynamic analysis method (dynamic pushover analysis) and it is intended to prove that the

statement that gravity systems can be ignored in FEMA P-695, Section 1.2.4 for the collapse performance examined according to the methodology of P-695 is not correct [24].

Within the scope of the article, two models were studied, including and without gravity frames in the buildings designed as 6-story office buildings. As shown in Figure 1.11, the pinned joints in gravity frames are modeled with zero-length nonlinear links of infinite rigidity, while the moment-rotation relationship proposed by Wen et al. has been used for beam-column joints in the moment frame [24]. Considering the building periods after modeling, it was seen that the models including gravity systems decreased 4% thanks to the lateral stiffness contribution.

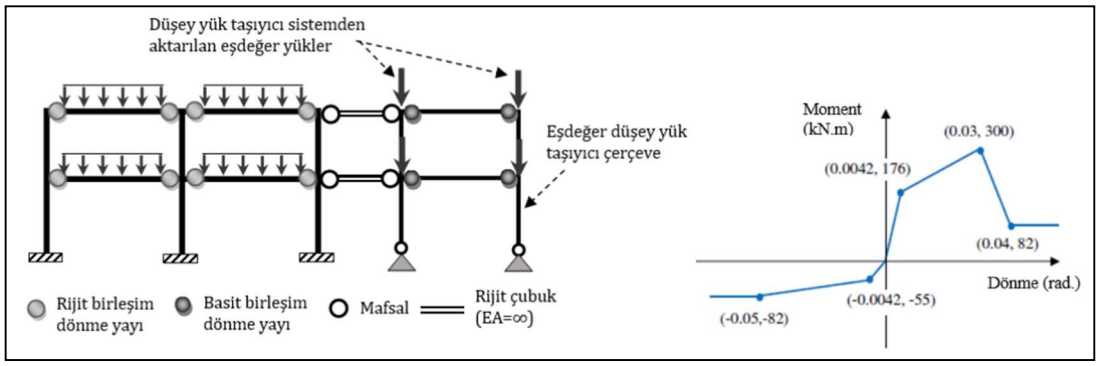


Figure 1.11: Numerical model and moment-rotation relationship for gravity beam-column connections.

In nonlinear incremental dynamic pushover analyzes applied to models with 20 earthquake recording compatible with the target spectrum, by increasing the spectral acceleration (S_{ae} (T_1)) corresponding to the natural vibration period of the structure in the elastic response spectrum of the selected earthquake acceleration record until the structures reach the drift angle of 0.10 rad, the structure has reached the collapse state. For the performance evaluation, fragility curves were created according to the relationship between the spectral acceleration value corresponding to the predominant vibration period of the models and the probability of collapse limit state.

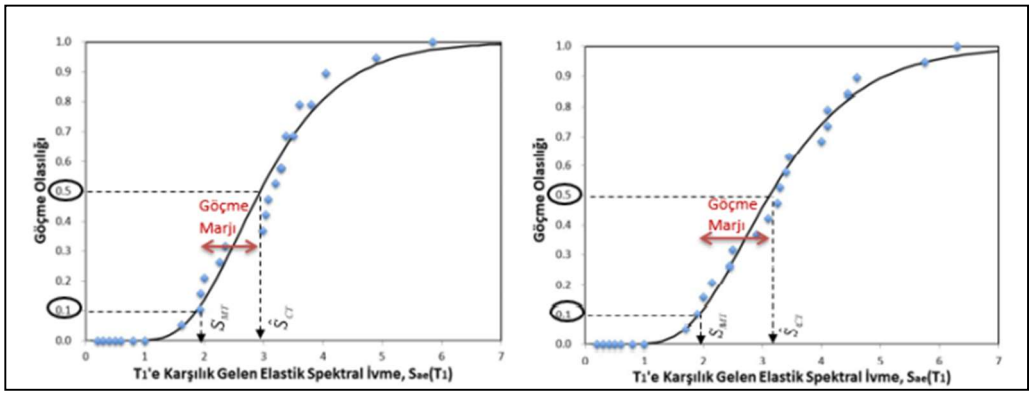


Figure 1.12: Fragility curves: a) For the moment frame only, b) For the moment frame with gravity frames.

According to ATC 63, adjusted collapse margin ratios (ACMR) were calculated using 10% and 50% collapse probabilities (Figure 1.12) and obtained as 1.877 for the bare moment frame and 1.993 for the moment frame with the gravity frame is included [24]. To compare ACMR, the probability of collapse has been obtained as 1.90 after the necessary assumptions. As a result of these assumptions, the bare moment frame ACMR value remained below the probability of collapse, that is, it could not meet the performance criterion and remained on the insecure side. However, the ACMR value of the gravity frame moment frame remained above 1.90. meeting the performance criterion. In other words, the moment frame with gravity frame has a higher collapse capacity than the bare moment frame. In this case, it is concluded that the uncertainties arising from the capacity-based design rules specified in the P-695 methodology reduce the capacity reserve and increase the risk of collapse [24].

2. STRUCTURAL MODELS

Typical low-rise (5-story) and medium-rise (10-story) steel structures are shown in Figure 2.1 and Figure 2.3 are designed following the design requirements of TBEC-2018 and AISC 360-2010 provisions. LRFSs of these structures consist of SMF and SCBF. The base plans of the two buildings with 5 and 10 floors are symmetrical to each other. In both of them, there are 5 spans with a length of 9.0 m in the direction of the moment frame and 4 spans with a length of 9.0 m in the direction of the braced frame. As seen in Figure 2.1 and Figure 2.2, the 5-story building has 36.0 m x 45.0 m plan dimensions and each floor height is 4.0 m. While all the columns in the moment frame are fixed to the foundation at ground level, the simple connection is used for the gravity frame columns.

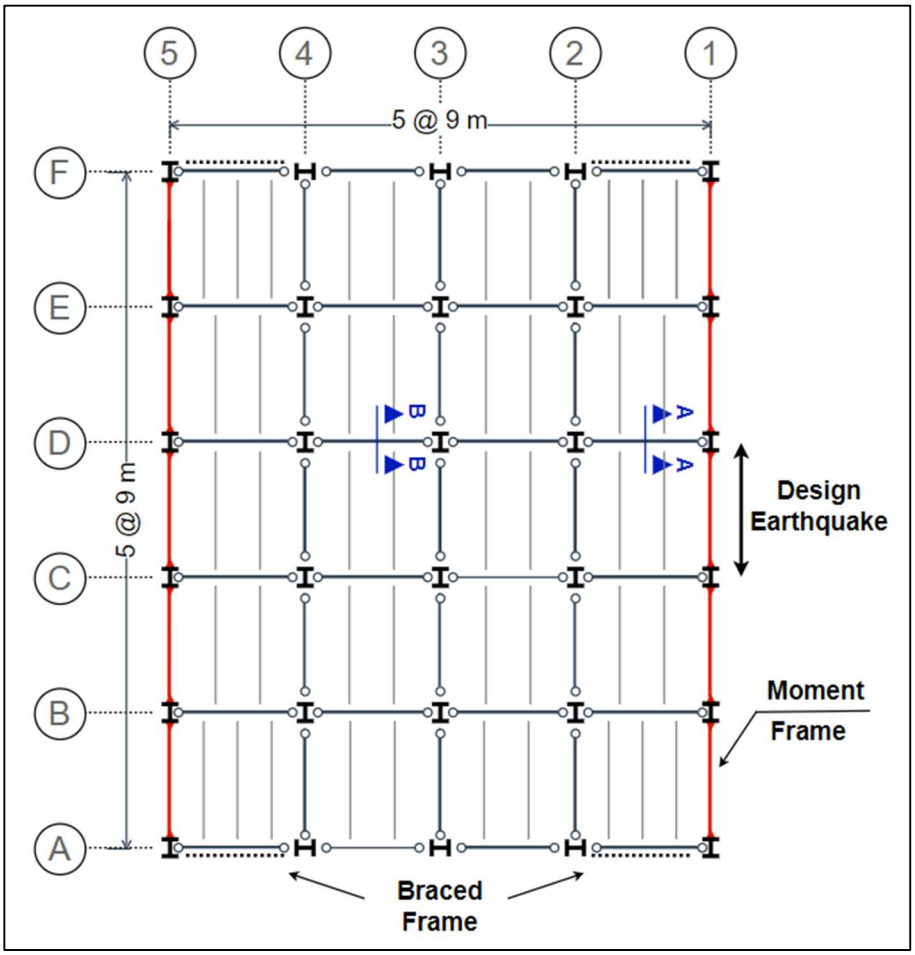


Figure 2.1: 5-story frame plan view.

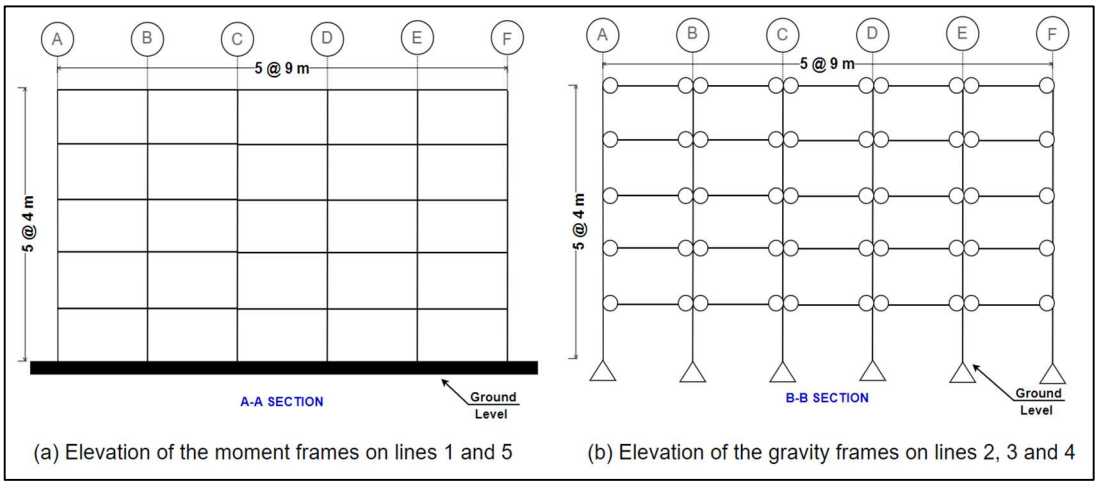


Figure 2.2: 5-story elevations.

Similarly, as seen in Figure 2.3, the plan dimensions of the ten-story building is 45.0 m by 36.0 m with 5.0 m x 9.0 m spans and 4.0 m x 9.0 m spans in two perpendicular directions, respectively. In the 10-story building, there is an additional 3.60 m height basement floor. Also, the normal floors have a height of 4.0 m as in the 5-story building, while the ground level has a height of 5.40 m. This structure is kept at ground level in x and y directions, and horizontal displacement of the basement walls is prevented. The columns are connected with the pin to the foundation at the basement level.

While the 5-story building has a long span in the north direction, the 10-story building has a long span designed from the moment frame to the east and the earthquake forces have been taken into account in the moment frame directions.

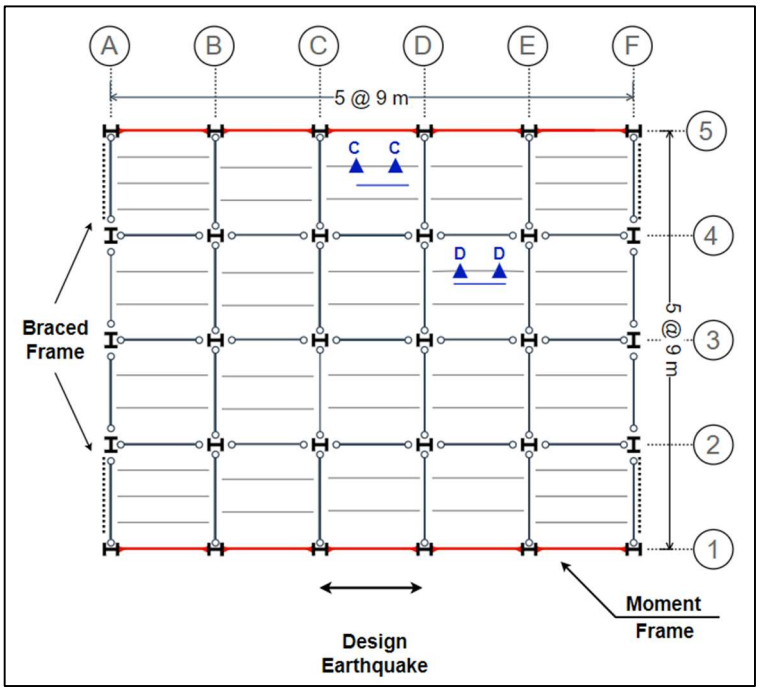


Figure 2.3: 10-story frame plan view.

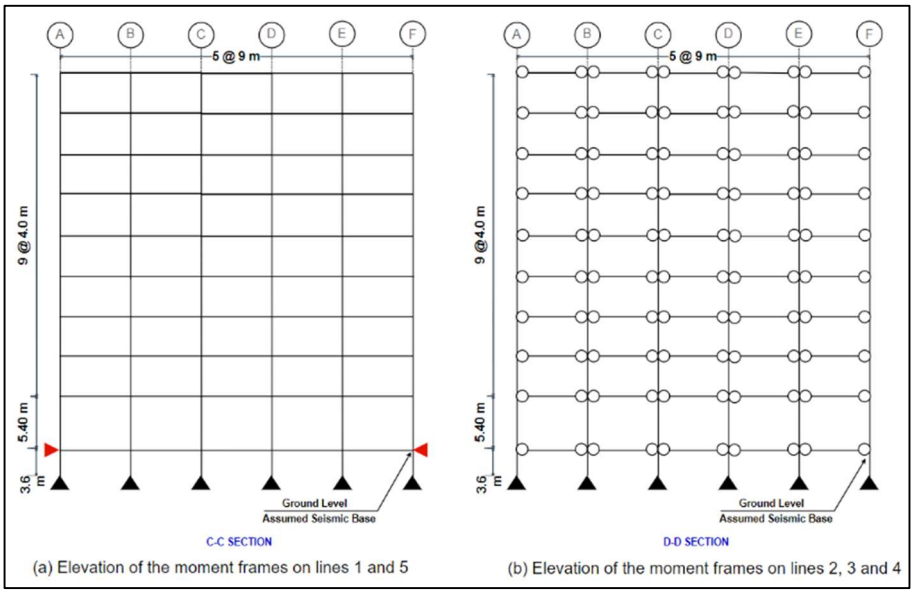


Figure 2.4: 10-story frame elevations.

As can be seen in Figure 2.2 and Figure 2.24 there are GFs that are pinned connection to other elements on the inner parts of both 5-story and 10-story structures and assume the task of carrying only gravity load. The structural system is designed from perimeter SMRFs and seismic lateral loads are met by two SMRFs in this perimeter, while internal GFs are not designed to resist lateral loads caused by seismic motions.

3. DESIGN REQUIREMENTS

3.1 Load Analyses

3.1.1 Dead Loads and Live Loads

Table 3.1: Dead loads.

Component	Floor	Roof
80 mm Light Concrete	0.20 kN/m^2/cm	0.20 kN/m^2/cm
38 mm Metal Deck	0.10 kN/m^2	0.10 kN/m^2
Steel Load-Bearing System (Self Weight)	0.90 kN/m^2	0.30 kN/m^2
Roofing / Insulation / Elevator Equipment	-	0.10 kN/m^2
Partition Walls	0.75 kN/m^2	-
Mechanical / Electrical Components	0.30 kN/m^2	0.30 kN/m^2
Flooring	0.50 kN/m^2	-
Suspended Ceiling	0.10 kN/m^2	0.10 kN/m^2
Fireproofing	0.10 kN/m^2	0.05 kN/m^2
Sprinkler	0.05 kN/m^2	0.05 kN/m^2
Total	**4.40 kN/m^2**	**3.00 kN/m^2**

Live loads were determined according to the "Uniformly Distributed Vertical Live Loads" chart in Turkish Standard-498 (TS-498) [18], Section 12.1. According to this chart, normal floors are 2.0 kN/m^2 while the penthouse is 1.50 kN/m^2.

3.1.2 Earthquake Loads

It is assumed that both buildings are located in Ataköy, Istanbul, on the seashore, in a location with high seismicity. The seismic data of these structures designed according to standard design earthquake ground motion level (DD-2) where the 10% probability of exceeding in 50 years, corresponding to a return period of 475 years and the local soil type of 'ZC', have been accessed from the Interactive Web Application of Turkey Earthquake Hazard Maps [25].

Table 3.2: Site-specific information.

Parameter	Site Specific Value	Reference
Mapped MCE_R spectral response acceleration parameter at short periods	S_S = 1.224 g	AFAD
Mapped MCE_R spectral response acceleration parameter at a period of 1 second	S_1 = 0.333 g	AFAD
Short period site coefficient	F_S = 1.200	Table 2.1. TBEC (2018)
Long period site coefficient	F1 = 1.500	Table 2.1. TBEC (2018)
Long-period transition period	T_L = 6 s	Section 2.3.4.1. TBEC (2018)

The design spectral response acceleration parameter at short periods, S_{DS}, and the design spectral response acceleration parameter at a period of 1 sec., S_{D1} were determined using Eqs. (3.1).

$$S_{DS} = S_S * F_S$$
$$S_{D1} = S_1 * F_1 \quad (3.1)$$

According to these equations, S_{DS} and S_{D1} acceleration values were calculated as 1.469 and 0.500. respectively. Then the horizontal design spectrum corner periods T_A and T_B were determined using Eqs. (3.2).

$$T_A = 0.2 \frac{S_{D1}}{S_{DS}}$$
$$T_B = \frac{S_{D1}}{S_{DS}} \quad (3.2)$$

Following the regulation, T_A and T_B corner periods were obtained as 0.068 s and 0.340 s, respectively.

3.1.3 Design Spectrum

Elastic design spectrum function determined according to TBEC-2018 conditions is given in Figure 3.1.

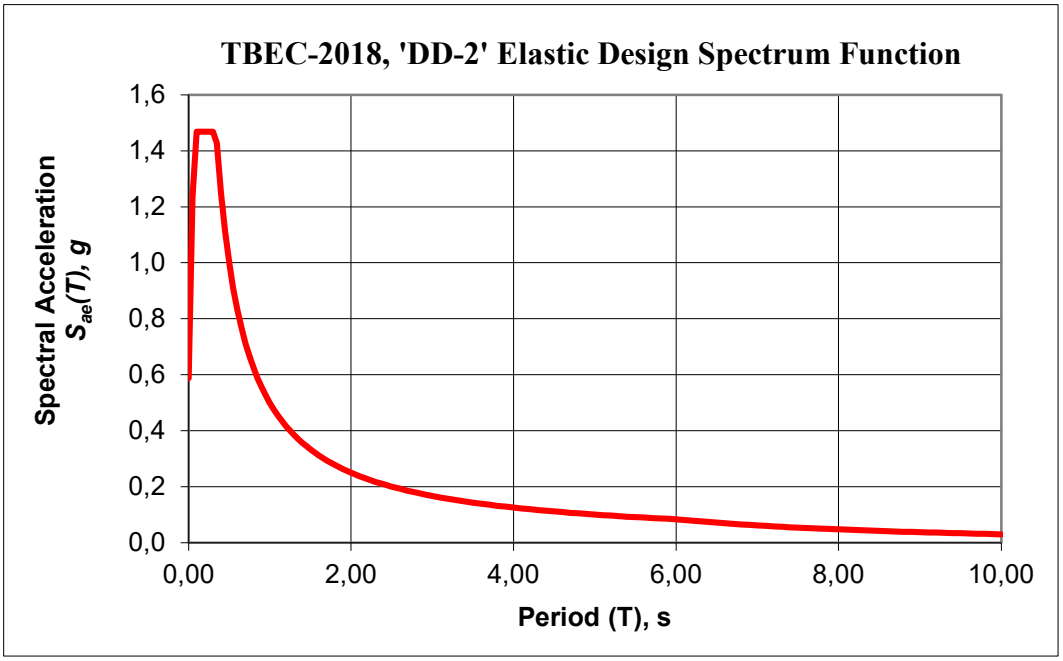


Figure 3.1: Elastic design spectrum function.

3.1.4 Structural Parameters

Table 3.3: Structural parameters for 5-story building.

Parameter	Coefficient	Reference
Seismic Force-Resisting System	SMF	
Building Height, h_n	20 m	
Response Modification Coefficient, R	8	Table 4.1, TBEC-2018
Overstrength Factor, Ω_0 (D)	3	Table 4.1, TBEC-2018
Building Height Class (BYS)	5	Table 3.3, TBEC-2018
Building Use Class (BKS)	3	Table 3.1, TBEC-2018
Building Importance Factor (I)	1.0	Table 3.1, TBEC-2018
Live Load Mass Participation Coefficient	0.3	Table 4.3, TBEC-2018
Earthquake Design Class (DTS)	1	Table 3.2, TBEC-2018
Permissible Height Class for Equivalent Seismic Load Method	BYS $\geq$ 4 ($H_N \leq$ 28 m)	Table 4.4, TBEC-2018

Table 3.4: Structural parameters.

Parameter	Coefficient	Reference
Seismic Force-Resisting System	SMF	
Building Height, h_n	41.4 m	
Response Modification Coefficient, R	8	Table 4.1, TBEC-2018
Overstrength Factor, Ω_0 (D)	3	Table 4.1, TBEC-2018
Building Height Class (BYS)	4	Table 3.3, TBEC-2018
Building Use Class (BKS)	3	Table 3.1, TBEC-2018
Building Importance Factor (I)	1.0	Table 3.1, TBEC-2018
Live Load Mass Participation Coefficient	0.3	Table 4.3, TBEC-2018
Earthquake Design Class (DTS)	1	Table 3.2, TBEC-2018
Permissible Height Class for Equivalent Seismic Load Method	BYS ≥ 4 (H_N ≤ 41.4 m)	Table 4.4, TBEC-2018

3.2 Special Moment Frame (SMF) Design

3.2.1 Seismic Base Shear

As a seismic calculation method, Modal Response Spectrum Analyses were used as a linear calculation method within the scope of design according to strength. It should be checked whether there is no irregularity in the plan and vertical in the building according to the regulation conditions. During the calculations, 5% additional eccentricity effects must be taken into account. In addition, the sufficient number of vibration modes in the modal analysis method, the base shear force calculated for each mode in the earthquake directions in Equation (4.30), TBEC-2018, must be determined so that the sum of the modal effective masses will not be less than 95% of the total building mass.

Considering these conditions, the total earthquake load (V_t) in the direction of the earthquake must be obtained according to the Modal Response Spectrum Method. Then, by calculating the total equivalent seismic load (base shear force) (V_{tE}) to be calculated according to the Equivalent Seismic Load Method, $V_t < \gamma_E V_{tE}$ control should be performed. If this condition specified in Section 4.8.4.1 of TBEC-2018 is not met, all reduced internal forces and displacement values obtained by the modal response spectrum analysis are equivalent base shear amplification coefficient β_{tE}

given in Equation (3.3) must be multiplied by. If there is no irregularity in the buildings, the alpha should be accepted as 0.80.

$$\beta_{tE} = \frac{\gamma_E \, V_{tE}}{V_t} \geq 1 \tag{3.3}$$

In direction of the earthquake considered, total equivalent seismic load (base shear force), V_{tE} is determined by Equation (3.4).

$$V_{tE} = m_t * S_{aR}(T_p) \geq 0.04 \, m_t \, I \, S_{DS} \, g \tag{3.4}$$

T_{pA}, which is the empirical fundamental natural period of vibration, will be calculated with Equation (3.5). The C_t parameter in this equation must be accepted as 0.08 for buildings consisting of steel frames. H_N is represented the building height.

$$T_{pA} = C_t \, H_N^{3/4} \tag{3.5}$$

The greatest value of T_p to be taken into consideration in the earthquake calculation cannot be more than 1.4 times the T_{pA} period according to Equation (3.6).

$$Max\,(T_p) = 1.4 \, T_{pA} \tag{3.6}$$

Horizontal elastic design spectral accelerations $S_{ae}\,(T)$, which are the ordinates of the horizontal elastic design acceleration spectrum, are defined in Equation (3.7) in terms of gravitational acceleration [g] depending on the natural vibration period.

$$\begin{aligned} S_{ae}\,(T) &= \left(0.4 + 0.6\,\frac{T}{T_A}\right) S_{DS} && (0 \leq T \leq T_A) \\ S_{ae}\,(T) &= S_{DS} && (T_A \leq T \leq T_B) \\ S_{ae}\,(T) &= \frac{S_{D1}}{T} && (T_B \leq T \leq T_L) \\ S_{ae}\,(T) &= \frac{S_{D1}\,T_L}{T^2} && (T_L \leq T) \end{aligned} \tag{3.7}$$

The earthquake load reduction coefficient $R_a\ (T)$, which will be taken as basis in reducing linear elastic earthquake loads, will be calculated according to the equations given in Eqs. (3.8.a) and (3.8.b).

$$R_a\ (T) = \frac{R}{I} \qquad (T > T_B) \qquad (3.8.a)$$

$$R_a\ (T) = D + \left(\frac{R}{I} - D\right) \frac{T}{T_B} \qquad (T \leq T_B) \qquad (3.8.b)$$

The reduced design spectral acceleration $S_{aR}(T_p)$ has given in Equation (3.4) will be calculated according to Equation (3.9).

$$S_{aR}(T_p) = \frac{S_{ae}(T)}{R_a(T)} \qquad (3.9)$$

Finally, the total mass of the buildings will be determined to calculate the equivalent seismic load. According to TBEC-2018 regulation, while all dead loads will be taken into account, 30% of live loads will be taken into account.

Then the total equivalent seismic load mentioned in Equation (3.4) above is calculated and it is checked whether the base shear force amplification factor is included in the calculations. All calculations related to this section are given in Appendix B1 for the 5-story building and Appendix D1 for the 10-story building.

3.2.2 Numerical Model

In the buildings, the outer perimeter frames consist of SMRF and SCBFs in perpendicular directions to each other as a seismic force-resisting system, while the inner parts consist of gravity frames. Full penetration welding was used for beam-column connections. Beam-columns in the moment frame were designed as rigid, while gravity frames were modeled with pin connections. Panel zone deformations were neglected. The columns were connected to the ground with fixed support. The floors were defined as composite concrete slab using C30 quality concrete and S355 quality structural steel materials, and all floors were designed as an infinite rigid

diaphragm within their planes. The deck ribs were placed parallel to the girder in the weak axis.

Linear analysis was made per the LRFD conditions specified in the SDCCSS. In normal floors, the dead loads, excluding the element weights, were applied to the building as 4.4 kN/m^2, the live loads as 2.0 kN/m^2 and likewise in the roof floors, the dead loads, excluding the element weights, were applied to building as 3.0 kN/m^2, the live loads as 1.5 kN/m^2. In the modeling of the building, structural steel quality rectangular hollow sections with a yield strength of 275 Mpa were used for the brace members, while European wide-head sections (HD, HE, IPE) with 355 Mpa quality were used for all remaining structural elements. Elasticity modulus was taken as 200.000 Mpa. All used sections have consisted of high ductility level, compact, and not slender elements.

In the dimensioning of the numerical model, load combinations are given in TBEC-2018, Section 9.2.5.1 will be used as load combinations including earthquake effects. The basic load combinations for strength design to be used for seismic design of moment and braced frames are as follows:

- $1.4\ G$
- $1.2\ G + 1.6\ Q + 0.5\ Q_r$
- $1.2\ G + 1.6\ Q_r + 1.0\ Q$
- $1.2\ G + +0.5\ Q + E_d^{(H)} + 0.3\ E_d^{(Z)}$
- $0.9\ G + E_d^{(H)} - 0.3\ E_d^{(Z)}$
- $1.2\ G + 0.5\ Q + \Omega_0\ E_d^{(H)} + 0.3\ E_d^{(Z)}$
- $0.9\ G + \Omega_0\ E_d^{(H)} - 0.3\ E_d^{(Z)}$

Ω_0 represents the overstrength coefficient (D). While this parameter is 3 for SMRFs, it takes the value 2 for SCBFs.

While $E_d^{(H)}$ represents the horizontal earthquake effect based on the design, $E_d^{(Z)}$ represents the vertical earthquake effect. The vertical earthquake effect is calculated with Equation (3.10).

$$E_d^{(Z)} \cong \left({}^{2}/_{3}\right) S_{DS}\ G \tag{3.10}$$

In this case, the combinations given above will be taken into account by arranging them as follows.

- $(1.2 + 0.2\,S_{DS})G + 0.5\,Q + E_d^{(H)}$
- $(0.9 - 0.2\,S_{DS})G + E_d^{(H)}$
- $(1.2 + 0.2\,S_{DS})G + 0.5\,Q + D\,E_d^{(H)}$
- $(0.9 - 0.2\,S_{DS})\,G + D\,E_d^{(H)}$

3.2.3 Story Drift Requirement

According to the limitations in Section 4.9.1 of the TBEC-2018 regulation, the story drift boundary condition of the buildings will be checked. According to the formula given in Equation (3.11) for flexible coupling detail or standalone of wall situation according to the regulation, all story drifts should be below the limit given for all floors.

$$\lambda \frac{\delta_{i,max}}{h_i} \leq 0.016\,\kappa \tag{3.11}$$

The κ parameter in this equation is accepted as 0.5 for steel structures. The λ coefficient, as expressed in Equation (3.12), is the ratio of the elastic spectral acceleration coefficient corresponding to the fundamental period for the DD-3 earthquake to the elastic spectral acceleration coefficient corresponding to the fundamental period for the DD-2 earthquake.

$$\lambda = \frac{S_{ae}^{DD3}(T_1)}{S_{ae}^{DD2}(T_1)} \tag{3.12}$$

δ_i is represented the effective story drift at the i'th floor and will be calculated with Equation (3.13). The expression Δ_i in this equation is represented the horizontal displacement difference between consecutive floors under the effect of reduced earthquake loads as stated in Eq (3.14).

$$\delta_i = \frac{R}{I} \Delta_i \tag{3.13}$$

$$\Delta_i = u_i - u_{i-1} \tag{3.14}$$

In the buildings, after pre-dimensioning, the story drift boundary condition will be checked whether met for all floors and the horizontal stiffness was sufficient.

As a result of the modal analysis made using sections that meet the story drift condition, it should be checked whether the first natural vibration period (T_1) of the structure is greater than the $1.4\,T_{pA}$ accepted at the beginning of the design. The acceleration value corresponding to the period obtained must be smaller than the acceleration value corresponding to $1.4\,T_{pA}$. If the condition is not met, the sections should be changed. Sections belonging to the pre-sizing and drift calculations are given in Appendix B2 for the 5-story building and Appendix D2 for the 10-story building.

3.2.4 Second Order Effects

Moment effects due to deformation are also taken into account in second-order effects. As a result of the additional moment effects that occur, the stiffness of the structure decreases, and the internal force values increase. Therefore, the Second Order Indicator Value $\theta_{II,i}$, included in Section 4.9.2 of the TBEC-2018 regulation must be calculated on each ith floor in the direction of the earthquake according to Equation (3.15).

$$\theta_{II,i} = \frac{(\Delta_i)_{ort} \sum_{k=i}^{N} w_k}{V_i\, h_i} \tag{3.15}$$

In case the maximum value of $\theta_{II,max}$ calculated for all floors satisfies the condition given in Equation (3.16), second-order effects are not required to be taken into account in the calculation of internal forces based on the design. C_h, parameter in the equation indicates a coefficient defined depending on the nonlinear hysteretic behavior of the carrier system and is taken as 1 in steel buildings.

$$\theta_{II,max} \leq 0.12 \frac{D}{C_h R} \tag{3.16}$$

In case the condition given in Equation (3.16) is not fulfilled, all internal forces for the earthquake direction are increased by multiplying the second-order amplification coefficient defined by Eq (3.17) by β_{II}.

$$\beta_{II} = 0.88 + \frac{C_h R}{D} \theta_{II,max} \geq 1 \tag{3.17}$$

Internal forces that arise due to the 2nd Order Effect must be checked whether need not to be taken into account at the building direction since the equation given in Equation (3.17). These checks are made in Appendix B3 for the 5-story building and Appendix D3 for the 10-story building.

3.2.5 Full Penetration Welded Joint

For column-beam connections in moment frames positioned in the direction of the earthquake and showing lateral resistance against earthquakes, 'Full Penetration Welded Joint' will be used. The connection detail given in Figure 3.2 will be designed according to the application limits stipulated in TBEC-2018, Annex 9B.4 [1].

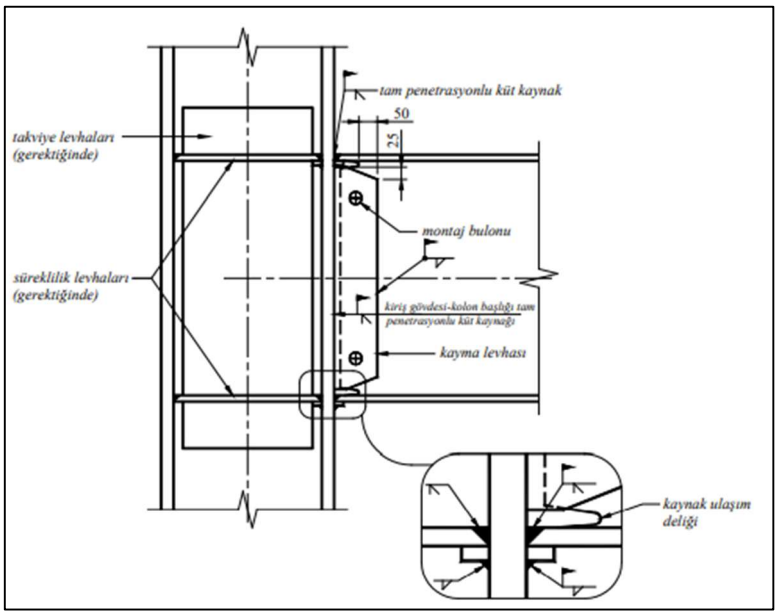


Figure 3.2: Full penetration welded connection detail.

The connection detail is capable of providing at least 0.04 radians or 0.02 radians story drift angle (story drift/story height). To use this connection, the conditions defined within the framework of the additional application limits given in Table 3.5 must be followed.

Table 3.5: Application limits of full penetration welded connection details.

Connection Detail Parameters	Application Limits
The distance of the plastic hinge from the column face	$l_h = 0$
Beam cross section height	≤ 920 mm
Beam span / cross section height ratio	≥ 7 (frames of high ductility level) ≥ 5 (frames of limited ductility level)
Beam flange thickness	≤ 25 mm
Column cross section height	≤ 920 mm (for I sections) ≤ 610 mm (for built-up sections)
Weld access hole	Required
Flange plate thickness	Full penetration weld
Capacity protected area	The region that includes the distance from the face of the column as much as the beam cross-section height

3.2.5.1 Probable Maximum Moment at Plastic Hinge

The probable maximum moment at the plastic hinge shall be:

$$M_{pr} = C_{pr} R_y F_{yb} W_{pb} \tag{3.18}$$

Where

R_y = ratio of the expected yield stress to the specified minimum yield stress,

F_{yb} = minimum yield strength of the beam

W_{pb} = plastic section modulus of the beam about the axis of bending, mm^3

C_{pr} = factor to account for peak connection strength, including strain hardening, local restraint, additional reinforcement, and other connected conditions.

In the calculation of the probable maximum moment at the plastic hinge, the C_{pr} value for welded connections is 1.4 as specified in TBEC-2018, Section 9B.4.3, R_y parameter will be taken as 1.25 for profiles made of S355 steel according to TBEC-2018, Table 9.2.

3.2.5.2 Required Shear Strength of The Connection

$$V_{uc} = V_d \mp (M_{pri} + M_{prj}) / l_n \tag{3.19}$$

Where

l_n = distance between plastic hinge locations, (mm)
V_d = beam shear force resulting from $1.2D + 0.5L + 0.2S$ combination, (N)
V_{uc} = required shear strength of beam and beam web-to-column connection, (N)

$$l_{n,left} = l - (2 * l_h + \left(\frac{d_{c,left}}{2} + \frac{d_{c,right}}{2}\right)) \tag{3.20.a}$$

$$l_{n,right} = l - (2 * l_h + \left(\frac{d_{c,left}}{2} + \frac{d_{c,right}}{2}\right)) \tag{3.21.b}$$

The distance of the plastic hinge from the column face, l_h, will be accepted as zero in full penetration welding application as stated in Table 3.5.

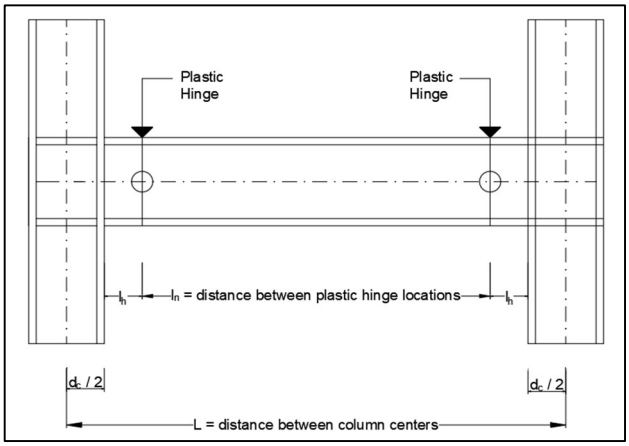


Figure 3.3: Shear force at the beam and web-to-column connection.

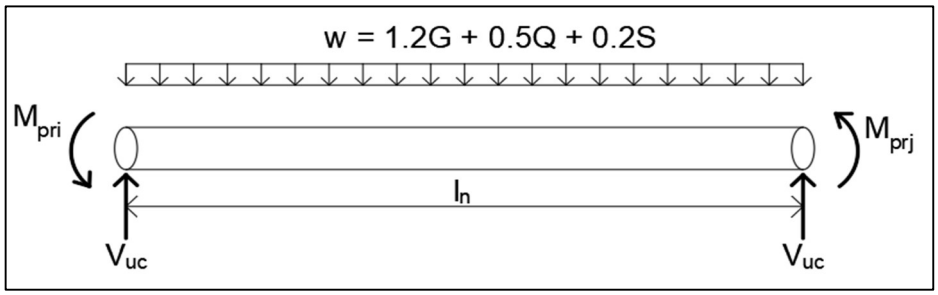


Figure 3.4: Computing the required shear strength.

3.2.6 Strong Column-Weak Beam Requirement

The strong-column/weak-beam (SC/WB) concept is a capacity-design approach intended to provide for frame columns strong enough to distribute frame (primarily beam) yielding over multiple stories. Columns at a beam-column joint must be stronger than beams. This principle is satisfied by taking the ratio of the sum of plastic moment capacities of columns at the joint, $\sum M_{pc}^{*}$ to the sum of plastic moment capacities of beams, $\sum M_{pb}^{*}$ at the intersection of the beam and column centerlines. SC/WB requirement for each beam-to-column connection will be checked according to Equation (3.22).

$$\frac{\sum M_{pc}^{*}}{\sum M_{pb}^{*}} > 1.0 \tag{3.22}$$

Where

$\sum M_{pc}^{*}$ = the sum of moments in the column above and below the joint at the intersection of the beam and column centerlines. $\sum M_{pc}^{*}$ is determined by summing the projections of the nominal flexural strengths of the columns above and below the joint to the beam centerline with a reduction for the axial force in the column. $\sum M_{pc}^{*}$ is based on the minimum specified yield stress of the column.

$$\sum M_{pc}^{*} = \sum W_{pc}\left(F_{yc} - \frac{P_{uc}}{A_g}\right) \tag{3.23}$$

$\sum M_{pb}^{*} =$ the sum of the moments in the beams at the intersection of the beam and column centerlines. $\sum M_{pb}^{*}$ is determined by summing the projections of the expected flexural strengths of the beams at the plastic hinge locations to the column centerline. $\sum M_{pb}^{*}$ is based on the expected yield stress of the beam and includes an allowance for strain hardening.

$$\sum M_{pb}^{*} = \sum (1.1\, R_y F_{yb} W_{pb} + M_{uv}) \tag{3.24}$$

A_g = cross-area of column, mm^2

F_{yb} = specified minimum yield stress of beam, MPa

F_{yc} = specified minimum yield stress of column, MPa

M_{uv} = additional moment due to shear amplification from the location of the plastic hinge to the column centerline ($= V_{uc} * \frac{d_c}{2}$), Nmm

P_{uc} = required axial compressive strength of the column, N.

W_{pc} = plastic section modulus of the column about the axis of bending, mm^3

W_{pb} = plastic section modulus of the beam about the axis of bending, mm^3

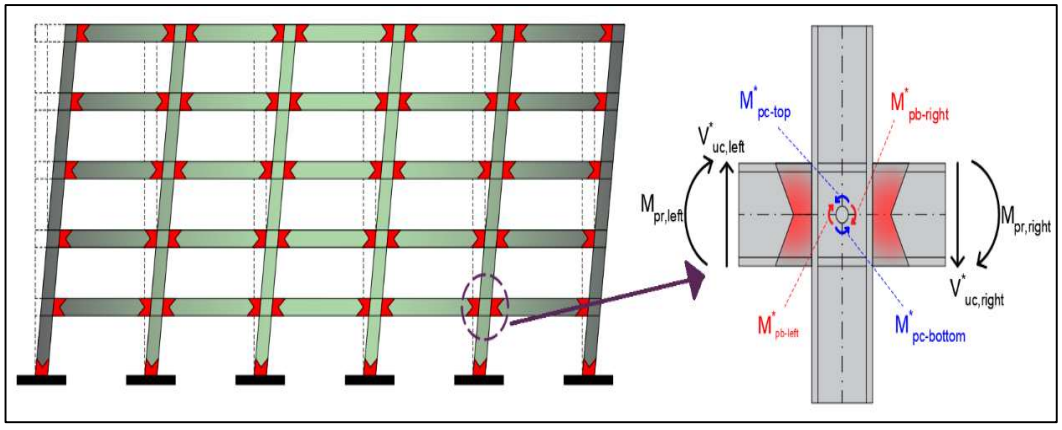


Figure 3.5: Shear and moment forces at the joint indicated by a circle.

While determining the required axial compressive strength, P_{uc}:

- The axial compressive force obtained from load combinations containing the earthquake effect;

$$(1.2 + 0.2\,S_{DS})G + 0.5\,Q + E_d^{(H)} + 0.2S$$

$$S_{DS} = 1.469 \;\rightarrow\; 1.469G + 0.5\,Q + E_d^{(H)} + 0.2S$$

- The greater of the axial compressive force obtained from the load combinations in which the overstrength is taken into account;

$$(1.2 + 0.2\,S_{DS})G + 0.5\,Q + D\,E_d^{(H)} + 0.2S$$

$$S_{DS} = 1.469 \;\rightarrow\; 1.469G + 0.5\,Q + D\,E_d^{(H)} + 0.2S$$

In the calculations, when overstrength is taken into consideration since the axial compressive strength values govern, the $1.469G + 0.5\,Q + 3\,E_d^{(H)} + 0.2S$ combination will be taken into consideration.

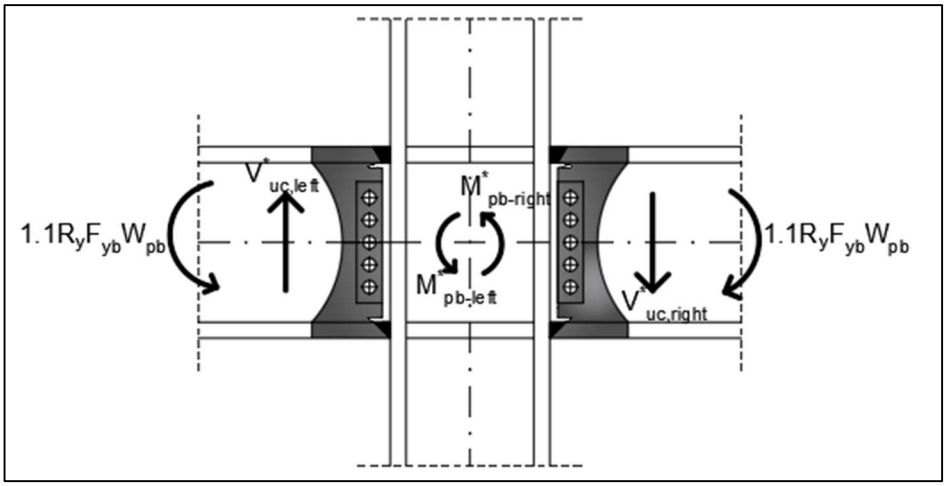


Figure 3.6: Sum of moments in beams.

According to the design requirements stated above, strong column-weak beam calculations are given in Appendix B4 for the 5-story building and Appendix D4 for the 10-story building.

3.2.7 Stability Analysis

All necessary calculations for the stability analysis described below are given in Appendix B5 for the 5-story building and Appendix D5 for the 10-story building.

3.2.7.1 Lateral Stiffnes Reduction

In the calculation according to the second-order theory with the direct analysis method, the stiffnesses of the elements will be reduced according to SDCCSS (2016), Section 6.2.3, to approximate the effect of nonlinear deformations on the stability analysis. The stiffnesses contributing to the stability of the structure will first be reduced by 20% by accepting the stiffness reduction coefficient $\tau_b = 1.0$. The axial rigidity will be taken '0.8EA' and flexural rigidity will be taken '0.8EI'. Then, this acceptance will be checked after obtaining the actual τ_b value determined according to the axial load level (Equation (3.25)).

It will be taken into consideration that if the axial load level is more than 50% of the yield strength (Equation (3.26)), the flexural rigidity must be reduced ($0.8\tau_b$EI) by multiplying it by the coefficient τ_b.

$$\frac{\alpha P_r}{P_{ns}} \leq 0.5 \rightarrow \tau_b = 1.0 \tag{3.25}$$

$$\frac{\alpha P_r}{P_{ns}} > 0.5 \rightarrow \tau_b = 4\left(\alpha \frac{P_r}{P_{ns}}\right)\left[1 - \left(\frac{\alpha P_r}{P_{ns}}\right)\right] \tag{3.26}$$

Where

P_{ns} = cross-section compressive strength ($F_y * A_g$)
P_r = required axial compressive strength
$\alpha = 1.0$ for LRFD

3.2.7.2 Notional Loads

There may be several geometric defects in the system manufacturing or the material. The column may have slipped out of its plumb line and this situation may affect stability, as shown in Figure 3.7. To take these effects into account, an imaginary horizontal load N_i is applied at each floor level. This applied load is called 'notional load'. And notional loads are only included in gravity load combinations. The incoming load is increased by 0.2% according to Equation (3.27).

$$N_i = 0.002\ \alpha\ Y_i \tag{3.27}$$

Where

N_i = horizontal load acting on the floor

Y_i = total vertical load acting on the floor at each floor level

$\alpha = 1.0$ for LRFD

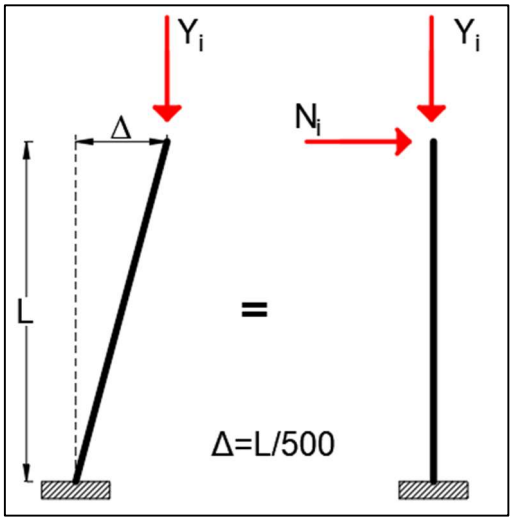


Figure 3.7: Notional load.

Gravity load combinations in which notional loads are included were given in Table 3.6.

Table 3.6: Load combinations including notional load effects.

Combination	Description
Comb#1	$1.4G \mp 1.4NG$
Comb#2	$1.2G + 1.6Q + 0.5Q_r \mp 1.2NG + 1.6NQ + 0.5NQ_r$
Comb#3	$1.2G + 1.6Q_r + 1.0Q \mp 1.2NG + 1.6NQ_r + 1.0NQ$
Comb#4	$(1.2 + 0.2\ S_{DS})\ G \mp 0.5\ Q + E_d^{(H)}$
Comb#5	$(0.9 - 0.2\ S_{DS})\ G \mp E_d^{(H)}$

According to SDCCSS (2016), Section 6.2.2.2, notional loads need not be included in load combinations containing horizontal loads, if the ratio of second-order displacements calculated using reduced stiffnesses to first-order displacements is equal to or less than 1.7.

3.2.7.3 Determination of Stiffness Reduction

Required compressive strengths P_r will be taken from the maximum axial force values at each floor obtained from the $(1.2 + 0.2\ S_{DS})G + 0.5\ Q + E$ combination.

If Equation (3.25) is provided for all columns, there is no need for an additional reduction coefficient in flexural stiffness. Thus, the assumption is correct. No need to introduce an additional factor for the flexural stiffness reduction. However, if this condition is not fulfilled, the reduction coefficient should be calculated as stated in Equation (3.26).

3.2.8 Strength Requirement

All necessary calculations for the strength requirement described below are given in Appendix B6 for the 5-story building and Appendix D6 for the 10-story building.

3.2.8.1 Design of Seismic SMRF Columns

Since the columns in the moment frame are subjected to bending moment and axial compressive force around their geometric axes, they are limited by the interaction curve shown in Figure 3.8.

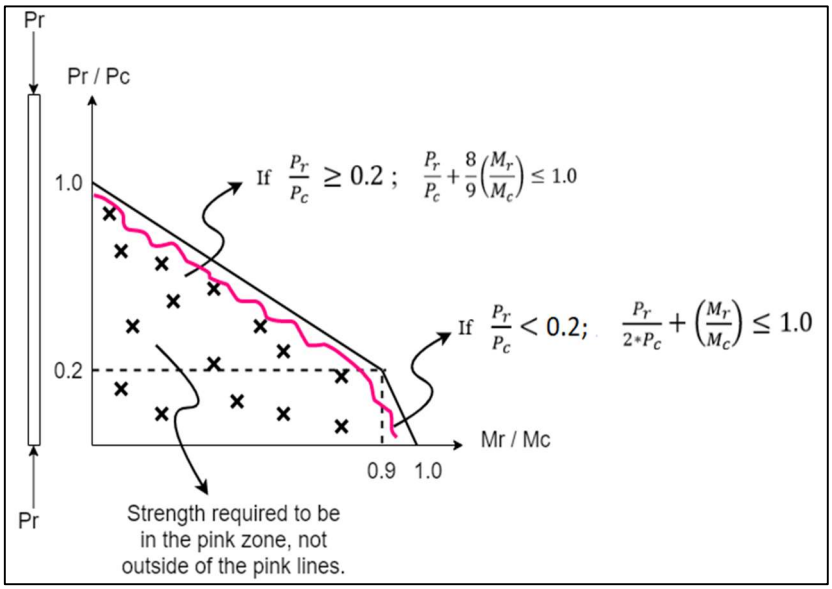


Figure 3.8: Axial force-moment interaction curve.

The ratio of the demand and capacities in the column elements should not exceed 1.0. that is, the capacity of the element should be sufficient to meet the coming forces. Calculations were made according to Equation (3.28.a) and (3.28.b).

$$If\ \frac{P_r}{P_c} \geq 0.2;\ \frac{P_r}{P_c} + \frac{8}{9}\left(\frac{M_r}{M_c}\right) \leq 1.0 \qquad (3.28.a)$$

$$If\ \frac{P_r}{P_c} < 0.2;\ \frac{P_r}{2P_c} + \left(\frac{M_{rx}}{M_{cx}} + \frac{M_{ry}}{M_{cy}}\right) \leq 1.0 \qquad (3.28.b)$$

Where

P_r = required axial strength using $(1.2 + 0.2S_{DS})G + E + 0.5Q + 0.2S$ load combinations (demand values).

P_c = design axial compressive strength (capacity values), $(= \emptyset_c P_n)$.

M_r = required flexural strength using $(1.2 + 0.2S_{DS})G + E + 0.5Q + 0.2S$ load comibnations (demand values).

M_c = design axial flexural strength (capacity values), $(= \emptyset_b M_n)$.

The size of the lengths L_b, L_p, and L_r should be checked for the calculation of the bending moment.

$$L_b \leq 0.086\, i_y \frac{E}{F_y} \tag{3.29}$$

$$L_p = 1.76\, i_y \sqrt{\frac{E}{F_y}} \tag{3.30}$$

$$L_r = 1.95\, i_{ts} \frac{E}{0.7F_y} \sqrt{\frac{J_c}{W_{ex}h_0} + \sqrt{(\frac{J_c}{W_{ex}h_0})^2 + 6.76(\frac{0.7F_y}{E})^2}} \tag{3.31}$$

Where

L_b= the element length between the points where lateral displacement and cross-section torsion in the compressive flange are prevented.
L_p= lateral unsupported boundary length for the yield boundary state.
L_r= limit length in non-elastic lateral-torsional buckling.

Since $L_b < L_p < L_r$, according to SDCCSS (2016), Section 9.2.2 (a), there is no need to consider the lateral-torsional buckling limit state. Therefore, characteristic bending moment strength for yield limit state will be calculated with Equation (3.32).

$$M_n = M_p = F_y W_{px} \tag{3.32}$$

However, in the case of $L_p < L_b < L_r$, inelastic lateral-torsional buckling may occur. In this case, the bending moment strength will be calculated with Equation (3.33).

$$M_n = C_b \left[M_p - \left(M_p - 0.7F_y W_{ex}\right)\left(\frac{L_b - L_p}{L_r - L_p}\right)\right] \leq M_p \tag{3.33}$$

In addition to the axial force-bending moment interaction, the columns must be inspected only under the axial load effect considering the overstrength earthquake effects ($(1.2 + 0.2S_{DS})G + 3E + 0.5Q + 0.2S$).

3.2.8.2 Design of Seismic SMRF Beams

Both flanges of beams should be laterally braced to satisfy the requirements for highly ductile members ($L_{b,max}$). According to Section 9.2.8.1a of TBEC-2018, lateral bracing of highly ductile beam members shall be calculated according to Equation (3.29).

The strength of the beam sections under shear force will be calculated according to Equation (3.34).

$$V_n = 0.6\, F_y\, A_w\, C_{v1} \tag{3.34}$$

In the case of $\frac{h}{t_w} \leq 2.24\sqrt{E/F_y}$, $\emptyset_v$ and C_{v1} parameters should be taken as 1.0.

Moment and shear force values that occurred in beams will be read from $(1.2 + 0.2S_{DS})G + E + 0.5Q + 0.2S$ combination.

3.2.8.3 Design of Non-Seismic GF Members

Since the columns in the gravity frames are only assigned to carry the gravity loads, their capacities under axial force should be checked according to the $(1.2G + 1.6Q_r)$ combination in the LRFD.

As with gravity columns, gravity beams carry only vertical loads. Therefore, the capacity calculation of the gravity beams should be made according to the $(1.2G + 1.6Q_r)$ combination.

According to AISC 360-10, Section L.3, the deflection value (L / 360) to be obtained according to the $(G + Q)$ combination in the gravity beams should not exceed the deflection limit.

3.2.9 Member Requirement

For members designated as highly ductile members, the width-to-thickness ratios of compression elements must not exceed the limiting width-to-thickness ratios, λ_{hd}, from Table 9.3, TBEC-2018.

The limiting width-to-thickness ratio is checked (Table 9.3- TBEC-2018):

$$\frac{b}{2t_f} < 0.30\sqrt{\frac{E}{F_y}} \tag{3.35}$$

$$\frac{h}{t_w} < \begin{cases} C_a \le 0.125\,;\, 2.45\sqrt{\dfrac{E}{F_y}}(1-0.93C_a) \\ C_a > 0.125\,;\, 0.77\sqrt{\dfrac{E}{F_y}}(2.93-C_a) \ge 1.49\sqrt{\dfrac{E}{F_y}} \end{cases} \tag{3.36}$$

$$C_a = \frac{P_u}{\emptyset_c(F_y A)} \tag{3.37}$$

- P_u, the value will be taken from the combination of $(1.2+0.2S_{DS})G + E + 0.5Q$ as the maximum axial force value in beams on each floor.

These checks are given in Appendix B7 for the 5-story building and Appendix D7 for the 10-story building.

3.3 Special Concentrically Braced Frame (SCBF) Design

3.3.1 Seismic Base Shear

As stated in Section 3.2.1 Modal Response Spectrum Analyses are also used for the direction of the braced frame of the buildings. According to this method, by calculating the total equivalent seismic load (base shear force) (V_{tE}) to be calculated according to the Equivalent Seismic Load Method, $V_t < \gamma_E V_{tE}$ control should be performed. If this condition specified in Section 4.8.4.1 of TBEC-2018 is not met, all reduced internal forces and displacement values obtained by the modal response spectrum analysis are equivalent base shear amplification coefficient β_{tE} given in Equation (3.3) must be multiplied by. All calculations related to this section are given in Appendix C1 for the 5-story building and Appendix E1 for the 10-story building.

3.3.2 Braces Design

At this stage, firstly, the dead load and live load areas on the braces must be determined. Since the axle spans of the 5 and 10 story buildings are the same, Figure 3.9 represents the load distribution for both models. Then, the forces (F_b) created by the dead and live loads on the braces in each floor according to the load areas should be calculated.

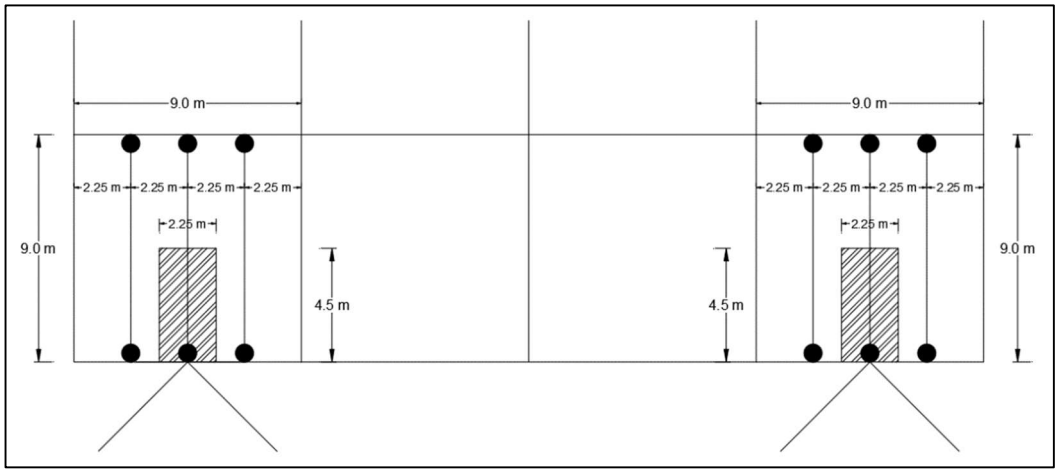


Figure 3.9: Load distribution.

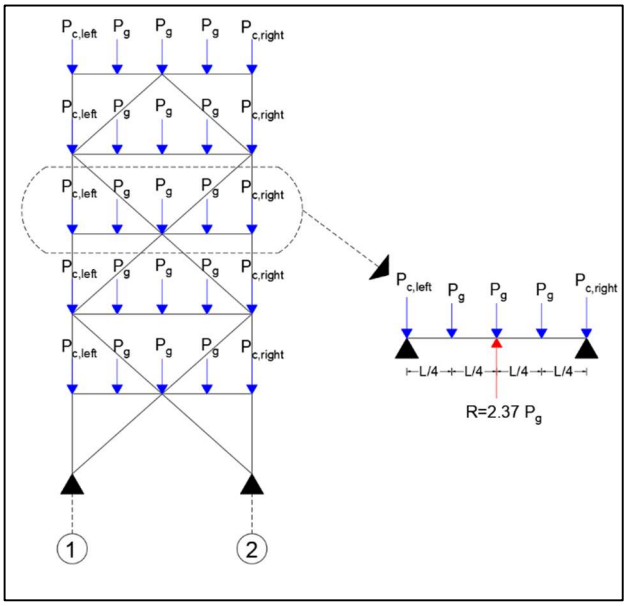


Figure 3.10: Point gravity loads.

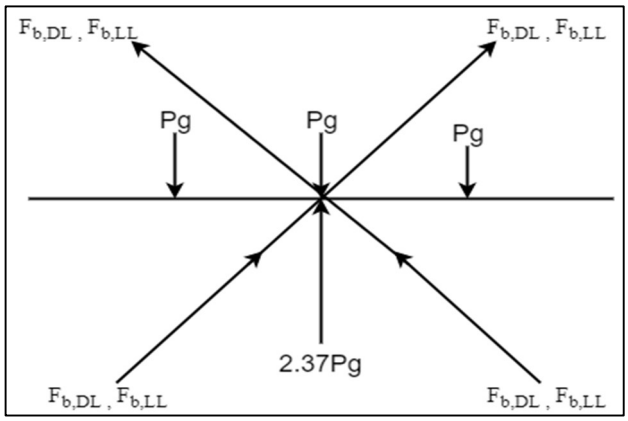


Figure 3.11: Forces caused by dead and live loads on the braces.

Then, the axial forces ($F_{b,QE}$) that the lateral seismic forces will create on the brace elements should be calculated.

After these forces are obtained, the axial force Demand (P_r) and capacity (P_c) values in the brace members should be compared. When calculating the axial force demand, the combination $(1.2 + 0.2S_{DS}) * F_{b,DL} + F_{b,QE} + F_{b,LL}$ should be taken as the basis and the demand value obtained should be divided by the number of brace members in the system.

For the capacity calculation, first of all, the width/thickness ratios for the brace members of the steel frames with highly ductility level should be checked. According to TBEC-2018, Table 9.3, the width/thickness limit state for the rectangular hollow sections with high ductility level is given in Eq (3.38).

$$\frac{b}{t} \leq \lambda_{hd} = 0.55\sqrt{\frac{E}{F_y}} \tag{3.38}$$

Also, slenderness ratios of all choosen brace members should be less than 200 according to TBEC-2018, Section 9.6.3.1:

$$\frac{L_c}{i} = \frac{KL_b}{i} \leq 200 \tag{3.39}$$

After determining the appropriate brace sections, the capacity calculation for these elements should be made in the order stated below and compared with the axial

force demand. If the selected brace sections do not meet the demand, the brace members must be replaced.

For obtaining the nominal compressive strength (P_n);

- $If\ \frac{\mathrm{L_c}}{\mathrm{i}} \leq\ 4.71\ *\sqrt{\frac{E}{F_y}}$;

Flexural buckling stress;

$$F_{cr} = \left(0.658^{\frac{F_y}{F_e}}\right) * F_y \tag{3.40}$$

Elastic buckling stress;

$$F_e = \frac{\pi^2 * E}{(\frac{k*L}{r})^2} \tag{3.41}$$

Characteristic axial compressive strength;

$$P_n = F_{cr} * A_g \tag{3.42}$$

The figuration of the axial forces that the lateral seismic forces will create on the brace elements and all calculations regarding the determination of brace sections are given in Appendix C2 for the 5-story building and Appendix E2 for the 10-story building.

3.3.3 Design of Beams in The Braced Bays

The first step in sizing the structural elements is to design the braces first in a CBF. Brace design is carried out by the lateral forces. Then, beams and columns are designed for the maximum forces imposed upon them by the braces. When the determining lateral seismic load effect capacity limits in the girders and columns, the following two structural analysis cases are required to be followed (Figure 3.12):

- Case I: A structural analysis in which all braces are assumed to resist forces corresponding to their expected strength in compression or tension,
- Case II: A structural analysis in which all braces in tension are assumed to resist forces corresponding to their expected strength and all braces in compression are assumed to resist their expected post-buckling strength.

The expected brace strength in tension, T_{ET}, expected brace strength in compression (or expected buckling strength), C_{EB}, and expected post-buckling brace strength, C_{EPB}, are given as;

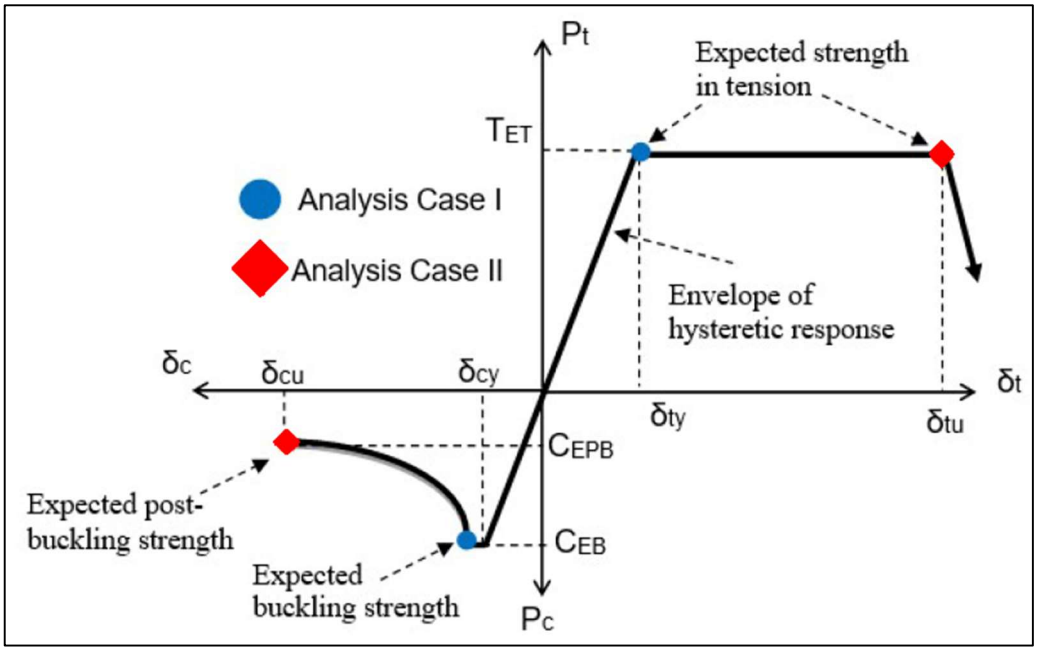


Figure 3.12: Illustration of T_{ET}, C_{EB} and C_{EPB} strengths to be used in the two structural analysis cases.

$$T_{ET} = R_y F_y A_g \tag{3.43}$$

$$C_{EB} = \min\{ R_y * F_y * A_g \; ; \; 1.14 * F_{cre} * A_g \} \tag{3.44}$$

$$C_{EPB} = 0.3 * C_{ET} \tag{3.45}$$

Where

T_{ET} = Expected tension strength

C_{EB} = Expected compression strength

C_{EPB} = Expected post-buckling strength

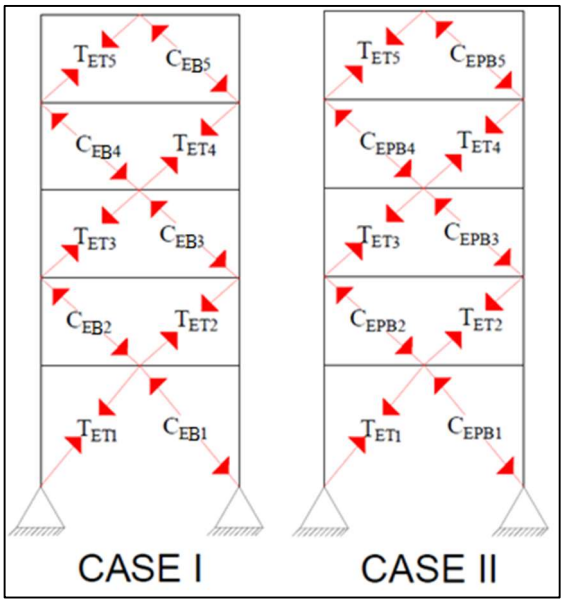


Figure 3.13: General view of cases.

Since Case II is governed in the design of beams, calculations have been made only for this case. To determine the applicable beam section to be used in the braced span, the brace section must be able to meet the bending moment demand. So, required flexural strength, M_r is obtained by reading the moment values of the beams in braced spans under $(1.2 + 0.2\,S_{DS})G + E + Q$ combination in the model created in the Etabs-2016. Then, a beam section will be selected according to the plastic strength moment value in the formula given in Equation (3.32) so that it is smaller than the M_r moment obtained. In addition, when selecting the cross-section, they must have high ductility and their flanges and webs must not exceed the limits.

The expected tensile and post-buckling strengths of the brace sections at each story and all calculations regarding the determination of the beam sections in the braced frame are given in Appendix C3 for the 5-story building and Appendix E3 for the 10-story building.

3.3.4 Design of Column

In the design of the columns, Case I govern. So, T_{ET}, C_{EB}, C_{EPB}, and seismic loads due to expected brace capacity acting on beams (F_u) will be calculated for all floors according to Case I. Afterwards, the building was cut from the right and left, and the moment at each floor level was taken and the axial force demand on the columns under the earthquake effect will be calculated.

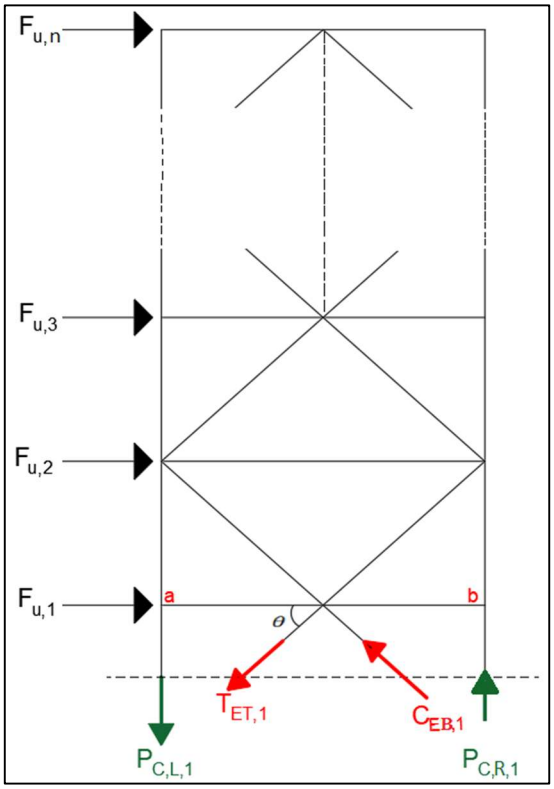


Figure 3.14: Tension and compression in 1st floor column as per Case I.

$$F_{u,n} = \left(\left(T_{ET,n} + C_{EB,n}\right) - \left(T_{ET,n+1} + C_{EB,n+1}\right)\right) * \sin(\theta)$$

3.3.4.1 Tension and Compression Forces That Occur In Columns

Afterward, the building was cut from the right and left, and the moment at each floor level was taken and the axial tension-compression force demand on the columns that will occur due to the earthquake forces effect will be determined.

For the 1st Floor:

$$Tension: P_{C,L,1} = \frac{\left[(F_{u,2}*h_2)+(F_{u,3}*h_3)+\cdots+(F_{u,n}*h_n)-(T_{ET,1}-C_{EB,1})*\sin(\theta)*\left(\frac{L}{2}\right)\right]}{L}$$

$$Compression: P_{C,R,1} = \frac{\left[(F_{u,2}*h_2)+(F_{u,3}*h_3)+\cdots+(F_{u,n}*h_n)+(T_{ET,1}-C_{EB,1})*\sin(\theta)*\left(\frac{L}{2}\right)\right]}{L}$$

- The formation of the tension force in the columns does not want. Therefore, this design should be made according to the compression force.

3.3.4.2 Calculation of Gravity Loads

First, the load areas of the columns and beam spans are determined as shown in Figure 3.15. Since the axis spans of both 5 and 10-story buildings in this study are the same, Figure 3.15 represents both structures. Then, vertical joint dead load and live loads that will affect determined load areas will be calculated. The total load acting on each floor is obtained by summing up cumulatively from top to bottom.

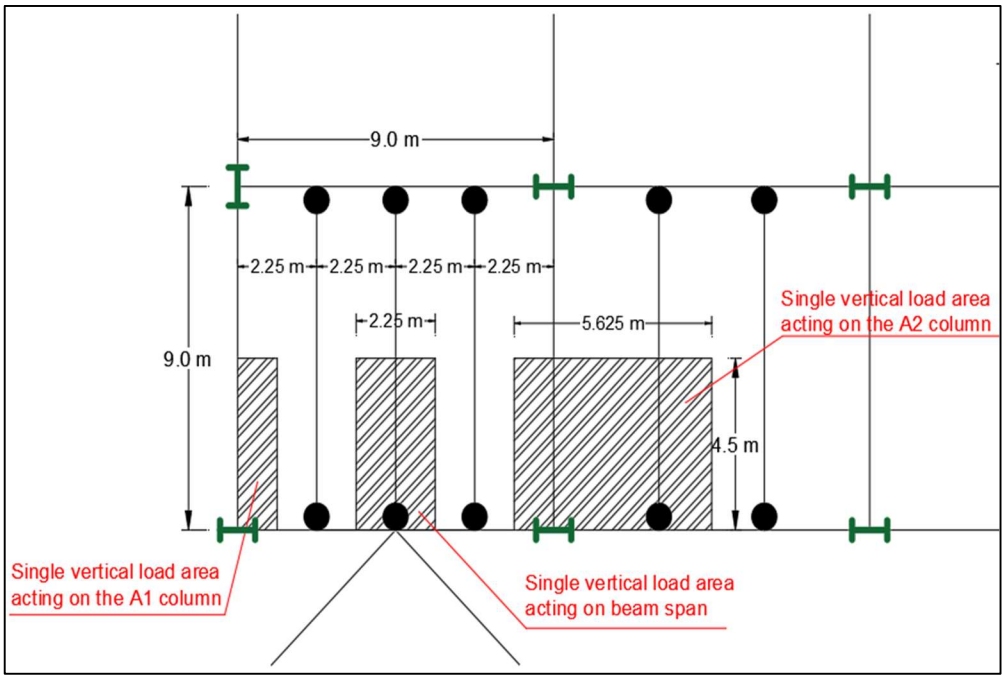


Figure 3.15: Load areas of SCBF columns.

3.3.4.3 Applicable Column Selection

To choose the applicable column section, the required axial strength demand that will occur in the columns should be calculated first. Compression design will be based. Axial forces caused by earthquakes and vertical loads will be superposed by the combination of $[(1.2 + 0.2S_{DS}) * P_G + P_{QE} + P_Q]$ to obtain the required axial strength (P_U).

Since there is no lateral support in the braced spans, the columns can be buckled in two directions. The axial force capacity of the columns (P_C) is calculated with Equation (3.42) and the conformity of the section should be checked by comparing it with the required axial force strength (P_U). Also buckling control must be made according to the boundary conditions for the flange and web parts of the column sections.

All the calculations made by following the guidelines mentioned above for the design of the columns in the braced frame and the figurations of the axial tension-compression forces that will occur due to the earthquake forces in the columns are given in Appendix C4 for the 5-story building and Appendix E4 for the 10-story building.

3.3.5 Story Drift Requirement

In the 5-story building, after pre-dimensioning, the story drift boundary condition must be met for all floors and the horizontal stiffness must be sufficient. The story drift in the direction of the braced frame should be calculated according to the rules mentioned in Section 3.2.3 and verified with boundary conditions. These checks are given in Appendix C5 for the 5-story building and Appendix E5 for the 10-story building.

4. NONLINEAR DYNAMIC TIME HISTORY ANALYSES

The structures behave within the generally accepted displacement, strain, and stress limits under operating loads, that is, they exhibit linear behavior. However, when the operational load limit of the structure is exceeded by external effects, as the deformation, displacement, and tension movements that occur in the system reach the end of the bearing capacity of the structure, they can take on values that are too large to be considered linear-elastic. In these cases, non-linear analyzes come into play with a performance-based seismic design approach, which takes into account the behavior beyond the linear elastic limit and enables numerical estimation of the damage to the structural elements subjected to earthquake loads. In this case, dynamic analysis methods in the time history performed by directly affecting the earthquake loads on the structure are the analyzes in which the behavior of the structure is obtained most accurately and realistically. With this method, it is aimed to check whether the structure can provide the expected performance level when the expected displacement occurs in the structure.

4.1 Nonlinear Models

The most basic feature of nonlinear dynamic analyzes is to consider the nonlinear behavior of the structural elements of the structures in the analyses. In this study, it is necessary to define the nonlinear behavior of the structural elements in the 5 and 10 story, structural models, to examine the contribution of MFs with together the GFs located in the interior to the seismic performance with the help of nonlinear analysis. Therefore, the existing structures were converted to nonlinear models using different connection properties and boundaries and then subjected to nonlinear dynamic time-history analyses.

The *'Reference Frame'*, the first of the nonlinear models, represents the typical analytical model in which the effects of gravity frames on lateral seismic resistance are not taken into account and are not included in the analysis. The conversion of the Reference Frame model to the nonlinear model is provided by the connections of the

moment frames in the structure. The non-linear behavior of the moment frame carrier system elements is represented by the plastic hinges defined at the endpoints of the rigidly connected elements. The properties of these plastic hinges are determined according to the cross-sectional effects and deformations that will occur in the structural elements. The properties of these plastic hinges are determined according to the deformations that will occur in the structural elements. While for beams the flexural hinges (M3) are defined by ignoring the axial load, the hinges (P-M2 or P-M3) for columns that take into account the interaction of axial load and bending moments should be defined according to the weak and strong axes. The plastification that will occur within the scope of nonlinear behavior is defined by nonlinear moment-curvature and interaction curves for beams and columns, which are revealed by various experiments and analyses.

The *'Set-1'* structure, which is another nonlinear model, represents the model in which 10% of the plastic rotational rigidity of gravity beams is taken into account in the connections of the moment frames and the gravity frames. While the nonlinear behavior is provided by plastic hinges in moment frames as mentioned above, in gravity frames, semi-rigid connections of the elements are achieved by using link elements. The multilinear moment-rotation relationship was used for link elements.

One of the last converted nonlinear models is the so-called *'Set-2'* model. In the Set-2 model, the structural elements have been resized so that gravity frames contribute 10% to the lateral load resistance system. In addition, considering the effects of a composite deck, link elements are modeled by using nonlinear models for the connections of gravity frames in nonlinear dynamic time-history analyses. Moment frames, on the other hand, as in other models, were provided nonlinear behavior by defining plastic hinges.

The aforementioned RF, Set-1, and Set-2 cases were modeled separately in 5-story and 10-story buildings. P-Delta effects were also taken into account when modeling all cases.

4.1.1 Nonlinear Modeling of Moment Frame Element Connections

The nonlinear behavior of columns and beams of moment-transferring frames is represented based on the lumped plasticity behavior approach. The plastification that will occur within the scope of nonlinear behavior is defined by nonlinear moment-curvature and interaction curves for beams and columns, which are revealed by various experiments and analyses.

Within the scope of this study, in determining the properties of plastic hinges to be formed in structural moment steel frame members, together with the a, b, c parameters and damage limitations defined in ASCE 41-13, Table 9.6, together with the performance limit states corresponding to the generalized load-strain curve for a ductile structural element shown in Figure 4.1 were used [12].

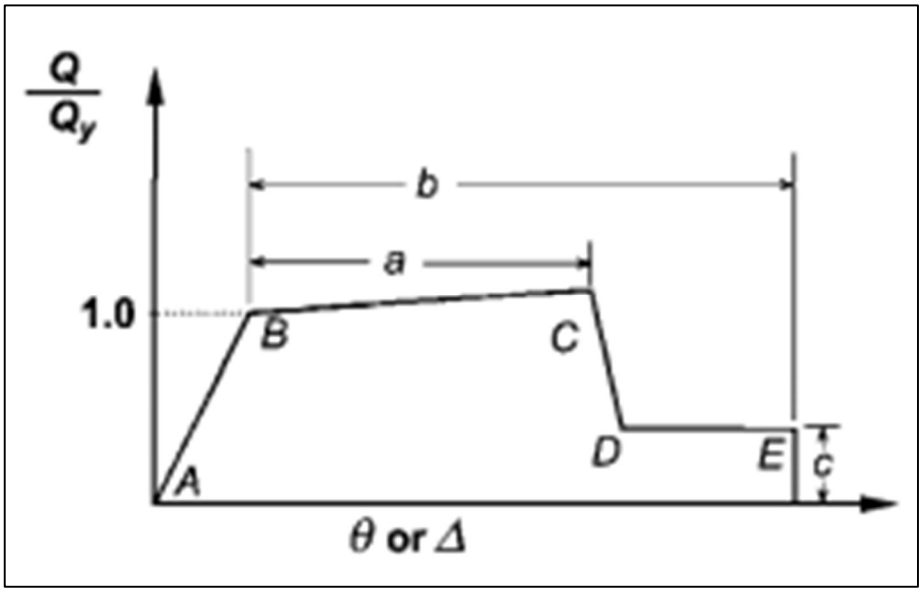


Figure 4.1: Generalized force-deformation relation for steel elements.

Parameters Q and Q_y in Figure 4.1 are generalized component strength and generalized component expected strength, respectively. For beams and columns, θ represents the total elastic and plastic rotation of the beam or column, while θ_y represents the rotation at yield. Δ is the total elastic and plastic displacement and Δ_y is the displacement at yield. The resistance at $\frac{Q}{Q_y} = 1.0$ is the yield value, and it appears that the load-deformation relationship adapts to the strain-hardening, while the element deforms to the expected strength with subsequent strain-hardening. The line AB shown

in the figure represents the linear response up to point B, which represents the effective yield point. The BC line represents the increase in strength due to strain hardening up to the strength of the C element. The residual strength at the CD line and point E indicates significant strength deterioration. However, within the scope of this study, the sudden drop from C to D shown in Figure 4.1 for the nonlinear behavior model of moment frames was not defined and ignored. Also, the parameters a and b shown in the figure represent the deformation portions that occur after yielding and plastic deformation, while parameter c shows the decreasing resistance after the sudden drop from C to D. The a, b, and c parameters are numerically defined in Table 4.1 and 4.2 for columns and beams with high ductility level, respectively.

Table 4.1: Modeling parameters and acceptance criteria for nonlinear procedures of columns.

	Modeling Parameters			**Acceptance Criteria**		
Component or Action	**Plastic Rotation Angle, Radians**		**Residual Strength Ratio**	**Plastic Rotation Angle, Radians**		
Column (Flexure)	**a**	**b**	**c**	**IO**	**LS**	**CP**
$\frac{b_f}{2t_f} \leq \frac{52}{\sqrt{F_y}}$ and $\frac{h}{t_w} \leq \frac{300}{\sqrt{F_y}}$	$9\theta_y$	$11\theta_y$	0.6	$1\theta_y$	$9\theta_y$	$11\theta_y$

Table 4.2: Modeling parameters and acceptance criteria for nonlinear procedures of beams.

	Modeling Parameters			**Acceptance Criteria**		
Component or Action	**Plastic Rotation Angle, Radians**		**Residual Strength Ratio**	**Plastic Rotation Angle, Radians**		
Beam (Flexure)	**a**	**b**	**c**	**IO**	**LS**	**CP**
$\frac{b_f}{2t_f} \leq \frac{52}{\sqrt{F_y}}$ and $\frac{h}{t_w} \leq \frac{418}{\sqrt{F_y}}$	$9\theta_y$	$11\theta_y$	0.6	$1\theta_y$	$9\theta_y$	$11\theta_y$

In the regulations, acceptable damage limits and damage zones are defined per the predicted performance levels at different earthquake intensities for the damage to the structural elements of the structural system. In the codes, the damage limits of the structural elements are examined under two headings as high ductility level and limited

ductility level. Performance levels for damage zones, on the other hand, are defined as immediate occupancy (IO), life safety (LS), and collapse prevention (CP) as specified in rotation-based limit states Table 4.1 and Table 4.2 in ASCE 41-13 [12]. Immediate occupancy (IO) represents the limited damage performance level, that is, the damage level where limited damage occurs in the load-bearing system elements of the building and the linear behavior is limited. LS represents the controlled damage performance level, that is, the level of damage that can be repaired in building elements to ensure life safety. Finally, CP is the performance level that represents the pre-collapse situation in which severe damage occurs in the structure.

The non-linear behavior of the moment frame elements of the RF, Set-1, and Set-2 models, which were sized and designed following the design requirements of SDCCSS-2016 and TBEC-2018 regulations, was modeled using ETABS [3] computer software. The plastic hinge details described above for the moment frame members of the structures are shown in Figure 4.2 and Figure 4.3.

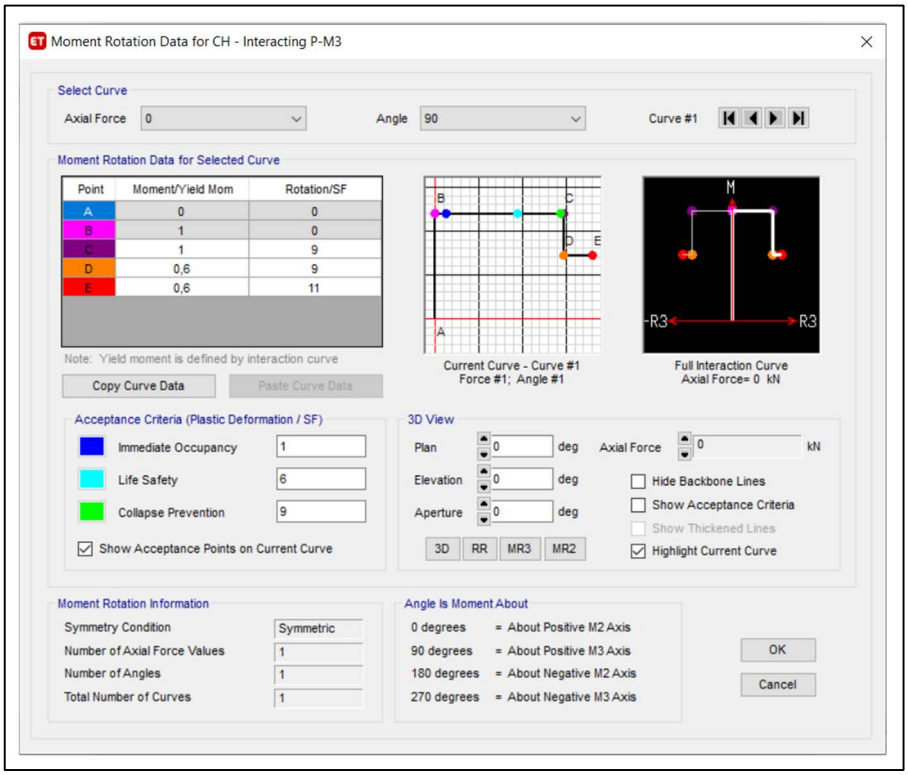


Figure 4.2: Moment frame column plastic hinge definition.

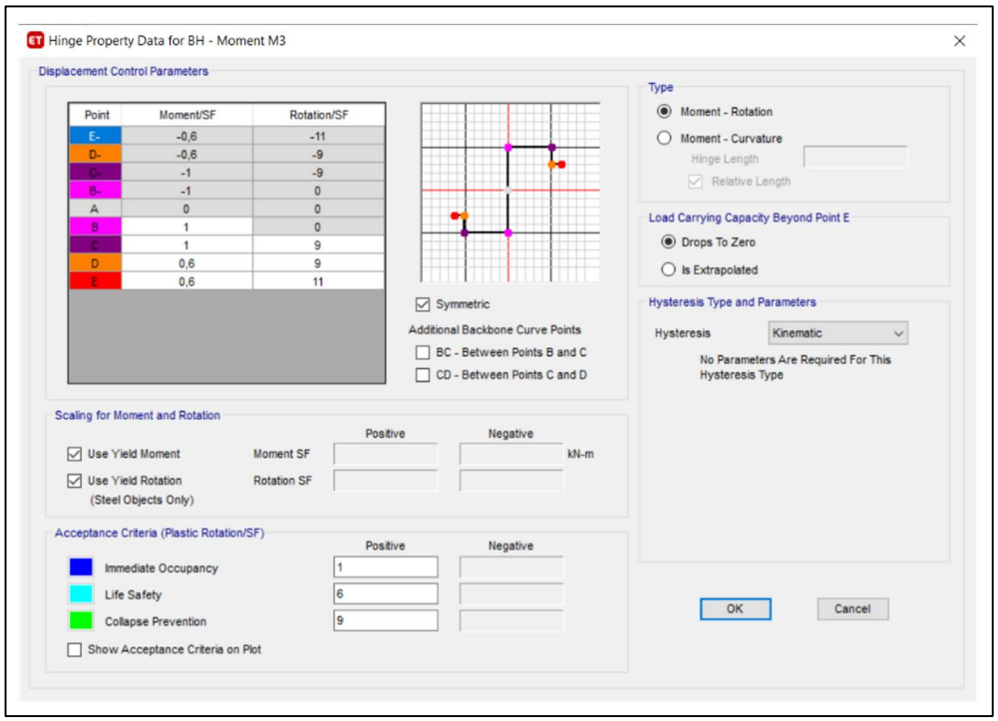


Figure 4.3: Moment frame beam plastic hinge definition.

According to TBEC-2019, Table 9B.3, it is predicted that the plastic hinge will form on the column face as shown in Figure 4.4 for a full penetration welded connection. For this reason, the hinges in the moment frame beam elements are assigned at a distance of half the depth of the column elements to which the beams are attached. This distance is named $l_{b,h}$ as seen in the figure.

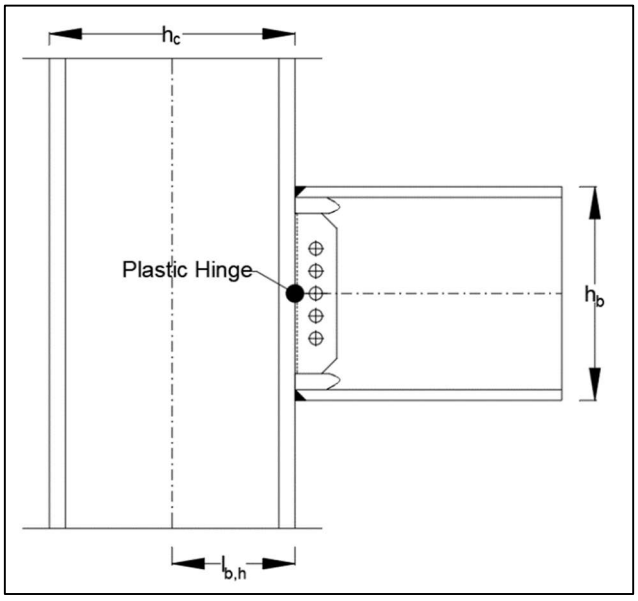


Figure 4.4: Beam hinges location.

The assignment of plastic hinges to moment frame beam-column elements of 5 and 10 story structures is shown in Figure 4.5.

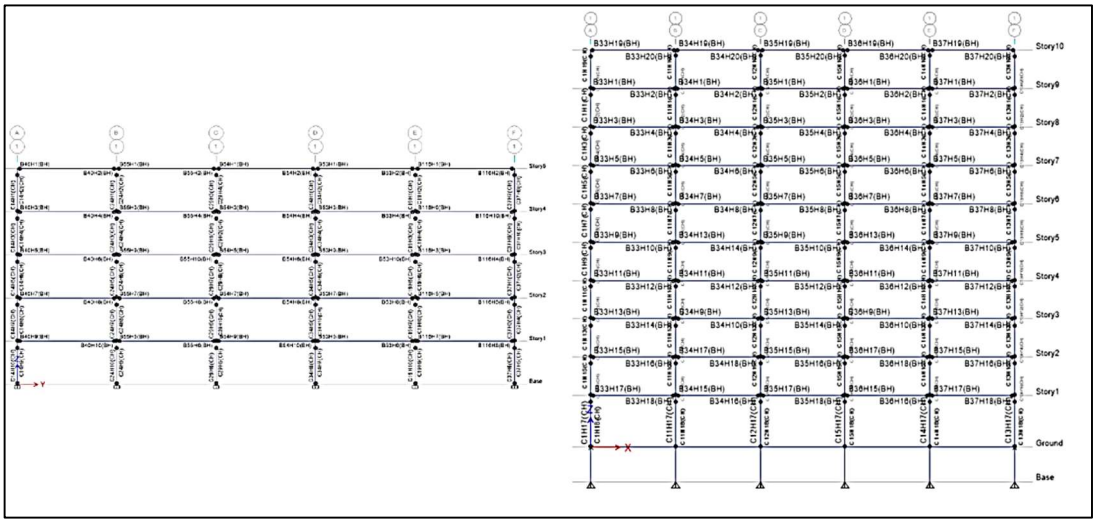


Figure 4.5: Assigning hinges to moment frame members.

4.1.2 Nonlinear Modeling of Gravity Frame Element Connections

In this study, semi-rigid connections were obtained by modeling multilinear plastic link elements for the connection of gravity beams to include gravity frames in the non-linear analysis in Set-1 and Set-2 structures.

In Set-1 models, semi-rigid connection models with 10% of the rotational rigidity ($\frac{4EI}{L}$) are idealized as the flexural strength of the gravity beams for link element connections.

In the Set-2 models of 5 and 10-story buildings, all the design requirements mentioned in Chapter 3 were repeated, and these structures were resized so that gravity frames could meet 10% of the total earthquake load that would come to the building. Since there are three gravity frames on the inside of the models, each frame carries 3.33% of the total earthquake load. A total base shear force was obtained 2448 kN in the 5-story Set-2 model. Gravity frames carry 10% of this base shear force, ie 244.8 kN. Since there are three gravity frames in total, each one is designed to withstand an earthquake load of 81.6 kN. Likewise, when this design approach is used for 10 stories, the total base shear force was 2740 kN, and each of the gravity frames can carry an earthquake load of 91.33 kN. Structural element sections belonging to these models

are given in Table 4.3. In addition, composite deck effects along with gravity frames were included in the analysis phase of Set-2 models.

Table 4.3: Sections of Set-2 models of 5 and 10 story buildings.

	Story	SMRFs_Columns		SMRFs_Beams	Gravity Frames_Columns		GFs_Beams
		Exterior	Interior		Exterior (Braced Bay)	Interior	
5-Story Building	5	HD 400 × 551	HD 400 × 509	HE 260 C	HE 450 B	HE 220 B	IPE O 400
	4	HD 400 × 551	HD 400 × 509	HE 500 A	HE 450 B	HE 220 B	IPE O 450
	3	HD 400 × 551	HD 400 × 509	HE 500 B	HE 450 B	HE 220 B	IPE O 450
	2	HD 400 × 551	HD 400 × 551	HE 550 B	HD 400 X 287	HE 600 B	IPE O 450
	1	HD 400 × 551	HD 400 × 551	HE 550 B	HD 400 X 287	HE 600 B	IPE O 450
10-Story Building	10	HD 400 × 216	HD 400 × 463	HE 500 A	HE 200 B	HE 240 C	IPE O 400
	9	HD 400 × 314	HD 400 × 463	HE 500 A	HE 240 B	HE 240 C	IPE O 450
	8	HD 400 × 314	HD 400 × 592	HE 550 A	HE 240 B	HE 260 C	IPE O 450
	7	HD 400 × 463	HD 400 × 592	HE 550 A	HD 320 × 198	HE 260 C	IPE O 450
	6	HD 400 × 463	HD 400 × 592	HE 550 B	HD 320 × 198	HE 260 C	IPE O 450
	5	HD 400 × 509	HD 400 × 677	HE 550 B	HD 400 × 347	HD 320 × 127	IPE O 450
	4	HD 400 × 509	HD 400 × 677	HE 550 B	HD 400 × 347	HD 320 × 127	IPE O 450
	3	HD 400 × 634	HD 400 × 677	HE 650 B	HD 400 × 382	HD 320 × 158	IPE O 450
	2	HD 400 × 634	HD 400 × 818	HE 650 B	HD 400 × 382	HD 400 × 237	IPE O 450
	1	HD 400 × 818	HD 400 × 818	HE 650 B	HD 400 × 592	HD 400 × 237	IPE O 450
	Basement	HD 400 × 818	HD 400 × 818	HE 500 A	HD 400 × 551	HD 400 × 237	IPE O 450

In this study, the analytical models suggested by Shen et al. [21] and Wen et. al [26], shown in Figure 4.6 and Figure 4.7, were used for the gravity beam-column connections in Set-1 and Set-2 models.

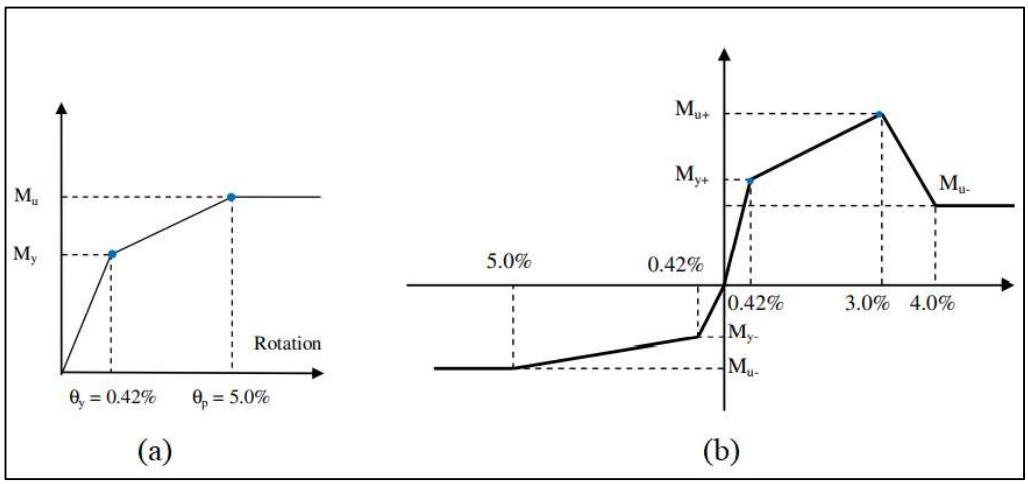
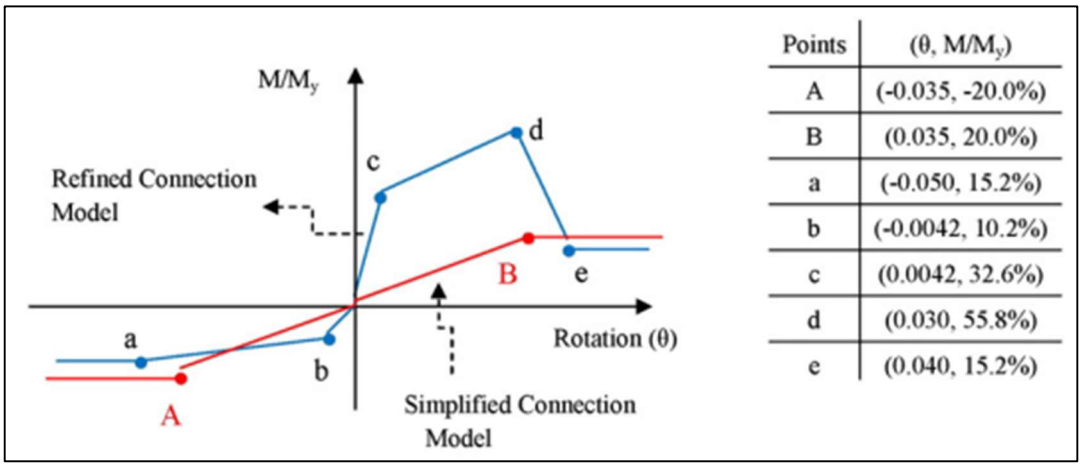


Figure 4.6: Connection models: a) Bare steel shear tab connection model, b) Composite steel shear tab connection model.



Points	(θ, M/My)
A	(-0.035, -20.0%)
B	(0.035, 20.0%)
a	(-0.050, 15.2%)
b	(-0.0042, 10.2%)
c	(0.0042, 32.6%)
d	(0.030, 55.8%)
e	(0.040, 15.2%)

Figure 4.7: Beam-to-column connection models in GFs.

The red line (A-B) in this behavior model represents the model in which the effects of the composite deck are not taken into account and only semi-rigid connections have 10% of the rotational stiffness of gravity beams. The line is shown in blue (a-e) shows the moment-rotation curvature that will be used in the design of gravity beam-column connections when composite deck effects are also taken into account. Also, it is seen that the simple shear connections modeled in the Set-1 structure underestimate the positive flexural strength by ignoring the concrete, but overestimate the negative flexural strength.

In the 5 and 10 story models, IPE O 400 is used as the gravity beam section on the top floor, while IPE O 450 section is used on the other floors. The moment-rotation and effective stiffnesses of the multilinear link elements to be assigned to these beams are calculated as explained below.

Plastic moment capacity (M_p) of IPE O 400 beam;

$$M_p = F_y * W_{py} * R_y = 355 \frac{kN^2}{m} * 269100^{mm^3} * 1.25 = 119.413\ kN - m$$

10% of plastic rotational stiffness ($4EI/L$) of IPE O 400 beam;

$$\theta = \frac{M_p}{\frac{4EI}{L}} = \frac{119.413^{kN-m}}{\frac{4*200000\frac{N}{mm^2}*(2.675E+\ mm^4)}{9000^{mm}}} * 10\% = 0.050\ rad$$

Effective stiffness;

$$K_{eff} = \frac{M_p}{\theta} = \frac{119.413^{kN-m}}{0.050^{rad}} = 2377.778\ kN - m/rad$$

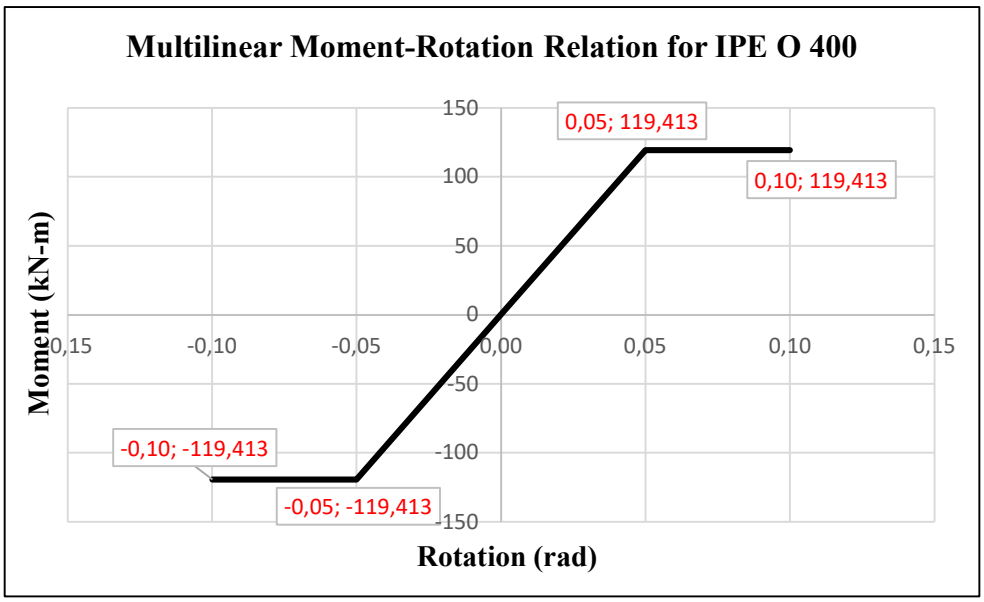


Figure 4.8: Moment-rotation relation of IPE O 400 for Set-1 models.

Plastic moment capacity (M_p) of IPE O 450 beam;

$$M_p = F_y * W_{py} * R_y = 355^{\frac{kN^2}{m}} * 34100^{mm^3} * 1.25 = 151.319\ kN - m$$

10% of plastic rotational stiffness ($4EI/L$) of IPE O 450 beam;

$$\theta = \frac{M_p}{\frac{4EI}{L}} = \frac{151.319^{kN-m}}{\frac{4*200000^{\frac{N}{mm}^2}*\left(4.09E+0\ mm^4\right)}{9000^{mm}}} * 10\% = 0.042\ rad$$

Effective stiffness;

$$K_{eff} = \frac{M_p}{\theta} = \frac{151.319^{kN-m}}{0.042^{rad}} = 3637.333\ kN - m/rad$$

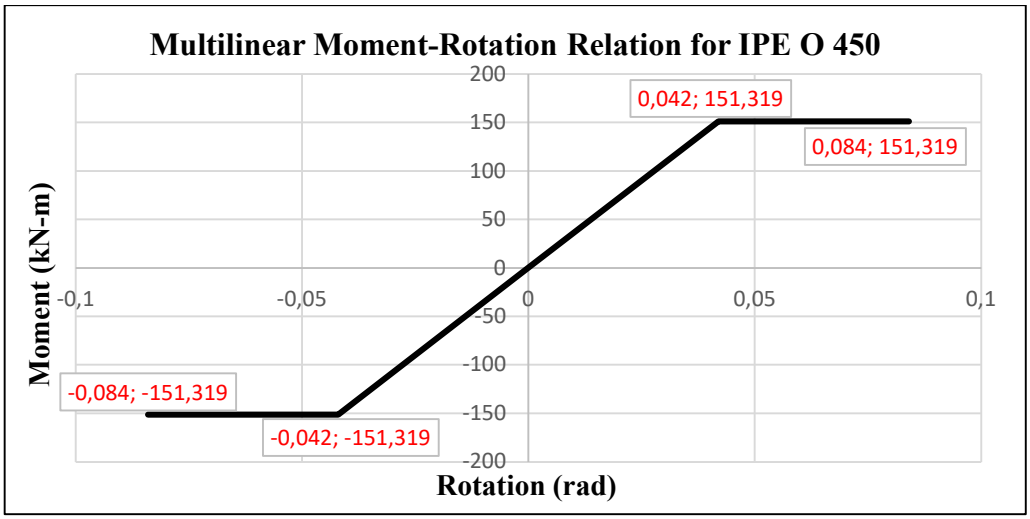


Figure 4.9: Moment-rotation relation of IPE O 450 for Set-1 models.

The method followed and equations used for the analytical model proposed by Shen et al [21] and Wen et al [26] in Figure 4.6 and Figure 4.7 were taken as the basis for the link element definitions of the gravity beam-column connections of the 5 and 10-story structures in Set-2 models.

Negative yielding moment (M_{y-}) and negative ultimate moment (M_{u-}) for the loading case when the concrete slab was subjected to tensile forces;

$$M_{y-} = \frac{1}{6} d_{st}^2 t_{st} F_y \tag{6.1}$$

$$M_{u-} = \frac{1}{4} d_{st}^2 t_{st} F_y \tag{6.2}$$

Positive yielding moment (M_{y+}) and positive ultimate moment (M_{u+}) for the loading case when the concrete slab was subjected to compressive forces.

- Yielding moment M_{y+} including concrete slab; The plastic neutral axis in the concrete slab by static equilibrium firstly must be found. The height of the compression slab zone a is:

$$a = \frac{\frac{1}{2} F_y d_{st} t_{st}}{b_{eff}\ x\ (0.3\ f_c')} \tag{6.3}$$

$$M_{y+} = \left(\frac{1}{2} F_y d_{st} t_{st}\right)(d_1 - \frac{a}{2} + 1.5 + \ d_{st}\ x\ \frac{2}{3}) \tag{6.4}$$

- Plastic moment M_{u+} including concrete slab; The height of the compression slab zone a is:

$$a = \frac{F_y d_{st} t_{st}}{b_{eff}\ x\ (0.85\ f_{cu})} \tag{6.5}$$

$$M_{u+} = (F_y d_{st} t_{st})(d_1 - \frac{a}{2} + 1.5 + \ d_{st}\ x\ \frac{1}{2}) \tag{6.6}$$

Where

d_{st} = Depth of connection plate's (mm).
t_{st} = Thickness of connection plate's (mm).
F_y = Yield strength of steel (MPa).
b_{eff} = Effective bay (mm).
$f_c^{'} = f_{cu}$ = Characteristic compressive strength (MPa).
d_1 = Depth of concrete deck (mm).

The welded connection model used to calculate these values is given in Figure 4.10 and the deck parametric properties are given in Figure 4.11 [23]. The single plate with dimensions of $390^{mm} x 125^{mm} x 8.5^{mm}$ in the shear tab connections of the GFs positioned in the interior is designed with five bolts on the beam webs.

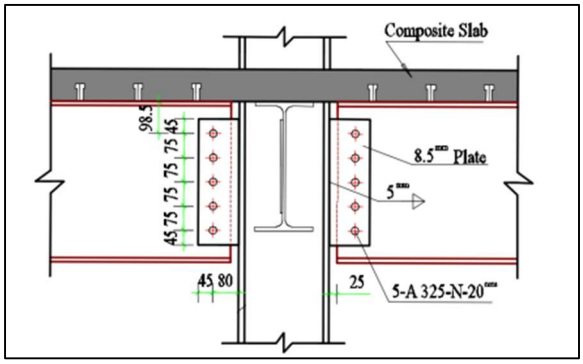


Figure 4.10: Typical GF shear tab connection detail.

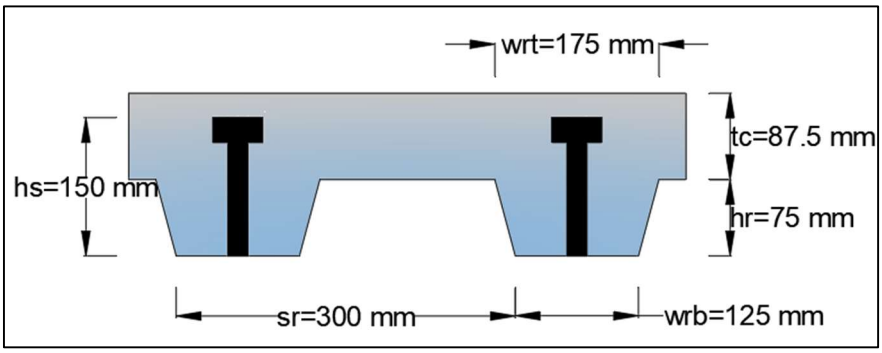


Figure 4.11: Filled deck properties.

Where

t_c = Slab depth (mm).

h_r = Rib depth (mm).

w_{rt} = Rib width top (mm).

w_{rb} = Rib bottom wrb (mm).

s_r = Rib spacing (mm).

h_s = Shear stud height (mm).

The moment-rotation relationship model calculated for the link elements of the Set-2 models according to the analytical model proposed by Shen et al. [21] and Wen et al. [26] and the formulations they used is given in Figure 4.12.

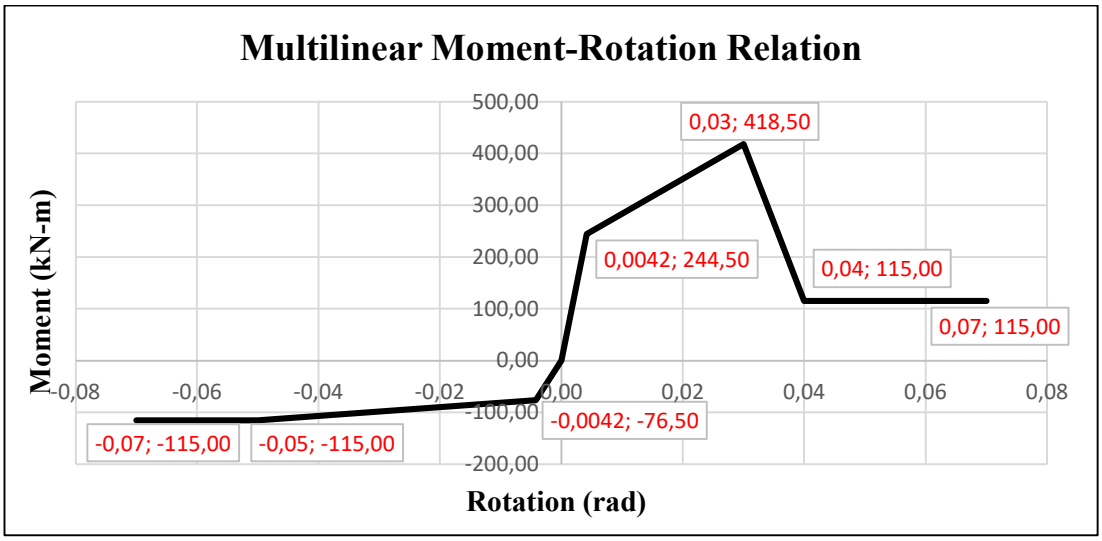


Figure 4.12: Moment-rotation relationship for Set-2 models.

The behavior models of the Set-1 and Set-2 connections for the IPE O 450 gravity beams are plotted together as shown in Figure 4.13 and appear to agree with the proposed analytical model in Figure 4.7.

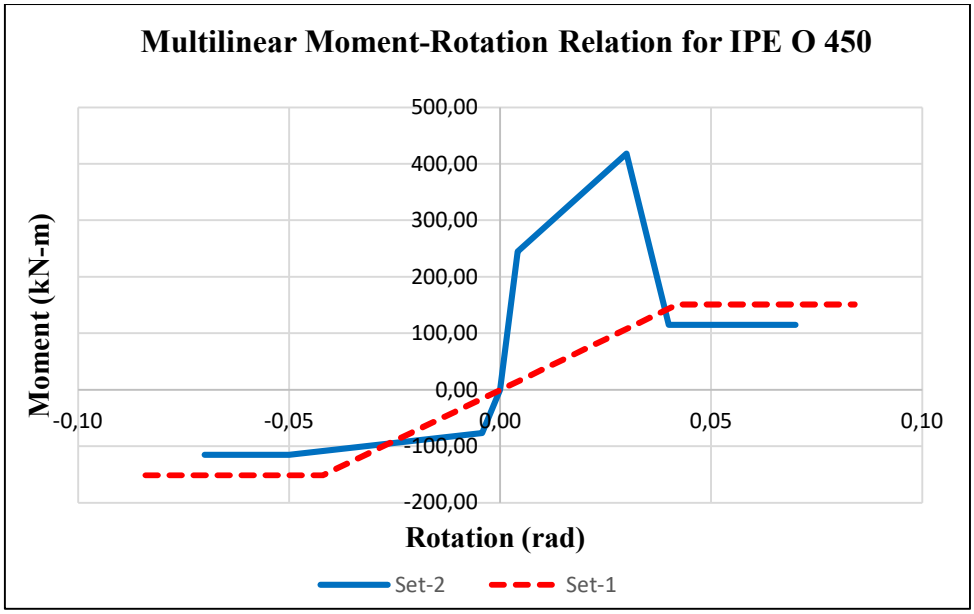


Figure 4.13: Moment-rotation models for Set-1 and Set-2.

Link elements whose connection models were determined were modeled with Etabs-2016 computer software as shown in Figure 4.14 [21]. Node 1, Node 2, and Node 3 are located in the same place as shown. The U_1, U_2, U_3 and R_1, R_2 of these nodes were modeled as fixed and have equal values for each node. In the R_3 direction, it was released and defined as nonlinear.

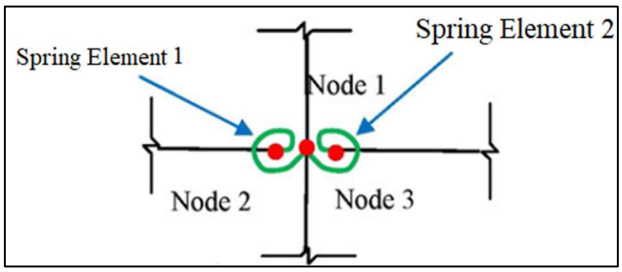


Figure 4.14: Spring elements.

Link elements defined for Set-1 and Set-2 models were assigned to gravity frame beams of 5- and 10-story buildings with a length of 20^{cm} as shown in Figure 4.15 and Figure 4.16.

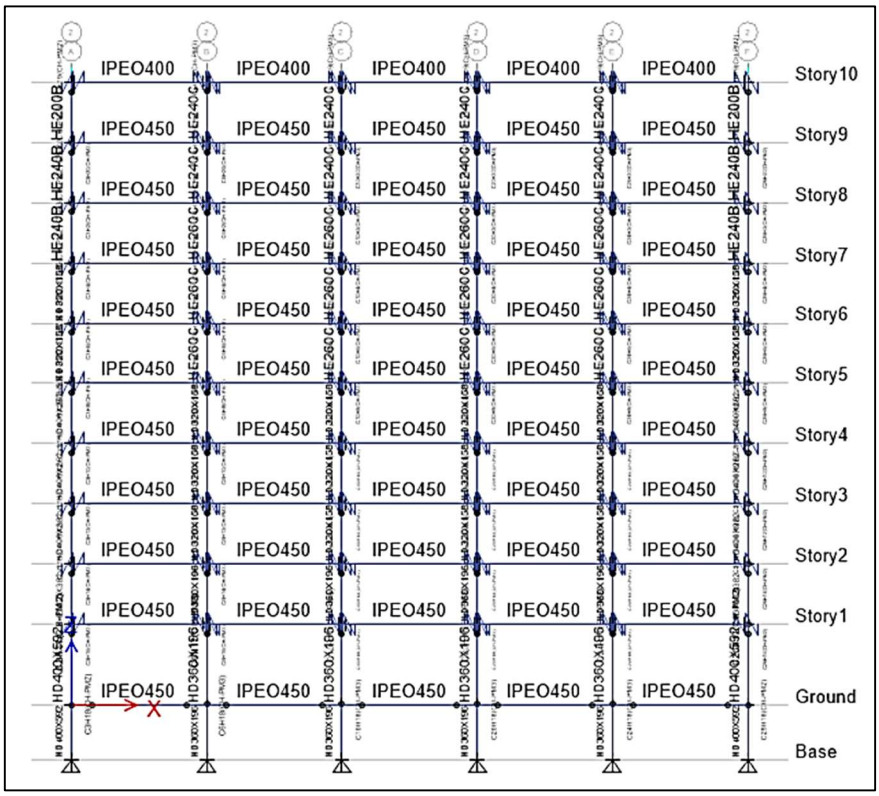


Figure 4.15: View of link elements in elevation.

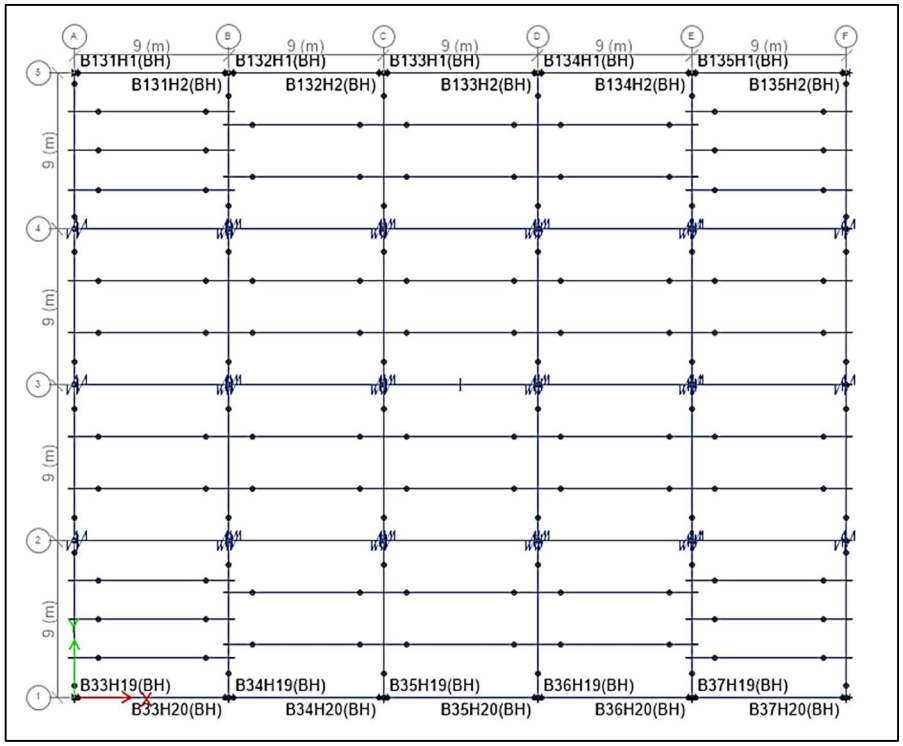


Figure 4.16: View of link elements in plan.

4.2 Earthquake Ground Motions in The Time History

The acceleration records to be used for nonlinear dynamic time history analysis directly affect the analysis results in terms of determining the behaviors and responses of the structures under the influence of ground motions. For this reason, it is very important to select the acceleration records to represent the earthquake hazard in a particular region for the analyzes to be made. Earthquake magnitudes compatible with the earthquake ground motion level based on the design, the duration of the earthquake, the maximum ground acceleration, fault distances, faulting mechanisms, and local soil conditions are the main factors that should be taken into account while making the selection.

In TBEC-2018, it is allowed to use artificially produced, previously recorded earthquake records (past earthquake records) or simulated earthquake ground motion records for non-linear time history earthquake calculations of buildings and building-type structures. However, it was stated that if there are past earthquake records compatible with the earthquake ground motion level based on the design in the area where the building is located, these records should be applied first. While past acceleration records provide information about factors such as sources, propagation environment, and soil that affect the records, they also contain sufficient and reliable information about the nature of ground motion and parameters such as amplitude, duration, phase, and frequency content. Therefore, it is healthier to select real earthquake records to perform nonlinear time history dynamic analyzes.

Ground motion records need to be scaled so that they can be used in analyzes in accordance with the design acceleration spectrum based on a particular earthquake zone and local soil type. In the scope of the study, the reason why the spectral acceleration values corresponding to the dominant periods of the structures in the elastic design spectrum are taken as a basis for scaling is that the mass participation ratios of the structures in the 1st mode dominant period are approximately 80%. In this method, the ordinates of the ground motion record are multiplied by a constant coefficient greater than or less than 1 and scaled up or down by the same amount in the time history. In this way, the most appropriate scaling is made according to the design spectrum obtained for the 5% damping rate of the real earthquake record in the desired period range. Since the process is done in the time history, there is no distortion in the frequency or the acceleration record itself. Since the acceleration value

corresponding to this period will be different for each earthquake at the desired period, the scaling process is done separately for all earthquake records to be used in the analysis.

In this study, earthquake records from the Pacific Earthquake Engineering Research (PEER) Center [11] strong ground motion database was used while selecting real earthquake records.

According to TBEC-2018, the design spectrum for the earthquake zone with DD-2 earthquake ground motion level and ZC soil type was given in Section 3.1.2. The design spectrum to be used as a basis for the selection and scaling of earthquake records is shown in Figure 4.17.

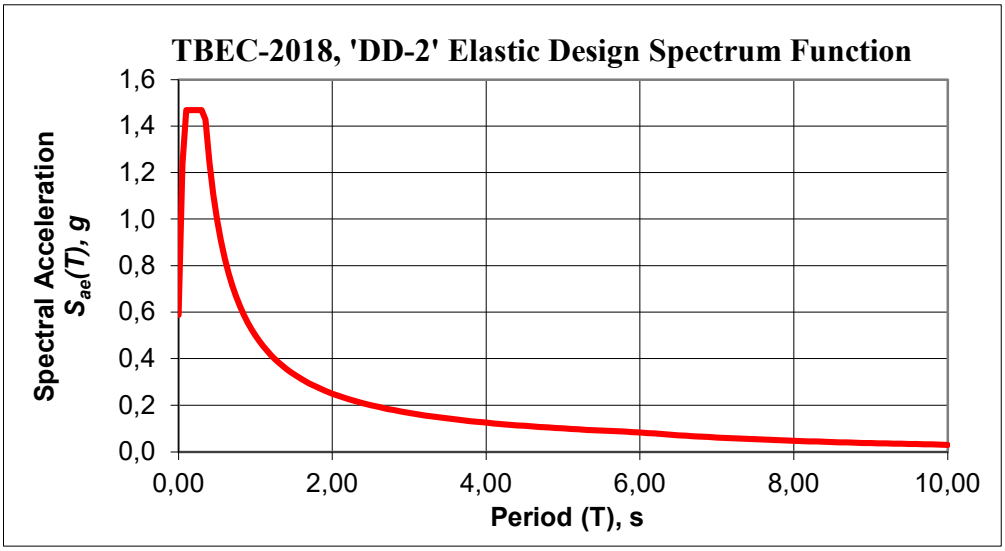


Figure 4.17: Elastic design spectrum function.

To determine the nonlinear behavior of the structures, 7 earthquake records were selected from the Peer strong ground motion database. It has been taken into account that the magnitudes of the selected earthquake ground motion records are greater than 6.00 and that the shear wave velocities of the soils ($(V_s)_{30}$) they are recorded are included in the ZC soil class in the range of 360-760 m/s as much as possible. The acceleration values corresponding to the periods of each of the RF, Set-1, and Set-2 models of the selected 7 earthquakes 5 and 10-story structures were scaled separately according to the response spectrum. In addition, while selecting the ground motion records, it has been paid attention that the scale factors calculated according to the response spectrum were between 1 ~ 5. The scale factors obtained as a result of scaling

according to the design spectrum represent the range in which each earthquake will begin to exhibit non-linear behavior when applied to the structures with its scale factor. The characteristics of the acceleration records and the scaling tables for each model and the figures containing the scaled acceleration-time spectrums with 5% damping are given below.

Table 4.4: Earthquake parameters and scale factors for 5-story RF.

5-Story_Reference Frame Model								
$T_1^{(Y)}$=	**1.459 s**							
NGA#	**$S_a^{(T)}$ (g)**	**Record**	**Scale Factor**	**Time (s)**	**Peak Ground Acc. (g)**	**Scaled Peak Ground Acc. (g)**	**Magnitude**	**$(V_s)_{30}$ (m/s)**
DD2/ZC	0.342	Design Specrum	1.000					
4132	0.158	PARK FIELD	**2.171**	21.2	0.367	0.797	6.00	467.76
4481	0.248	L'AQUILA	**1.380**	40.0	0.325	0.449	6.30	685.00
4840	0.228	CHUETSU	**1.500**	60.0	0.091	0.136	6.80	334.01
587	0.139	NEWZEALAND	**2.463**	49.3	0.241	0.593	6.60	551.30
1111	0.215	KOBE	**1.594**	41.0	0.483	0.771	7.08	609.00
451	0.093	MORGAN HILL	**3.675**	30.0	0.387	1.421	6.19	561.43
8166	0.155	DUZCE	**2.209**	35.0	0.396	0.875	7.14	425.00

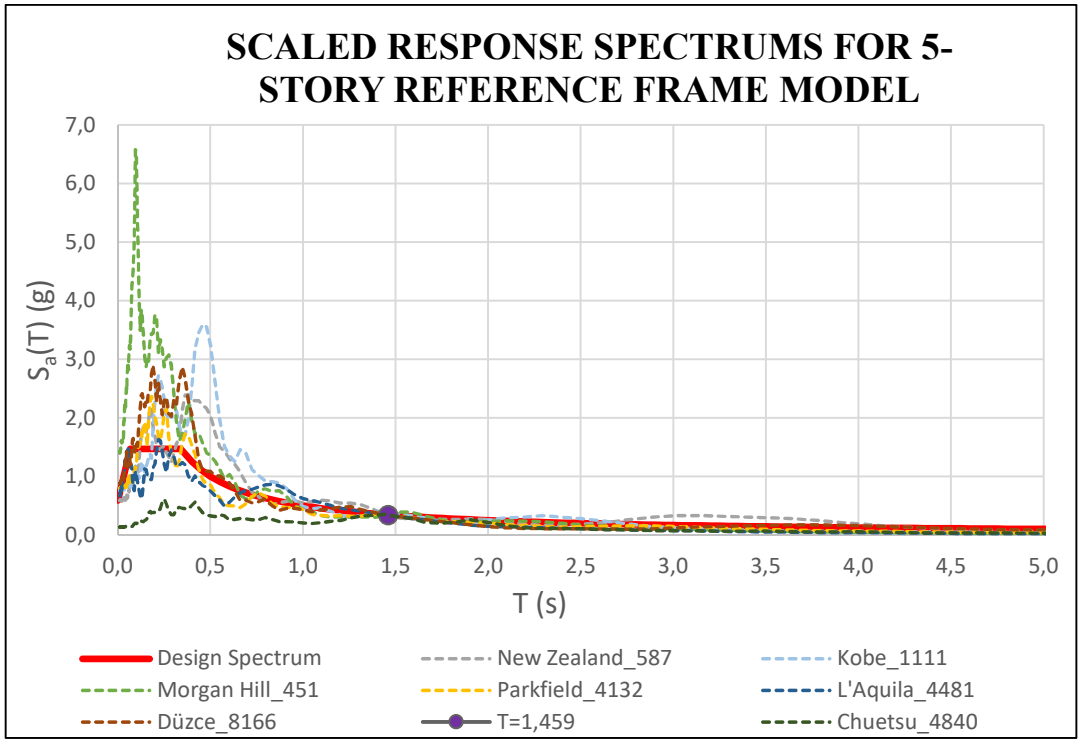


Figure 4.18: Scaled response spectrums for 5 story RF.

Table 4.5: Earthquake parameters and scale factors for 5-story Set-1.

5-Story_SET 1 Model								
$T_1^{(Y)}$=	**1.426 s**							
NGA#	**$S_a^{(T)}$ (g)**	**Record**	**Scale Factor**	**Time (s)**	**Peak Ground Acc. (g)**	**Scaled Peak Ground Acc. (g)**	**Magnitude**	**$(V_s)_{30}$ (m/s)**
DD2/ZC	0.350	Design Specrum	1.000					
4132	0.162	PARK FIELD	**2.164**	21.2	0.367	0.794	6.00	467.76
4481	0.258	L'AQUILA	**1.357**	40.0	0.325	0.442	6.30	685.00
4840	0.231	CHUETSU	**1.516**	60.0	0.091	0.138	6.80	334.01
587	0.154	NEW ZEALAND	**2.272**	49.3	0.241	0.547	6.60	551.30
1111	0.212	KOBE	**1.649**	41.0	0.483	0.797	7.08	609.00
451	0.087	MORGAN HILL	**4.010**	30.0	0.387	1.551	6.19	561.43
8166	0.163	DUZCE	**2.147**	35.0	0.396	0.851	7.14	425.00

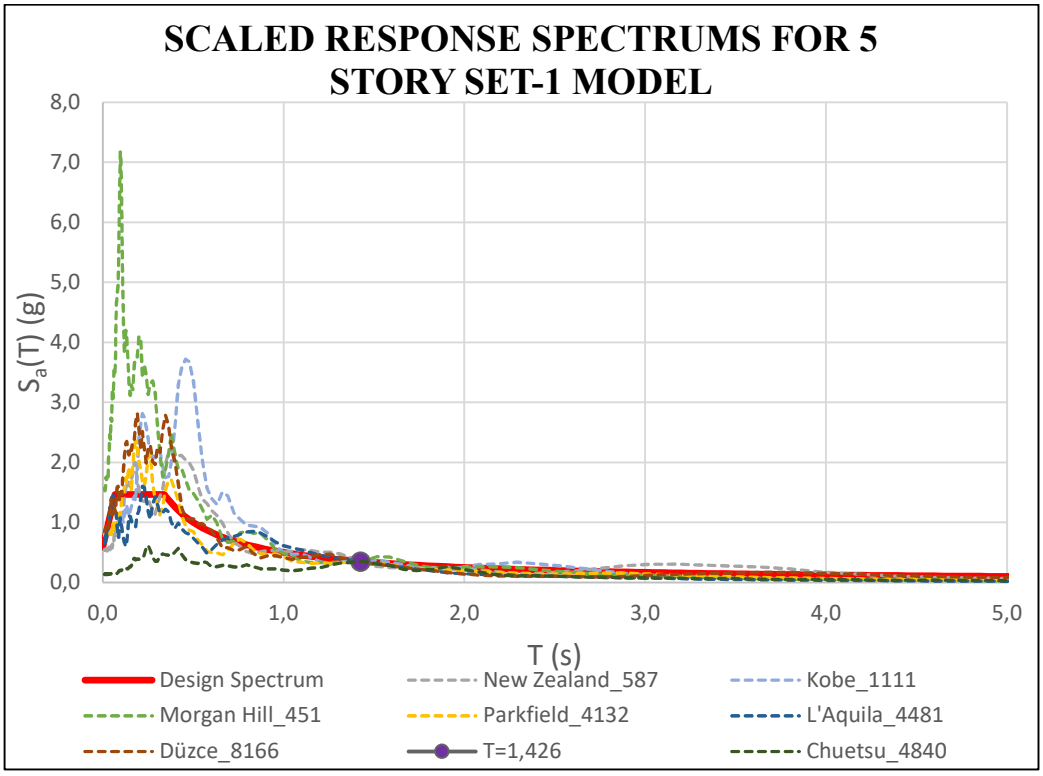


Figure 4.19: Scaled response spectrums for 5 story Set-1.

Table 4.6: Earthquake parameters and scale factors for 5-story Set-2.

5-Story_SET 2 Model								
$T_1^{(Y)}$=	1.39 s							
NGA#	**$S_a^{(T)}$ (g)**	**Record**	**Scale Factor**	**Time (s)**	**Peak Ground Acc. (g)**	**Scaled Peak Ground Acc. (g)**	**Magnitude**	**$(V_s)_{30}$ (m/s)**
DD2/ZC	0.360	Design Specrum	1.000					
4132	0.164	PARK FIELD	**2.198**	21.2	0.367	0.807	6.00	467.76
4481	0.269	L'AQUILA	**1.335**	40.0	0.325	0.434	6.30	685.00
4840	0.226	CHUETSU	**1.591**	60.0	0.091	0.145	6.80	334.01
587	0.173	NEW ZEALAND	**2.076**	49.3	0.241	0.500	6.60	551.30
1111	0.213	KOBE	**1.686**	41.0	0.483	0.815	7.08	609.00
451	0.083	MORGAN HILL	**4.320**	30.0	0.387	1.671	6.19	561.43
8166	0.173	DUZCE	**2.077**	35.0	0.396	0.823	7.14	425.00

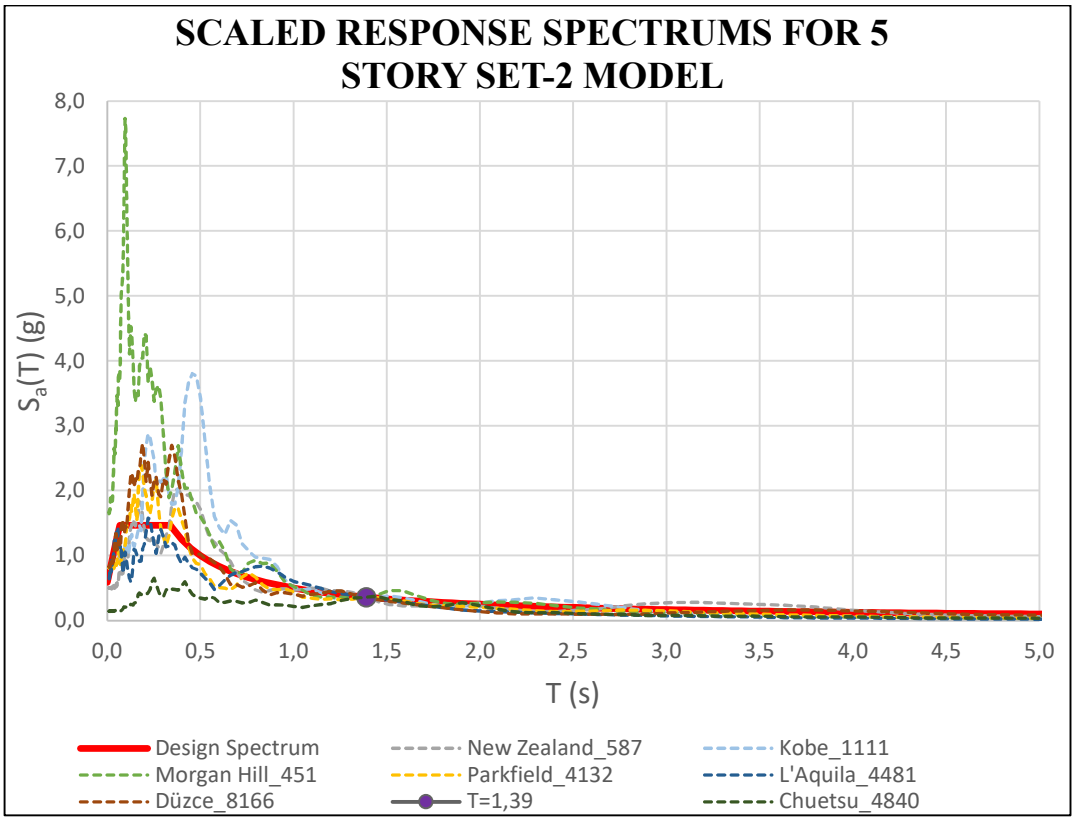


Figure 4.20: Scaled response spectrums for 5 story Set-2.

Table 4.7: Earthquake parameters and scale factors for 10-story RF.

10-Story_Reference Frame Model								
$T_1^{(X)}$=	2.773 s							
NGA#	**$S_a^{(T)}$ (g)**	**Record**	**Scale Factor**	**Time (s)**	**Peak Ground Acc. (g)**	**Scaled Peak Ground Acc. (g)**	**Magnitude**	**$(V_s)_{30}$ (m/s)**
DD2/ZC	0.180	Design Specrum	1.000					
4132	0.073	PARK FIELD	**2.466**	21.2	0.367	0.905	6.00	467.76
4481	0.063	L'AQUILA	**2.842**	40.0	0.325	0.925	6.30	685.00
4840	0.058	CHUETSU	**3.112**	60.0	0.091	0.283	6.80	334.01
587	0.108	NEW ZEALAND	**1.665**	49.3	0.241	0.401	6.60	551.30
1111	0.116	KOBE	**1.558**	41.0	0.483	0.753	7.08	609.00
451	0.033	MORGAN HILL	**5.420**	30.0	0.387	2.096	6.19	561.43
8166	0.045	DUZCE	**4.027**	35.0	0.396	1.596	7.14	425.00

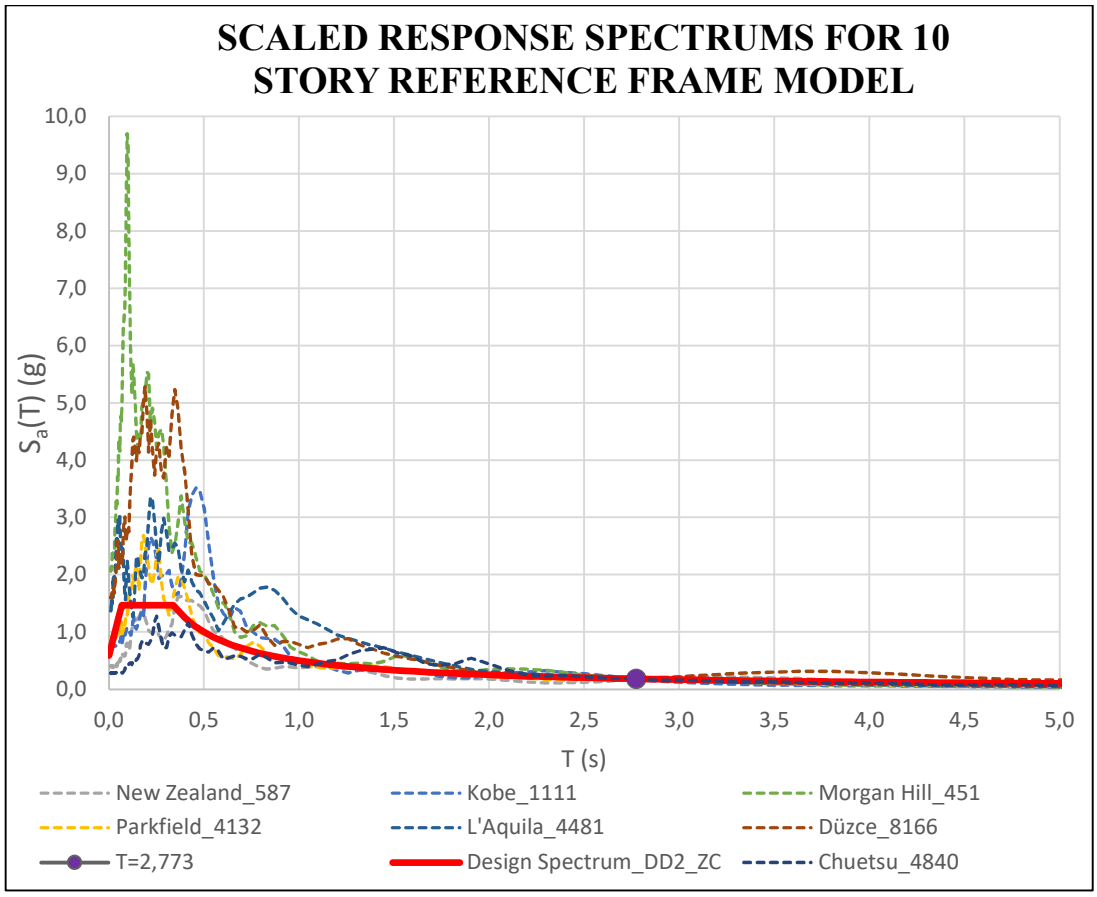


Figure 4.21: Scaled response spectrums for 10 story RF.

Table 4.8: Earthquake parameters and scale factors for 10-story Set-1.

10-Story_SET 1 Model								
$T_1^{(X)}$=	2.733 s							
NGA#	**$S_a^{(T)}$ (g)**	**Record**	**Scale Factor**	**Time (s)**	**Peak Ground Acc. (g)**	**Scaled Peak Ground Acc. (g)**	**Magnitude**	**$(V_s)_{30}$ (m/s)**
DD2/ZC	0.183	Design Specrum	1.000					
4132	0.072	PARK FIELD	**2.531**	21.2	0.367	0.929	6.00	467.76
4481	0.065	L'AQUILA	**2.806**	40.0	0.325	0.913	6.30	685.00
4840	0.060	CHUETSU	**3.074**	60.0	0.091	0.279	6.80	334.01
587	0.102	NEW ZEALAND	**1.790**	49.3	0.241	0.431	6.60	551.30
1111	0.125	KOBE	**1.469**	41.0	0.483	0.710	7.08	609.00
451	0.035	MORGAN HILL	**5.255**	30.0	0.387	2.032	6.19	561.43
8166	0.045	DUZCE	**4.086**	35.0	0.396	1.619	7.14	425.00

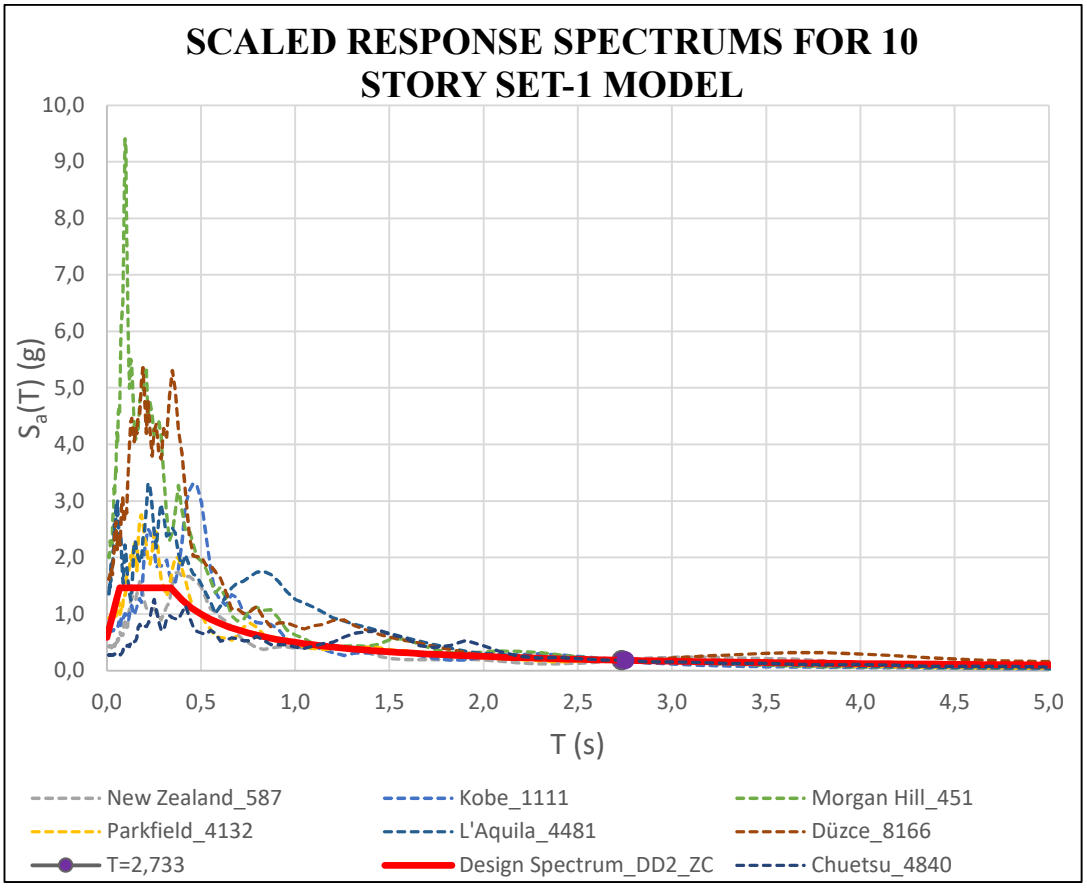


Figure 4.22: Scaled response spectrums for 10 story Set-1.

Table 4.9: Earthquake parameters and scale factors for 10-story Set-2.

10-Story_SET 2 Model								
$T_1^{(X)}$=	2.635 s							
NGA#	**$S_a^{(T)}$ (g)**	**Record**	**Scale Factor**	**Time (s)**	**Peak Ground Acc. (g)**	**Scaled Peak Ground Acc. (g)**	**Magnitude**	**$(V_s)_{30}$ (m/s)**
DD2/ZC	0.189	Design Specrum	1.000					
4132	0.068	PARK FIELD	**2.770**	21.2	0.367	1.017	6.00	467.76
4481	0.070	L'AQUILA	**2.707**	40.0	0.325	0.880	6.30	685.00
4840	0.062	CHUETSU	**3.069**	60.0	0.091	0.279	6.80	334.01
587	0.087	NEW ZEALAND	**2.184**	49.3	0.241	0.526	6.60	551.30
1111	0.147	KOBE	**1.286**	41.0	0.483	0.621	7.08	609.00
451	0.040	MORGAN HILL	**4.689**	30.0	0.387	1.813	6.19	561.43
8166	0.047	DUZCE	**4.051**	35.0	0.396	1.605	7.14	425.00

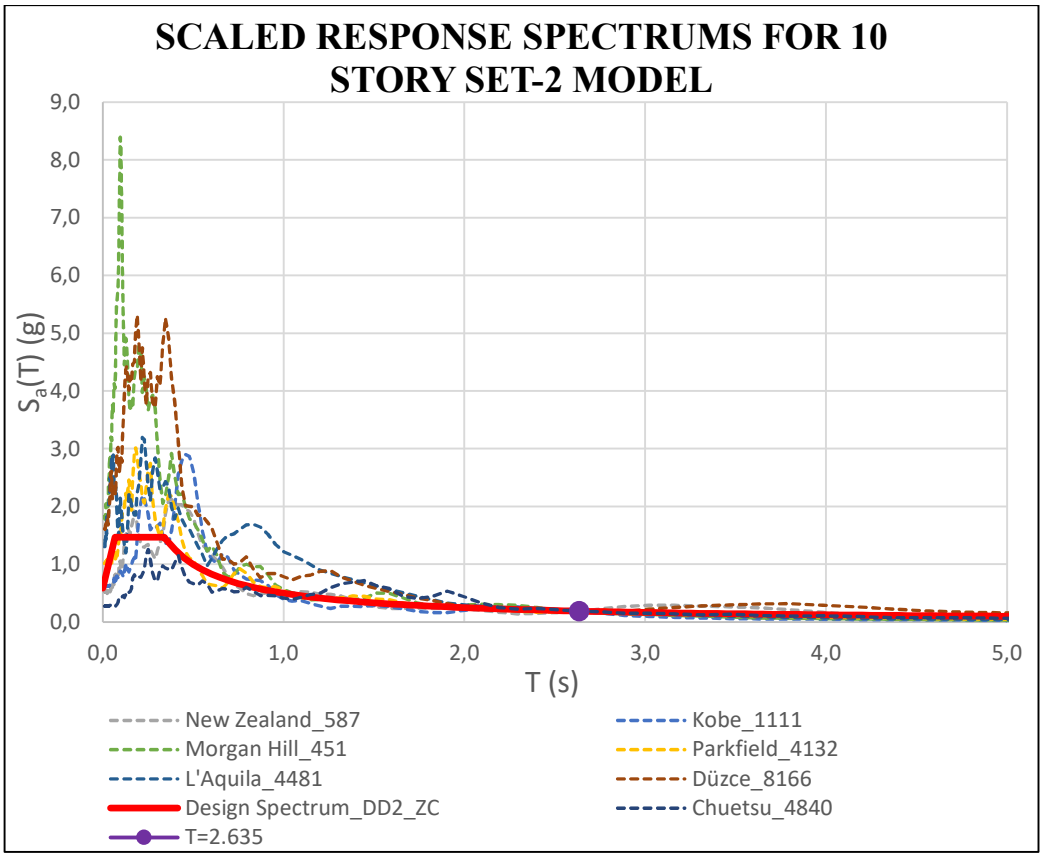


Figure 4.23: Scaled response spectrums for 10 story Set-2.

5. INCREMENTAL DYNAMIC ANALYSES

Incremental dynamic analysis (IDA) is a parametric analysis method in which the parameters in the nonlinear dynamic time history analysis are made by changing and used to more comprehensively evaluate the seismic performance of structures under the influence of lateral loads. IDAs are performed by exposing structural models to ground motion records, each scaled to multiple intensity levels, and by generating parameterized response curves against intensity levels by nonlinear multiple dynamic analyzes of structural models. Scale factors (SF) are determined by increasing the ground motion intensities from the range where the structures will behave elastically to the range where will behave inelastically and until the structure collapses. Numerous nonlinear dynamic analyzes are performed of structural models subjected to a series of ground motion records scaled to multiple intensity levels.

The IDA advantages are as follows [27]:

- Thorough understanding of the range of response or demands versus the range of potential levels of a ground motion record,
- Better understanding of the structural implication of rarer/more severs ground motion levels,
- Better understanding of the changes in the nature of the structural response as the intensity of ground motion increases,
- Producing estimates of the dynamic capacity of the global structural system,
- Finally, given a multi-record IDA study, understanding how stable (or variable) all these items are from one ground motion record to another.

Within the scope of this study, 7 earthquake records were applied one by one to 5 and 10 story 3D models (RF, Set-1, and Set-2) with incremental dynamic analysis. The scale factor was determined in such a way that the ground motion intensity with a scale factor of SF would have a spectral acceleration, Sa, equal to g. To exemplify, a SF of 1.0 corresponds to 1.0 g spectral acceleration at the ‘first mode’ fundamental period of the scaled ground motion [23]. In other words, it was obtained by dividing the increased acceleration intensities of ground motions to the earthquake response spectrum acceleration value corresponding to the building fundamental period. As a

result of the modeling, the fundamental periods of the 5-story buildings were obtained as 1.459 s, 1.426 s, and 1.39 s for the RF, Set-1, and Set-2 models, respectively. In 10-story buildings, the fundamental periods were obtained as 2.773 s, 2.733 s, and 2.635 s. Due to the significant differences in the fundamental periods, SFs were calculated using increment magnitudes of 0.2g for the 5-story models and 0.1g for the 10-story models in incremental dynamic analysis. The acceleration densities of ground motions have been increased for all structures until the Set-2 models of 5 and 10 story structures exceed the relative story drift limit calculated according to TBEC-2018.

All analyzes were performed using the 'non-linear direct integration' method in the time-history via Etabs software. At the time of defining the loadings, the first fundamental period of the structure period and the period value in which the mass participation rate exceeds 90% were used for the damping of the structure, and the damping ratio was accepted as 5% for all models. Hilber-Hughes-Taylor method was preferred for time integration parameters. For all increased ground motion intensities, individual loading conditions were defined using SFs, and analyzes were carried out.

In this study, SFs were calculated for each model and for each earthquake record to can make incremental dynamic analyses. Then when the acceleration intensities obtained according to the design spectrum and corresponding to the SFs at which nonlinear behavior will start, are applied to the structural models, and the hinging states and plastic rotation demands that occur in the models were examined. Maximum drift ratios, maximum top displacements, base shear forces, and base shear forces corresponding to peak displacements (capacity curves) corresponding to the increased acceleration intensities for each model and each earthquake record were read from the analysis results and examined according to the regulation limits by the graph. In addition, by determining the SFs and acceleration intensities of the Set-2 models when they reach their maximum drift ratios, the hinging of all structures at this moment, plastic rotation demands, and the distribution of the drift ratios that occur along the story in the structures was scrutinized. After all the analyzes were completed, the responses of the structures were obtained by taking the averages of the results obtained for 7 earthquake records.

The maximum story drift ratio obtained according to TBEC-2018 is 2.00%. Within the scope of this study, two times of the drift limit obtained within the limits of the regulation was taken into account, and the acceleration intensities of the structures when they reach 4.00% were investigated.

The maximum top displacements of the models were limited by the peak displacement values obtained from the linear analysis. As a result of the linear analysis, the maximum peak displacement was obtained as 274 mm and 619 mm for the 5-story 10-story structure, respectively, and these values were accepted as the boundary conditions for the peak displacement values obtained as a result of the incremental dynamic analysis. For the base shear forces obtained as a result of the analyses, the limit values of 1849.288 kN and 2007.115 kN, which are mentioned in Appendix B1 for 5-story and in Appendix D1 for 10-story, were accepted, respectively. In addition, boundary conditions IO ≤ 1θy <LS ≤ 9θy <CP ≤ 11θy were used for the plastic rotation angles representing the IO, LS, and CP performance levels in the hinging of the structures, as specified in Section 4.1.1.

SFs calculated for each model and responses of the structures under the increased acceleration intensities are shown in tables and figures in the next section.

5.1 IDA For 5-Story Building Models

5.1.1 Düzce_8166 Earthquake

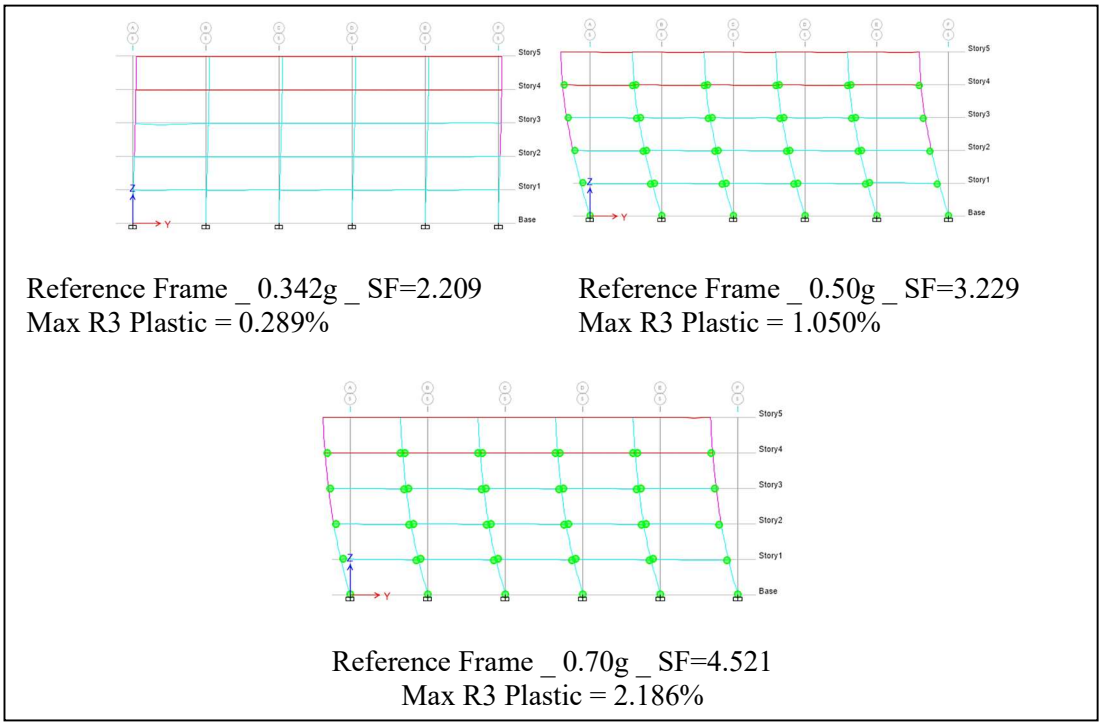
Table 5.1: SFs for 5-story models under the Düzce earthquake.

5 Story_Reference Frame		
(S_a)	(SF)	Scale
g	unitless	mm/s²
0,100	0,646	6333,79
0,155	1,000	9806,65
0,300	1,938	19001,381
0,342	**2,209**	**21661,5**
0,500	3,229	31668,97
0,700	4,521	44336,56
0,900	5,813	57004,14
1,100	7,105	69671,73
1,300	8,396	82339,32
1,500	9,688	95006,91
1,700	10,980	107674,49
1,900	12,271	120342,08

5 Story_Set 1		
(S_a)	(SF)	Scale
g	unitless	mm/s²
0,100	0,613	6011,51
0,163	1,000	9806,65
0,300	1,839	18034,53
0,350	**2,147**	**21054,71**
0,500	3,065	30057,54
0,700	4,291	42080,56
0,900	5,517	54103,58
1,100	6,743	66126,60
1,300	7,969	78149,61
1,500	9,195	90172,63
1,700	10,421	102195,65
1,900	11,647	114218,67

5 Story_Set 2		
(S_a)	(SF)	Scale
g	unitless	mm/s²
0,100	0,578	5664,75
0,173	1,000	9806,65
0,300	1,733	16994,25
0,360	**2,077**	**20370,44**
0,500	2,888	28323,75
0,700	4,044	39653,24
0,900	5,199	50982,74
1,100	6,354	62312,24
1,300	7,509	73641,74
1,500	8,665	84971,24
1,700	9,820	96300,74
1,900	10,975	107630,24

Application of acceleration intensities to 5-story models under Düzce earthquake in three stages starting from the acceleration intensities corresponding to the SF obtained from the design spectrum;

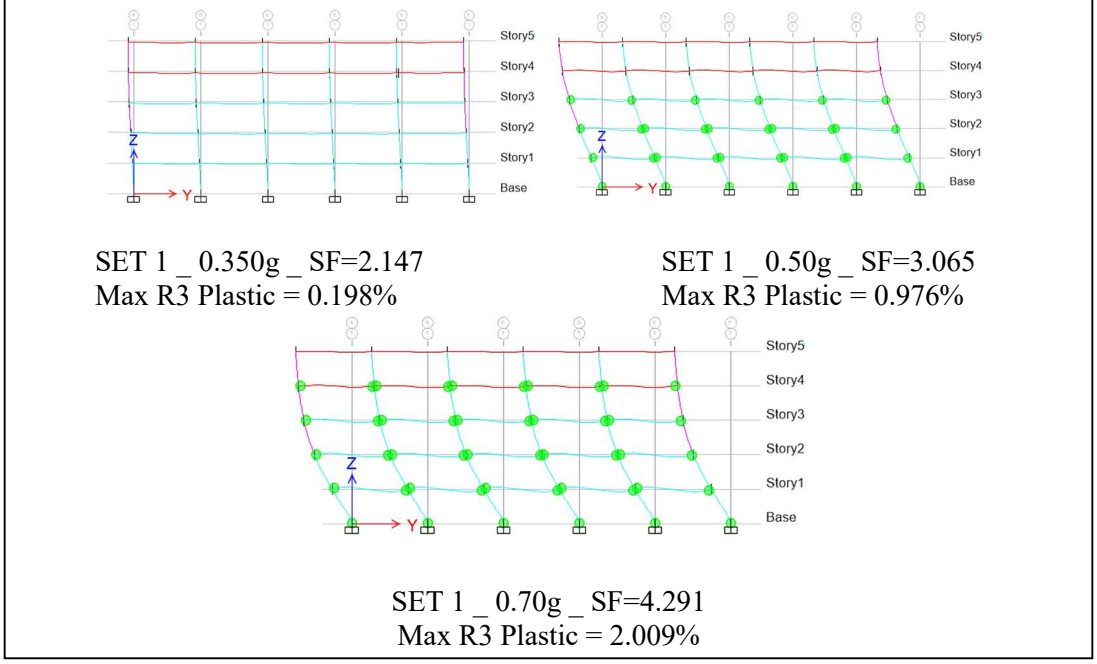


Reference Frame _ 0.342g _ SF=2.209
Max R3 Plastic = 0.289%

Reference Frame _ 0.50g _ SF=3.229
Max R3 Plastic = 1.050%

Reference Frame _ 0.70g _ SF=4.521
Max R3 Plastic = 2.186%

Figure 5.1: Hingings and plastic rotation demands of 5-story RFs under the Düzce earthquake.



SET 1 _ 0.350g _ SF=2.147
Max R3 Plastic = 0.198%

SET 1 _ 0.50g _ SF=3.065
Max R3 Plastic = 0.976%

SET 1 _ 0.70g _ SF=4.291
Max R3 Plastic = 2.009%

Figure 5.2: Hingings and plastic rotation demands of 5-story Set-1 under the Düzce earthquake.

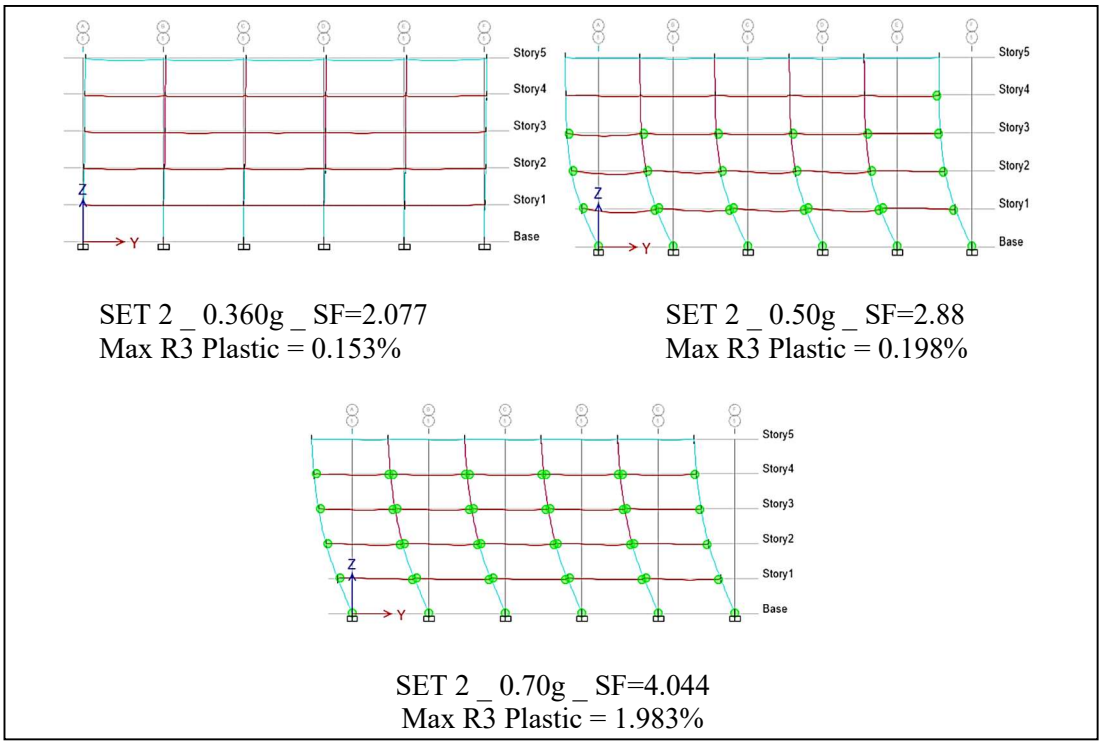


Figure 5.3: Hingings and plastic rotation demands of 5-story Set-2 under the Düzce earthquake.

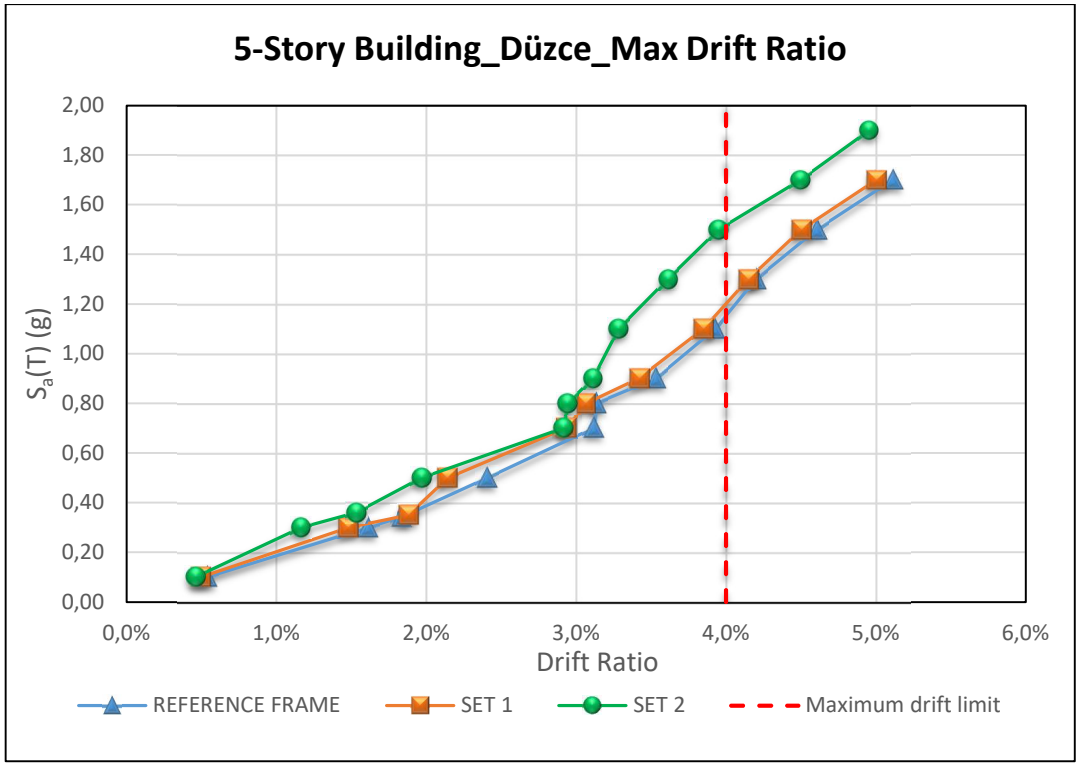


Figure 5.4: Max drift ratios of 5-story models under Düzce earthquake acceleration intensities.

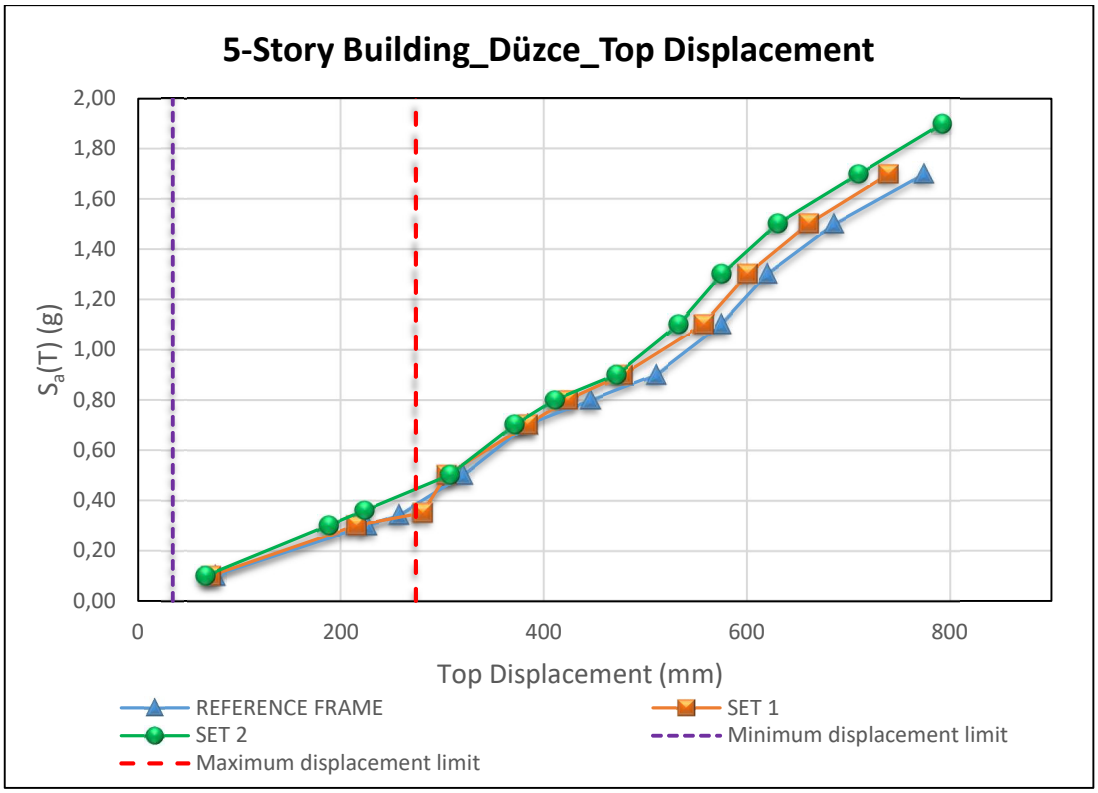


Figure 5.5: Max top displacements of 5-story models under Düzce earthquake acceleration intensities.

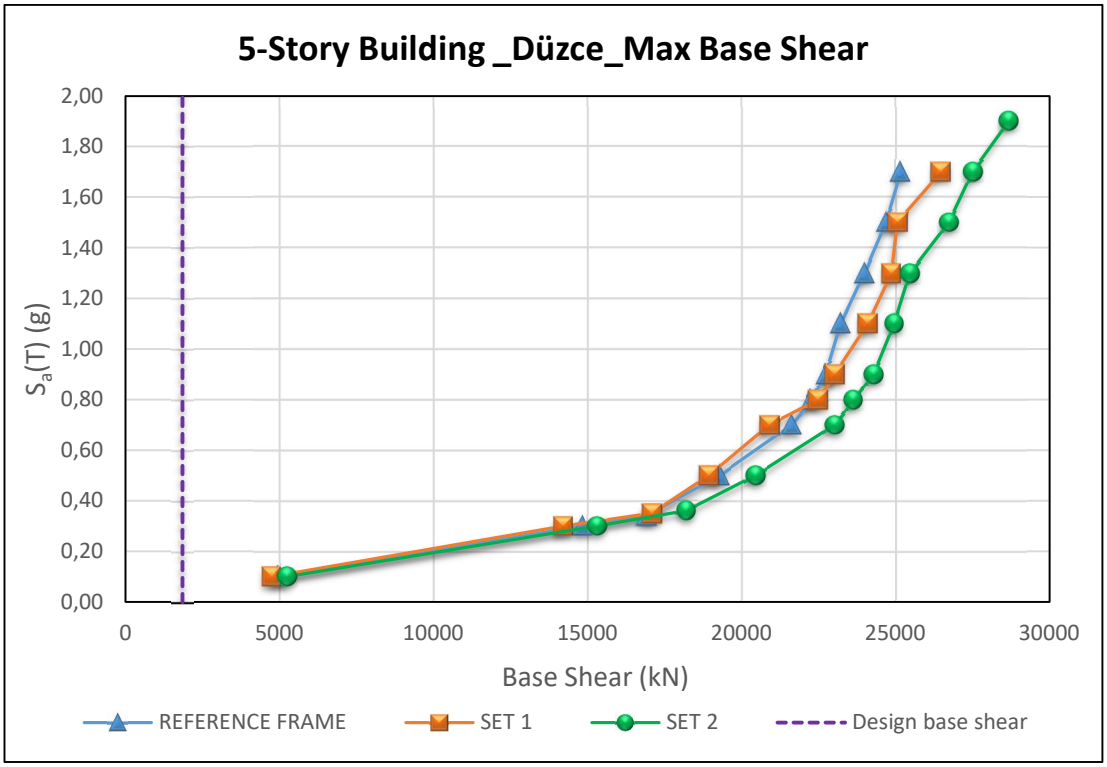


Figure 5.6: Max base shears of 5-story models under Düzce earthquake acceleration intensities.

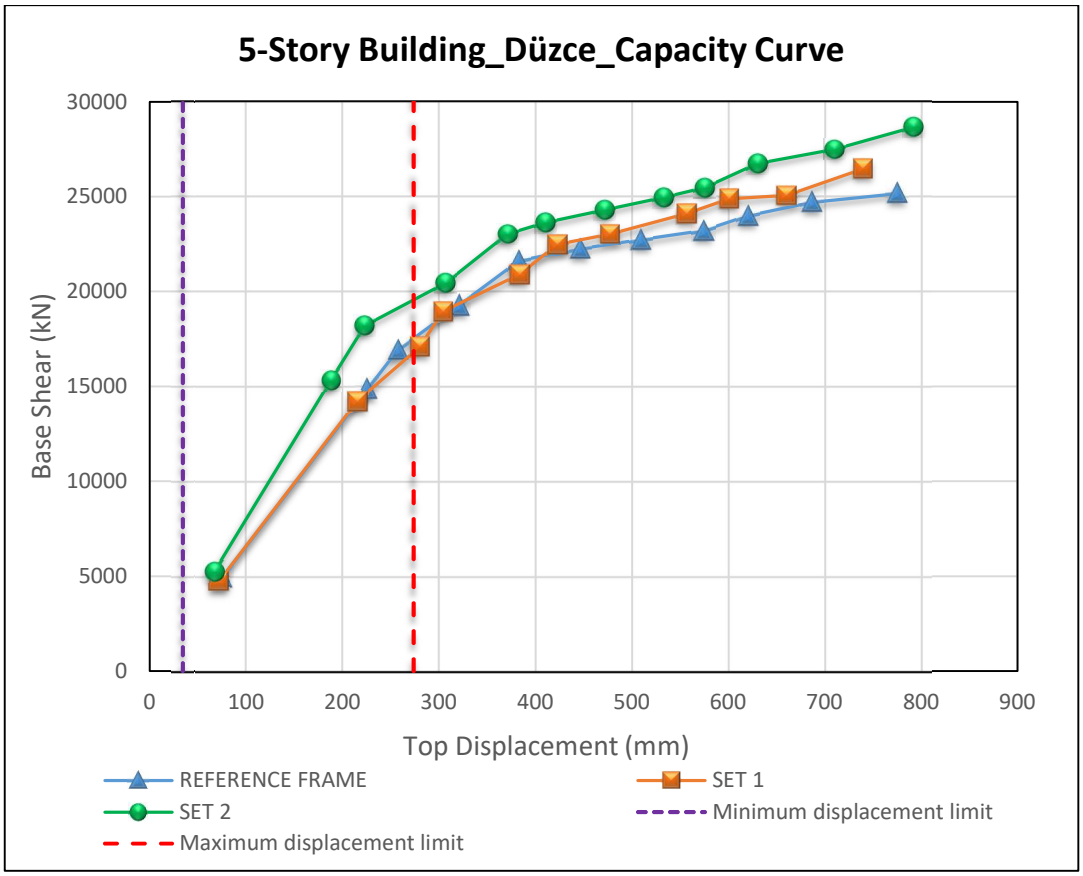


Figure 5.7: Capacity curves of 5-story models under Düzce earthquake acceleration intensities.

Table 5.2: Responses of 5-story models under Düzce earthquake.

DUZCE / 5-STORY	$S_a(T)$ values corresponding to drift ratio limit	$S_a(T)$ values corresponding to maximum top displacement limit	The base shears corresponding to maximum top displacement
Reference Frame	1.15 g	0.38 g	17536.96 kN
Set-1	1.20 g	0.35 g	16818.73 kN
Set-2	1.50 g	0.45 g	19565.37 kN

The hinging and plastic rotation demands and drift ratio distributions along the structure height of all models at 1.50 g acceleration intensity, where the 5-story Set-2 structure under the Düzce earthquake reached the 4.00% drift ratio limit;

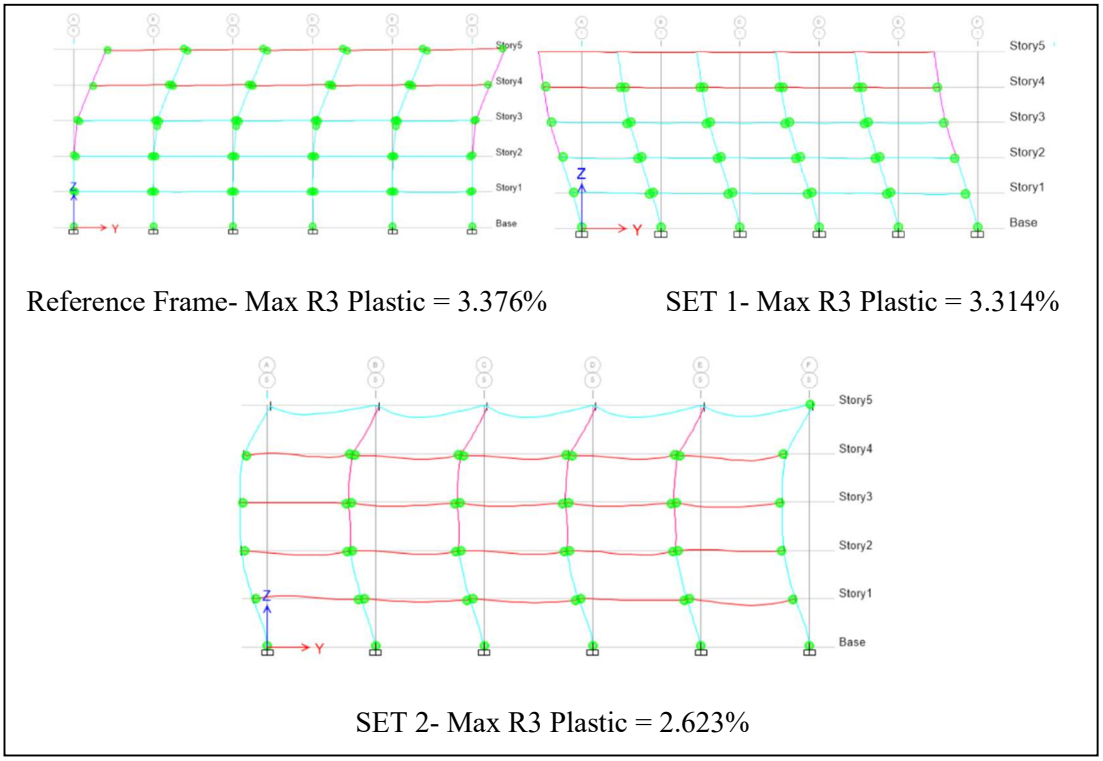


Figure 5.8: Hinging and plastic rotation demands of 5-story models at S_a=1.50g under the Düzce earthquake.

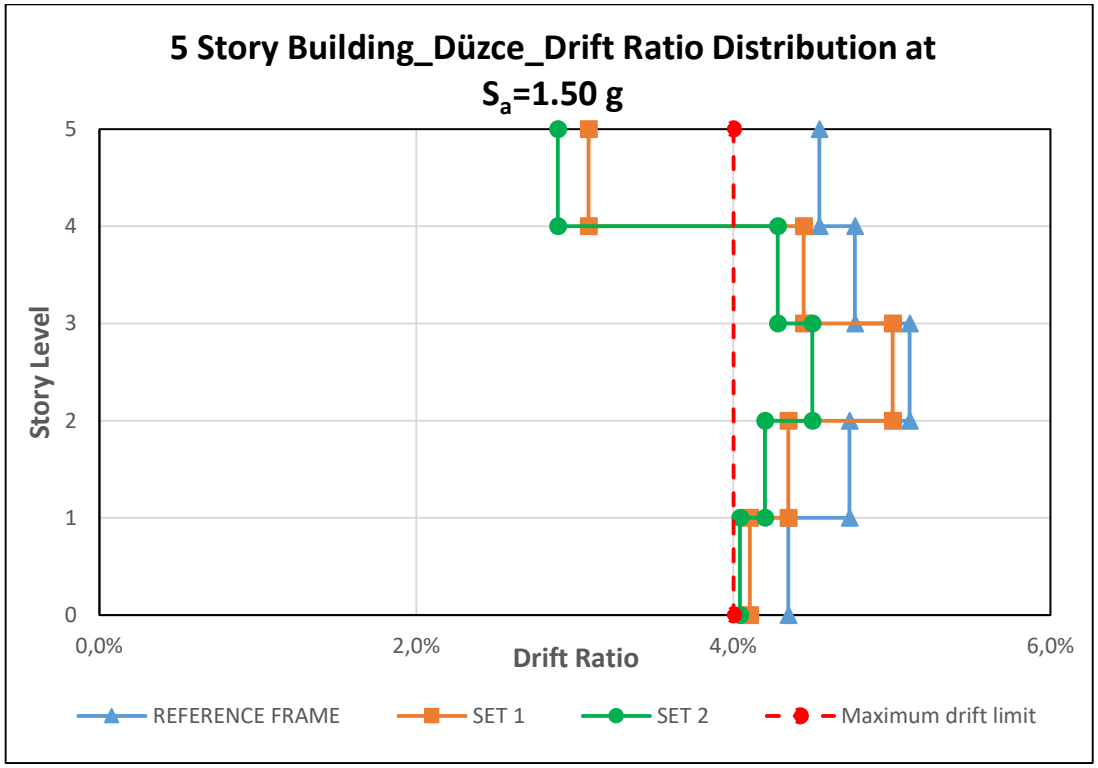


Figure 5.9: Drift ratio distributions along 5-story models' height at S_a=1.50g under the Düzce earthquake.

5.1.2 Park Field_4132 Earthquake

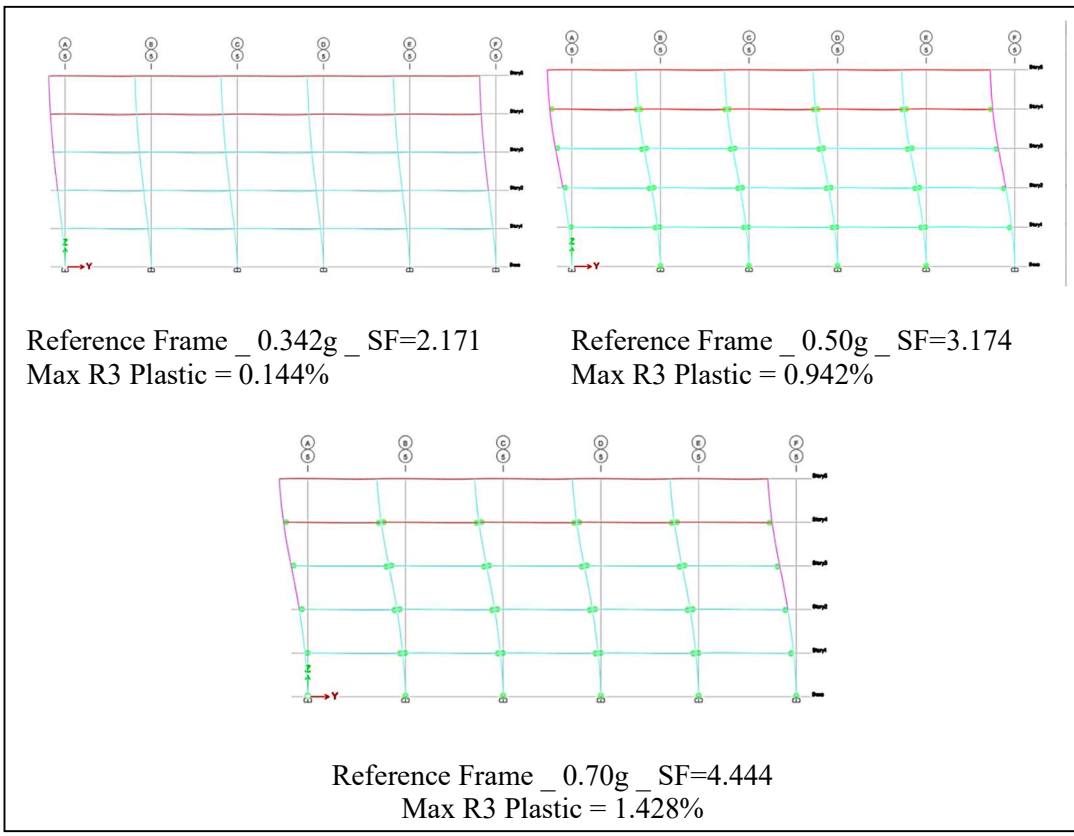
Table 5.3: SFs for 5-story models under the Park Field earthquake.

5 Story_Reference Frame		
(S_a)	(SF)	Scale
g	unitless	mm/s²
0,100	0,635	6225,887
0,158	1,000	9806,650
0,300	1,905	18677,661
0,342	**2,171**	**21293,778**
0,500	3,174	31129,434
0,700	4,444	43581,208
0,900	5,714	56032,982
1,100	6,984	68484,755
1,300	8,253	80936,529
1,500	9,523	93388,303
1,700	10,793	105840,076
1,900	12,062	118291,850

5 Story_Set 1		
(S_a)	(SF)	Scale
g	unitless	mm/s²
0,100	0,618	6057,930
0,162	1,000	9806,650
0,300	1,853	18173,790
0,350	**2,164**	**21217,295**
0,500	3,089	30289,651
0,700	4,324	42405,511
0,900	5,560	54521,371
1,100	6,795	66637,232
1,300	8,031	78753,092
1,500	9,266	90868,952
1,700	10,502	102984,812
1,900	11,737	115100,673

5 Story_Set 2		
(S_a)	(SF)	Scale
g	unitless	mm/s²
0,100	0,611	5993,948
0,164	1,000	9806,650
0,300	1,853	18173,790
0,360	**2,198**	**21554,236**
0,500	3,089	30289,651
0,700	4,324	42405,511
0,900	5,560	54521,371
1,100	6,795	66637,232
1,300	8,031	78753,092
1,500	9,266	90868,952
1,700	10,502	102984,812
1,900	11,737	115100,673

Application of acceleration intensities to 5-story models under Park Field earthquake in three stages starting from the acceleration intensities corresponding to the SF obtained from the design spectrum;

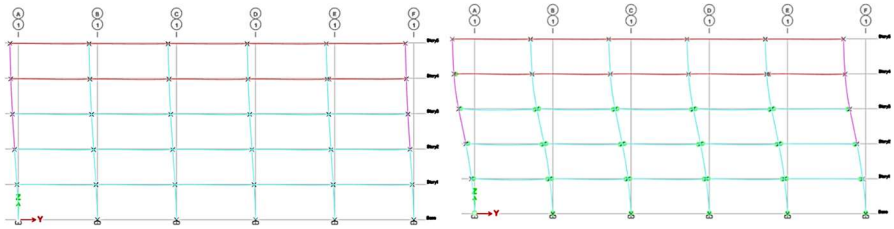


Reference Frame _ 0.342g _ SF=2.171
Max R3 Plastic = 0.144%

Reference Frame _ 0.50g _ SF=3.174
Max R3 Plastic = 0.942%

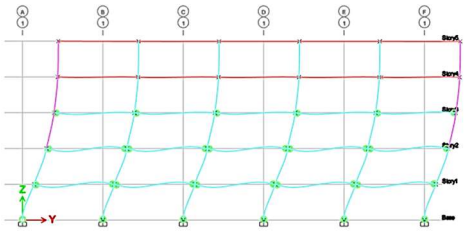
Reference Frame _ 0.70g _ SF=4.444
Max R3 Plastic = 1.428%

Figure 5.10: Hingings and plastic rotation demands of 5-story RFs under the Park Field earthquake.



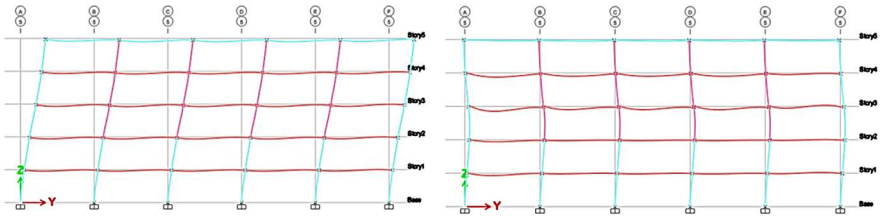
SET 1 _ 0.350g _ SF=2.164
Max R3 Plastic = 0.144%

SET 1 _ 0.50g _ SF=3.089
Max R3 Plastic = 1.004%



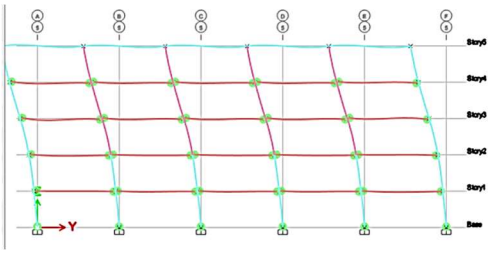
SET 1 _ 0.70g _ SF=4.324
Max R3 Plastic = 1.439%

Figure 5.11: Hingings and plastic rotation demands of 5-story Set-1 under the Park Field earthquake.



SET 2 _ 0.360g _ SF=2.198
Max R3 Plastic = 0.159%

SET 2 _ 0.50g _ SF=3.089
Max R3 Plastic = 0.842%



SET 2 _ 0.70g _ SF=4.324
Max R3 Plastic = 2.067%

Figure 5.12: Hingings and plastic rotation demands of 5-story Set-2 under the Park Field earthquake.

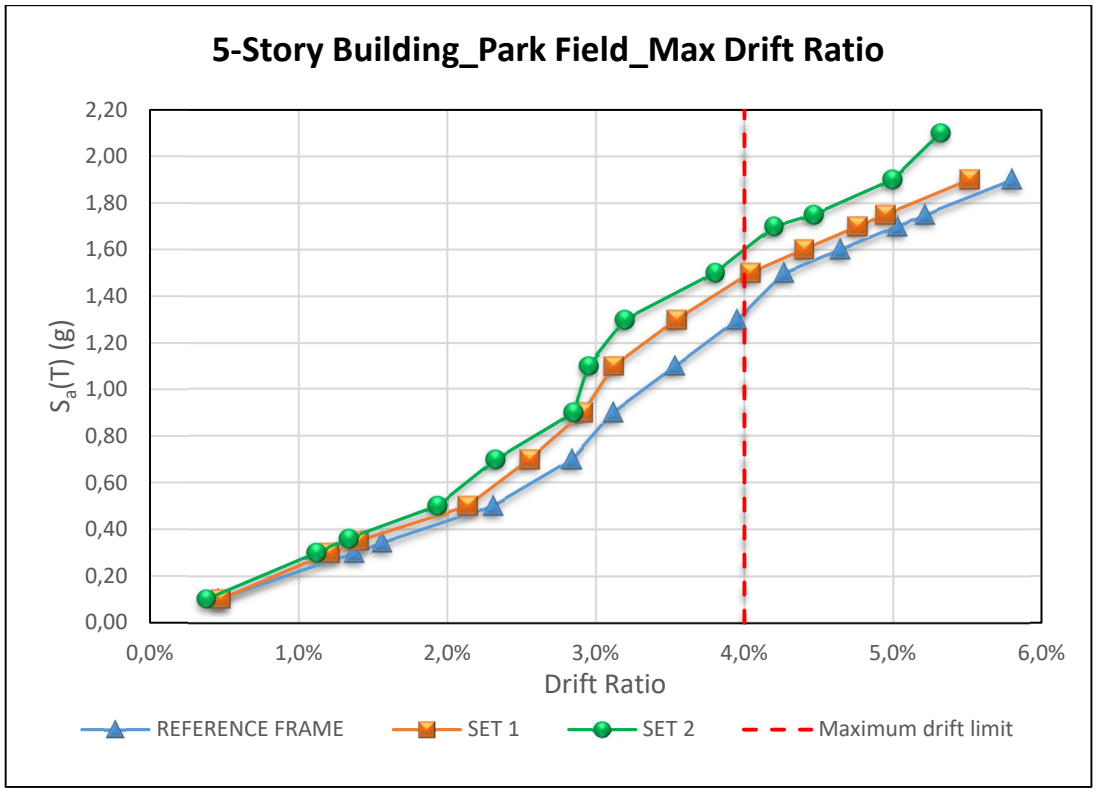


Figure 5.13: Max drift ratios of 5-story models under Park Field earthquake acceleration intensities.

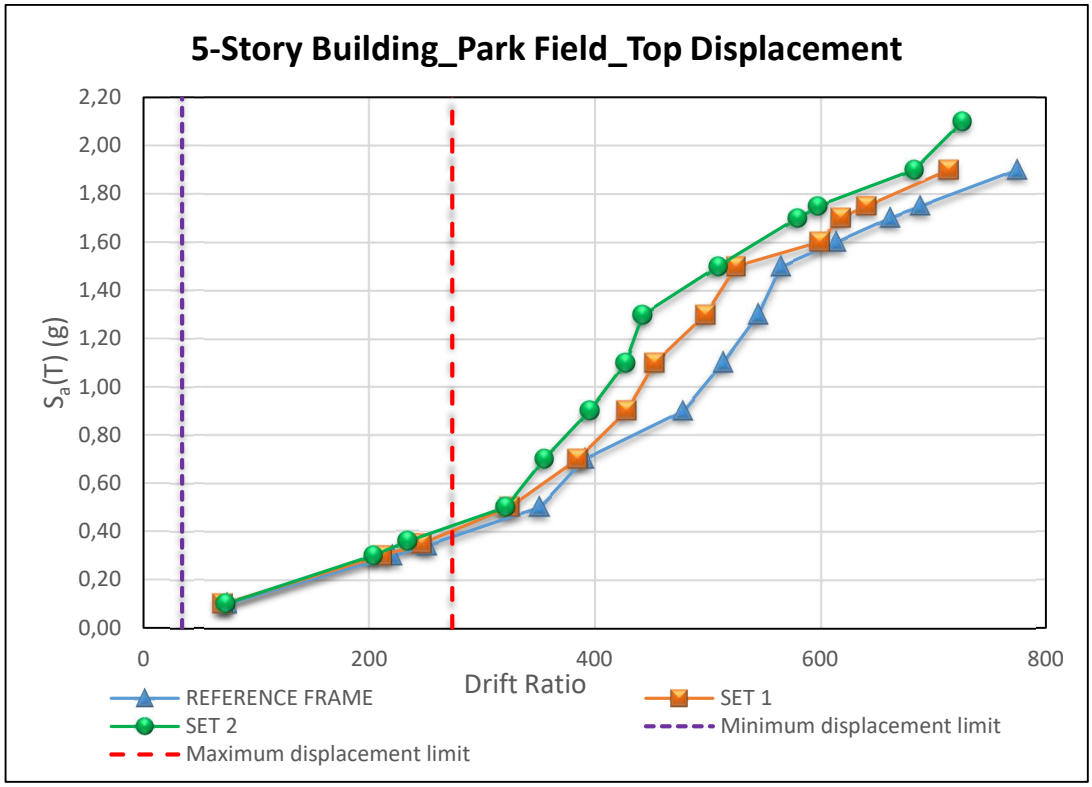


Figure 5.14: Max top displacements of 5-story models under Park Field earthquake acceleration intensities.

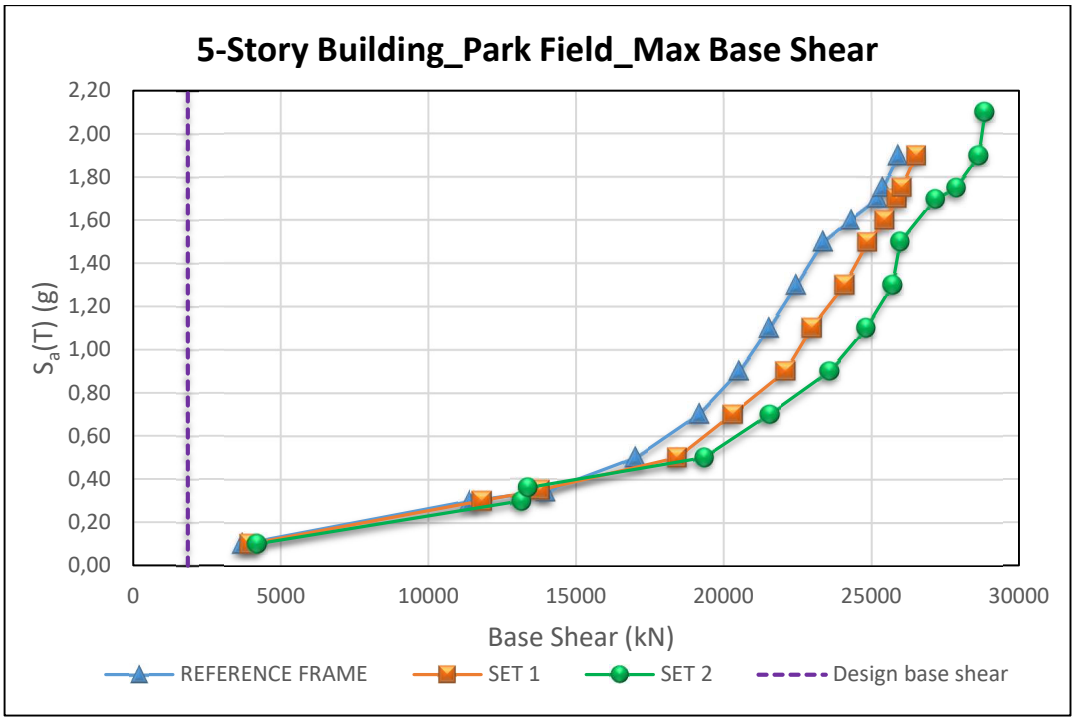


Figure 5.15: Max base shears of 5-story models under Park Field earthquake acceleration intensities.

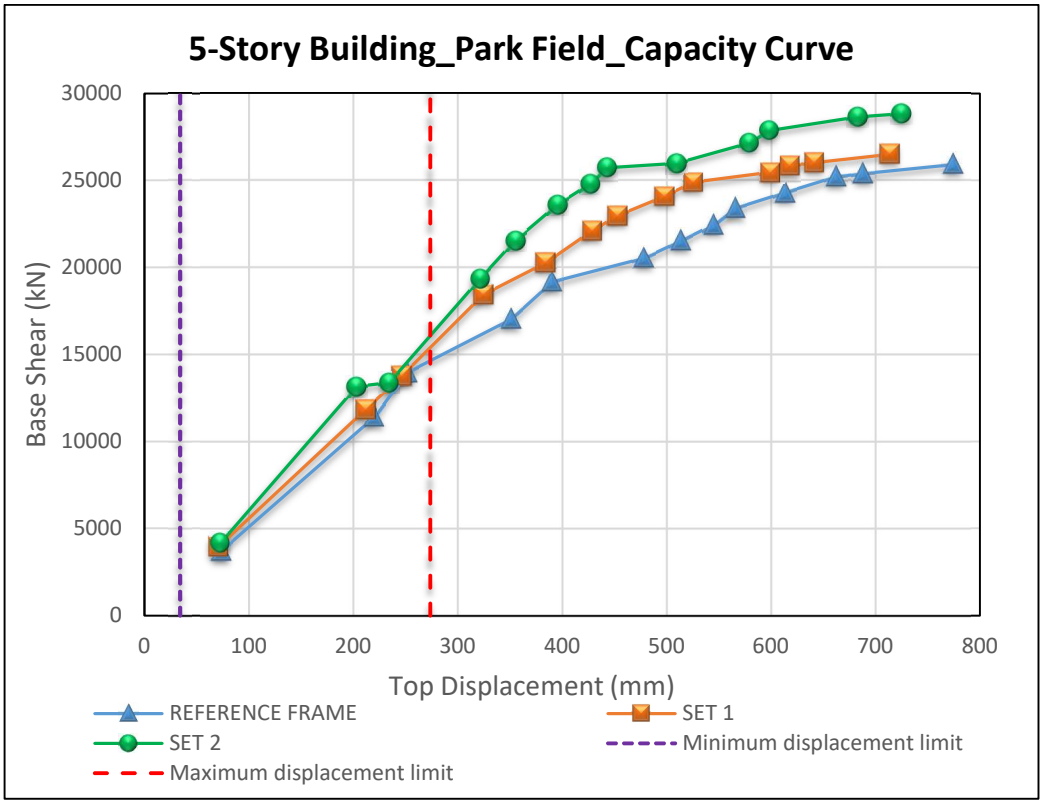
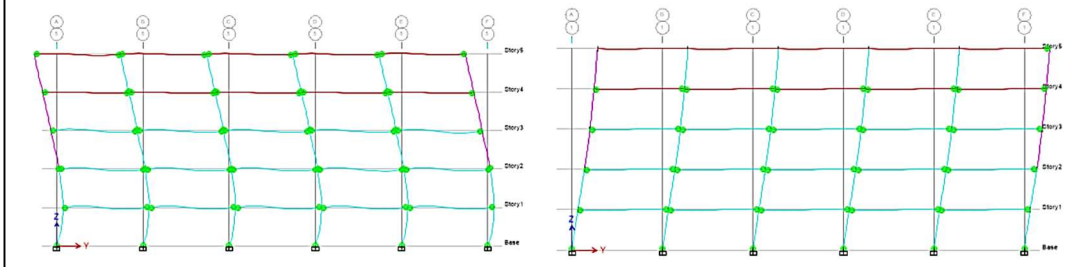


Figure 5.16: Capacity curves of 5-story models under Park Field earthquake acceleration intensities.

Table 5.4: Responses of 5-story models under Park Field earthquake.

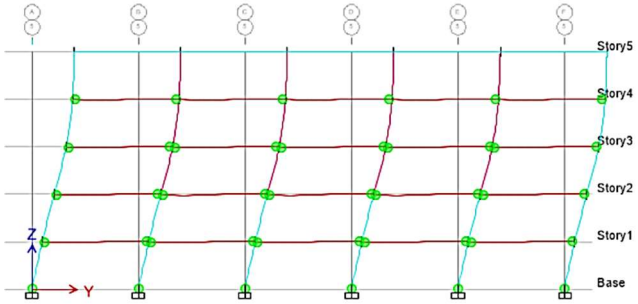
PARKFIELD / 5-STORY	S_a(T) values corresponding to drift ratio limit	S_a(T) values corresponding to maximum top displacement limit	The base shears corresponding to maximum top displacement
Reference Frame	1.30 g	0.38 g	14646.10 kN
Set-1	1.50 g	0.40 g	15404.23 kN
Set-2	1.60 g	0.43 g	16087.61 kN

The hinging and plastic rotation demands and drift ratio distributions along the structure height of all models at 1.60g acceleration intensity, where the 5-story Set-2 structure under the Park Field earthquake reached the 4.00% drift ratio limit;



Reference Frame- Max R3 Plastic = 3.880%

SET 1- Max R3 Plastic = 3.667%



SET 2- Max R3 Plastic = 3.321%

Figure 5.17: Hinging and plastic rotation demands of 5-story models at S_a=1.60g under the Park Field earthquake.

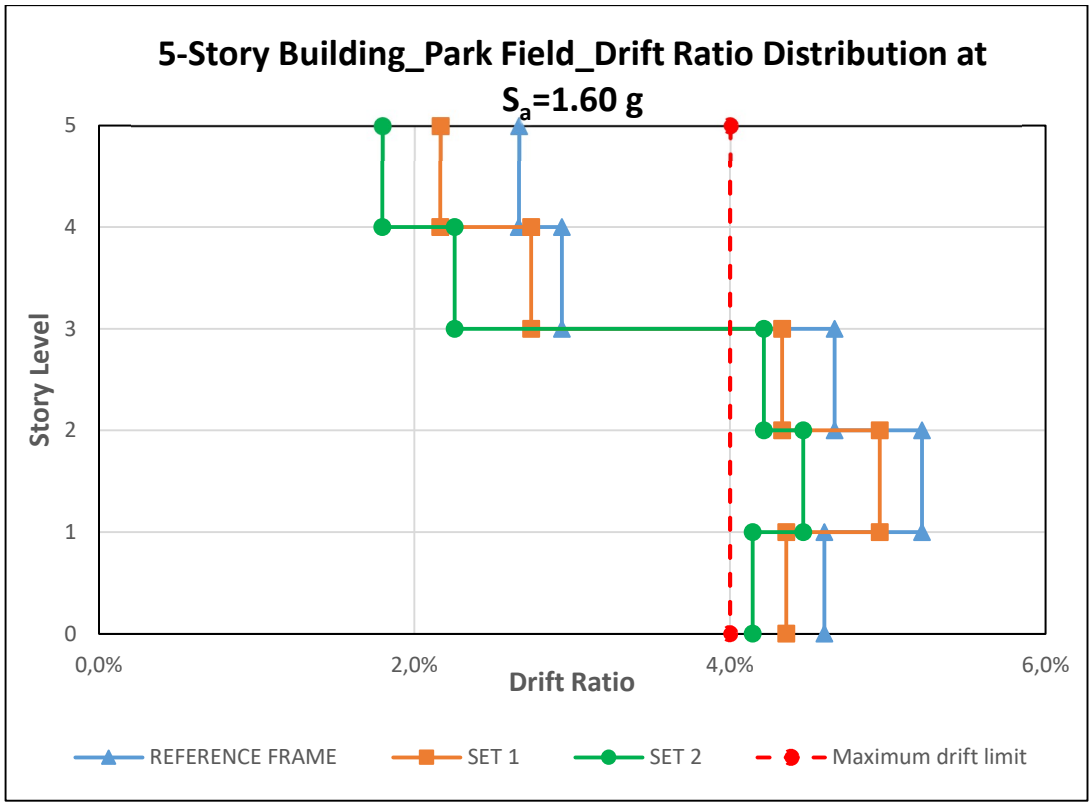


Figure 5.18: Drift ratio distributions along 5-story models' height at S_a=1.60g under the Park Field earthquake.

5.1.3 L'Aquila_4481 Earthquake

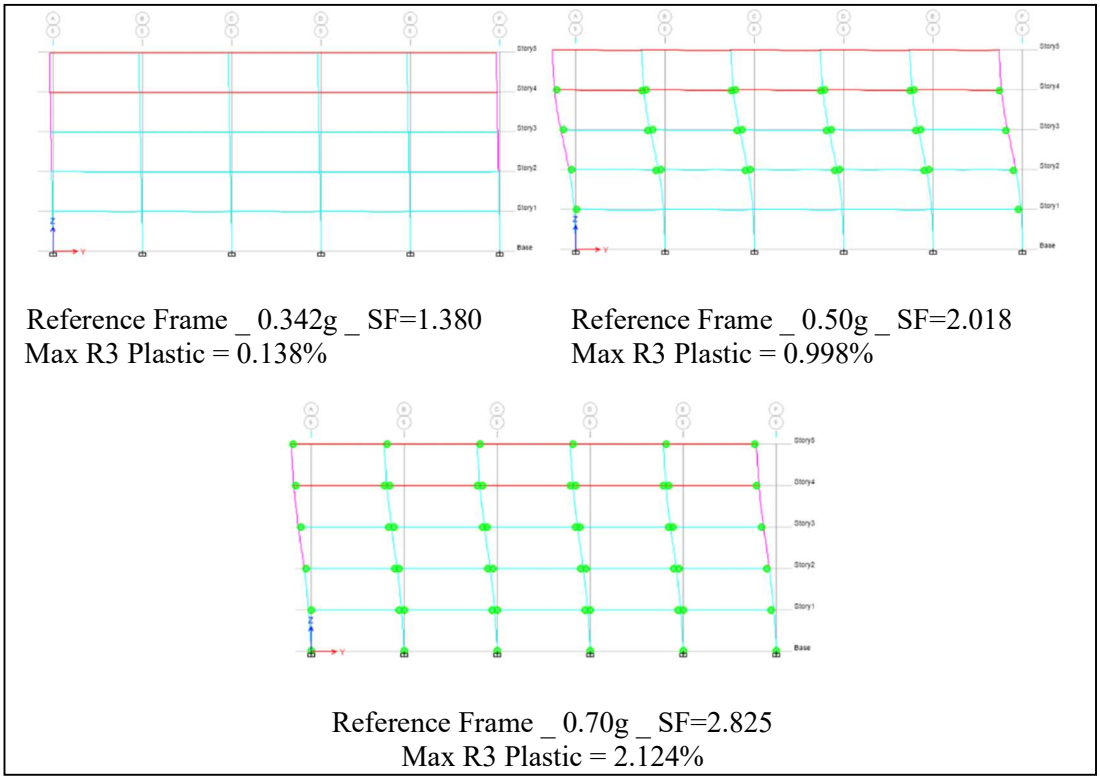
Table 5.5: SFs for 5-story models under the L'Aquila earthquake.

5 Story_Reference Frame		
(S_a)	(SF)	Scale
g	unitless	mm/s²
0,100	0,404	3957,197
0,200	0,807	7914,394
0,248	1,000	9806,650
0,342	**1,380**	**13534,405**
0,500	2,018	19785,985
0,700	2,825	27700,378
0,900	3,632	35614,772
1,100	4,439	43529,166
1,300	5,246	51443,560
1,500	6,053	59357,954

5 Story_Set 1		
(S_a)	(SF)	Scale
g	unitless	mm/s²
0,100	0,388	3800,709
0,200	0,775	7601,418
0,258	1,000	9806,650
0,350	**1,357**	**13311,603**
0,500	1,938	19003,545
0,700	2,713	26604,963
0,900	3,488	34206,380
1,100	4,263	41807,798
1,300	5,038	49409,216
1,500	5,813	57010,634

5 Story_Set 2		
(S_a)	(SF)	Scale
g	unitless	mm/s²
0,100	0,371	3641,187
0,200	0,743	7282,375
0,269	1,000	9806,650
0,360	**1,335**	**13093,710**
0,500	1,856	18205,937
0,700	2,599	25488,312
0,900	3,342	32770,687
1,100	4,084	40053,062
1,300	4,827	47335,437
1,500	5,569	54617,812

Application of acceleration intensities to 5-story models under L'Aquila earthquake in three stages starting from the acceleration intensities corresponding to the SF obtained from the design spectrum;

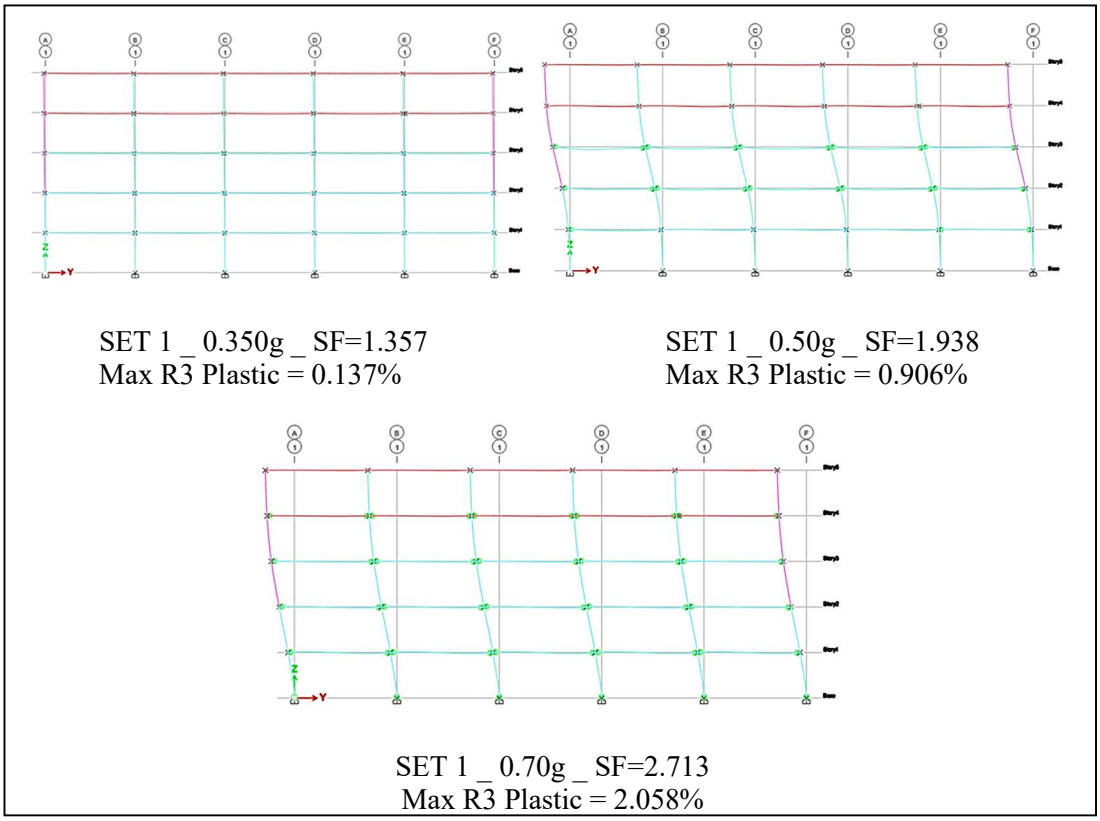


Reference Frame _ 0.342g _ SF=1.380
Max R3 Plastic = 0.138%

Reference Frame _ 0.50g _ SF=2.018
Max R3 Plastic = 0.998%

Reference Frame _ 0.70g _ SF=2.825
Max R3 Plastic = 2.124%

Figure 5.19: Hingings and plastic rotation demands of 5-story RFs under the L'Aquila earthquake.



SET 1 _ 0.350g _ SF=1.357
Max R3 Plastic = 0.137%

SET 1 _ 0.50g _ SF=1.938
Max R3 Plastic = 0.906%

SET 1 _ 0.70g _ SF=2.713
Max R3 Plastic = 2.058%

Figure 5.20: Hingings and plastic rotation demands of 5-story Set-1 under the L'Aquila earthquake.

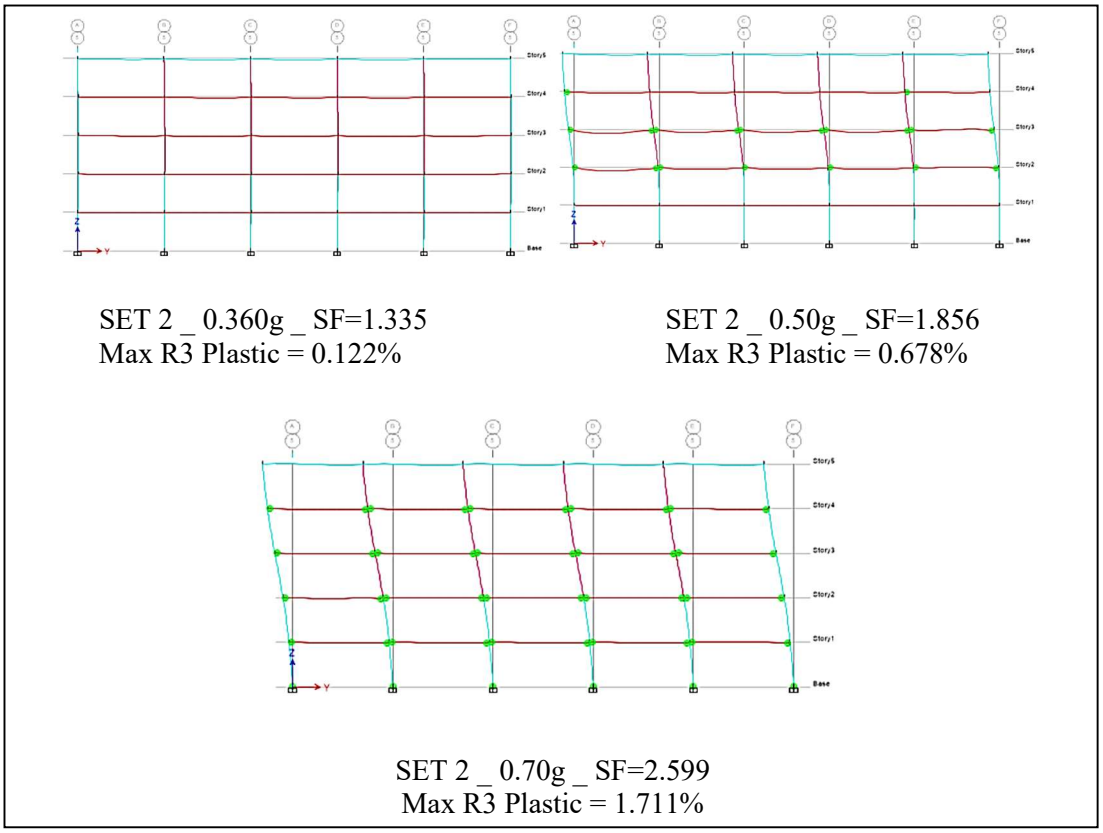


Figure 5.21: Hingings and plastic rotation demands of 5-story Set-2 under the L'Aquila earthquake.

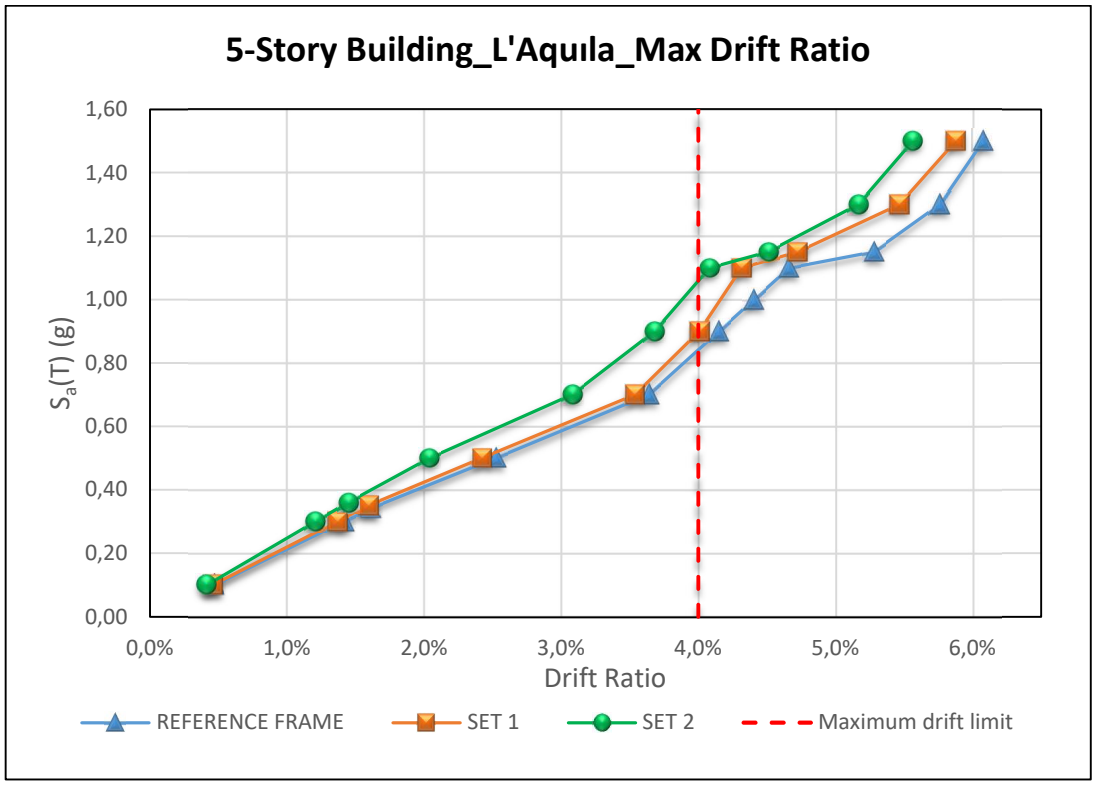


Figure 5.22: Max drift ratios of 5-story models under L'Aquila earthquake acceleration intensities.

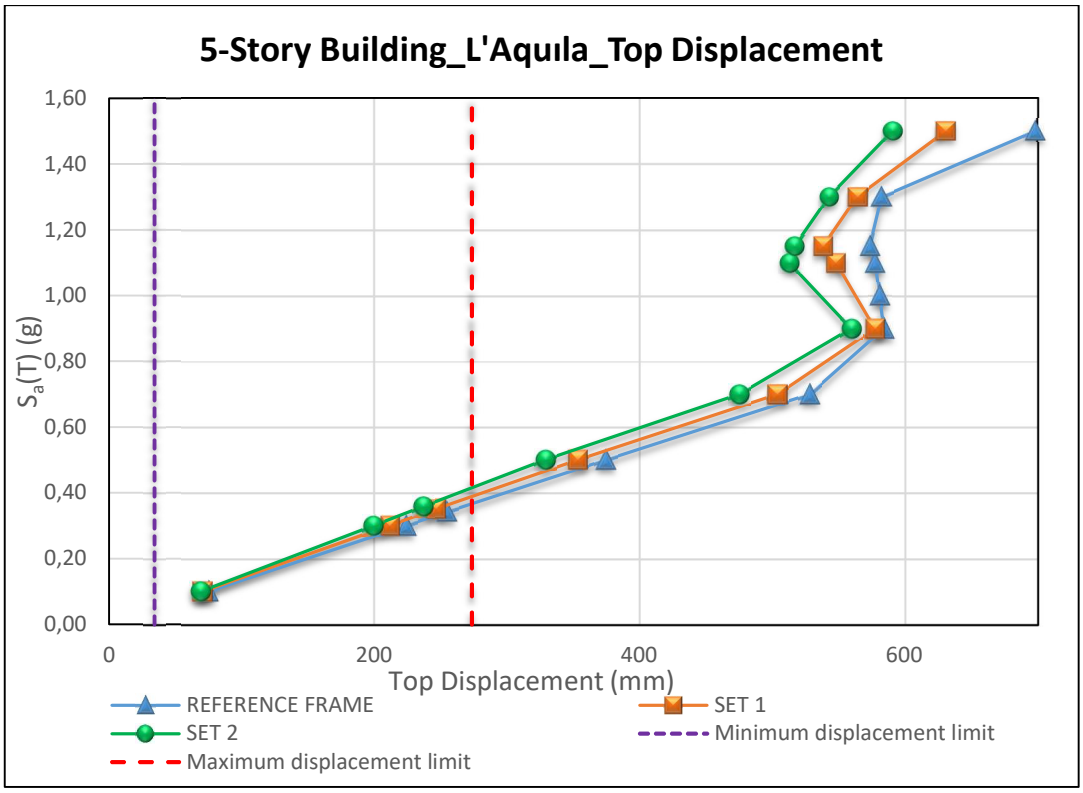


Figure 5.23: Max top displacements of 5-story models under L'Aquila earthquake acceleration intensities.

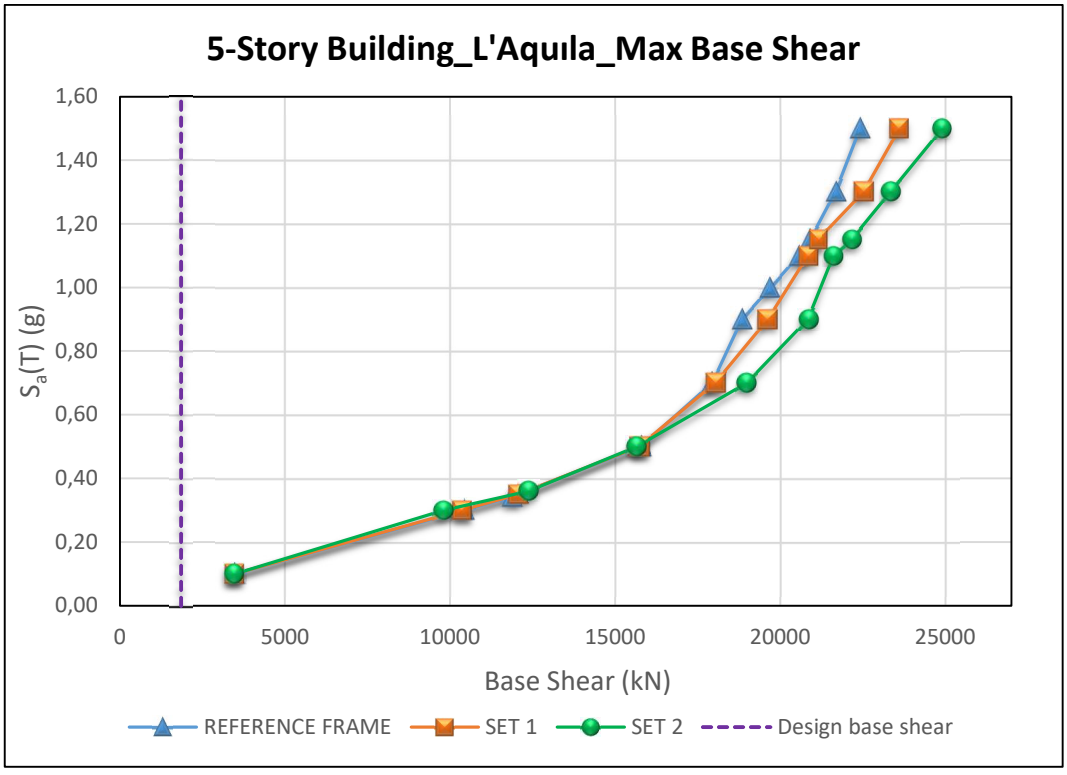


Figure 5.24: Max base shears of 5-story models under L'Aquila earthquake acceleration intensities.

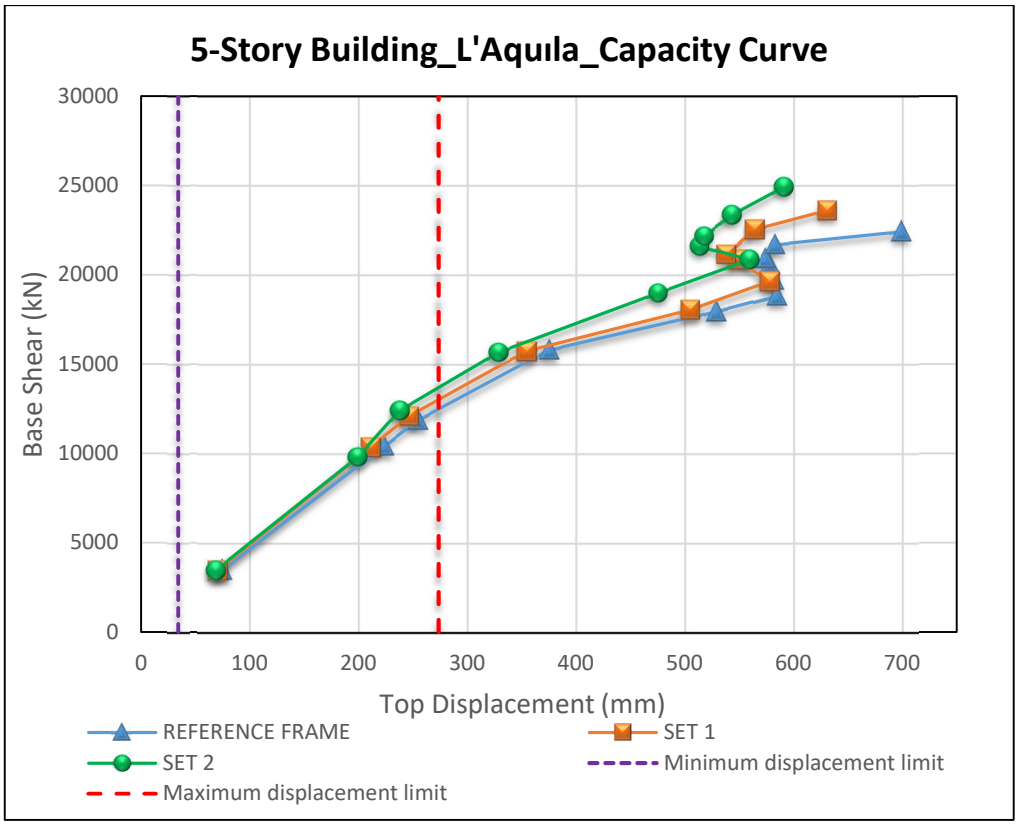


Figure 5.25: Capacity curves of 5-story models under L'Aquila earthquake acceleration intensities.

Table 5.6: Responses of 5-story models under L'Aquila earthquake.

LAQUILA / 5-STORY	$S_a(T)$ values corresponding to drift ratio limit	$S_a(T)$ values corresponding to maximum top displacement limit	The base shears corresponding to maximum top displacement
Reference Frame	0.85 g	0.36 g	12483.86 kN
Set-1	0.90 g	0.39 g	13004.10 kN
Set-2	1.10 g	0.42 g	13683.06 kN

The hinging and plastic rotation demands and drift ratio distributions along the structure height of all models at 1.10g acceleration intensity, where the 5-story Set-2 structure under the L'Aquila earthquake reached the 4.00% drift ratio limit;

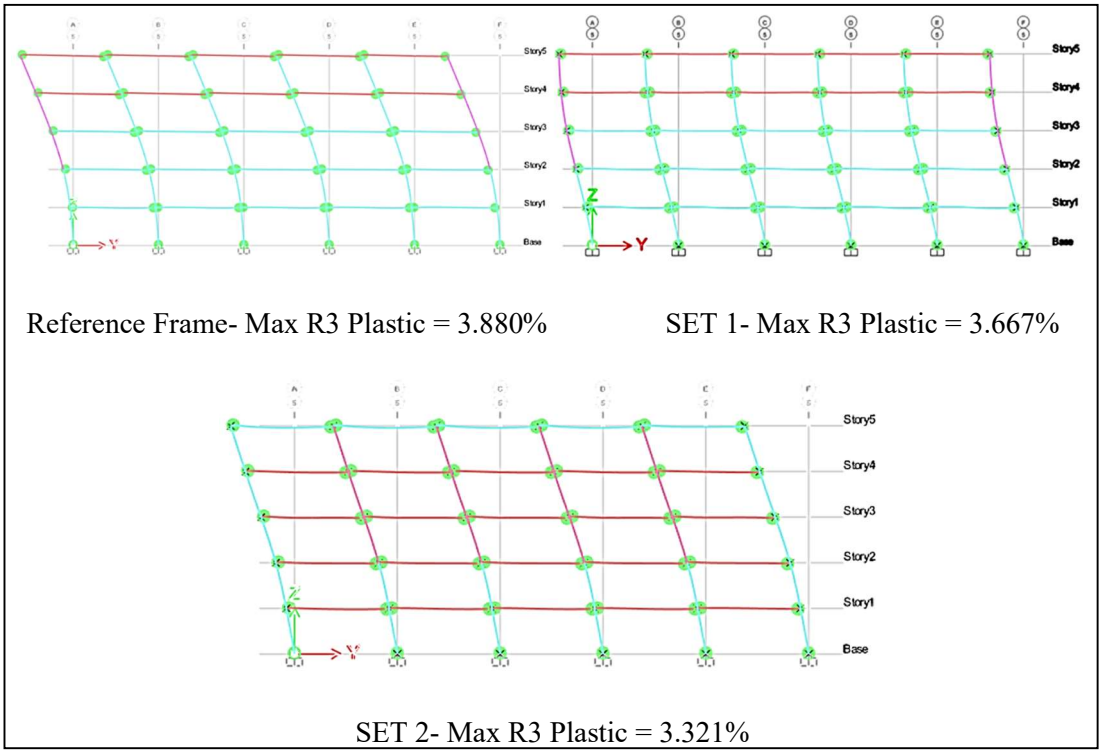


Figure 5.26: Hinging and plastic rotation demands of 5-story models at S_a=1.10g under the L'Aquila earthquake.

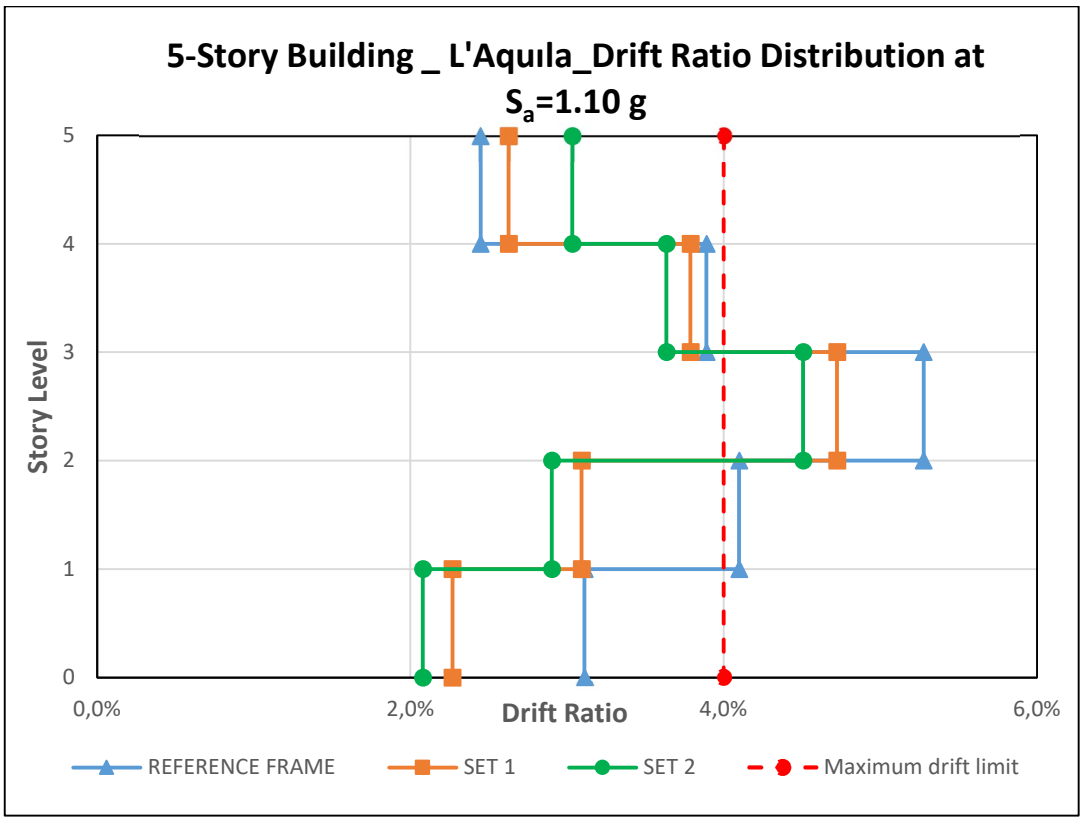


Figure 5.27: Drift ratio distributions along 5-story models' height at S_a=1.10g under the L'Aquila earthquake.

5.1.4 Kobe_1111 Earthquake

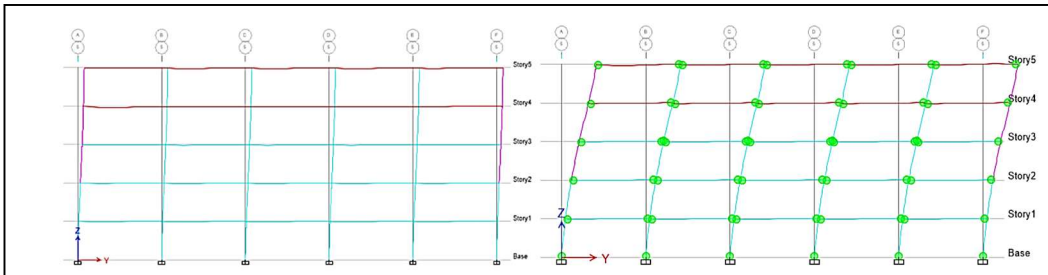
Table 5.7: SFs for 5-story models under the Kobe earthquake.

5 Story_Reference Frame		
(S_a)	(SF)	Scale
g	unitless	mm/s²
0,100	0,466	4571,769
0,200	0,932	9143,537
0,215	1,000	9806,650
0,300	1,399	13715,306
0,342	**1,594**	**15636,363**
0,500	2,331	22858,843
0,700	3,263	32002,380
0,800	3,730	36574,148

5 Story_Set 1		
(S_a)	(SF)	Scale
g	unitless	mm/s²
0,100	0,471	4616,965
0,200	0,942	9233,929
0,212	1,000	9806,650
0,300	1,412	13850,894
0,350	**1,649**	**16170,457**
0,500	2,354	23084,823
0,700	3,296	32318,752
0,800	3,766	36935,716

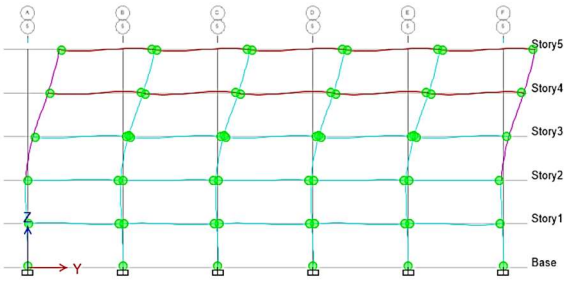
5 Story_Set 2		
(S_a)	(SF)	Scale
g	unitless	mm/s²
0,100	0,469	4599,096
0,200	0,938	9198,192
0,213	1,000	9806,650
0,300	1,407	13797,289
0,360	**1,686**	**16538,350**
0,500	2,345	22995,481
0,700	3,283	32193,673
0,800	3,752	36792,770

Application of acceleration intensities to 5-story models under Kobe earthquake in three stages starting from the acceleration intensities corresponding to the SF obtained from the design spectrum;



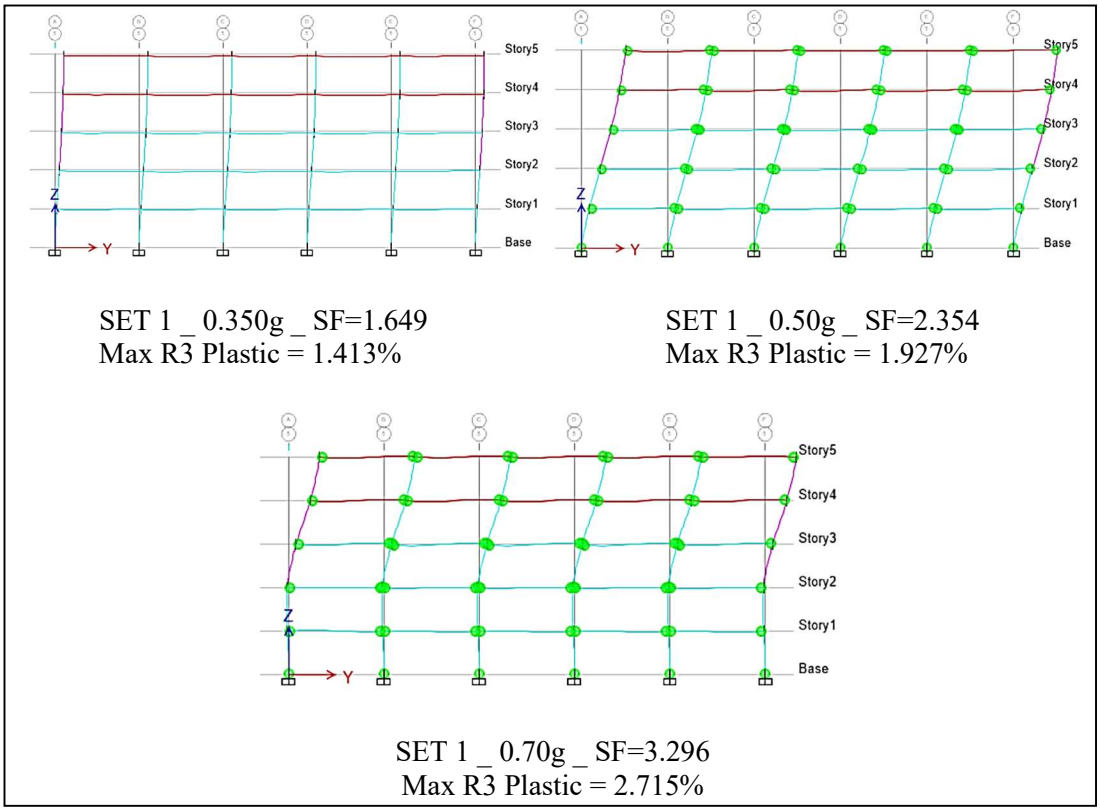
Reference Frame _ 0.342g _ SF=1.594
Max R3 Plastic = 1.524

Reference Frame _ 0.50g _ SF=2.331
Max R3 Plastic = 2.022%



Reference Frame _ 0.70g _ SF=3.263
Max R3 Plastic = 2.939%

Figure 5.28: Hingings and plastic rotation demands of 5-story RFs under the Kobe earthquake.

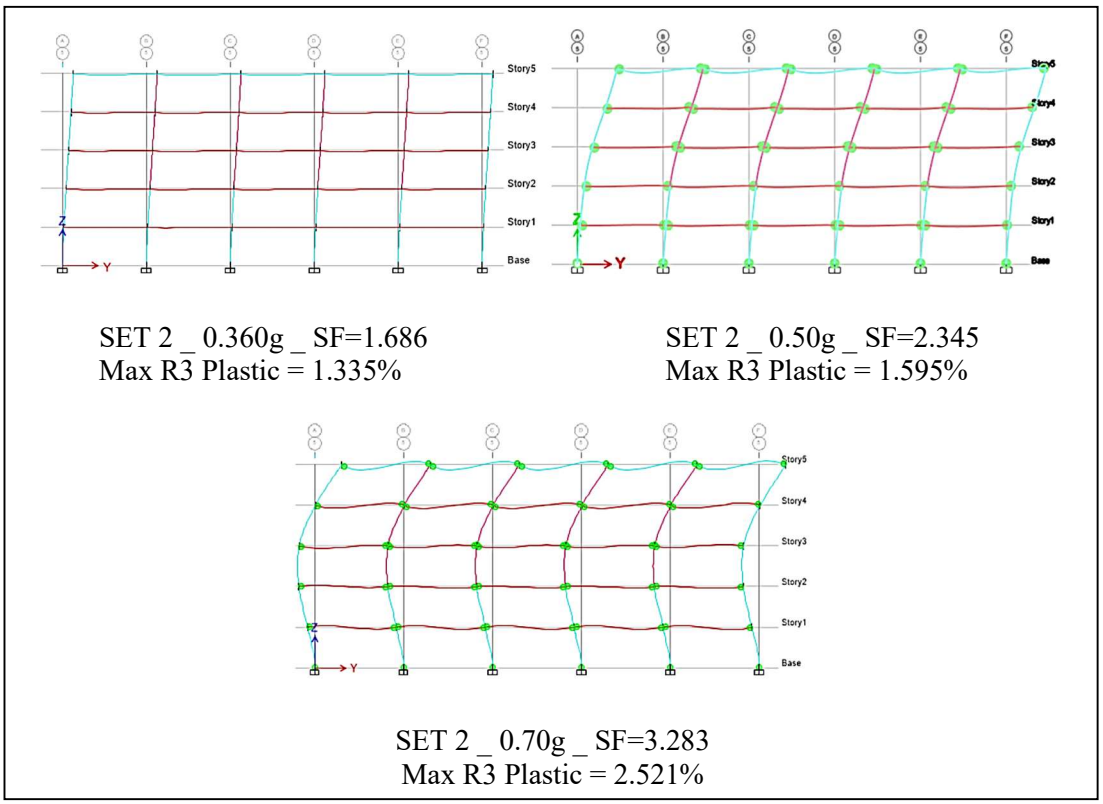


SET 1 _ 0.350g _ SF=1.649
Max R3 Plastic = 1.413%

SET 1 _ 0.50g _ SF=2.354
Max R3 Plastic = 1.927%

SET 1 _ 0.70g _ SF=3.296
Max R3 Plastic = 2.715%

Figure 5.29: Hingings and plastic rotation demands of 5-story Set-1 under the Kobe earthquake.



SET 2 _ 0.360g _ SF=1.686
Max R3 Plastic = 1.335%

SET 2 _ 0.50g _ SF=2.345
Max R3 Plastic = 1.595%

SET 2 _ 0.70g _ SF=3.283
Max R3 Plastic = 2.521%

Figure 5.30: Hingings and plastic rotation demands of 5-story Set-2 under the Kobe earthquake.

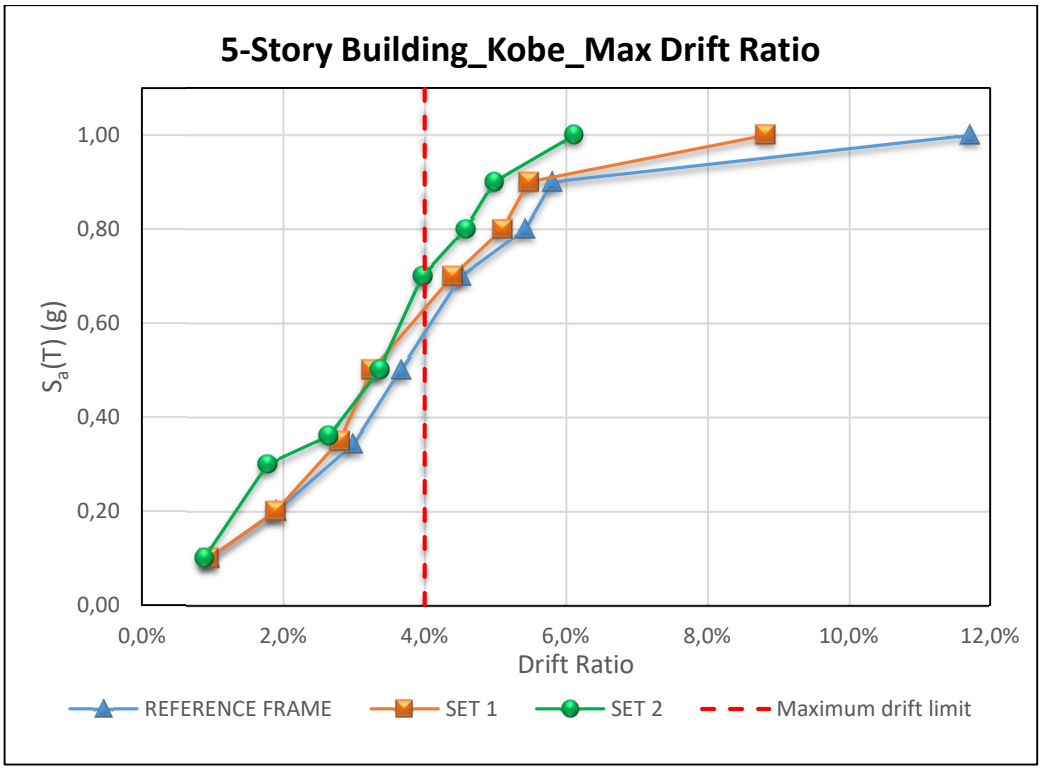


Figure 5.31: Max drift ratios of 5-story models under Kobe earthquake acceleration intensities.

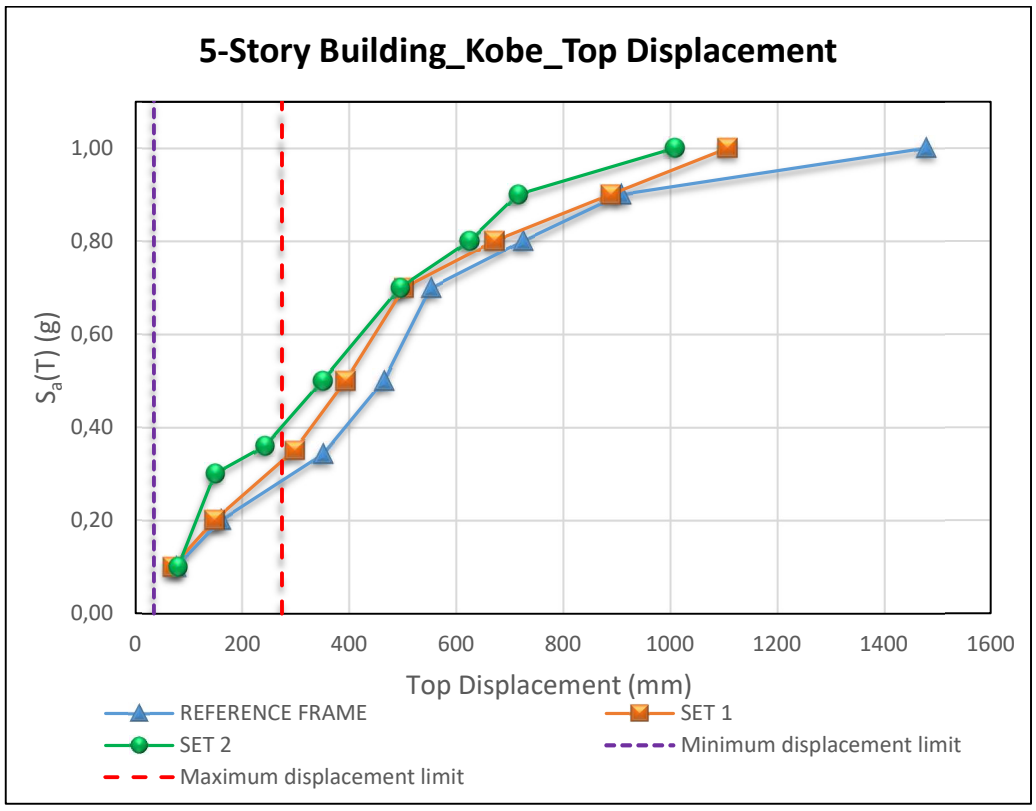


Figure 5.32: Max top displacements of 5-story models under Kobe earthquake acceleration intensities.

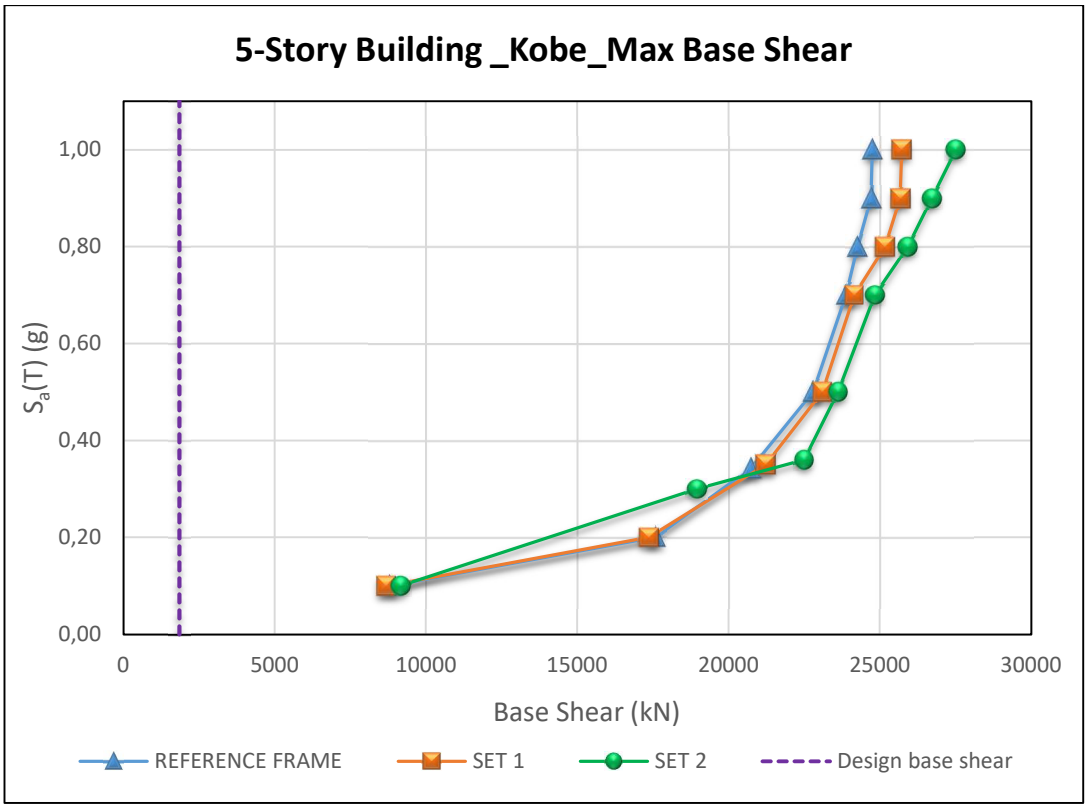


Figure 5.33: Max base shears of 5-story models under Kobe earthquake acceleration intensities.

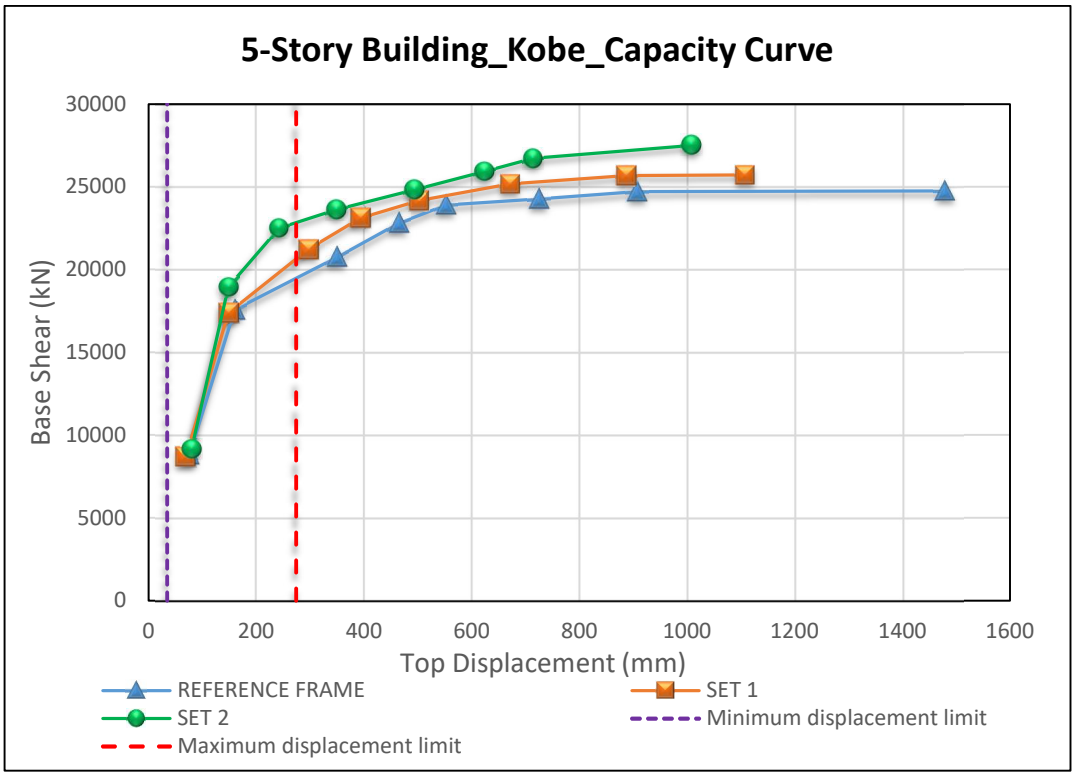


Figure 5.34: Capacity curves of 5-story models under Kobe earthquake acceleration intensities.

Table 5.8: Responses of 5-story models under Kobe earthquake.

KOBE / 5-STORY	$S_a(T)$ values corresponding to drift ratio limit	$S_a(T)$ values corresponding to maximum top displacement limit	The base shears corresponding to maximum top displacement
Reference Frame	0.58 g	0.29 g	19743.00 kN
Set-1	0.63 g	0.33 g	20640.88 kN
Set-2	0.70 g	0.40 g	22826.58 kN

The hinging and plastic rotation demands and drift ratio distributions along the structure height of all models at 0.70g acceleration intensity, where the 5-story Set-2 structure under the Kobe earthquake reached the 4.00% drift ratio limit;

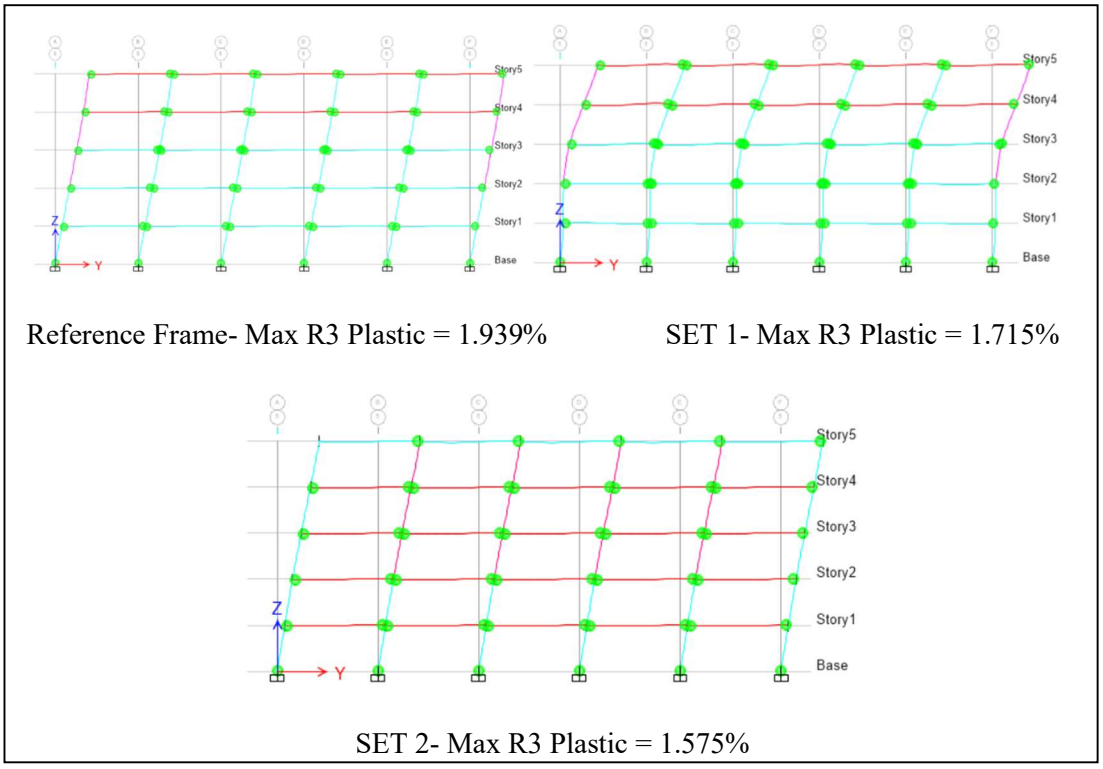


Figure 5.35: Hinging and plastic rotation demands of 5-story models at S_a=0.70g under the Kobe earthquake.

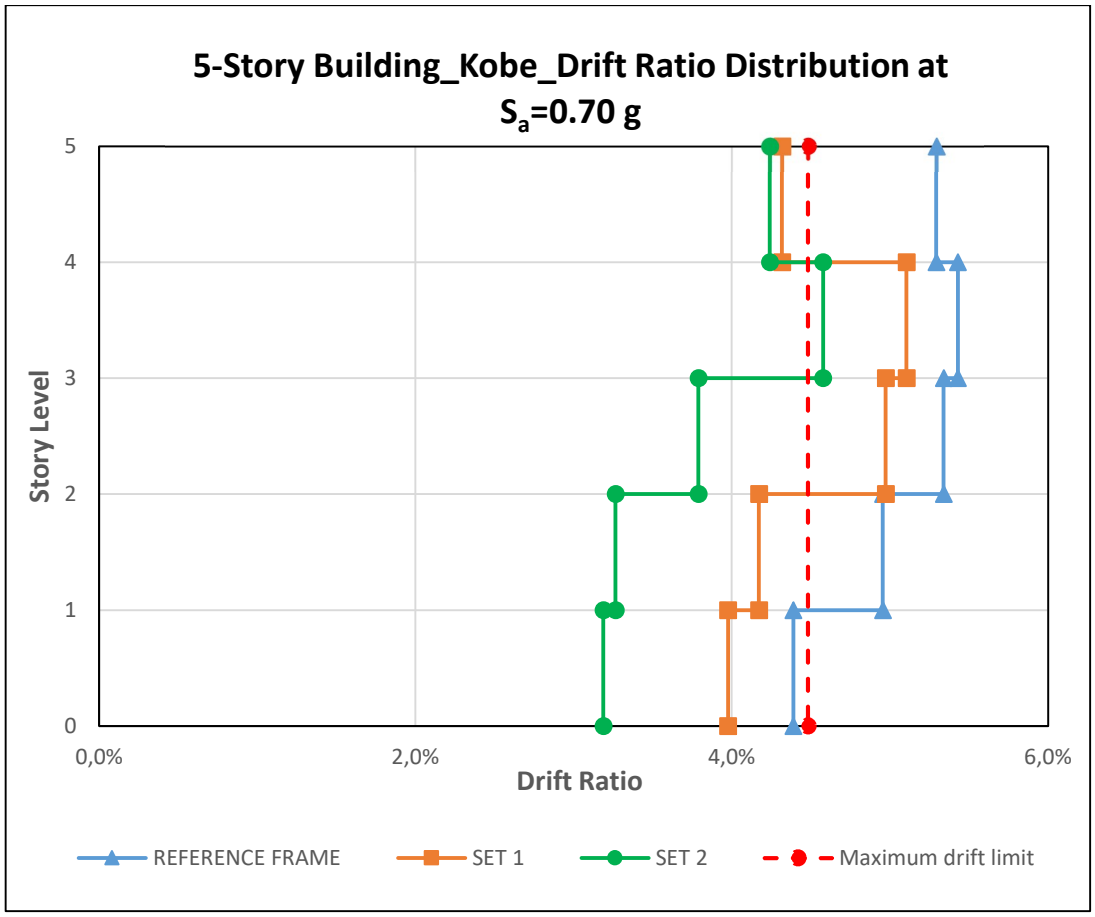


Figure 5.36: Drift ratio distributions along 5-story models' heightt at S_a=0.70g under the Kobe earthquake.

5.1.5 New Zealand_587 Earthquake

Table 5.9: SFs for 5-story models under the New Zealand earthquake.

5 Story_Reference Frame		
(S_a)	(SF)	Scale
g	unitless	mm/s²
0,100	0,720	7063,238
0,139	1,000	9806,650
0,200	1,440	14126,477
0,342	**2,463**	**24157,688**
0,500	3,601	35316,192
0,700	5,042	49442,669
0,900	6,482	63569,146
1,100	7,923	77695,623
1,300	9,363	91822,100
1,500	10,804	105948,577

5 Story_Set 1		
(S_a)	(SF)	Scale
g	unitless	mm/s²
0,100	0,649	6362,914
0,154	1,000	9806,650
0,200	1,298	12725,828
0,350	**2,272**	**22285,469**
0,500	3,244	31814,569
0,700	4,542	44540,397
0,900	5,840	57266,224
1,100	7,137	69992,052
1,300	8,435	82717,879
1,500	9,733	95443,707

5 Story_Set 2		
(S_a)	(SF)	Scale
g	unitless	mm/s²
0,100	0,577	5661,973
0,173	1,000	9806,650
0,200	1,155	11323,945
0,360	**2,076**	**20360,454**
0,500	2,887	28309,864
0,700	4,042	39633,809
0,900	5,196	50957,755
1,100	6,351	62281,700
1,300	7,506	73605,645
1,500	8,660	84929,591

Application of acceleration intensities to 5-story models under New Zealand earthquake in three stages starting from the acceleration intensities corresponding to the SF obtained from the design spectrum;

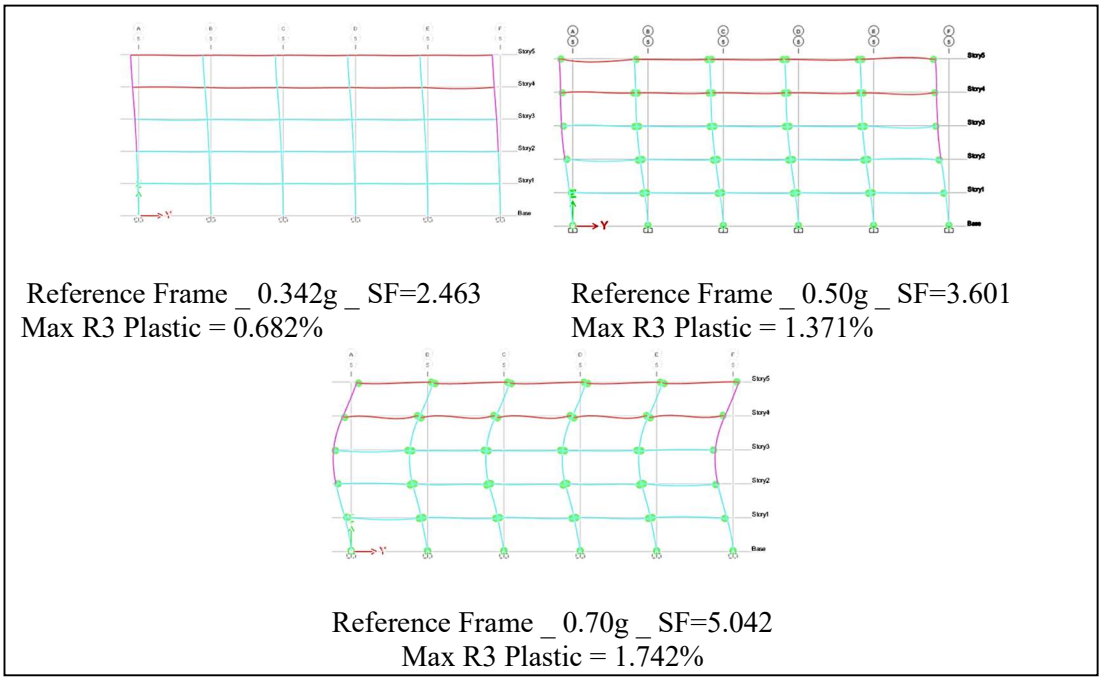


Figure 5.37: Hingings and plastic rotation demands of 5-story RFs under the New Zealand earthquake.

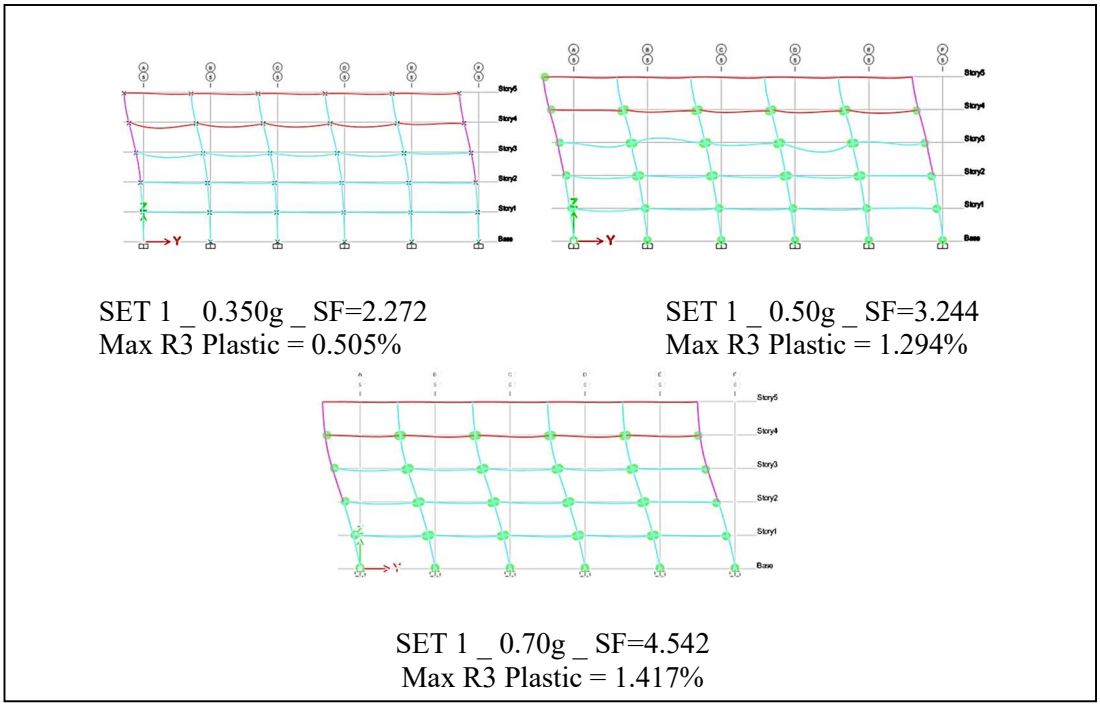


Figure 5.38: Hingings and plastic rotation demands of 5-story Set-1 under the New Zealand earthquake.

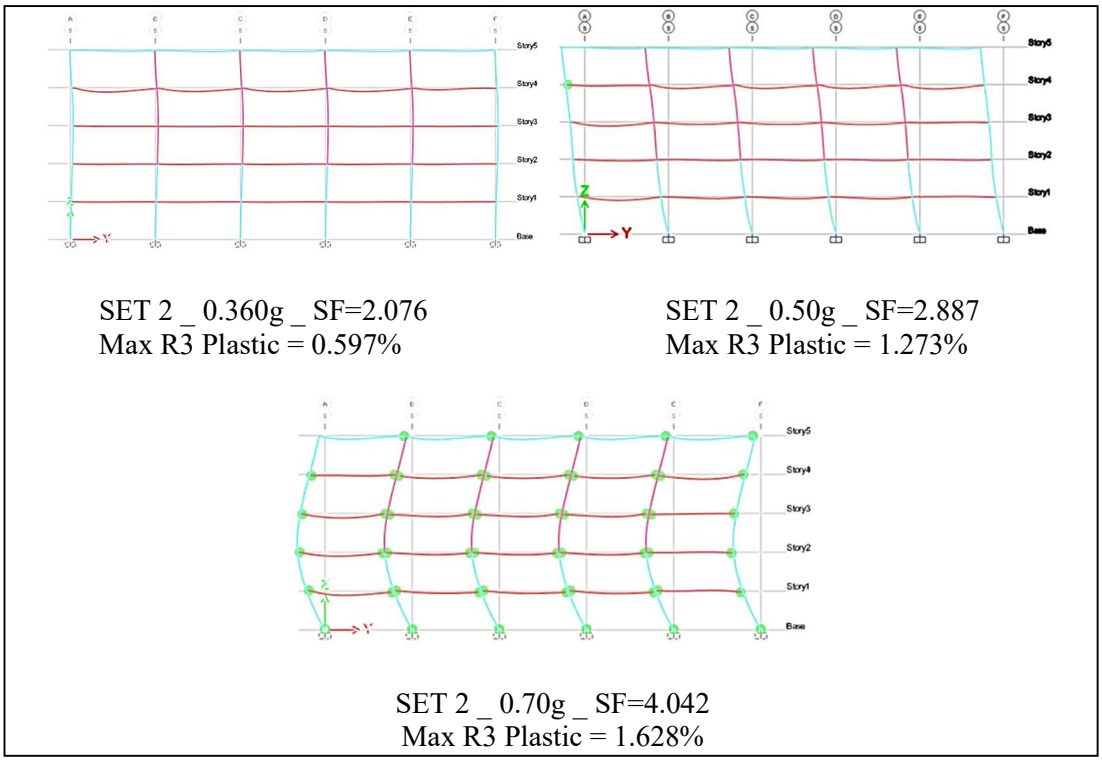


Figure 5.39: Hingings and plastic rotation demands of 5-story Set-2 under the New Zealand earthquake.

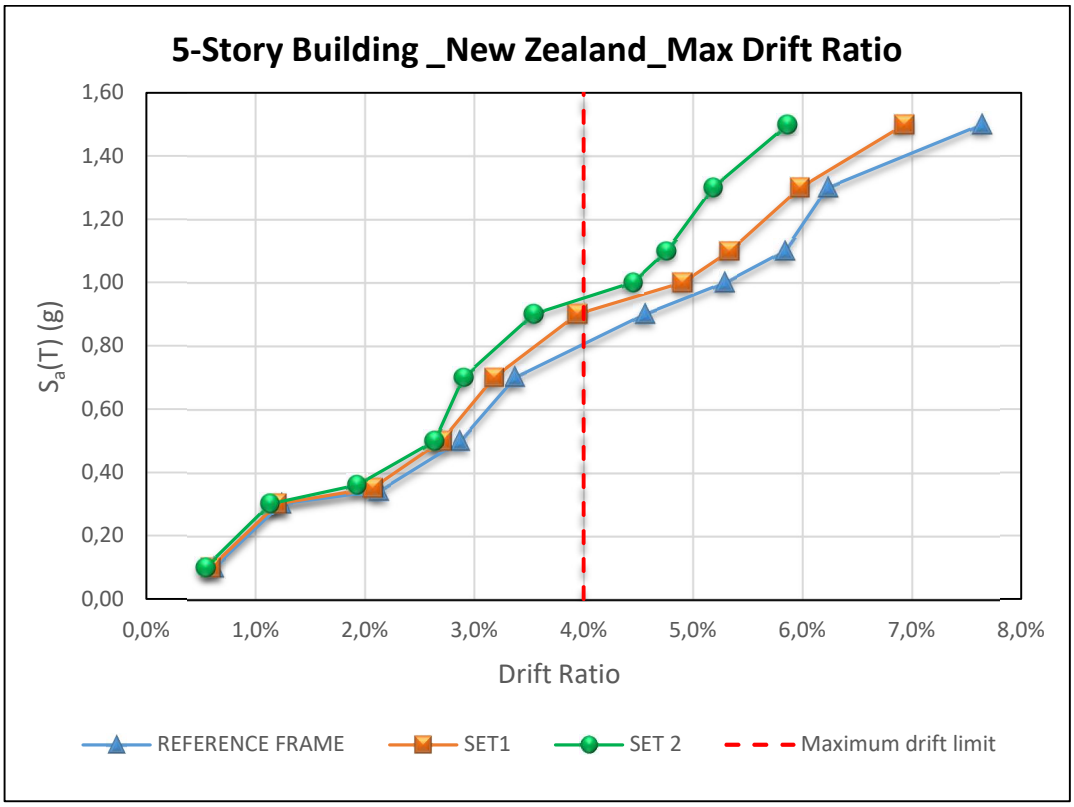


Figure 5.40: Max drift ratios of 5-story models under New Zealand earthquake acceleration intensities.

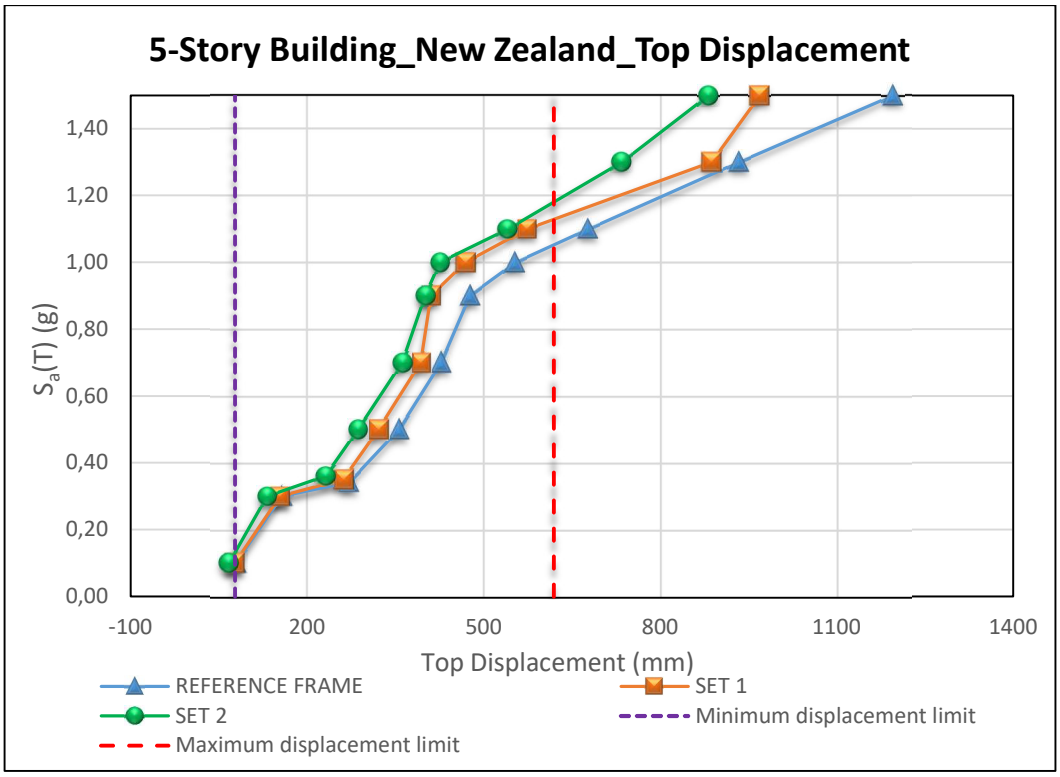


Figure 5.41: Max top displacements of 5-story models under New Zealand earthquake acceleration intensities.

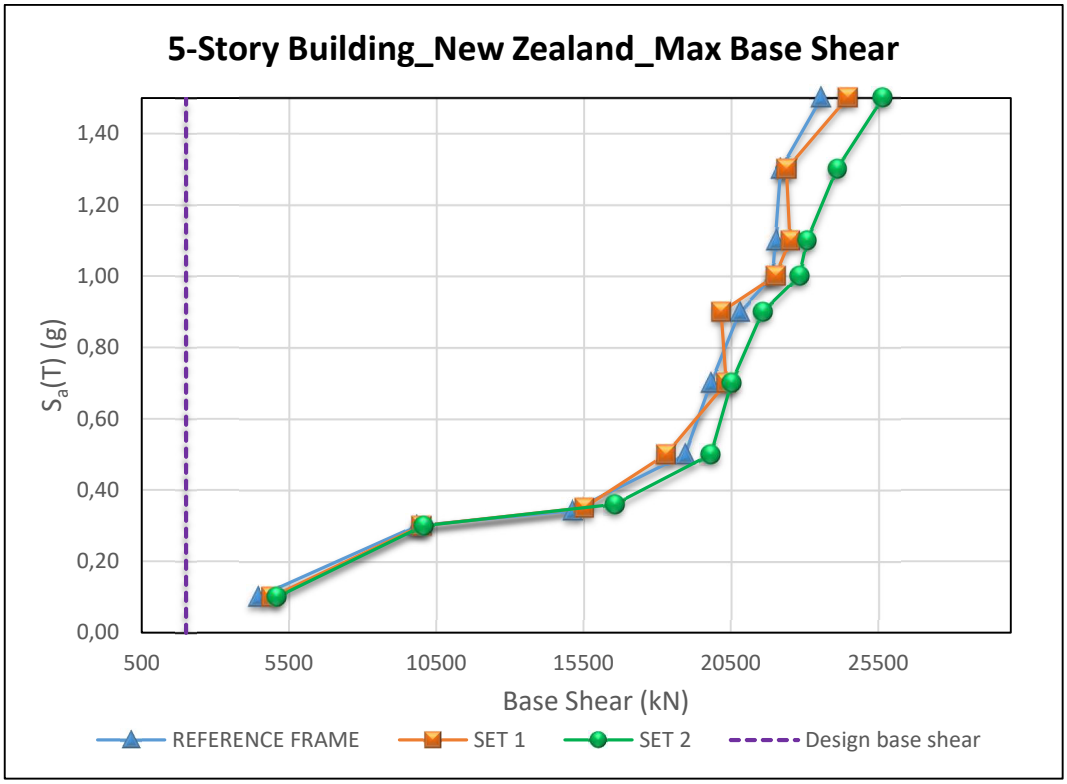


Figure 5.42: Max base shears of 5-story models under New Zealand earthquake acceleration intensities.

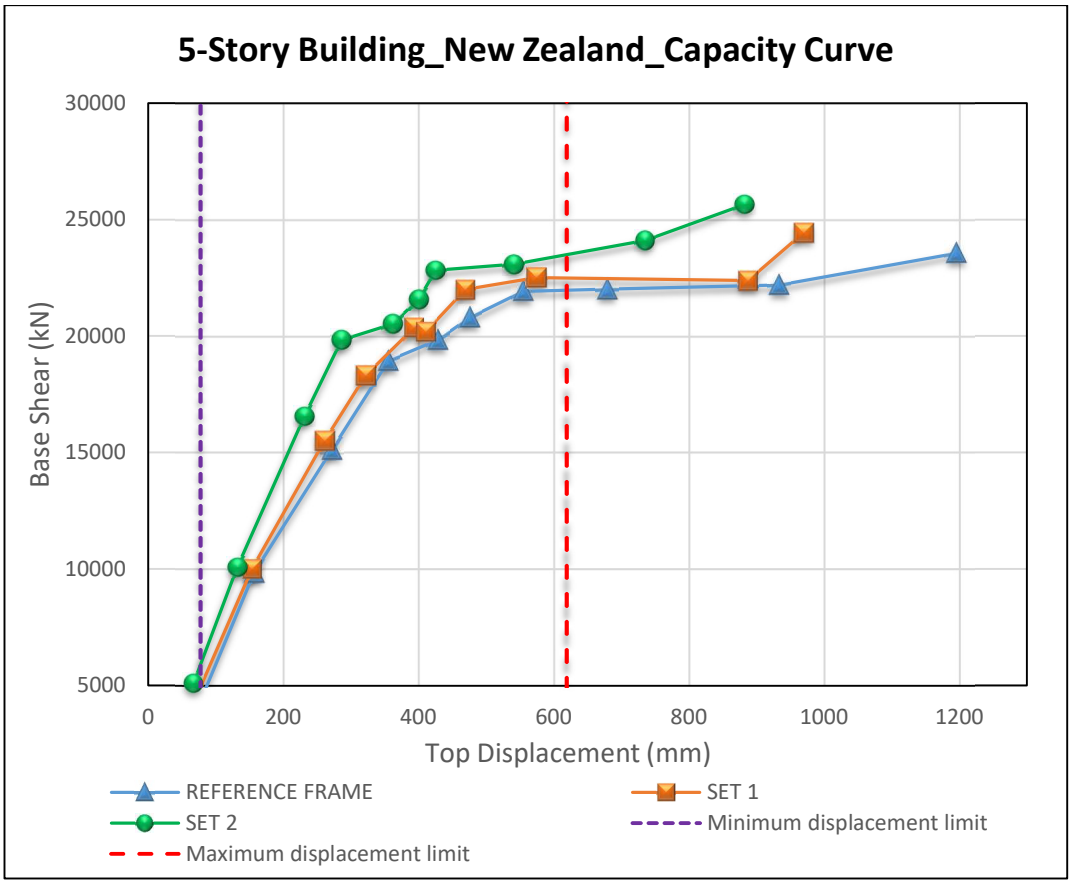


Figure 5.43: Capacity curves of 5-story models under New Zealand earthquake acceleration intensities.

Table 5.10: Responses of 5-story models under New Zealand earthquake.

NEW ZEALAND / 5-STORY	$S_a(T)$ values corresponding to drift ratio limit	$S_a(T)$ values corresponding to maximum top displacement limit	The base shears corresponding to maximum top displacement
Reference Frame	0.80 g	0.35 g	15226.72 kN
Set-1	0.90 g	0.38 g	16099.83 kN
Set-2	0.95 g	0.47 g	19093.38 kN

The hinging and plastic rotation demands and drift ratio distributions along the structure height of all models at 0.95g acceleration intensity, where the 5-story Set-2 structure under the New Zealand earthquake reached the 4.00% drift ratio limit;

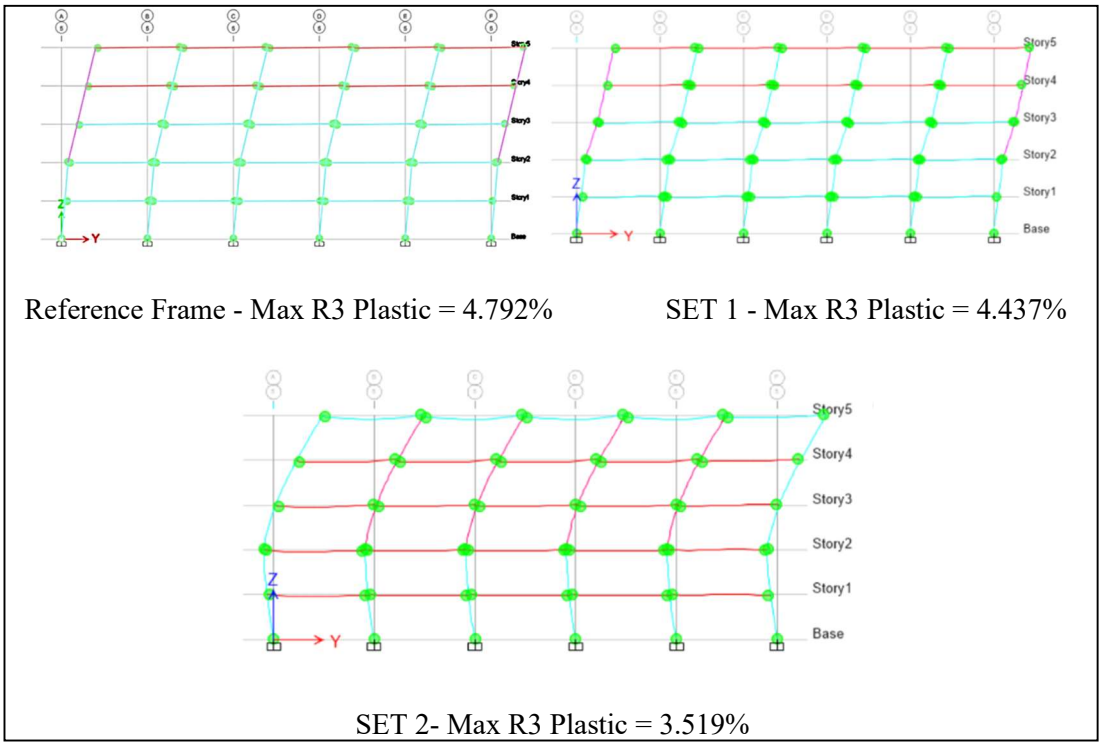


Figure 5.44: Hinging and plastic rotation demands of 5-story models at S_a=0.95g under the New Zealand earthquake.

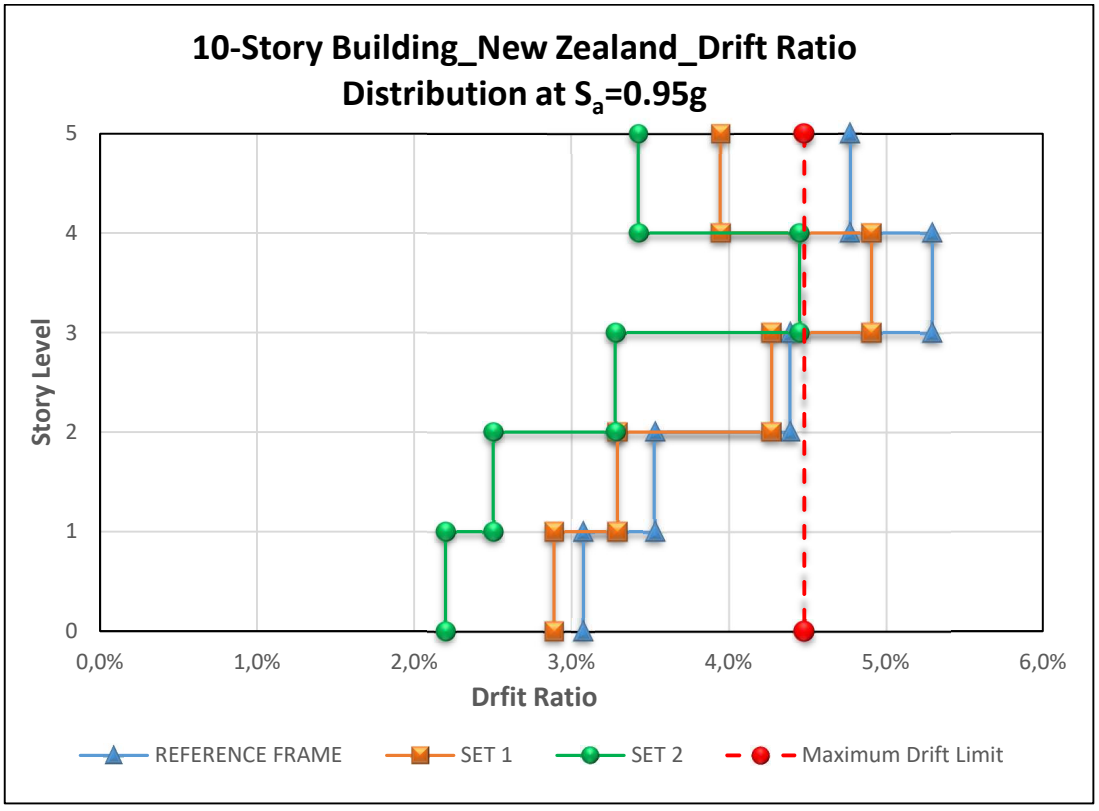


Figure 5.45: Drift ratio distributions along 5-story models' height at S_a=0.95g under the New Zealand earthquake.

5.1.6 Morgan Hill_451 Earthquake

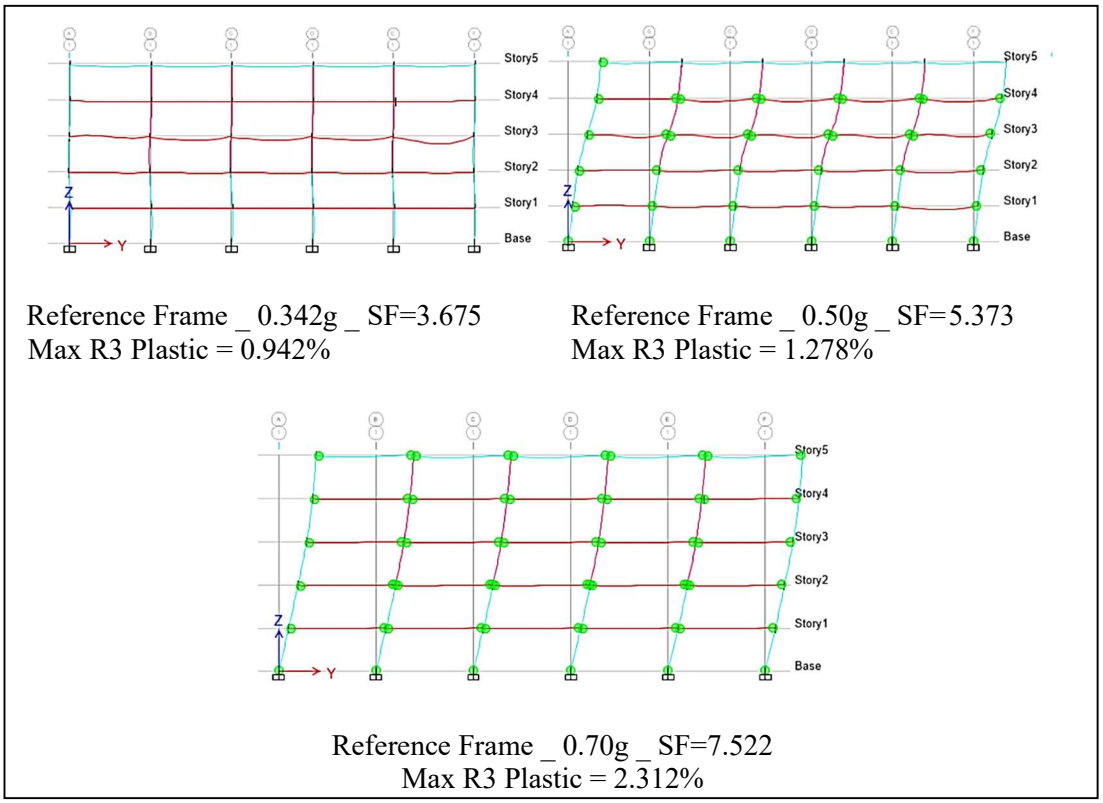
Table 5.11: SFs for 5-story models under the Morgan Hill earthquake.

5 Story_Reference Frame		
(S_a)	(SF)	Scale
g	unitless	mm/s²
0,093	1,000	9806,650
0,100	1,075	10537,706
0,200	2,149	21075,413
0,342	**3,675**	**36041,063**
0,500	5,373	52688,532
0,700	7,522	73763,944
0,900	9,671	94839,357
1,100	11,820	115914,770
1,300	13,969	136990,182

5 Story_Set 1		
(S_a)	(SF)	Scale
g	unitless	mm/s²
0,100	1,145	11228,170
0,087	1,000	9806,650
0,200	2,290	22456,341
0,350	**4,010**	**39325,544**
0,500	5,725	56140,851
0,700	8,015	78597,192
0,900	10,305	101053,532
1,100	12,595	123509,873
1,300	14,884	145966,213

5 Story_Set 2		
(S_a)	(SF)	Scale
g	unitless	mm/s²
0,100	1,201	11781,71
0,083	1,000	9806,65
0,200	2,403	23563,41
0,360	**4,320**	**42367,01**
0,500	6,007	58908,53
0,700	8,410	82471,94
0,900	10,813	106035,35
1,100	13,215	129598,76
1,300	15,618	153162,17

Application of acceleration intensities to 5-story models under Morgan Hill earthquake in three stages starting from the acceleration intensities corresponding to the SF obtained from the design spectrum;

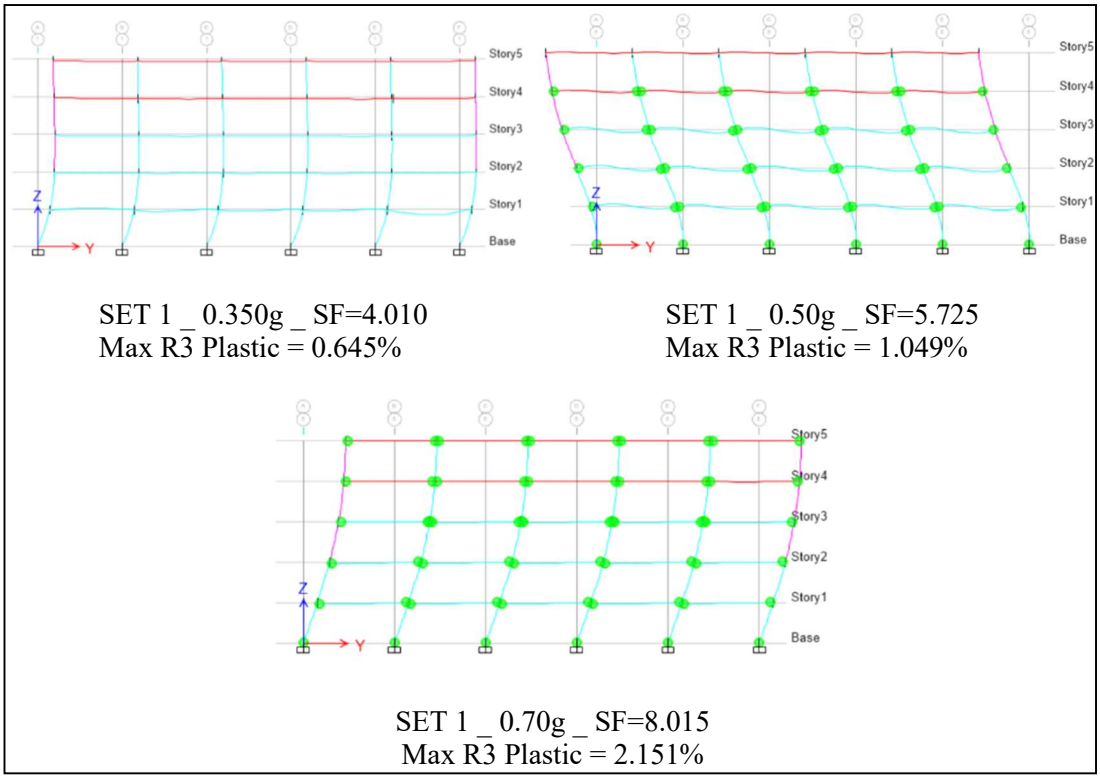


Reference Frame _ 0.342g _ SF=3.675
Max R3 Plastic = 0.942%

Reference Frame _ 0.50g _ SF=5.373
Max R3 Plastic = 1.278%

Reference Frame _ 0.70g _ SF=7.522
Max R3 Plastic = 2.312%

Figure 5.46: Hingings and plastic rotation demands of 5-story RFs under the Morgan Hill earthquake.

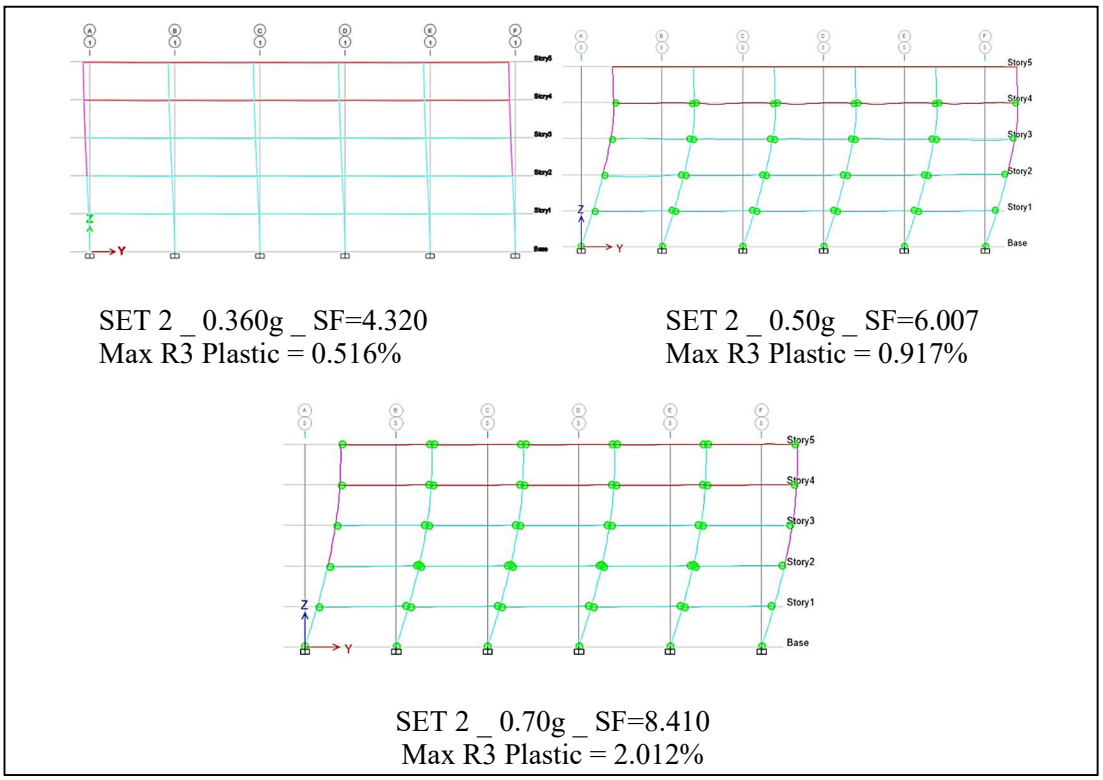


SET 1 _ 0.350g _ SF=4.010
Max R3 Plastic = 0.645%

SET 1 _ 0.50g _ SF=5.725
Max R3 Plastic = 1.049%

SET 1 _ 0.70g _ SF=8.015
Max R3 Plastic = 2.151%

Figure 5.47: Hingings and plastic rotation demands of 5-story Set-1 under the Morgan Hill earthquake.



SET 2 _ 0.360g _ SF=4.320
Max R3 Plastic = 0.516%

SET 2 _ 0.50g _ SF=6.007
Max R3 Plastic = 0.917%

SET 2 _ 0.70g _ SF=8.410
Max R3 Plastic = 2.012%

Figure 5.48: Hingings and plastic rotation demands of 5-story Set-2 under the Morgan Hill earthquake.

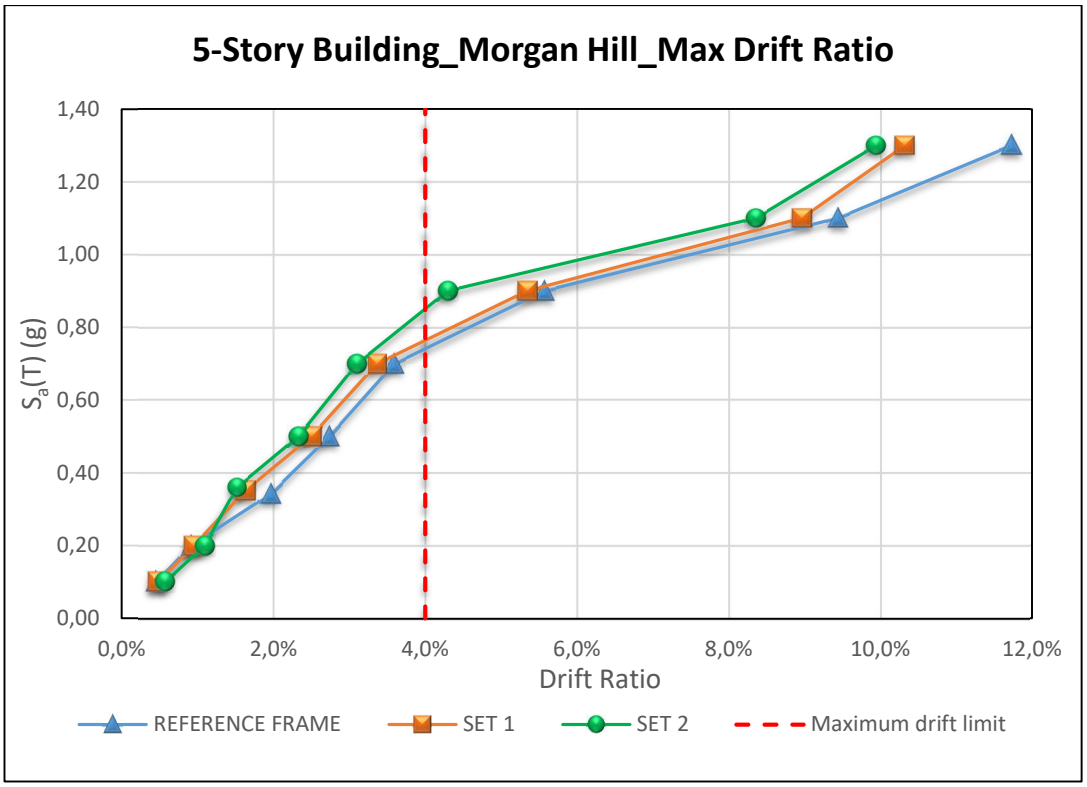


Figure 5.49: Max drift ratios of 5-story models under Morgan Hill earthquake acceleration intensities.

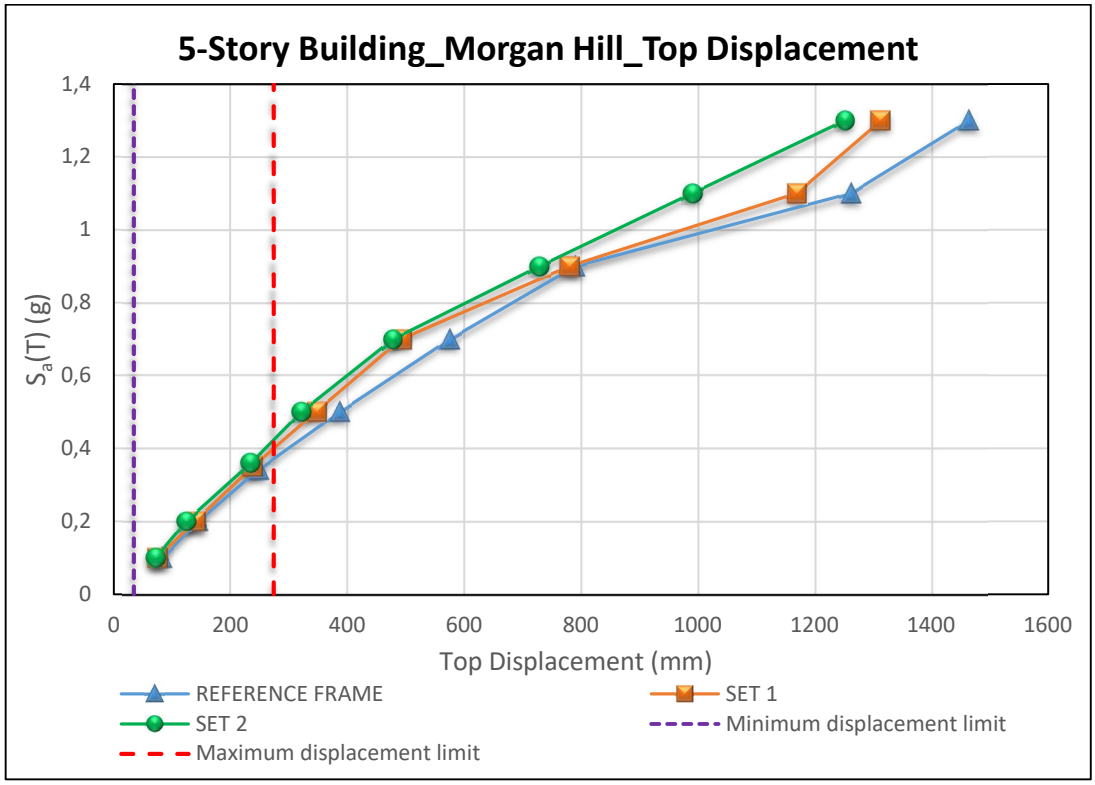


Figure 5.50: Max top displacements of 5-story models under Morgan Hill earthquake acceleration intensities.

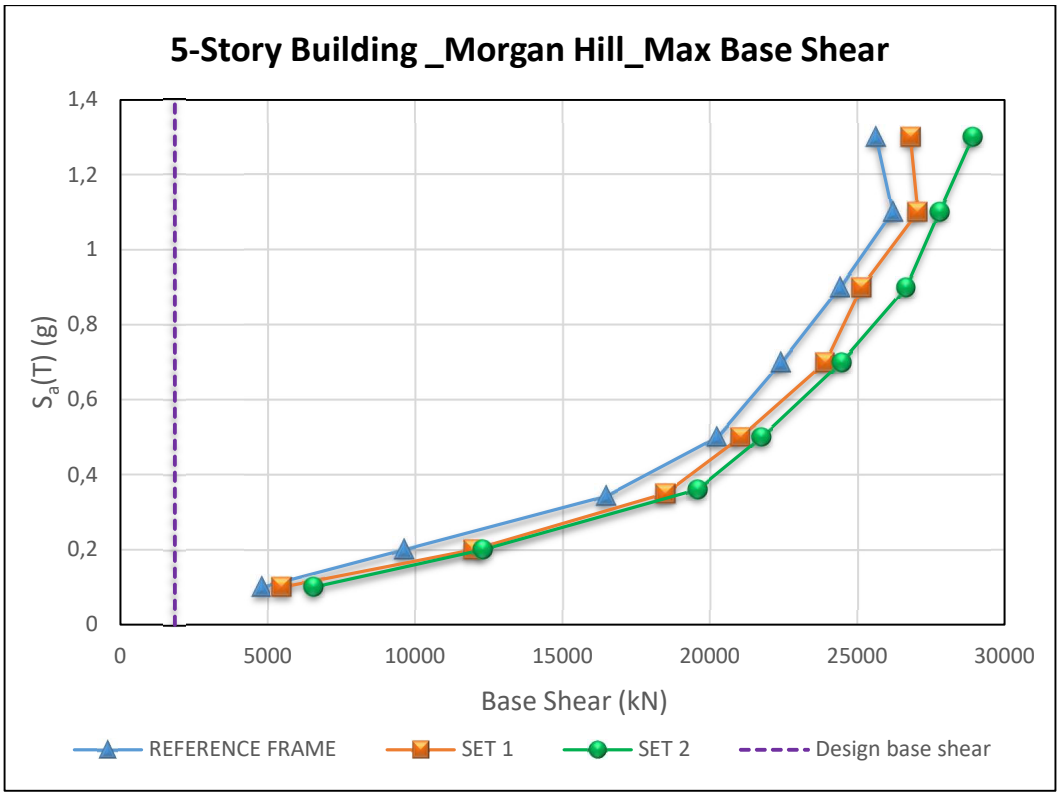


Figure 5.51: Max base shears of 5-story models under Morgan Hill earthquake acceleration intensities.

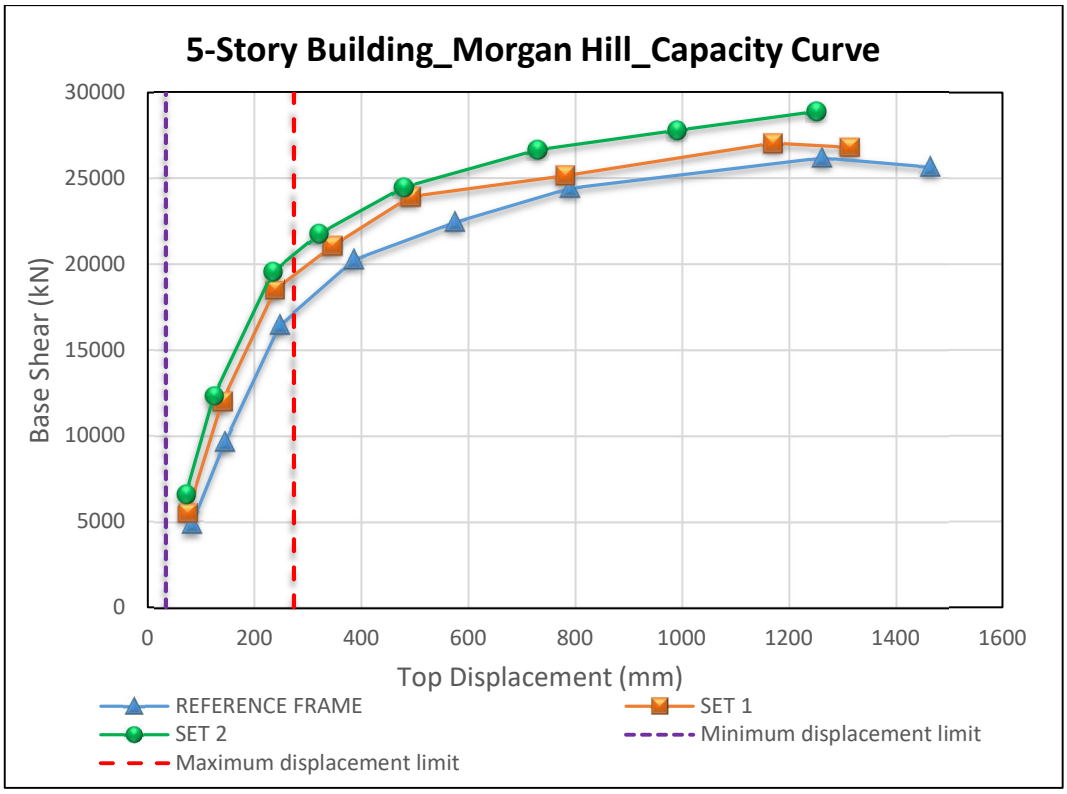


Figure 5.52: Capacity curves of 5-story models under Morgan Hill earthquake acceleration intensities.

Table 5.12: Responses of 5-story models under Morgan Hill earthquake.

MORGAN HILL / 5-STORY	S_a(T) values corresponding to drift ratio limit	S_a(T) values corresponding to maximum top displacement limit	The base shears corresponding to maximum top displacement
Reference Frame	0.74 g	0.37 g	17187.01 kN
Set-1	0.76 g	0.40 g	19346.13 kN
Set-2	0.85 g	0.42 g	20560.72 kN

The hinging and plastic rotation demands and drift ratio distributions along the structure height of all models at 0.85g acceleration intensity, where the 5-story Set-2 structure under the Morgan Hill earthquake reached the 4.00% drift ratio limit;

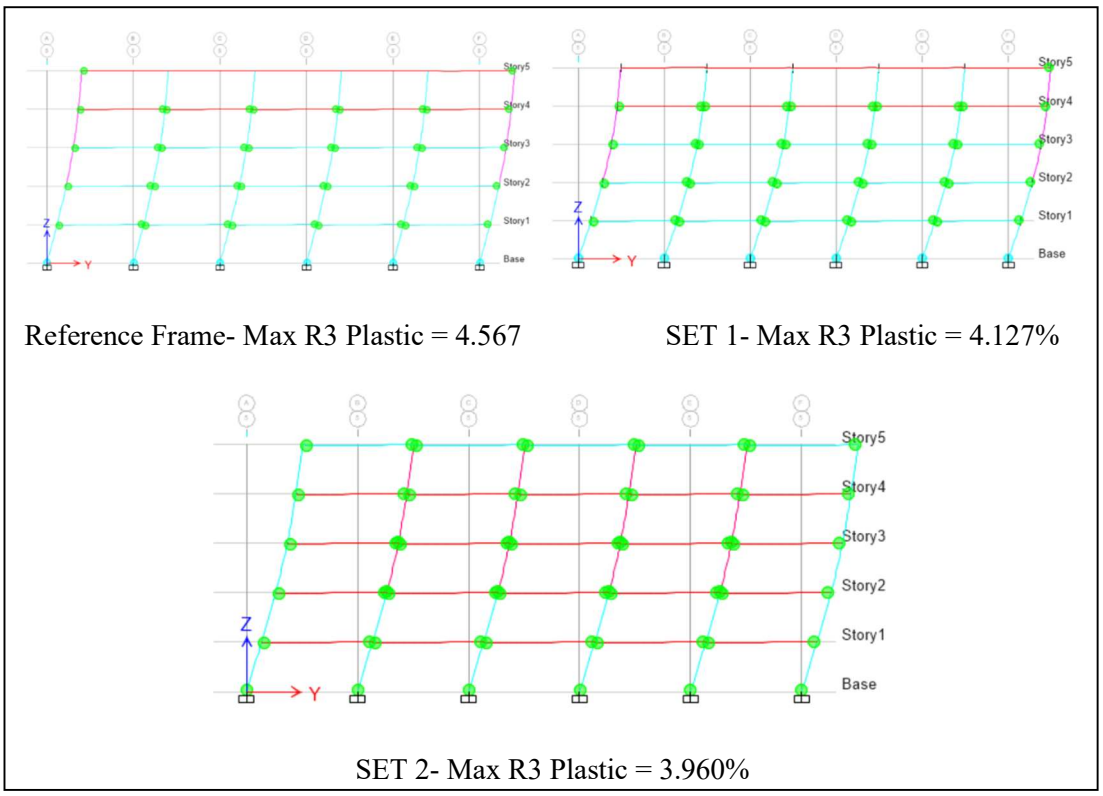


Figure 5.53: Hinging and plastic rotation demands of 5-story models at S_a=0.85g under the Morgan Hill earthquake.

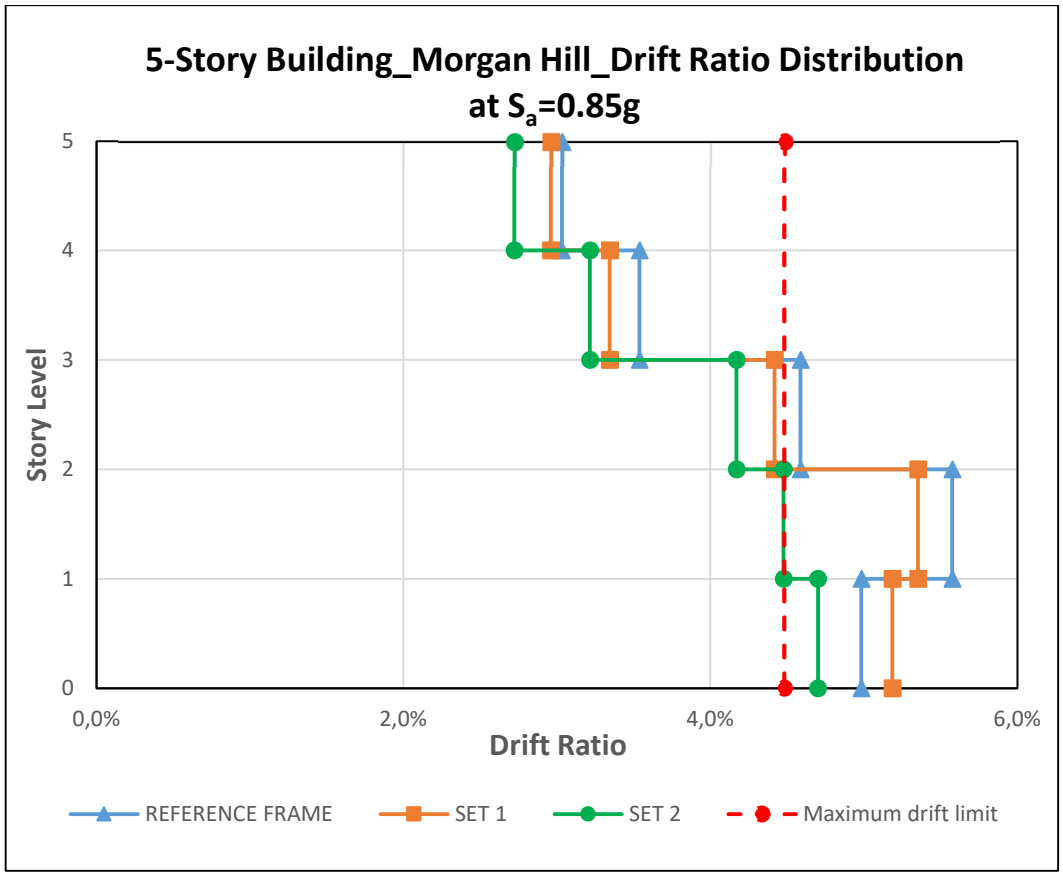


Figure 5.54: Drift ratio distributions along 5-story models' height at S_a=0.85g under the Morgan Hill earthquake.

5.1.7 Chuetsu_4840 Earthquake

Table 5.13: SFs for 5-story models under the Chuetsu earthquake.

5 Story_Reference Frame		
(S_a)	(SF)	Scale
g	unitless	mm/s²
0,100	0,438	4299,681
0,228	1,000	9806,650
0,300	1,315	12899,044
0,342	**1,500**	**14705,770**
0,500	2,192	21498,406
0,700	3,069	30097,769
0,900	3,946	38697,131
1,100	4,823	47296,494
1,300	5,700	55895,856
1,500	6,577	64495,219
1,700	7,454	73094,582
1,900	8,330	81693,944

5 Story_Set 1		
(S_a)	(SF)	Scale
g	unitless	mm/s²
0,100	0,433	4245,433
0,231	1,000	9806,650
0,300	1,299	12736,298
0,350	**1,516**	**14869,203**
0,500	2,165	21227,163
0,700	3,030	29718,028
0,900	3,896	38208,893
1,100	4,762	46699,758
1,300	5,628	55190,623
1,500	6,494	63681,488
1,700	7,360	72172,353
1,900	8,225	80663,218

5 Story_Set 2		
(S_a)	(SF)	Scale
g	unitless	mm/s²
0,100	0,443	4339,81
0,226	1,000	9806,65
0,300	1,328	13019,43
0,360	**1,591**	**15605,96**
0,500	2,213	21699,05
0,700	3,098	30378,67
0,900	3,983	39058,29
1,100	4,868	47737,91
1,300	5,753	56417,53
1,500	6,638	65097,15
1,700	7,523	73776,77
1,900	8,408	82456,39

Application of acceleration intensities to 5-story models under Chuetsu earthquake in three stages starting from the acceleration intensities corresponding to the SF obtained from the design spectrum;

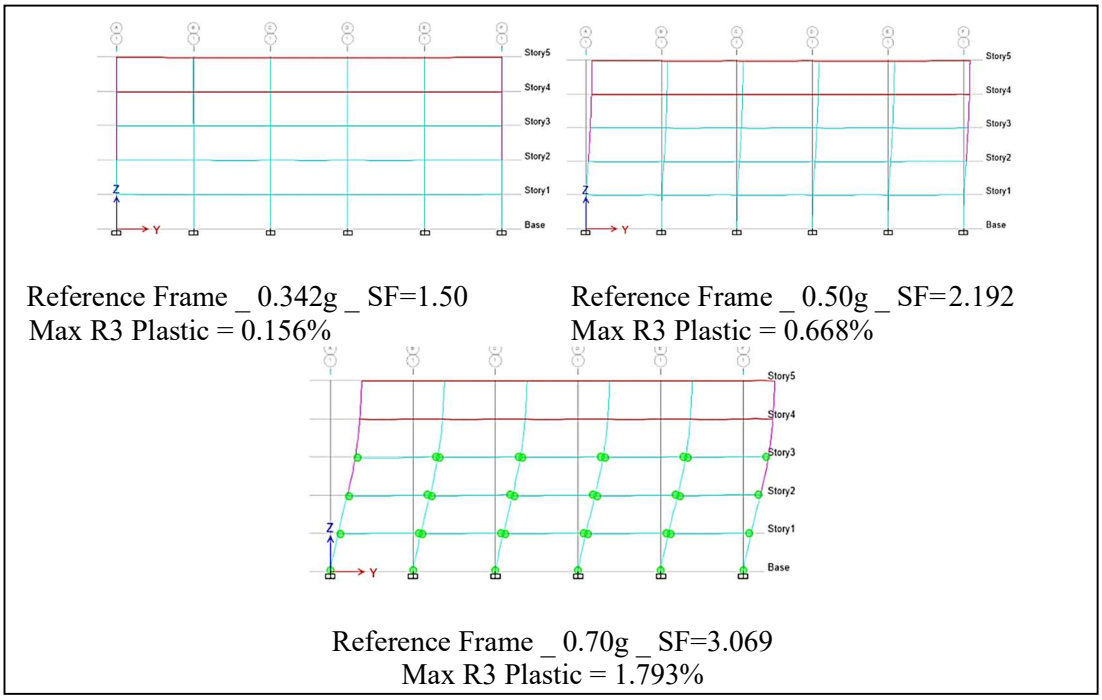


Figure 5.55: Hingings and plastic rotation demands of 5-story RFs under the Chuetsu earthquake.

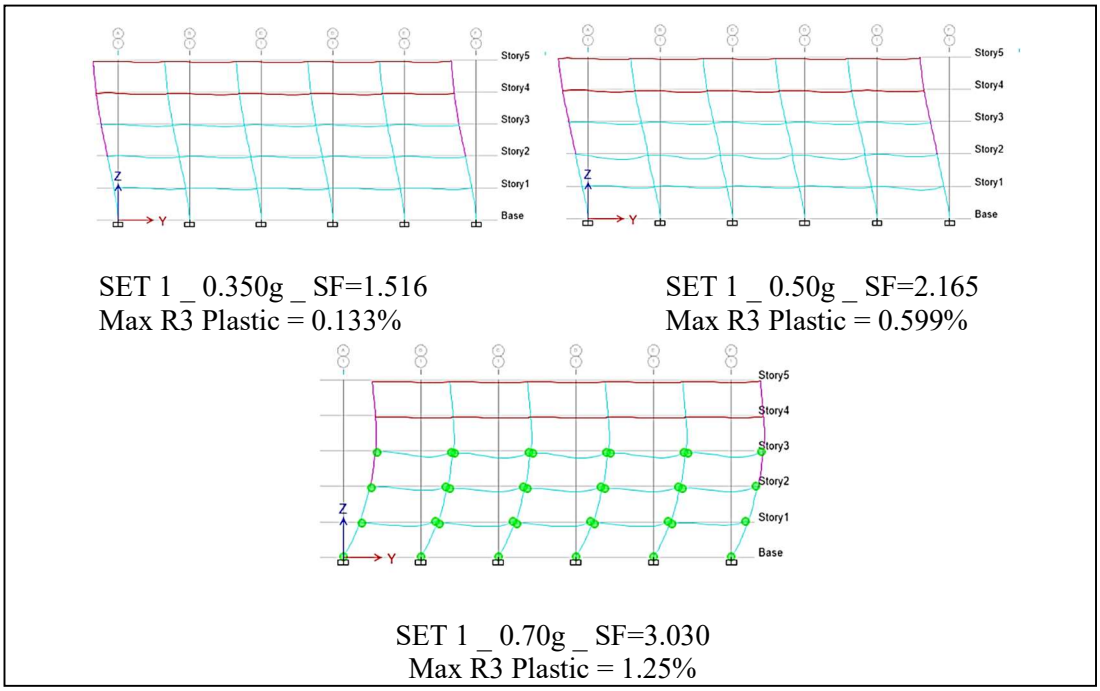


Figure 5.56: Hingings and plastic rotation demands of 5-story Set-1 under the Chuetsu earthquake.

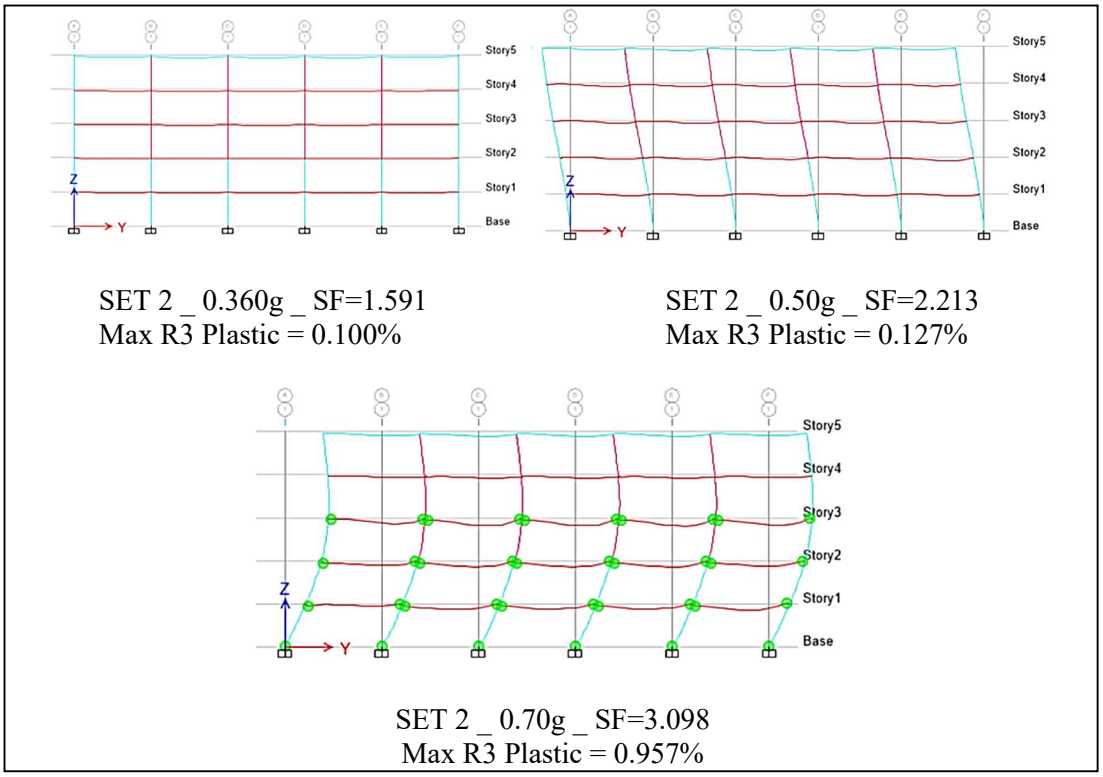


Figure 5.57: Hingings and plastic rotation demands of 5-story Set-2 under the Chuetsu earthquake.

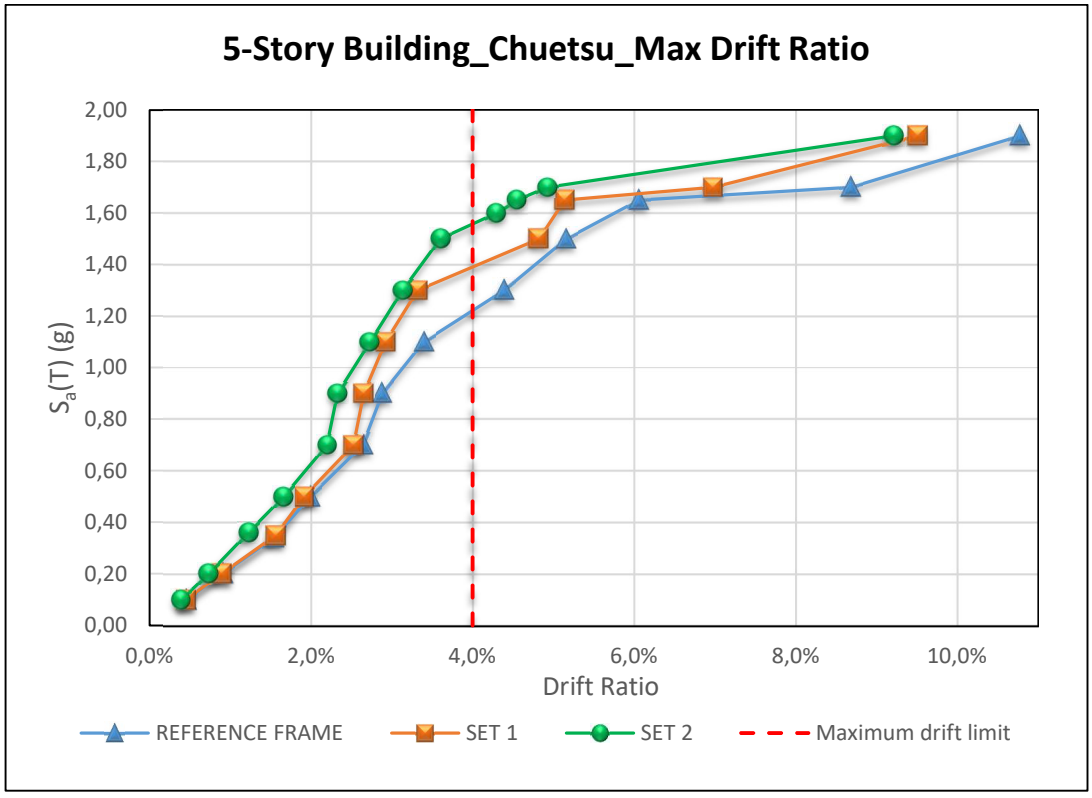


Figure 5.58: Max drift ratios of 5-story models under Chuetsu earthquake acceleration intensities.

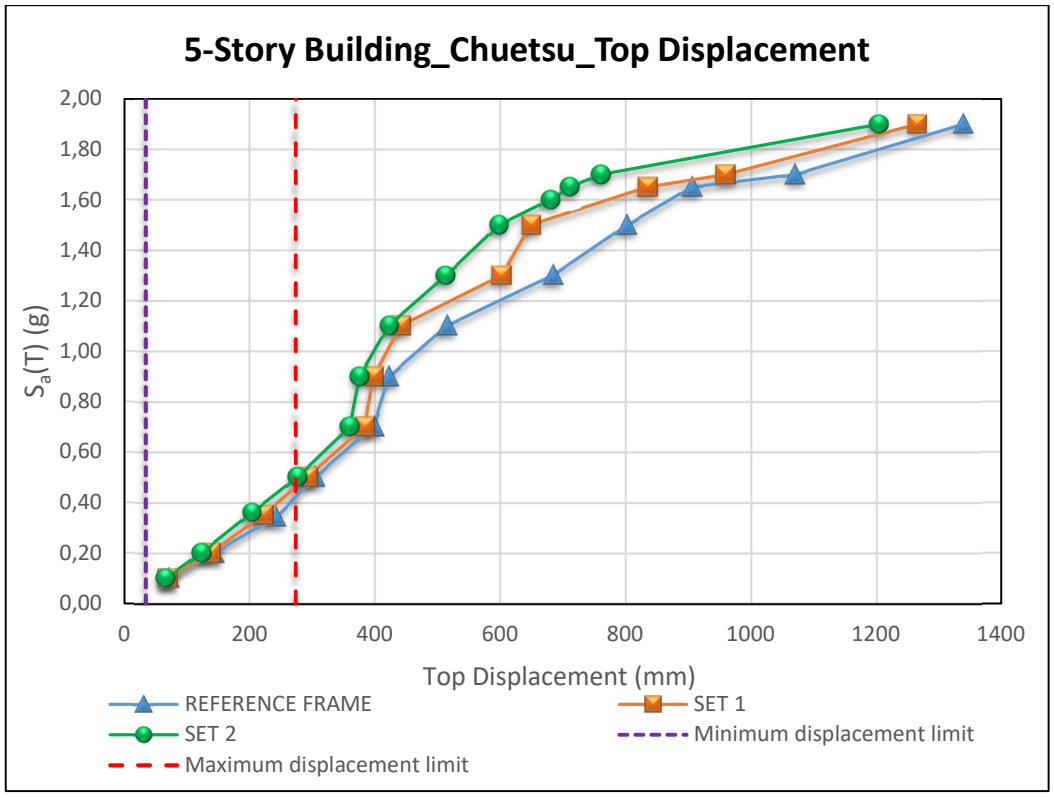


Figure 5.59: Max top displacements of 5-story models under Chuetsu earthquake acceleration intensities.

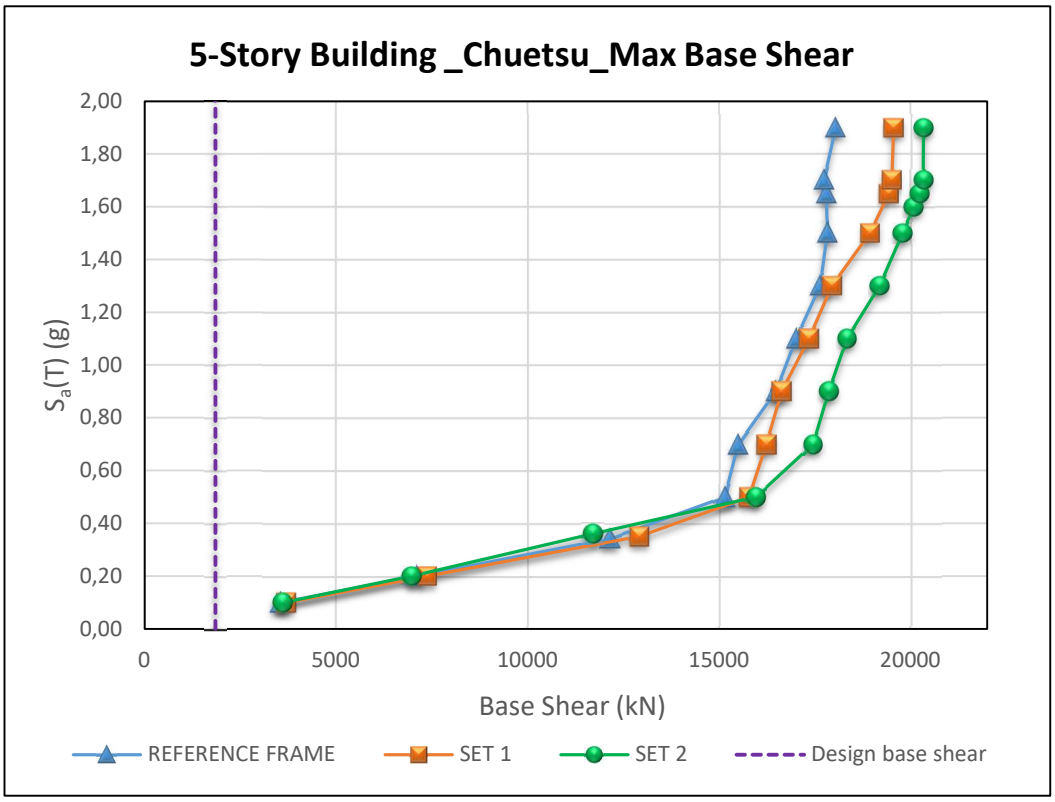


Figure 5.60: Max base shears of 5-story models under Chuetsu earthquake acceleration intensities.

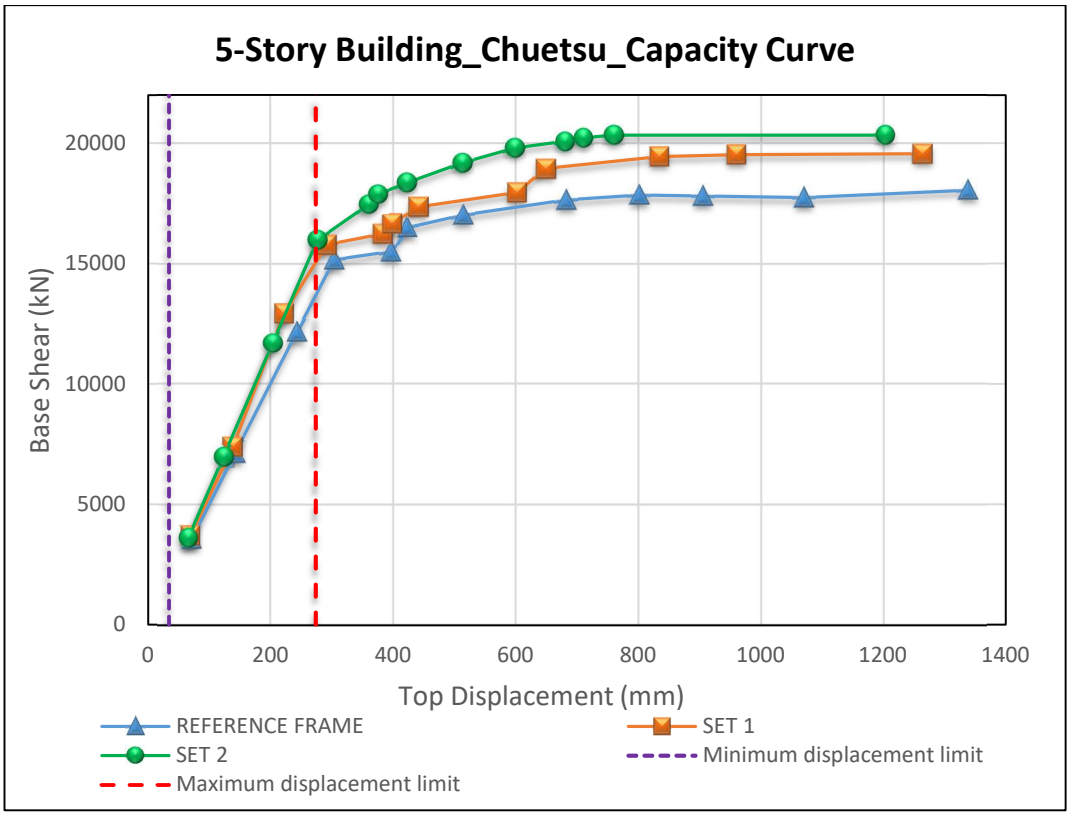


Figure 5.61: Capacity curves of 5-story models under Chuetsu earthquake acceleration intensities.

Table 5.14: Responses of 5-story models under Chuetsu earthquake.

CHUETSU / 5-STORY	$S_a(T)$ values corresponding to drift ratio limit	$S_a(T)$ values corresponding to maximum top displacement limit	The base shears corresponding to maximum top displacement
Reference Frame	1.20 g	0.42 g	13684.06 kN
Set-1	1.40 g	0.46 g	15043.39 kN
Set-2	1.55 g	0.50 g	15821.46 kN

The hinging and plastic rotation demands and drift ratio distributions along the structure height of all models at 1.55g acceleration intensity, where the 5-story Set-2 structure under the Chuetsu earthquake reached the 4.00% drift ratio limit;

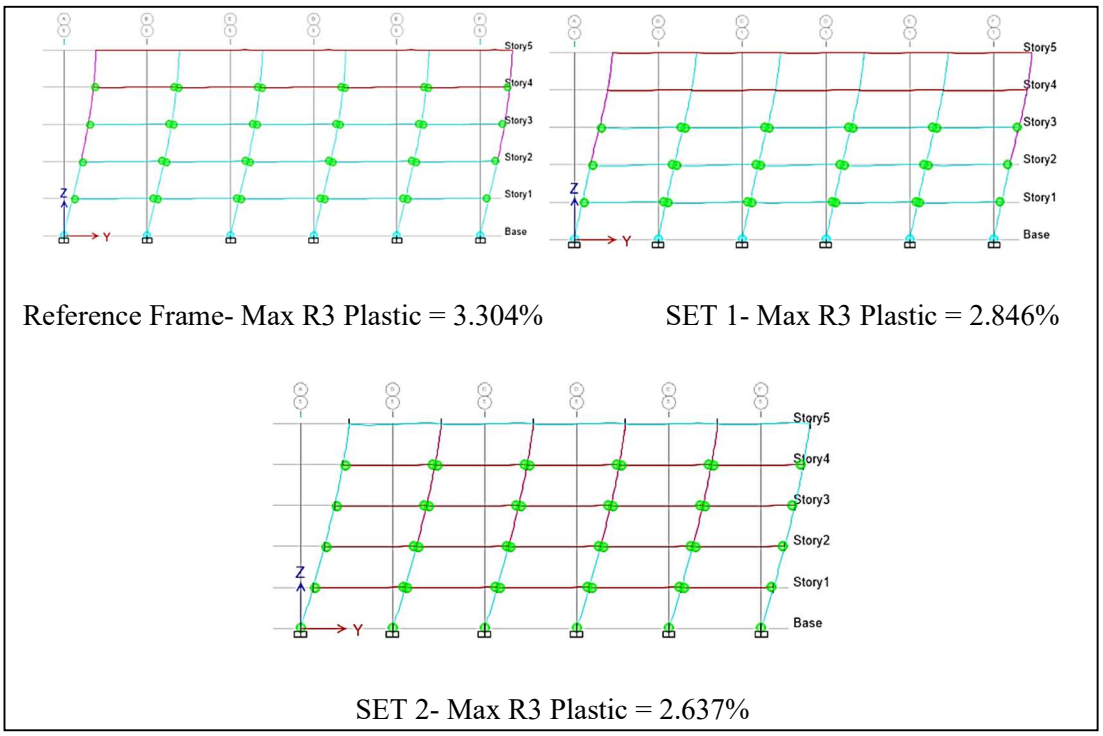


Figure 5.62: Hinging and plastic rotation demands of 5-story models at S_a=1.55g under the Chuetsu earthquake.

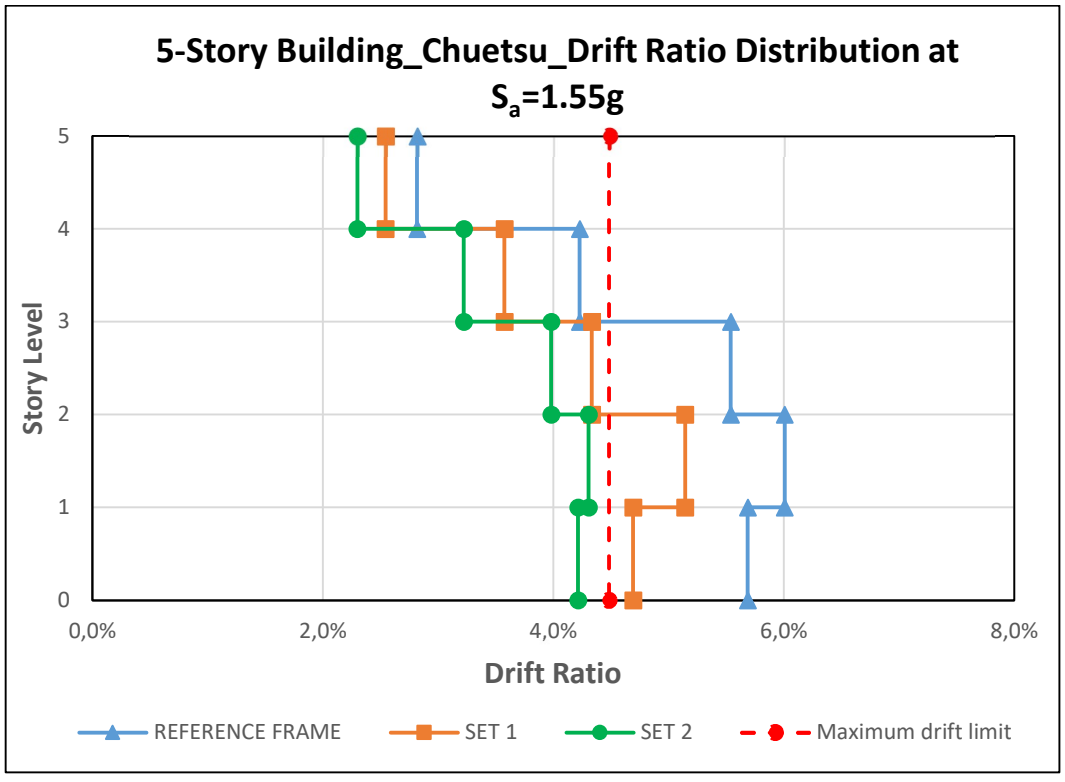


Figure 5.63: Drift ratio distributions along 5-story models' height at S_a=1.55g under the Chuetsu earthquake.

5.2 IDA For 10-Story Building Models

5.2.1 Düzce_8166 Earthquake

Table 5.15: SFs for 10-story models under the Düzce earthquake.

10 Story_Reference Frame		
(S_a)	(SF)	Scale
g	unitless	mm/s²
0,045	1,000	9806,650
0,100	2,235	21919,045
0,180	**4,023**	**39454,281**
0,200	4,470	43838,090
0,300	6,705	65757,135
0,400	8,940	87676,180
0,500	11,176	109595,225
0,600	13,411	131514,270
0,700	15,646	153433,315
0,800	17,881	175352,360

10 Story_Set 1		
(S_a)	(SF)	Scale
g	unitless	mm/s²
0,045	1,000	9806,650
0,100	2,232	21891,858
0,183	**4,085**	**40062,100**
0,200	4,465	43783,716
0,300	6,697	65675,574
0,400	8,929	87567,432
0,500	11,162	109459,290
0,600	13,394	131351,148
0,700	15,626	153243,006
0,800	17,859	175134,864

10 Story_Set 2		
(S_a)	(SF)	Scale
g	unitless	mm/s²
0,047	1,000	9806,650
0,100	2,141	20997,243
0,189	**4,051**	**39726,783**
0,200	4,282	41994,485
0,300	6,423	62991,728
0,400	8,564	83988,970
0,500	10,706	104986,213
0,600	12,847	125983,455
0,700	14,988	146980,698
0,800	17,129	167977,940

Application of acceleration intensities to 10-story models under Düzce earthquake in three stages starting from the acceleration intensities corresponding to the SF obtained from the design spectrum;

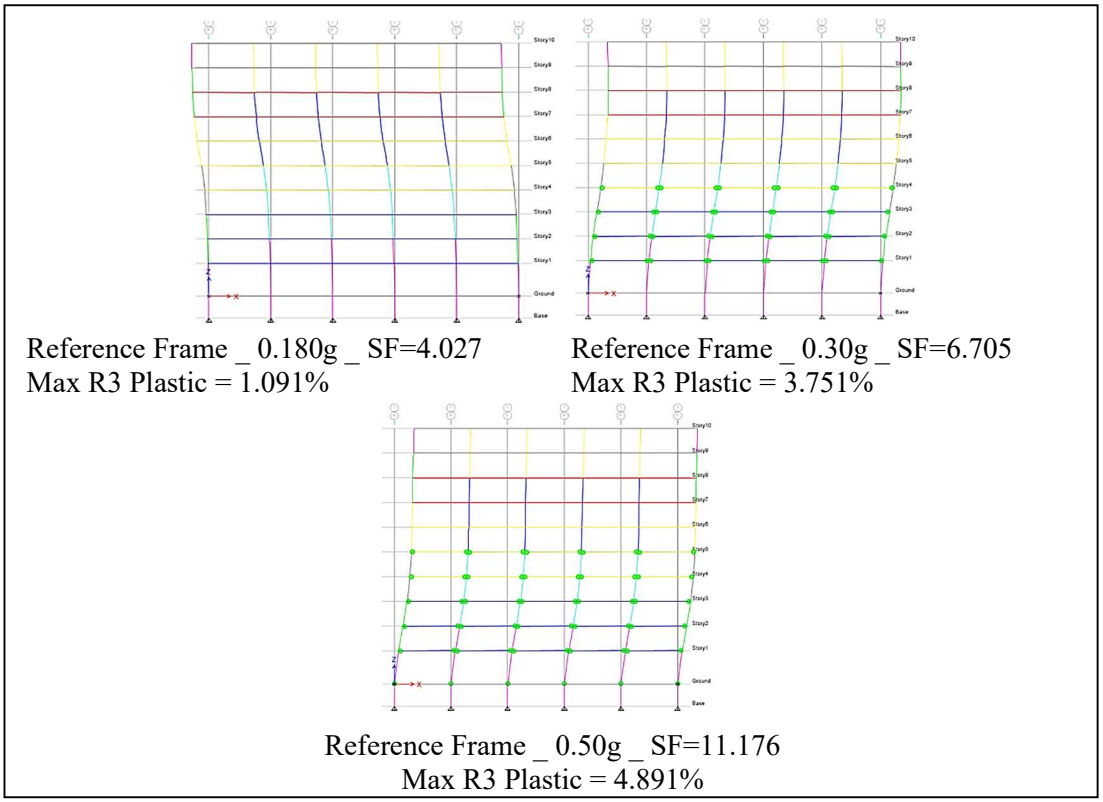
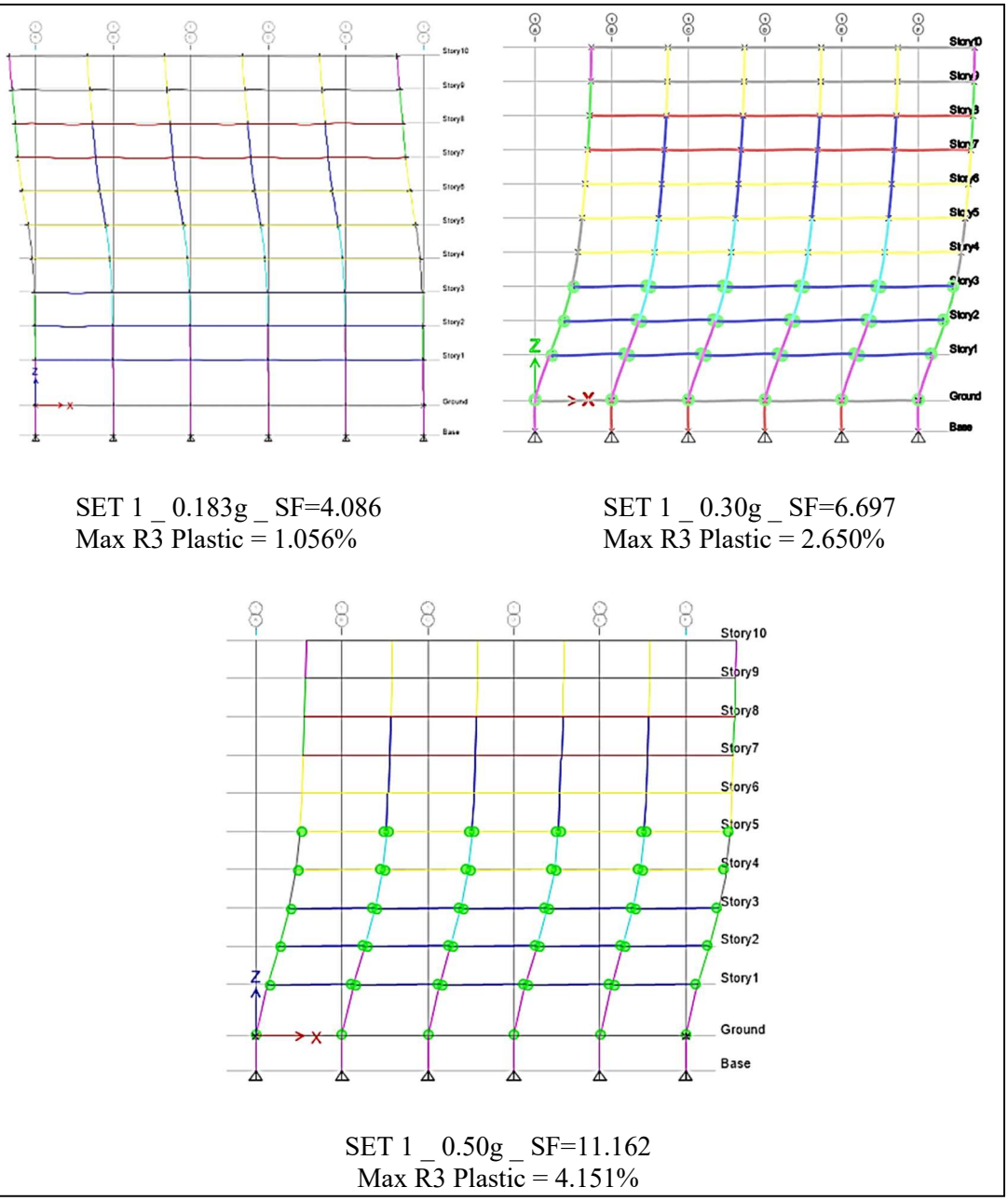


Figure 5.64: Hingings and plastic rotation demands of 10-story RFs under the Düzce earthquake.

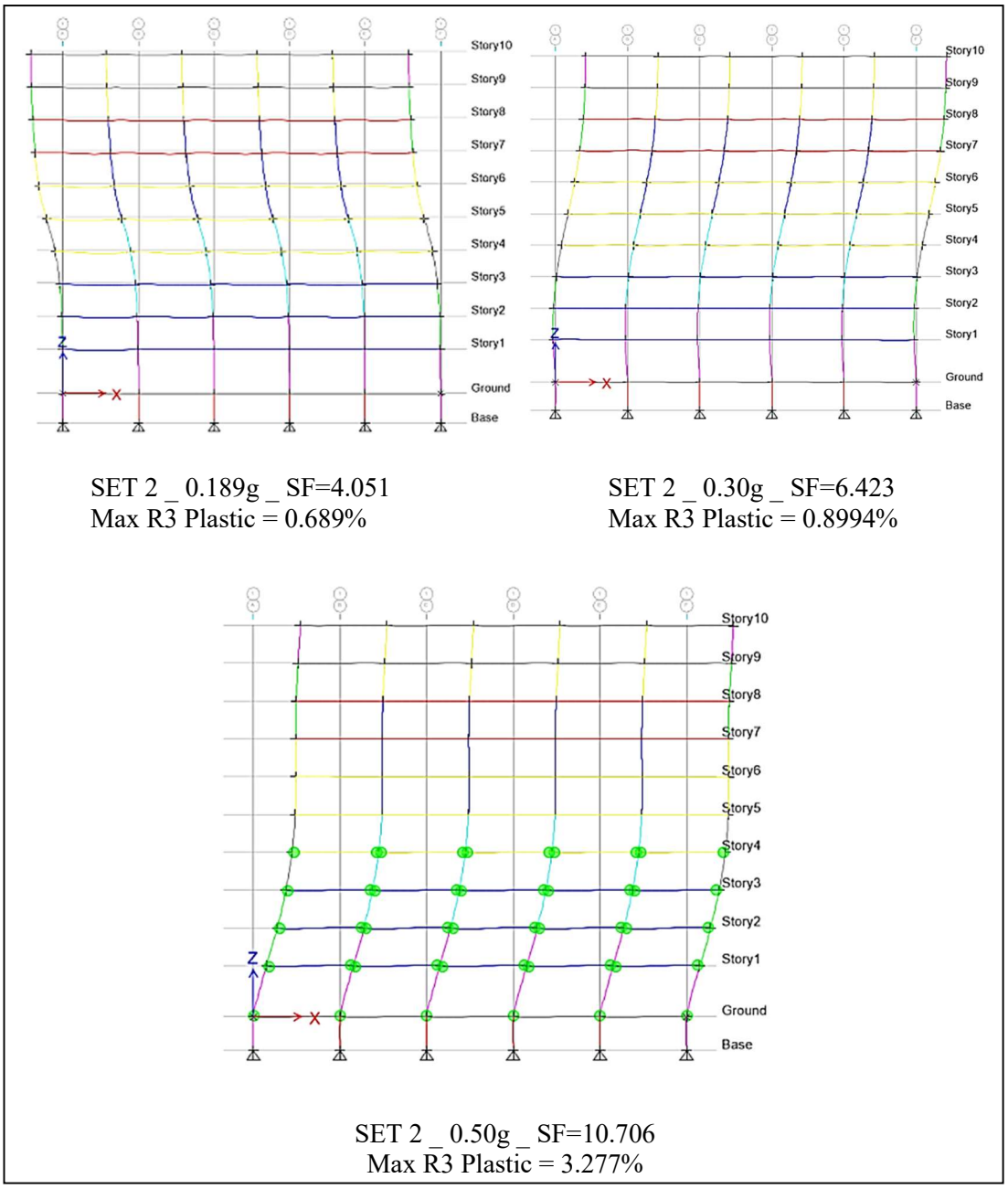


SET 1 _ 0.183g _ SF=4.086
Max R3 Plastic = 1.056%

SET 1 _ 0.30g _ SF=6.697
Max R3 Plastic = 2.650%

SET 1 _ 0.50g _ SF=11.162
Max R3 Plastic = 4.151%

Figure 5.65: Hingings and plastic rotation demands of 10-story Set-1 under the Düzce earthquake.



SET 2 _ 0.189g _ SF=4.051
Max R3 Plastic = 0.689%

SET 2 _ 0.30g _ SF=6.423
Max R3 Plastic = 0.8994%

SET 2 _ 0.50g _ SF=10.706
Max R3 Plastic = 3.277%

Figure 5.66: Hingings and plastic rotation demands of 10-story Set-2 under the Düzce earthquake.

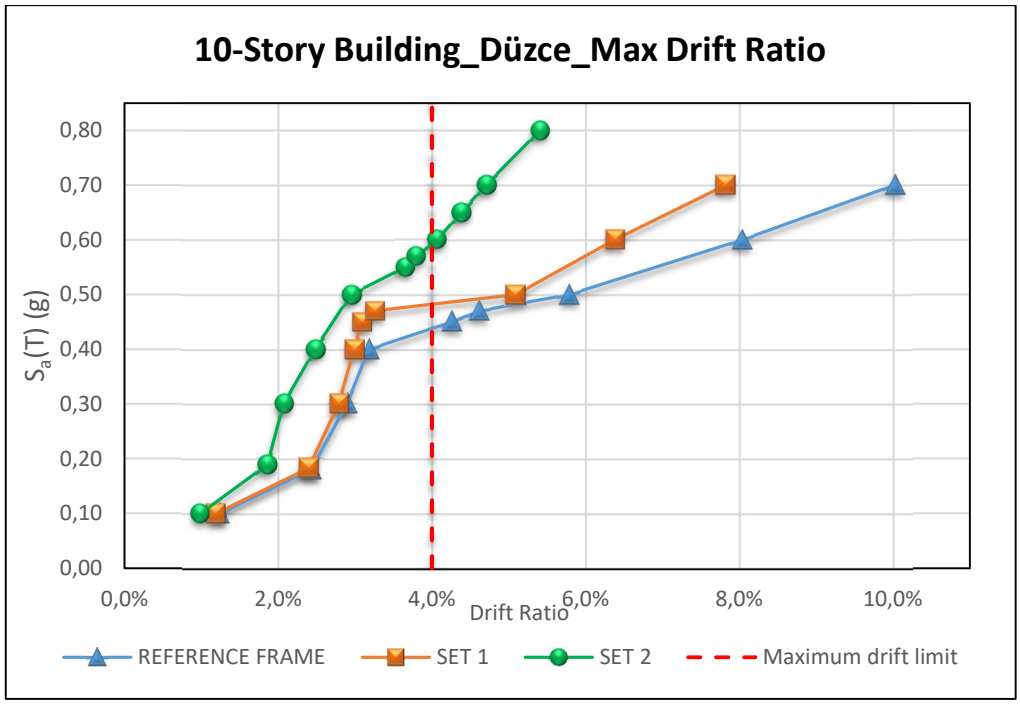


Figure 5.67: Max drift ratios of 10-story models under Düzce earthquake acceleration intensities.

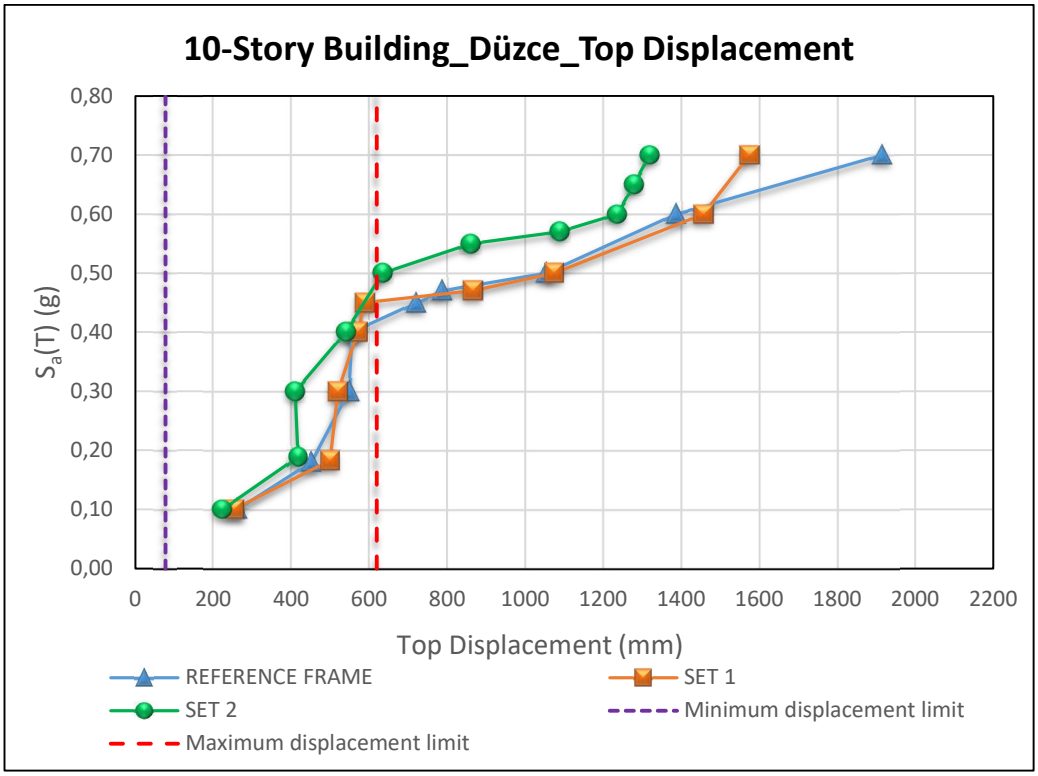


Figure 5.68: Max top displacements of 10-story models under Düzce earthquake acceleration intensities.

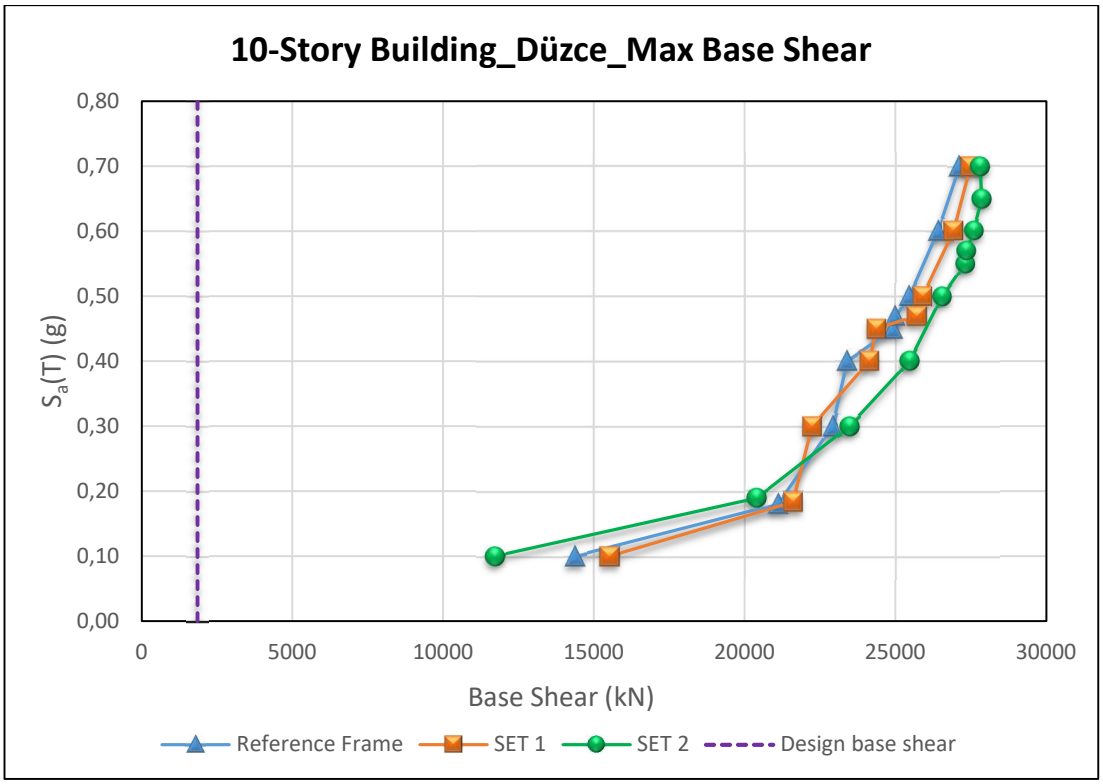


Figure 5.69: Max base shears of 10-story models under Düzce earthquake acceleration intensities.

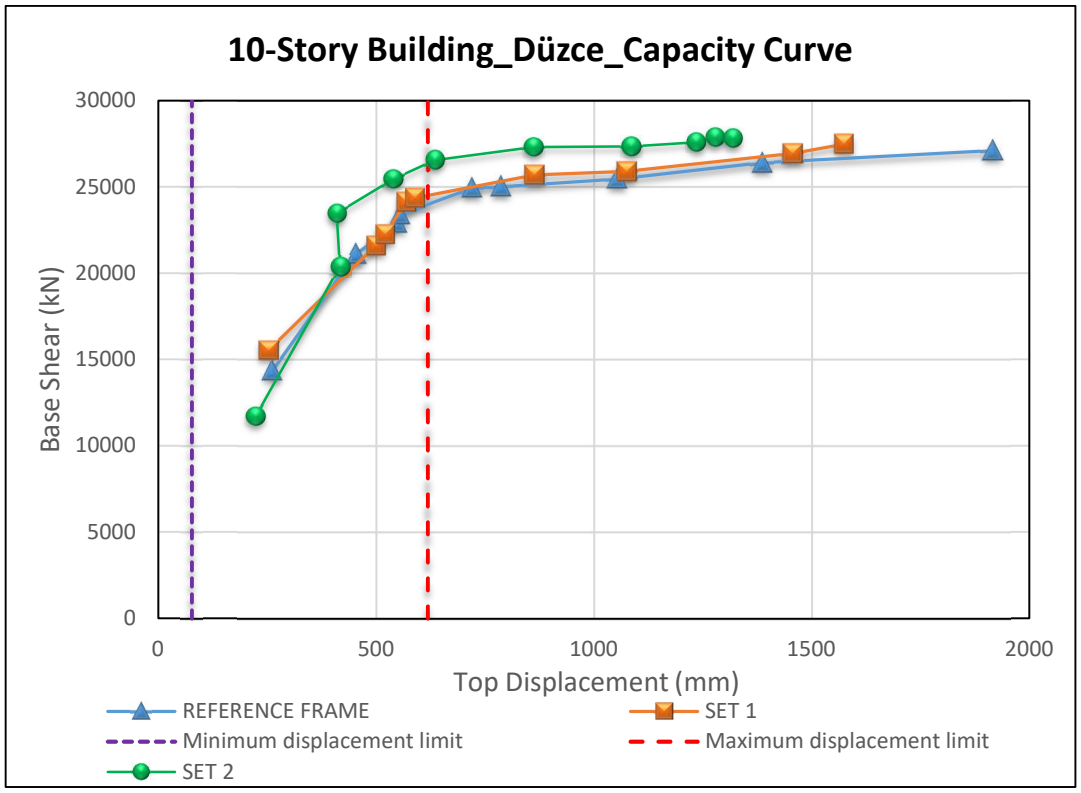
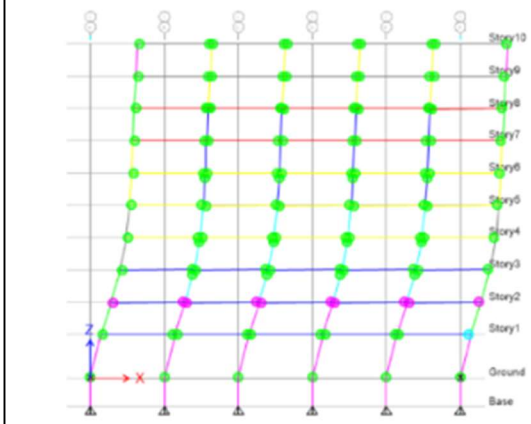


Figure 5.70: Capacity curves of 10-story models under Düzce earthquake acceleration intensities.

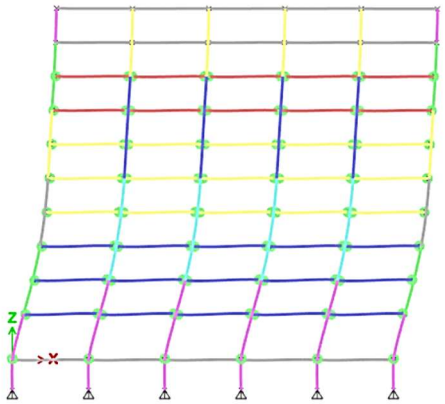
Table 5.16: Responses of 10-story models under Düzce earthquake.

DUZCE / 10-STORY	S_a(T) values corresponding to drift ratio limit	S_a(T) values corresponding to maximum top displacement limit	The base shears corresponding to maximum top displacement
Reference Frame	0.44 g	0.42 g	23981.27 kN
Set-1	0.48 g	0.45 g	24513.24 kN
Set-2	0.60 g	0.48 g	26365.33 kN

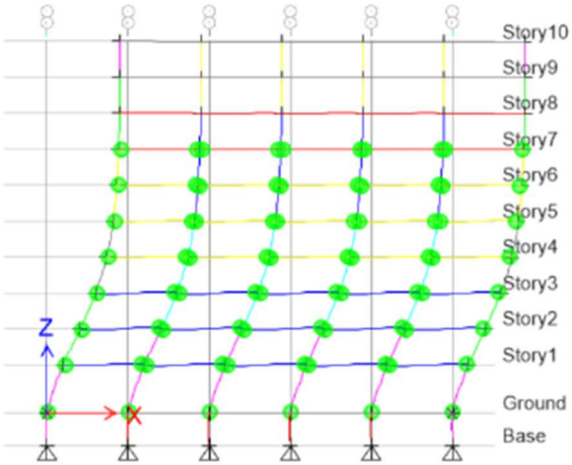
The hinging and plastic rotation demands and drift ratio distributions along the structure height of all models at 0.60g acceleration intensity, where the 10-story Set-2 structure under the Düzce earthquake reached the 4.00% drift ratio limit;



Reference Frame- Max R3 Plastic = 10.510%



SET 1- Max R3 Plastic = 3.911%



SET 2- Max R3 Plastic = 3.812%

Figure 5.71: Hinging and plastic rotation demands of 10-story models at S_a=0.60g under the Düzce earthquake.

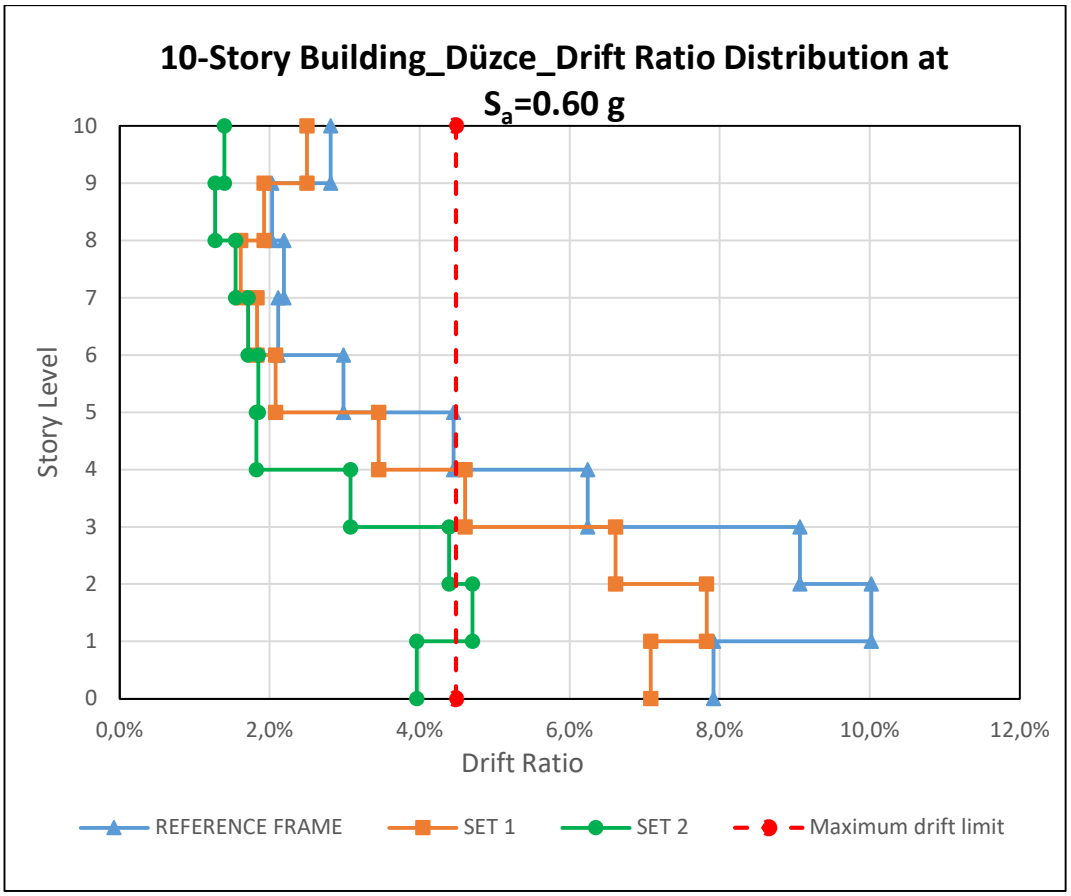


Figure 5.72: Drift ratio distributions along 10-story models' height at S_a=0.60g under the Düzce earthquake.

5.2.2 Park Field_4132 Earthquake

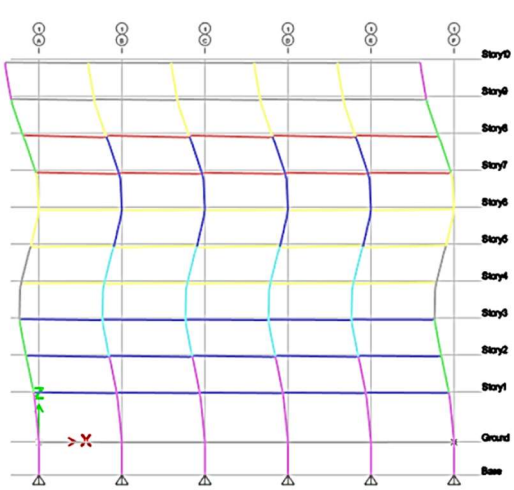
Table 5.17: SFs for 10-story models under the Park Field earthquake.

10 Story_Reference Frame		
(S_a)	(SF)	Scale
g	unitless	mm/s²
0,073	1,000	9806,650
0,100	1,369	13420,800
0,180	**2,466**	**24178,914**
0,200	2,737	26841,601
0,300	4,106	40262,401
0,400	5,474	53683,202
0,500	6,843	67104,002
0,600	8,211	80524,803
0,700	9,580	93945,603
0,800	10,948	107366,403
0,900	12,317	120787,204

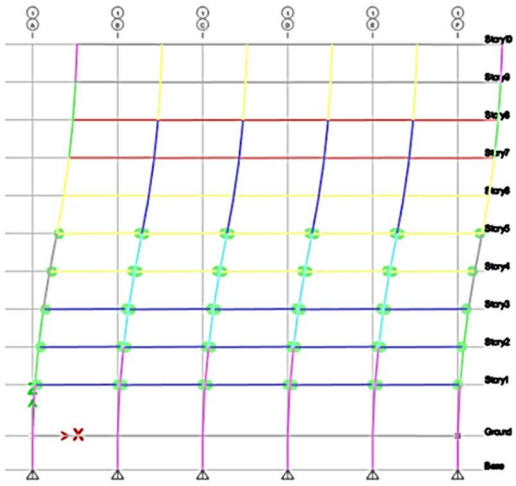
10 Story_Set 1		
(S_a)	(SF)	Scale
g	unitless	mm/s²
0,072	1,000	9806,650
0,100	1,383	13561,991
0,183	**2,531**	**24821,156**
0,200	2,766	27123,983
0,300	4,149	40685,974
0,400	5,532	54247,965
0,500	6,915	67809,956
0,600	8,298	81371,948
0,700	9,681	94933,939
0,800	11,064	108495,930
0,900	12,446	122057,922

10 Story_Set 2		
(S_a)	(SF)	Scale
g	unitless	mm/s²
0,068	1,000	9806,650
0,100	1,464	14358,940
0,189	**2,770**	**27167,114**
0,200	2,928	28717,880
0,300	4,393	43076,820
0,400	5,857	57435,760
0,500	7,321	71794,700
0,600	8,785	86153,640
0,700	10,249	100512,580
0,800	11,714	114871,520
0,900	13,178	129230,460

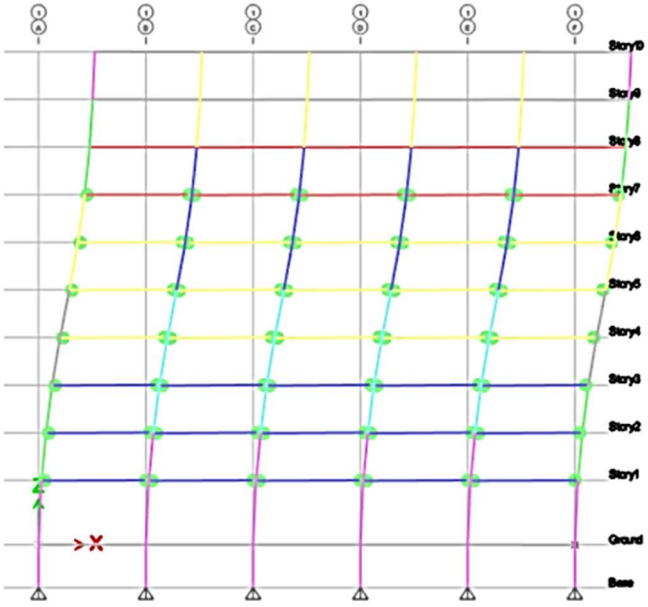
Application of acceleration intensities to 10-story models under Park Field earthquake in three stages starting from the acceleration intensities corresponding to the SF obtained from the design spectrum;



Reference Frame _ 0.180g _ SF=2.466
Max R3 Plastic = 0.801%

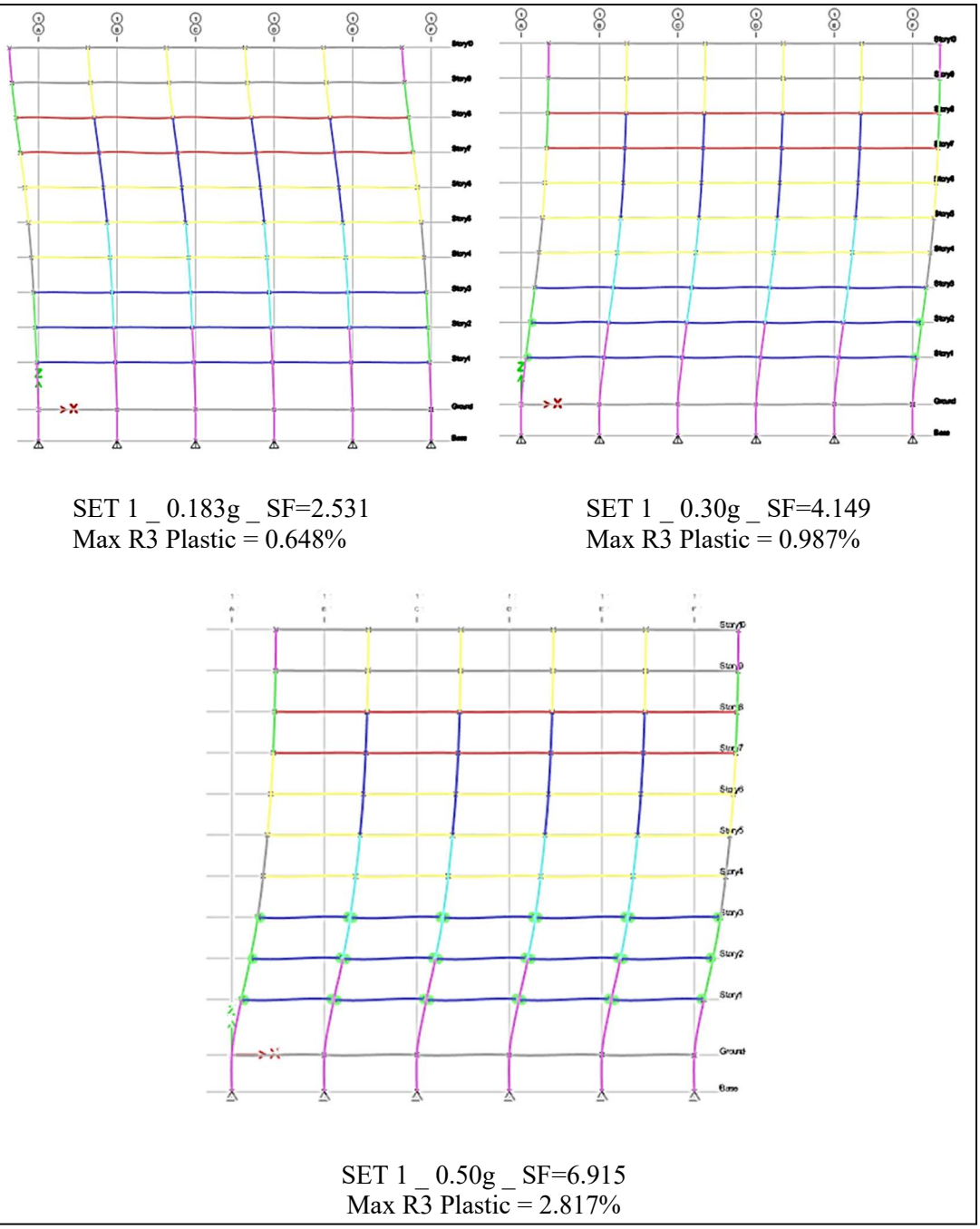


Reference Frame _ 0.30g _ SF=4.106
Max R3 Plastic = 1.066%



Reference Frame _ 0.50g _ SF=6.843
Max R3 Plastic = 3.567%

Figure 5.73: Hingings and plastic rotation demands of 10-story RFs under the Park Field earthquake.

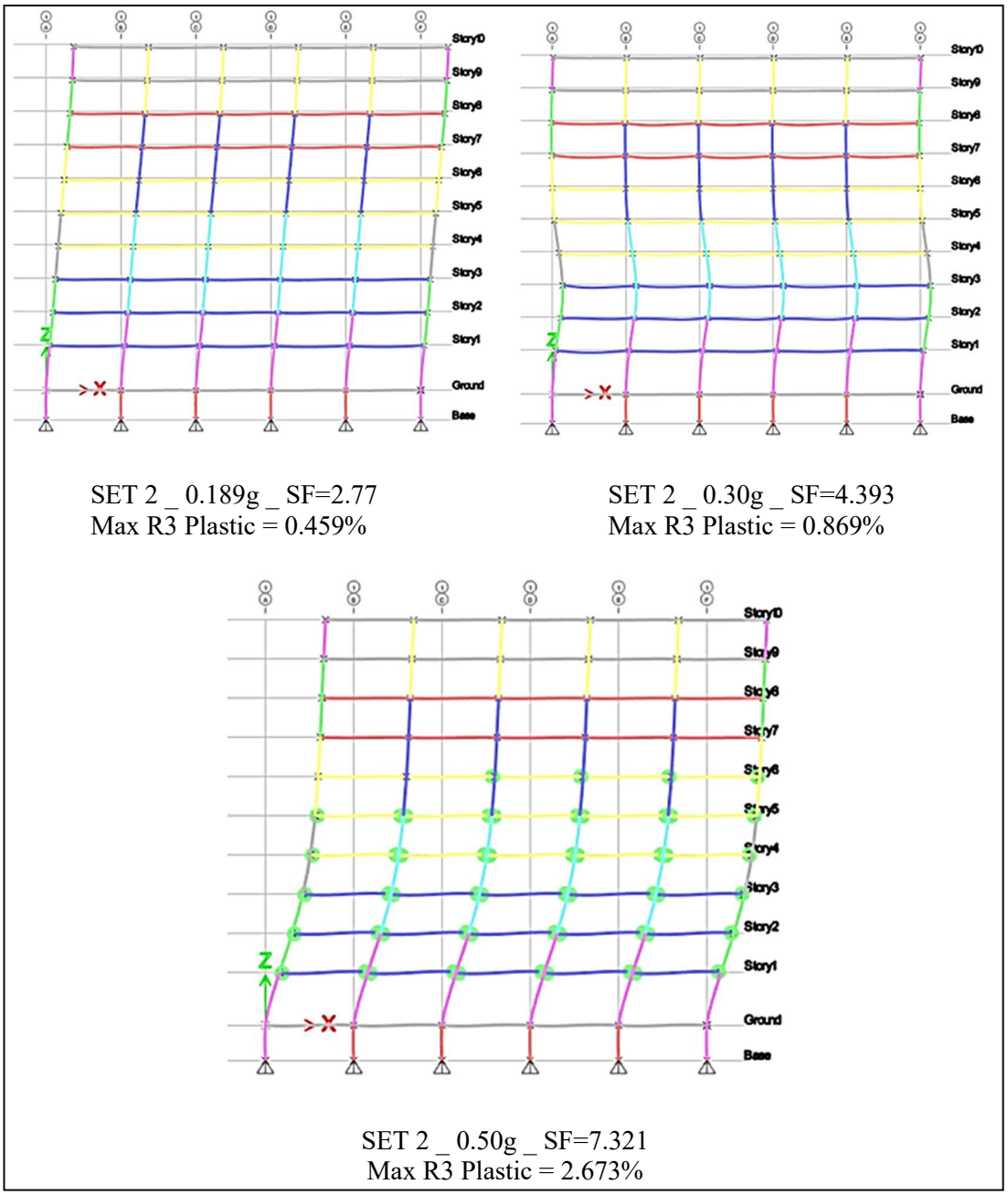


SET 1 _ 0.183g _ SF=2.531
Max R3 Plastic = 0.648%

SET 1 _ 0.30g _ SF=4.149
Max R3 Plastic = 0.987%

SET 1 _ 0.50g _ SF=6.915
Max R3 Plastic = 2.817%

Figure 5.74: Hingings and plastic rotation demands of 10-story Set-1 under the Park Field earthquake.



SET 2 _ 0.189g _ SF=2.77
Max R3 Plastic = 0.459%

SET 2 _ 0.30g _ SF=4.393
Max R3 Plastic = 0.869%

SET 2 _ 0.50g _ SF=7.321
Max R3 Plastic = 2.673%

Figure 5.75: Hingings and plastic rotation demands of 10-story Set-2 under the Park Field earthquake.

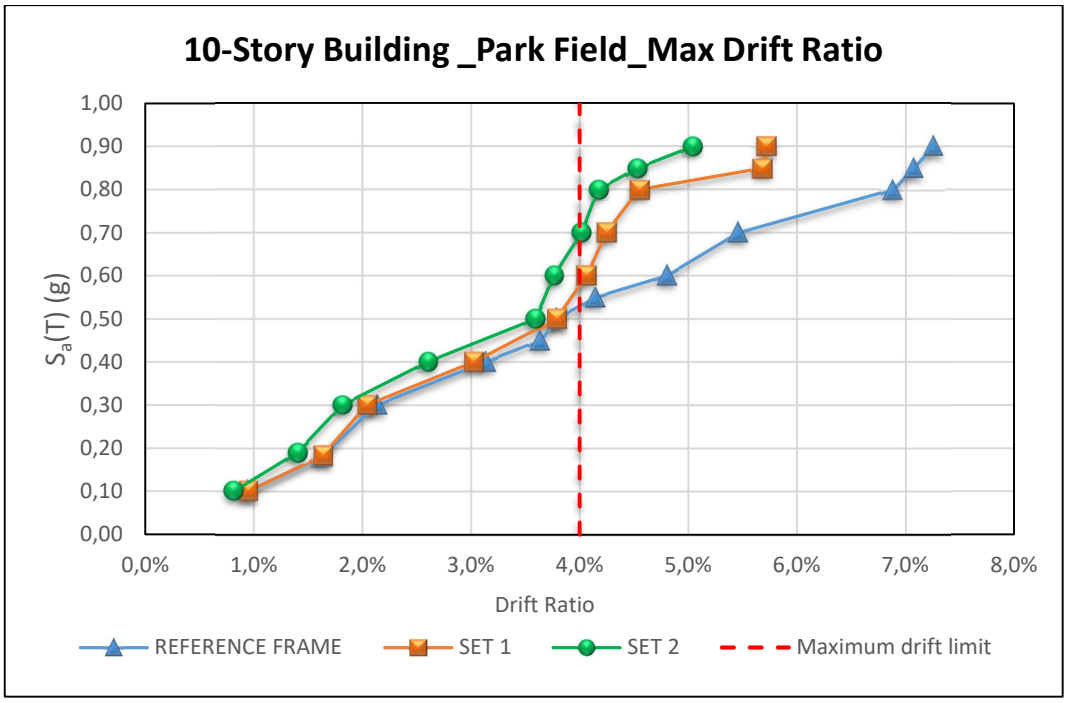


Figure 5.76: Max drift ratios of 10-story models under Park Field earthquake acceleration intensities.

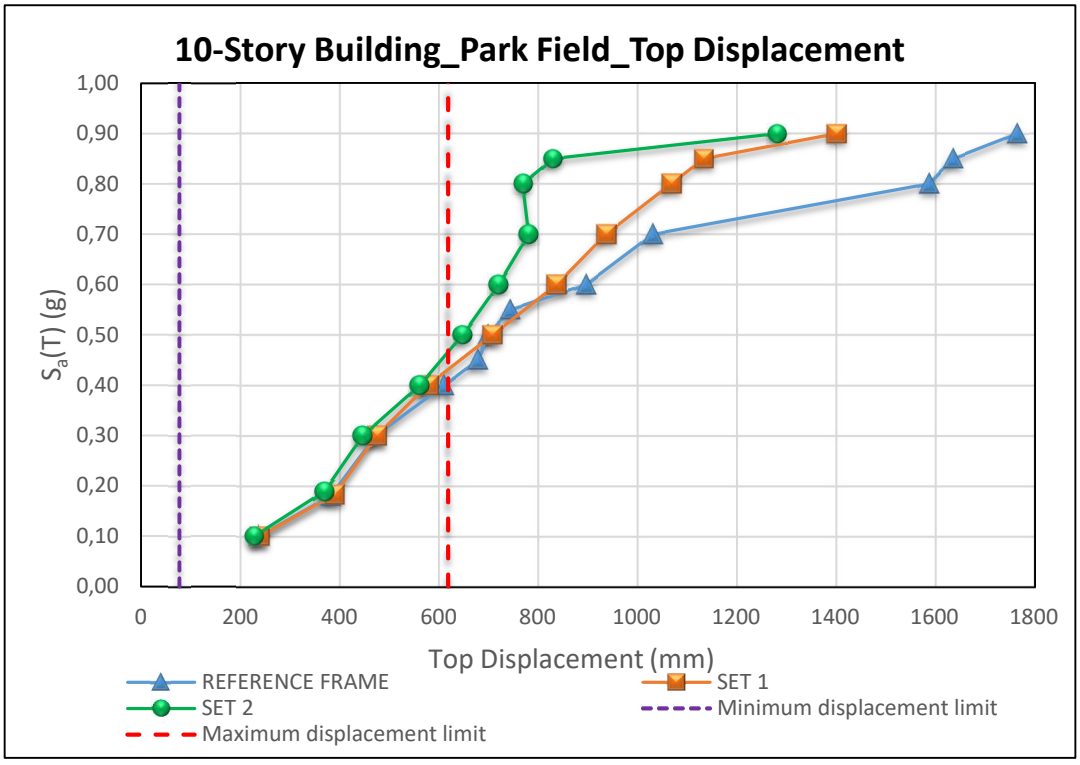


Figure 5.77: Max top displacements of 10-story models under Park Field earthquake acceleration intensities.

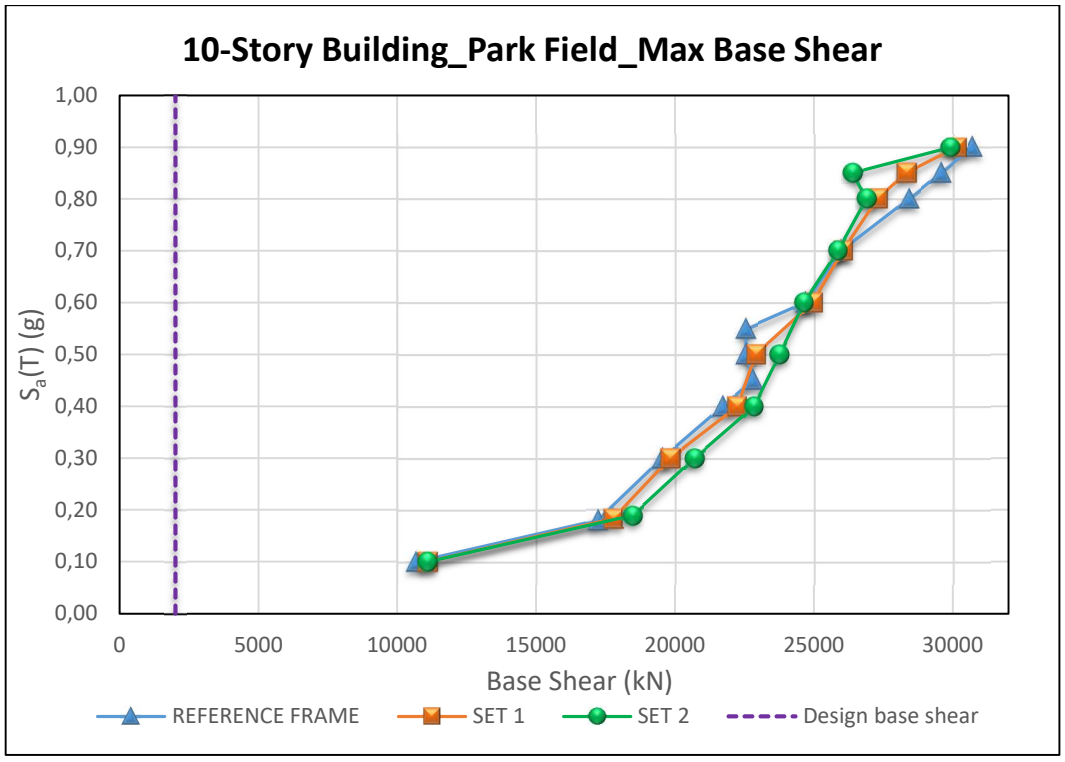


Figure 5.78: Max base shears of 10-story models under Park Field earthquake acceleration intensities.

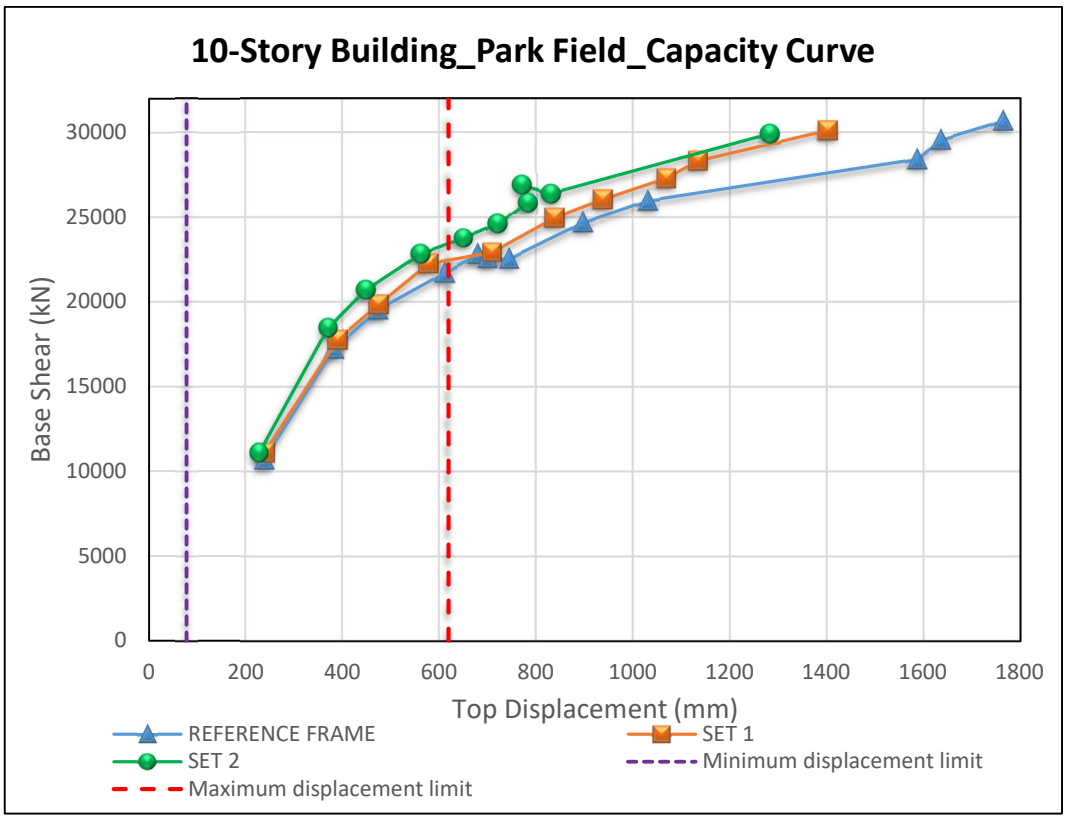
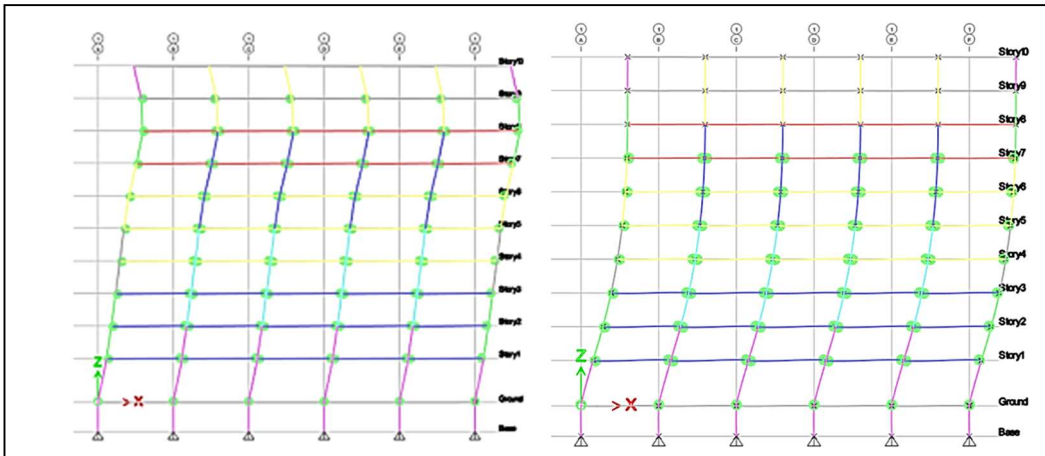


Figure 5.79: Capacity curves of 10-story models under Park Field earthquake acceleration intensities.

Table 5.18: Responses of 10-story models under Park Field earthquake.

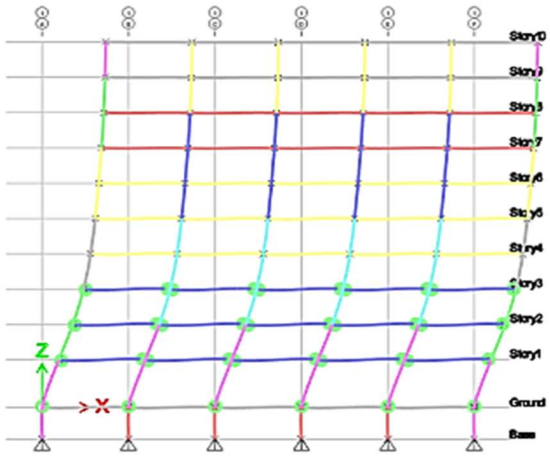
PARKFIELD / 10-STORY	S_a(T) values corresponding to drift ratio limit	S_a(T) values corresponding to maximum top displacement limit	The base shears corresponding to maximum top displacement
Reference Frame	0.53 g	0.40 g	21837.18 kN
Set-1	0.60 g	0.43 g	22453.48 kN
Set-2	0.70 g	0.47 g	23454.07 kN

The hinging and plastic rotation demands and drift ratio distributions along the structure height of all models at 0.70g acceleration intensity, where the 10-story Set-2 structure under the Park Field earthquake reached the 4.00% drift ratio limit;



Reference Frame- Max R3 Plastic = 6.006%

SET 1- Max R3 Plastic = 5.312 %



SET 2- Max R3 Plastic = 3.278%

Figure 5.80: Hinging and plastic rotation demands of 10-story models at S_a=0.70g under the Park Field earthquake.

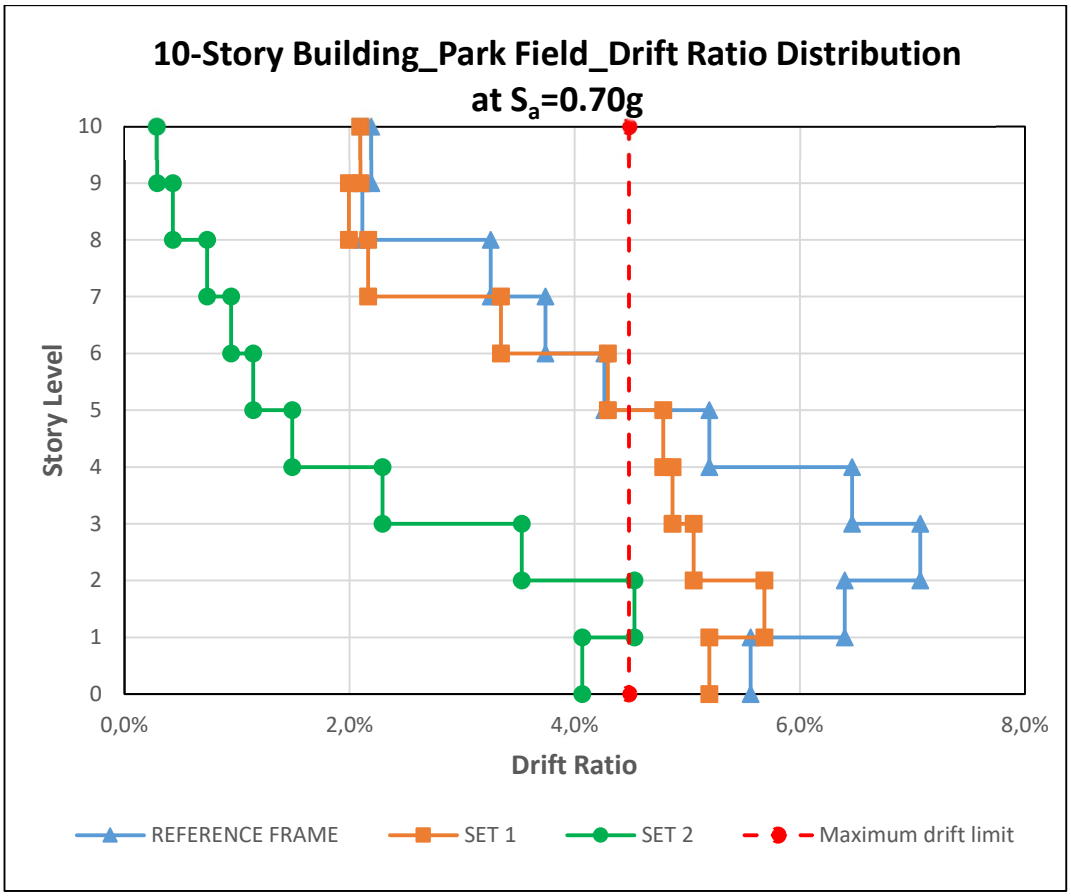


Figure 5.81: Drift ratio distributions along 10-story models' height at S_a=0.70g under the Park Field earthquake.

5.2.3 L'Aquila_4481 Earthquake

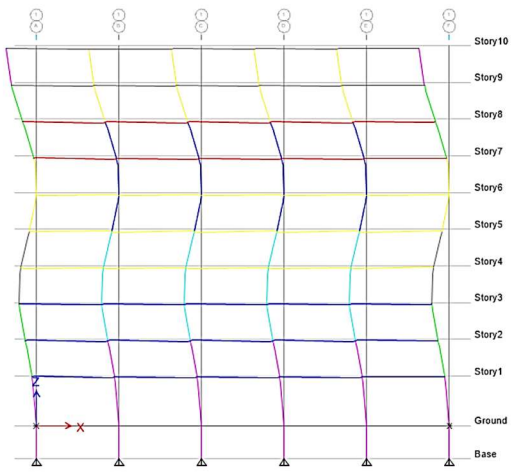
Table 5.19: SFs for 10-story models under the L'Aquila earthquake.

10 Story_Reference Frame		
(S_a)	(SF)	Scale
g	unitless	mm/s²
0,063	1,000	9806,650
0,100	1,578	15472,454
0,180	**2,842**	**27875,174**
0,200	3,156	30944,909
0,300	4,733	46417,363
0,400	6,311	61889,818
0,500	7,889	77362,272
0,600	9,467	92834,726

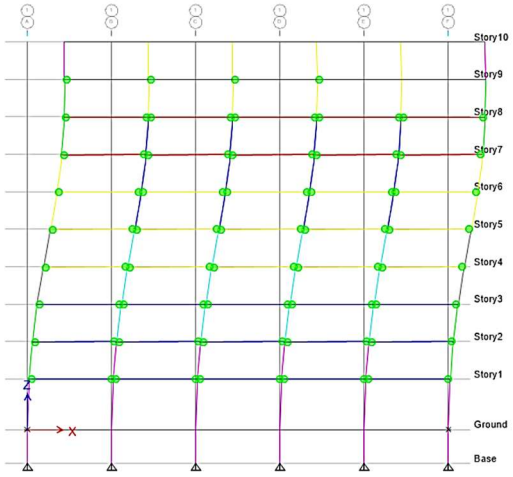
10 Story_Set 1		
(S_a)	(SF)	Scale
g	unitless	mm/s²
0,065	1,000	9806,650
0,100	1,533	15037,309
0,183	**2,806**	**27521,283**
0,200	3,067	30074,618
0,300	4,600	45111,927
0,400	6,134	60149,235
0,500	7,667	75186,544
0,600	9,200	90223,853

10 Story_Set 2		
(S_a)	(SF)	Scale
g	unitless	mm/s²
0,070	1,000	9806,650
0,100	1,431	14029,478
0,189	**2,707**	**26543,773**
0,200	2,861	28058,957
0,300	4,292	42088,435
0,400	5,722	56117,914
0,500	7,153	70147,392
0,600	8,584	84176,870

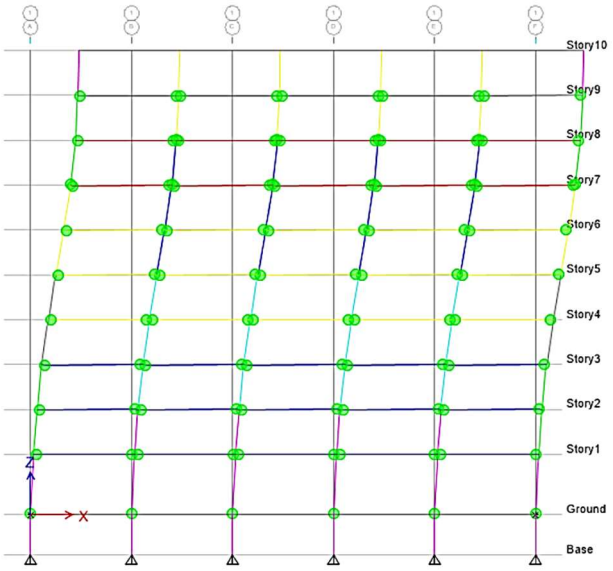
Application of acceleration intensities to 10-story models under L'Aquila earthquake in three stages starting from the acceleration intensities corresponding to the SF obtained from the design spectrum;



Reference Frame _ 0.180g _ SF=2.842
Max R3 Plastic = 0.097%

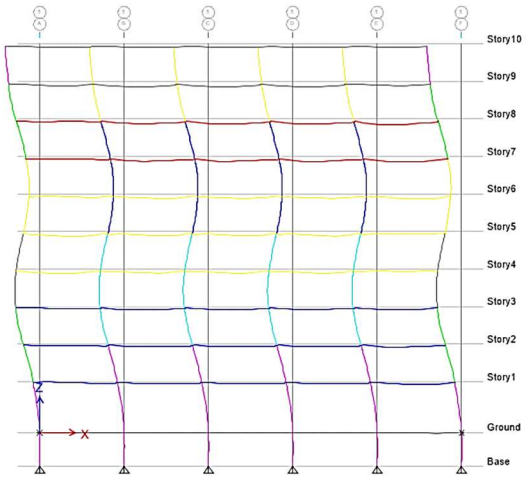


Reference Frame _ 0.30g _ SF=4.733
Max R3 Plastic = 1.263%

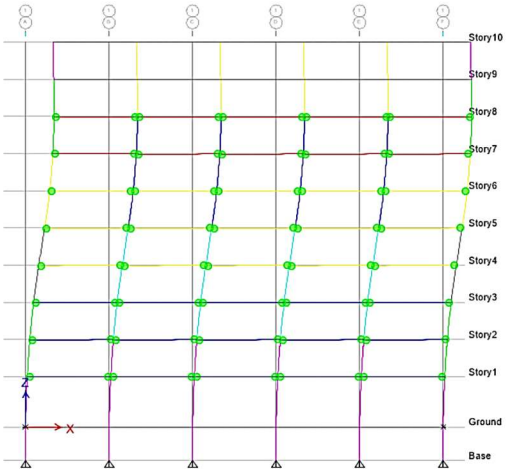


Reference Frame _ 0.50g _ SF=7.889
Max R3 Plastic = 4.821%

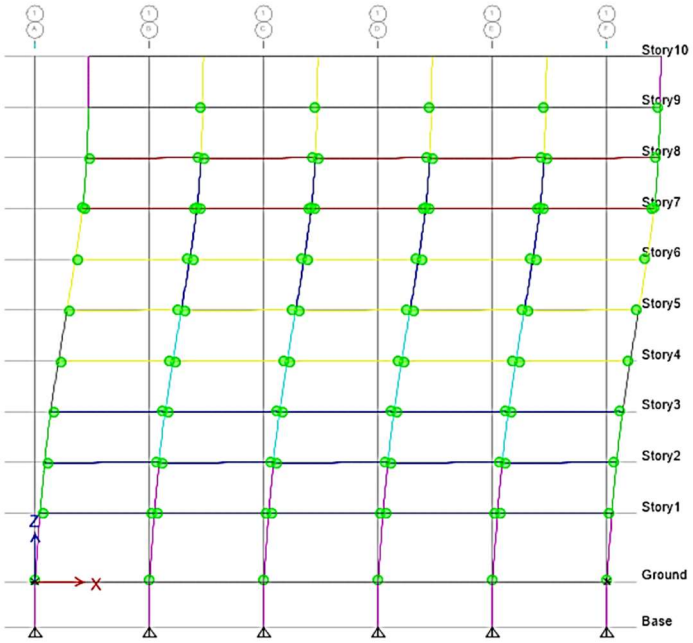
Figure 5.82: Hingings and plastic rotation demands of 10-story RFs under the L'Aquila earthquake.



SET 1 _ 0.183g _ SF=2.806
Max R3 Plastic = 0.102%



SET 1 _ 0.30g _ SF=4.600
Max R3 Plastic = 1.120%



SET 1 _ 0.50g _ SF=7.667
Max R3 Plastic = 4.594%

Figure 5.83: Hingings and plastic rotation demands of 10-story Set-1 under the L'Aquila earthquake.

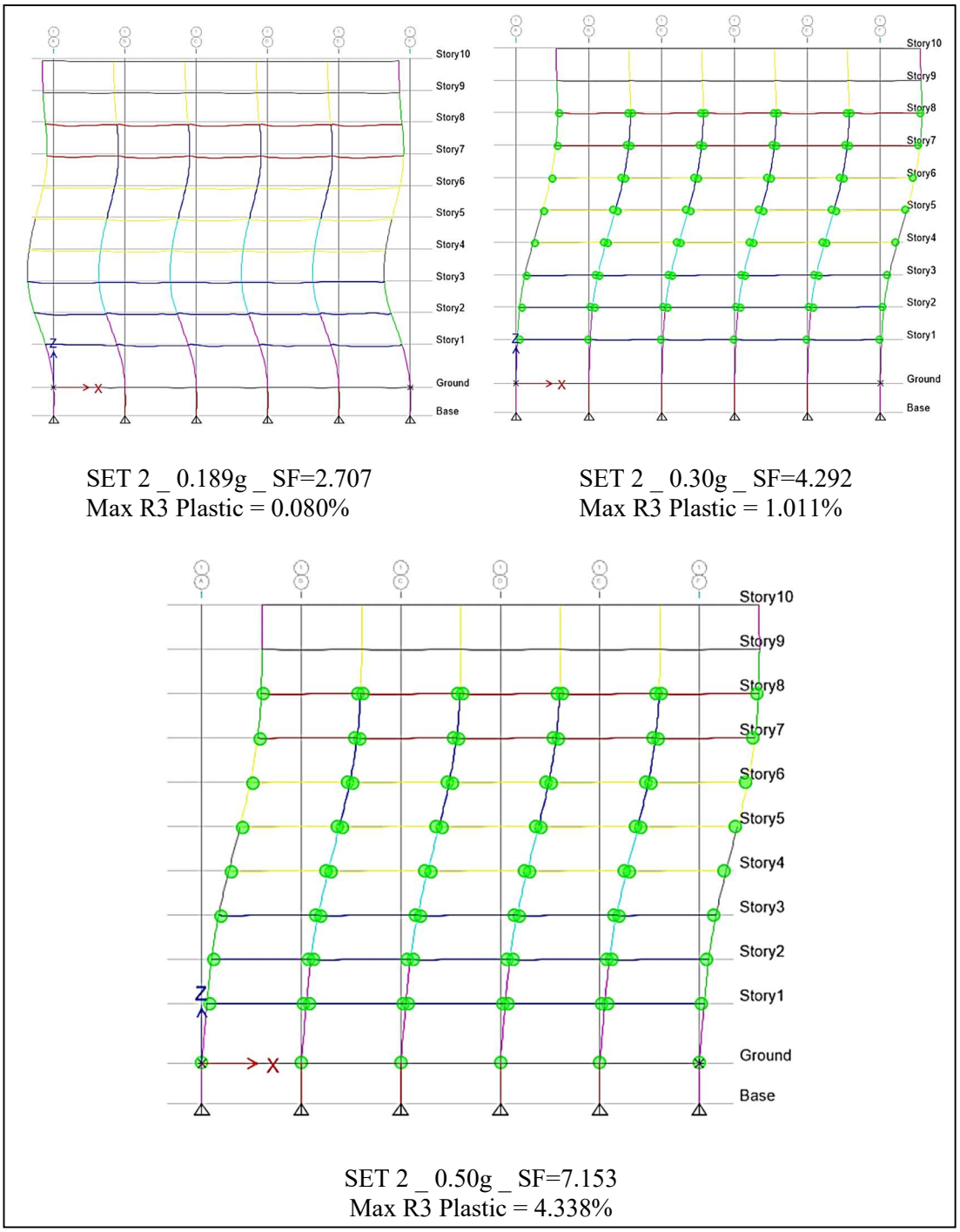


Figure 5.84: Hingings and plastic rotation demands of 10-story Set-2 under the L'Aquila earthquake.

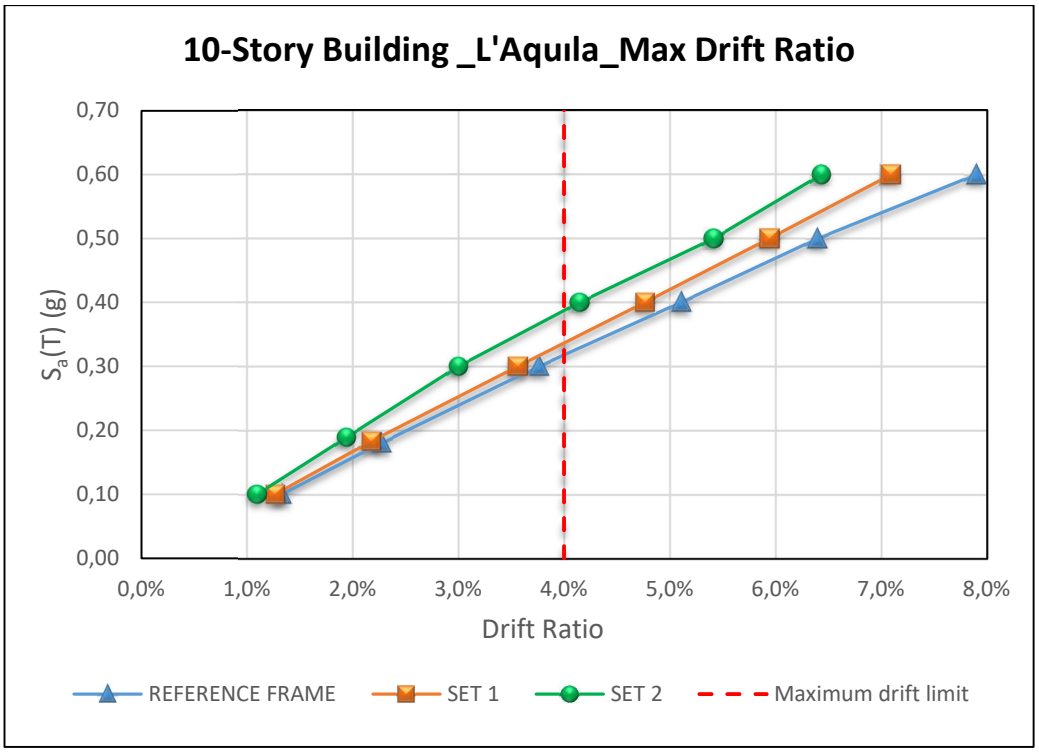


Figure 5.85: Max drift ratios of 10-story models under L'Aquila earthquake acceleration intensities.

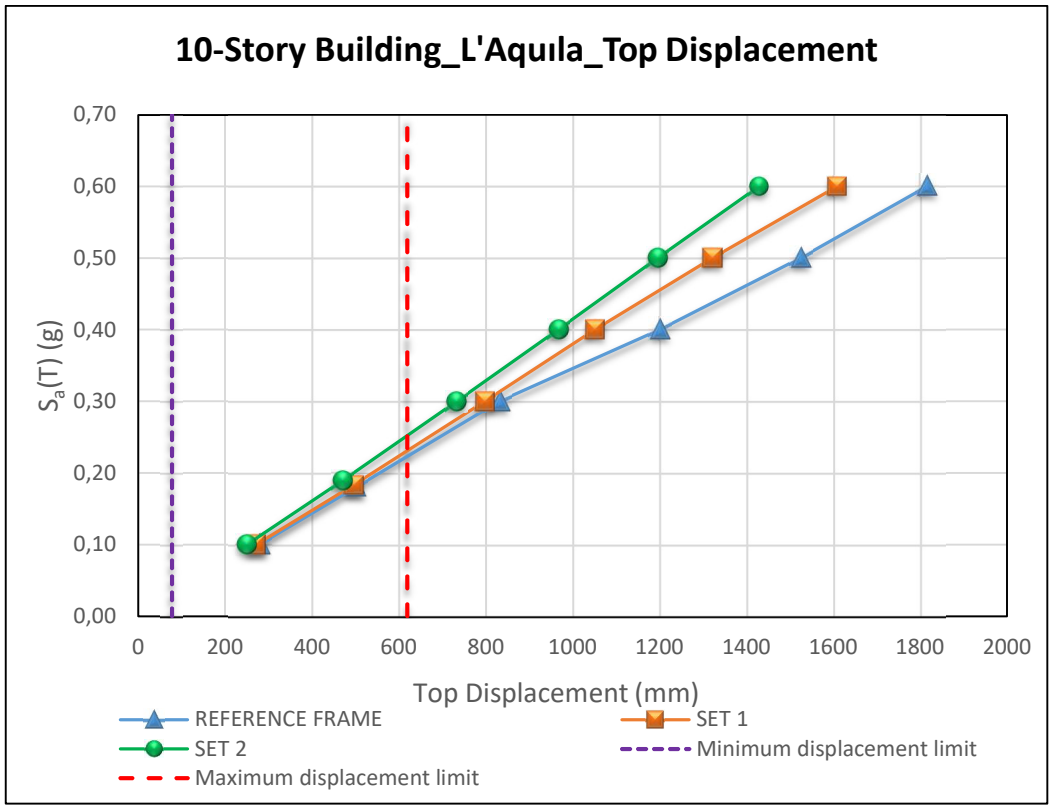


Figure 5.86: Max top displacements of 10-story models under L'Aquila earthquake acceleration intensities.

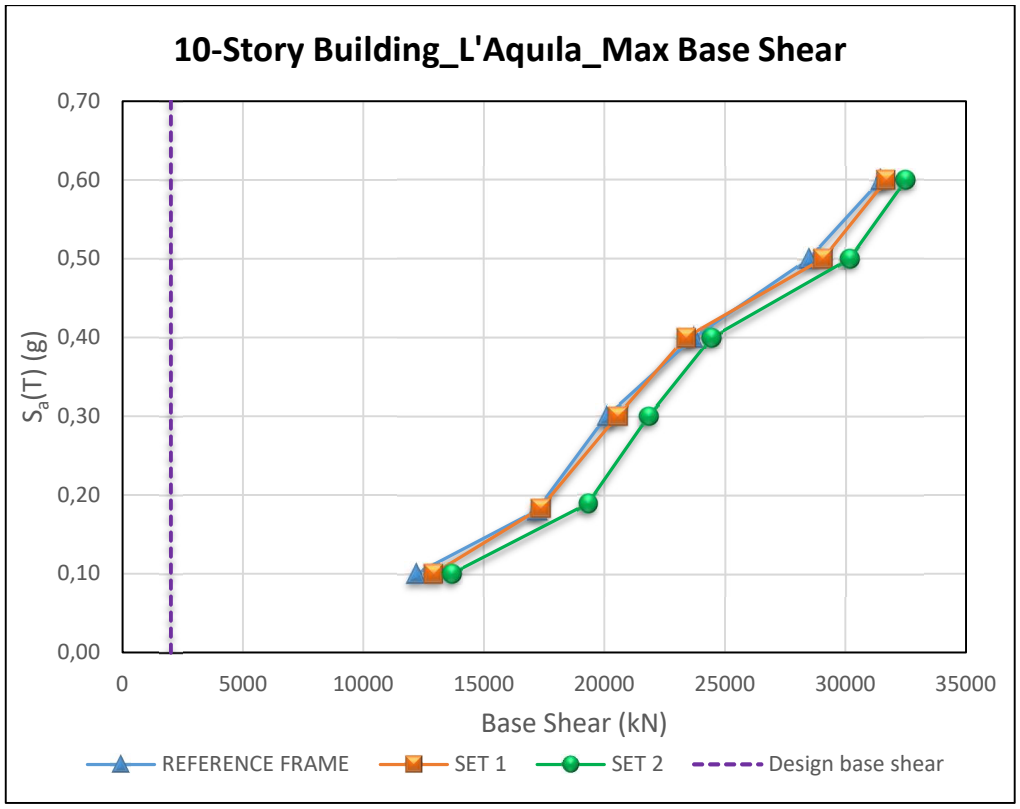


Figure 5.87: Max base shears of 10-story models under L'Aquila earthquake acceleration intensities.

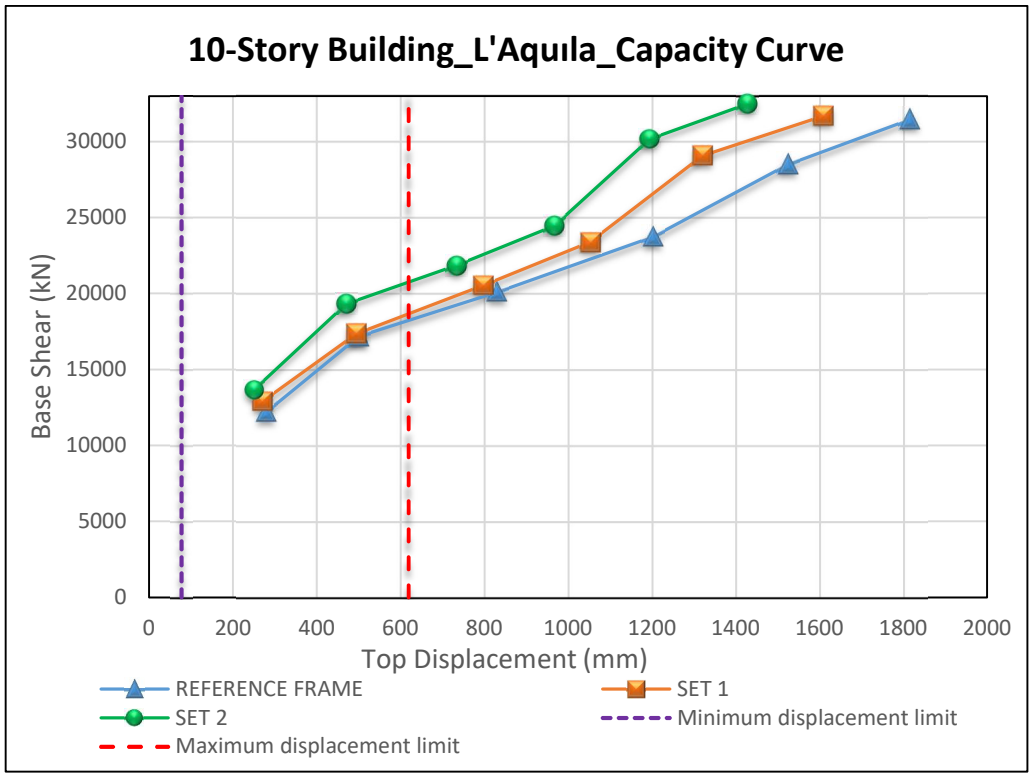
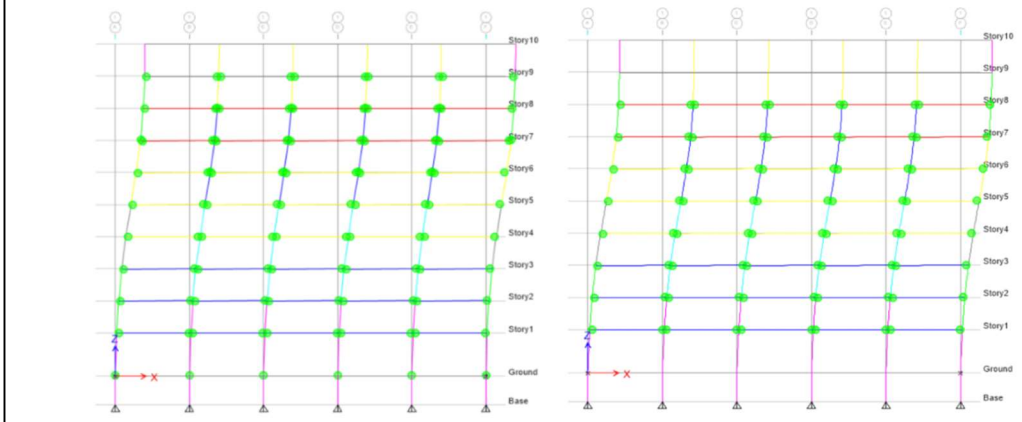


Figure 5.88: Capacity curves of 10-story models under L'Aquila earthquake acceleration intensities.

Table 5.20: Responses of 10-story models under L'Aquila earthquake.

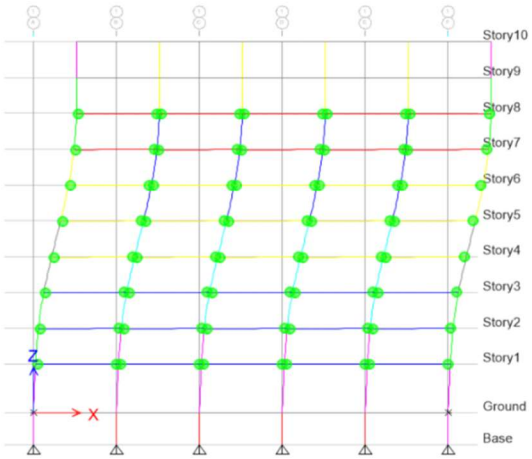
LAQUILA / 10-STORY	S_a(T) values corresponding to drift ratio limit	S_a(T) values corresponding to maximum top displacement limit	The base shears corresponding to maximum top displacement
Reference Frame	0.32 g	0.22 g	18218.19 kN
Set-1	0.34 g	0.23 g	18645.32 kN
Set-2	0.40 g	0.25 g	20738.92 kN

The hinging and plastic rotation demands and drift ratio distributions along the structure height of all models at 0.40g acceleration intensity, where the 10-story Set-2 structure under the L'Aquila earthquake reached the drift ratio limit;



Reference Frame- Max R3 Plastic = 4.192%

SET 1- Max R3 Plastic = 3.716%



SET 2- Max R3 Plastic = 3.214%

Figure 5.89: Hinging and plastic rotation demands of 10-story models at S_a=0.40g under the L'Aquila earthquake.

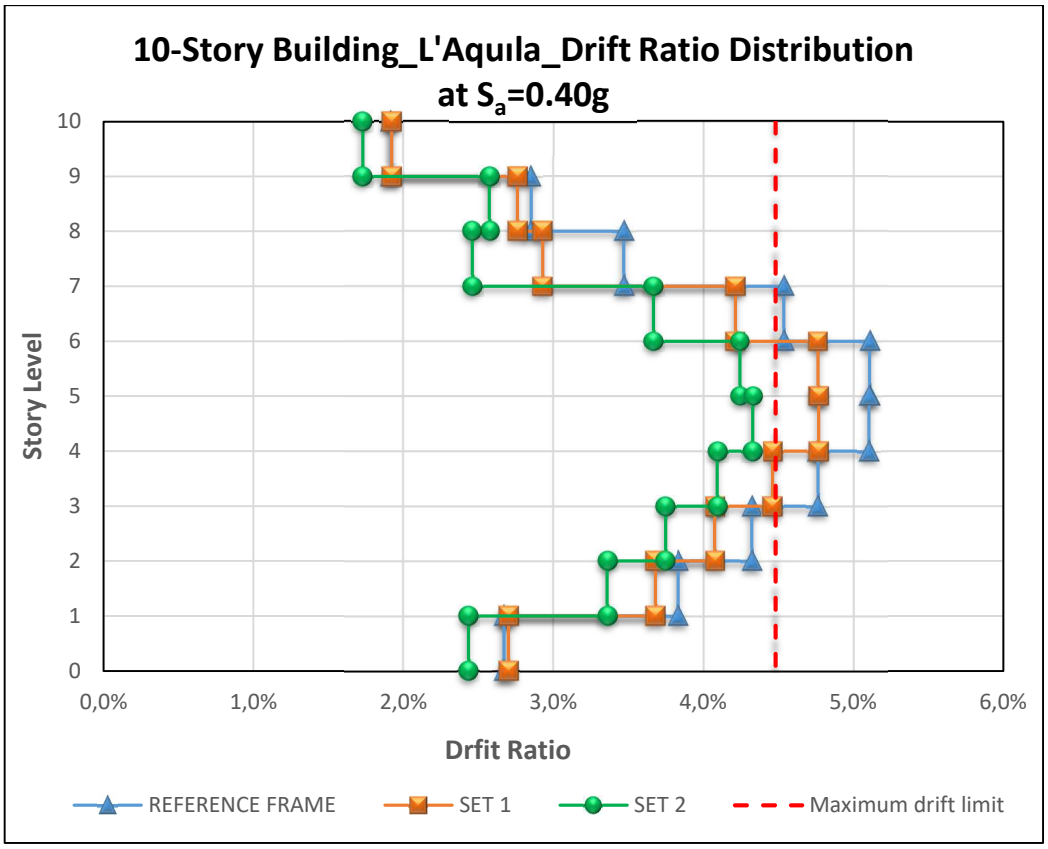


Figure 5.90: Drift ratio distributions along 10-story models' height at S_a=0.40g under the L'Aquila earthquake.

5.2.4 Kobe_1111 Earthquake

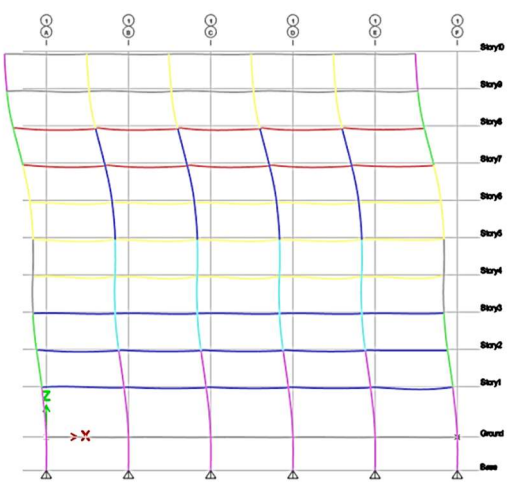
Table 5.21: SFs for 10-story models under the Kobe earthquake.

10 Story_Reference Frame		
(S_a)	(SF)	Scale
g	unitless	mm/s²
0,100	0,865	8478,393
0,116	1,000	9806,650
0,180	**1,558**	**15274,672**
0,200	1,729	16956,785
0,300	2,594	25435,178
0,400	3,458	33913,570
0,500	4,323	42391,963
0,600	5,187	50870,356
0,700	6,052	59348,748
0,800	6,916	67827,141
0,900	7,781	76305,534
1,000	8,646	84783,926
1,100	9,510	93262,319

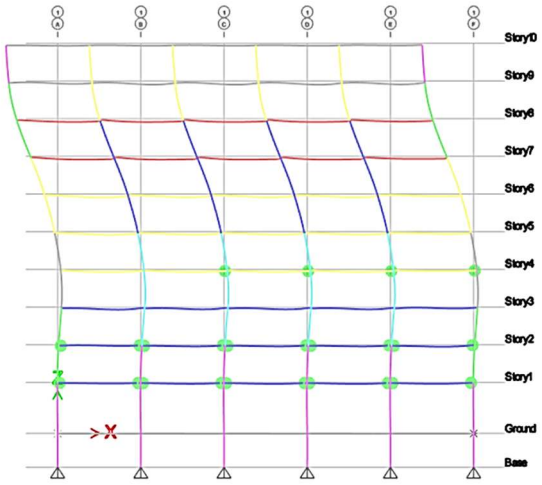
10 Story_Set 1		
(S_a)	(SF)	Scale
g	unitless	mm/s²
0,100	0,803	7873,237
0,125	1,000	9806,650
0,183	**1,469**	**14409,598**
0,200	1,606	15746,473
0,300	2,409	23619,710
0,400	3,211	31492,946
0,500	4,014	39366,183
0,600	4,817	47239,420
0,700	5,620	55112,656
0,800	6,423	62985,893
0,900	7,226	70859,129
1,000	8,028	78732,366
1,100	8,831	86605,603

10 Story_Set 2		
(S_a)	(SF)	Scale
g	unitless	mm/s²
0,100	0,680	6664,544
0,147	0,999	9796,879
0,189	**1,286**	**12609,317**
0,200	1,359	13329,087
0,300	2,039	19993,631
0,400	2,718	26658,174
0,500	3,398	33322,718
0,600	4,078	39987,262
0,700	4,757	46651,805
0,800	5,437	53316,349
0,900	6,116	59980,893
1,000	6,796	66645,436
1,100	7,476	73309,980

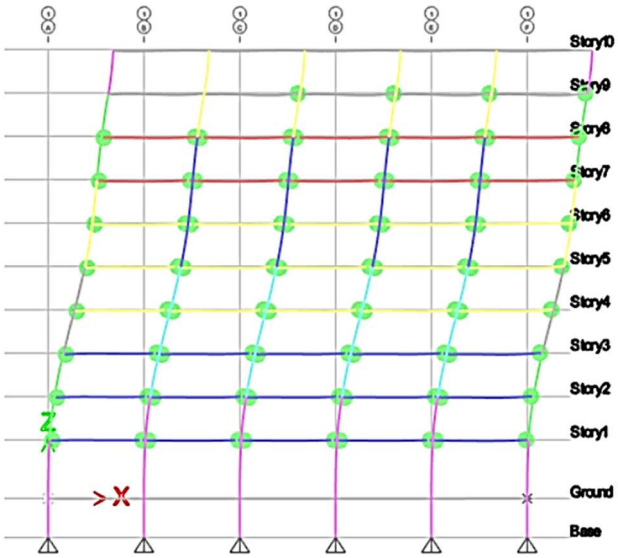
Application of acceleration intensities to 10-story models under Kobe earthquake in three stages starting from the acceleration intensities corresponding to the SF obtained from the design spectrum;



Reference Frame _ 0.180g _ SF= 1.558
Max R3 Plastic = 0.676%



Reference Frame _ 0.30g _ SF= 2.594
Max R3 Plastic = 1.545%



Reference Frame _ 0.50g _ SF=4.323
Max R3 Plastic = 3.718%

Figure 5.91: Hingings and plastic rotation demands of 10-story RFs under the Kobe earthquake.

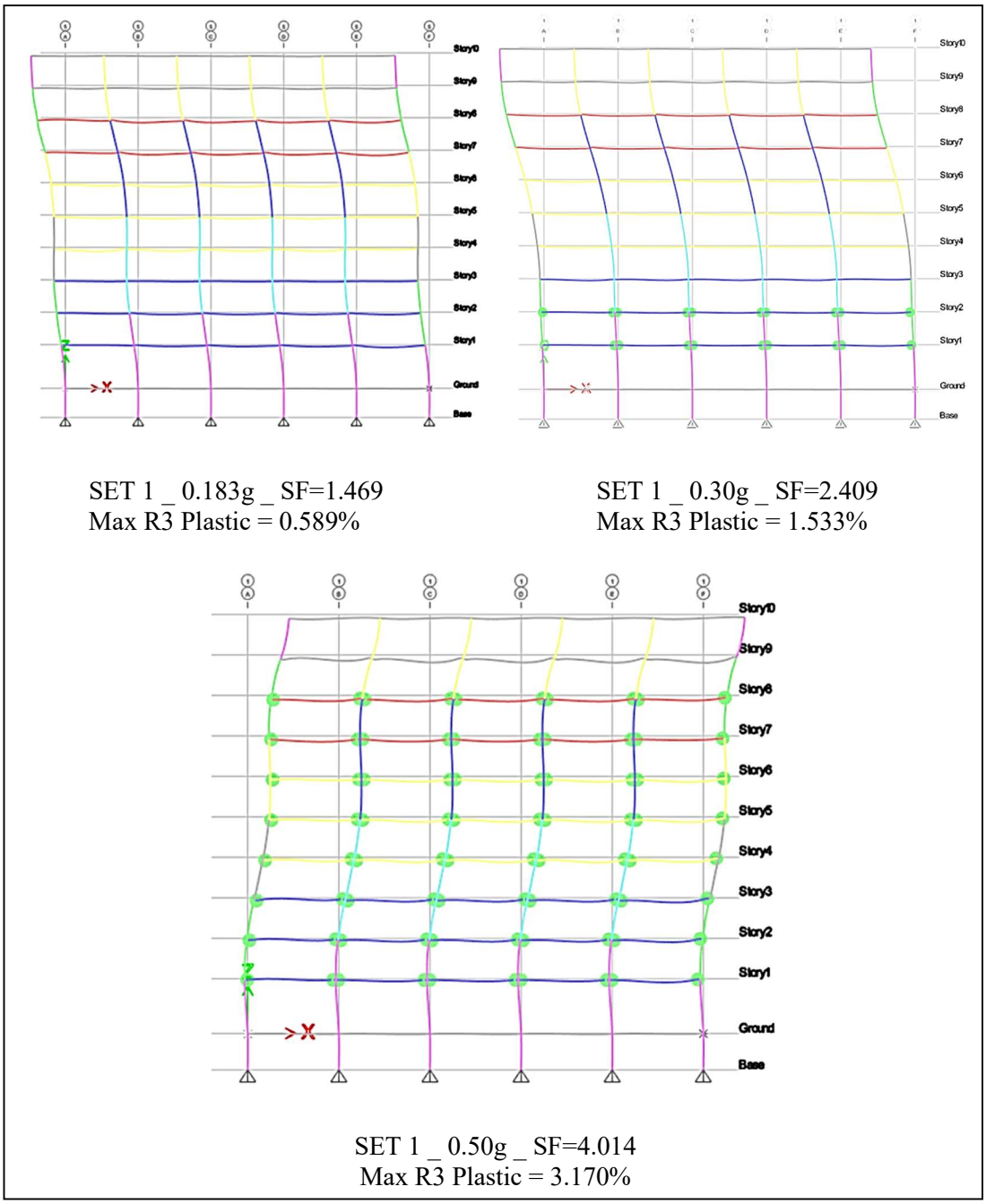
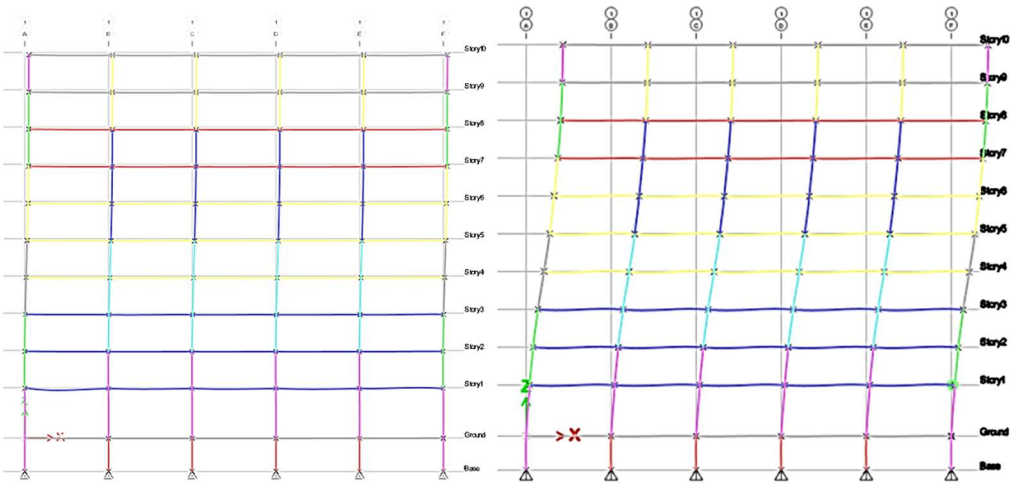
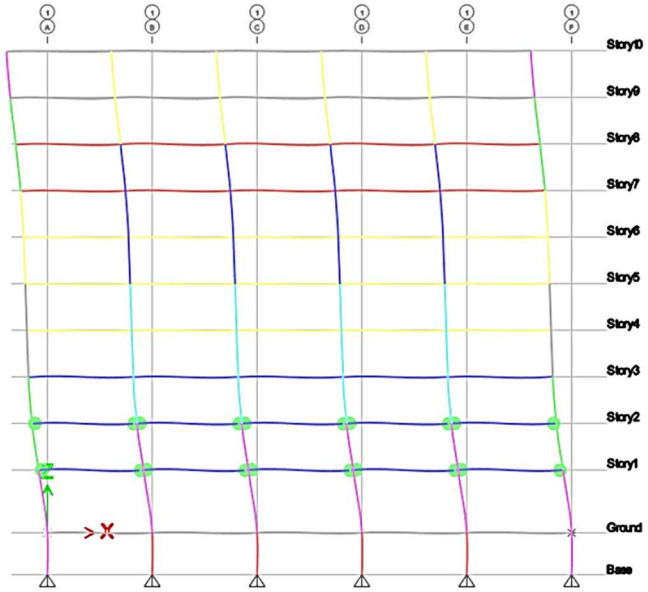


Figure 5.92: Hingings and plastic rotation demands of 10-story Set-1 under the Kobe earthquake.



SET 2 _ 0.189g _ SF=1.286
Max R3 Plastic = 0.368%

SET 2 _ 0.30g _ SF=2.039
Max R3 Plastic = 0.961%



SET 2 _ 0.50g _ SF=3.398
Max R3 Plastic = 2.187%

Figure 5.93: Hingings and plastic rotation demands of 10-story Set-2 under the Kobe earthquake.

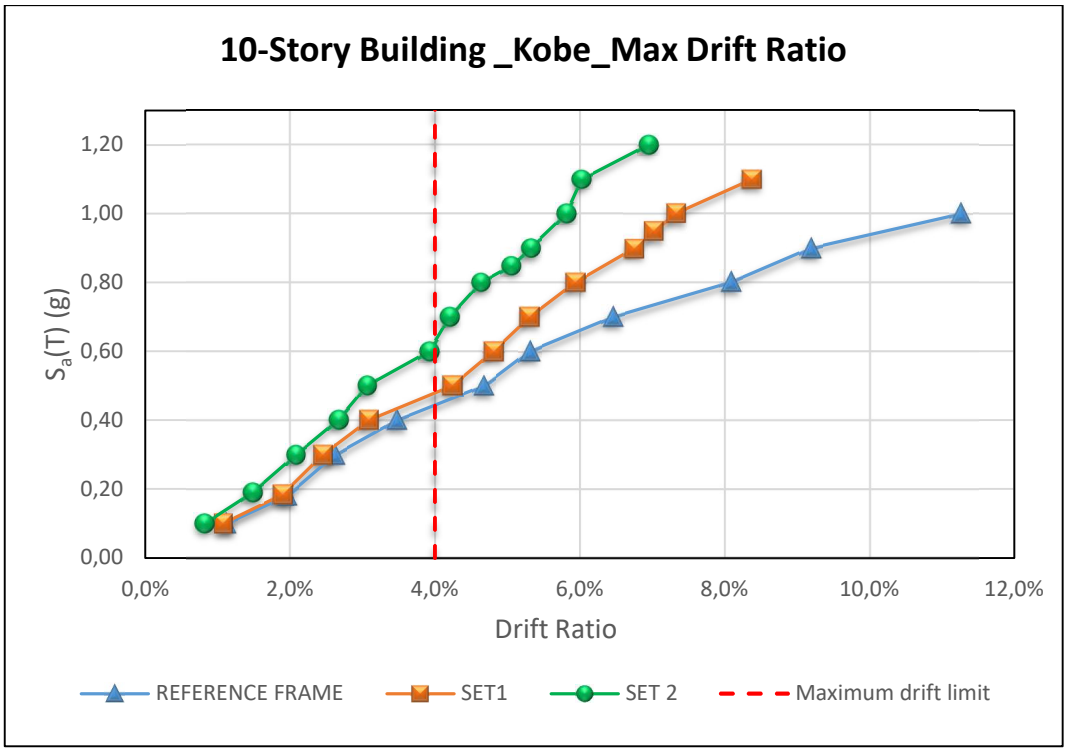


Figure 5.94: Max drift ratios of 10-story models under Kobe earthquake acceleration intensities.

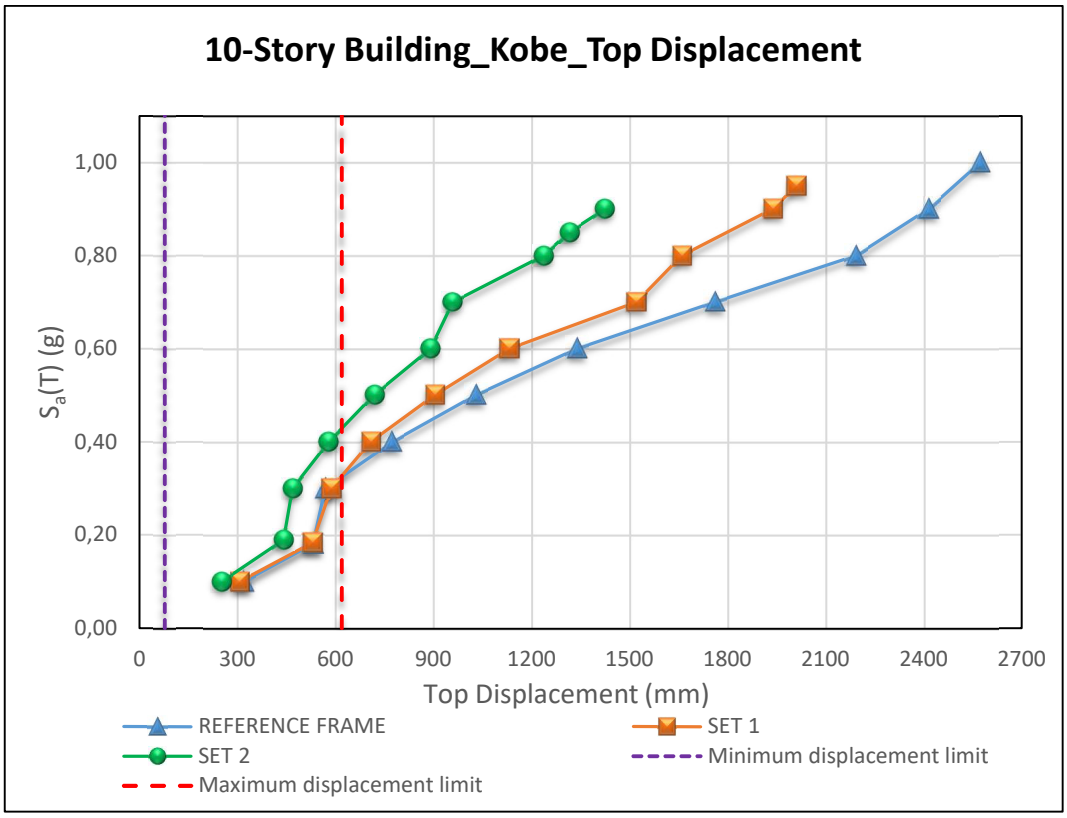


Figure 5.95: Max top displacements of 10-story models under Kobe earthquake acceleration intensities.

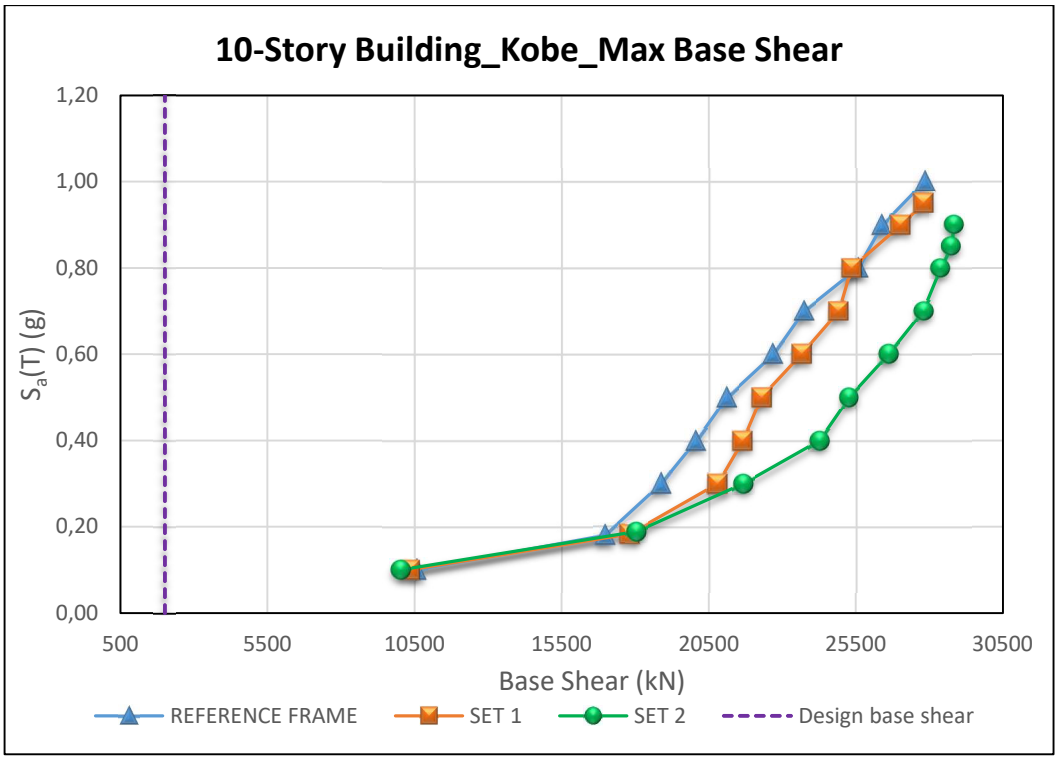


Figure 5.96: Max base shears of 10-story models under Kobe earthquake acceleration intensities.

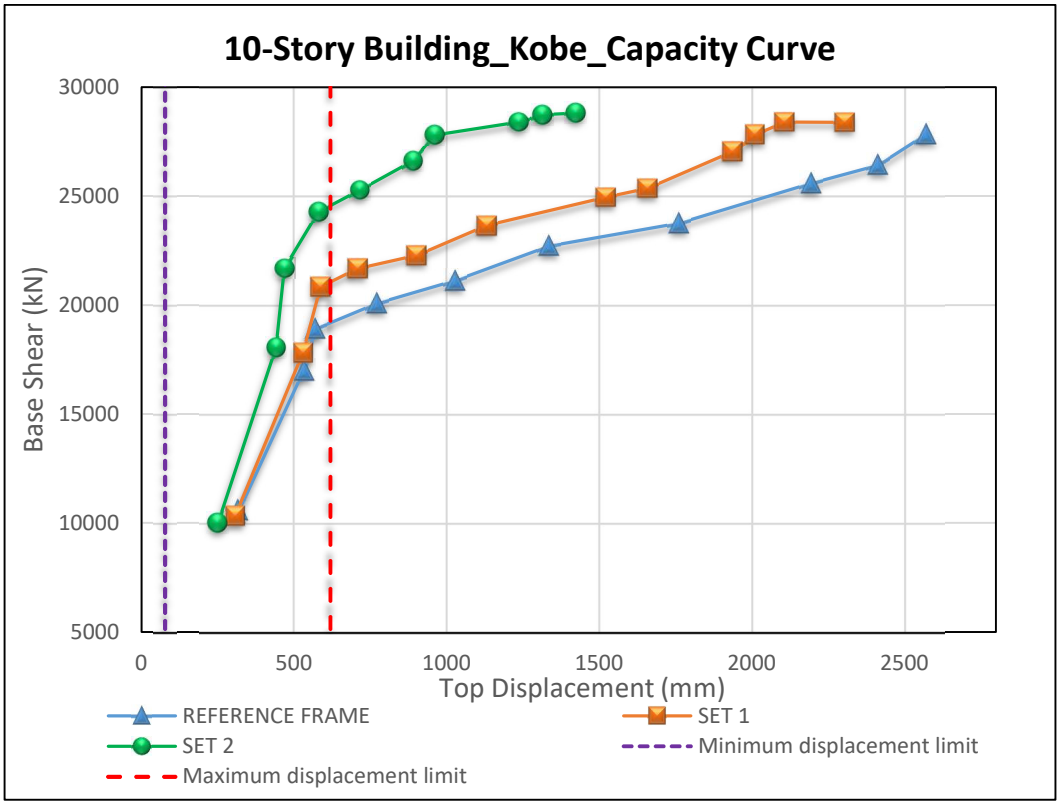
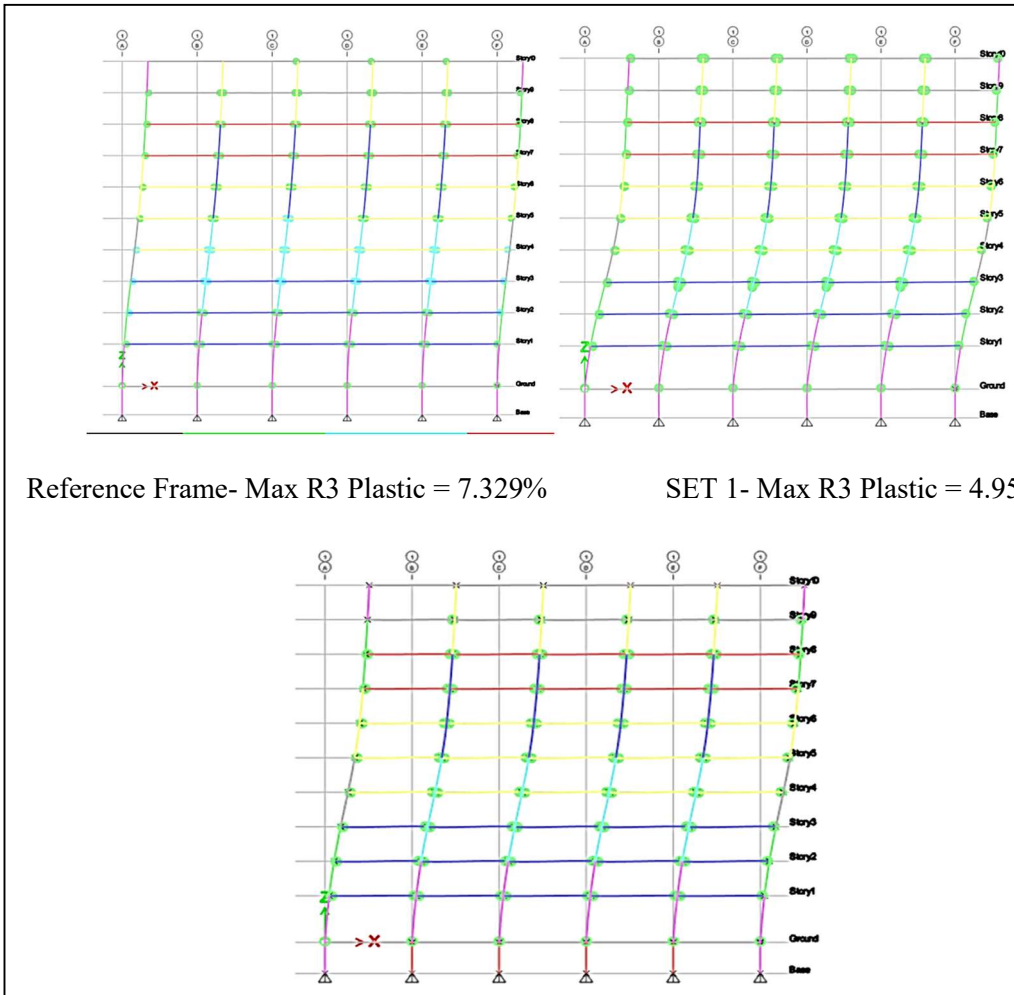


Figure 5.97: Capacity curves of 10-story models under Kobe earthquake acceleration intensities.

Table 5.22: Responses of 10-story models under Kobe earthquake.

KOBE / 10-STORY	S_a(T) values corresponding to drift ratio limit	S_a(T) values corresponding to maximum top displacement limit	The base shears corresponding to maximum top displacement
Reference Frame	0.44 g	0.32 g	19180.66 kN
Set-1	0.48 g	0.33 g	21046.16 kN
Set-2	0.60 g	0.43 g	24556.03 kN

The hinging and plastic rotation demands and drift ratio distributions along the structure height of all models at 0.60g acceleration intensity, where the 10-story Set-2 structure under the Kobe earthquake reached the 4.00% drift ratio limit;



Reference Frame- Max R3 Plastic = 7.329%

SET 1- Max R3 Plastic = 4.959%

SET 2- Max R3 Plastic = 4.392%

Figure 5.98: Hinging and plastic rotation demands of 10-story models at S_a=0.60g under the Kobe earthquake.

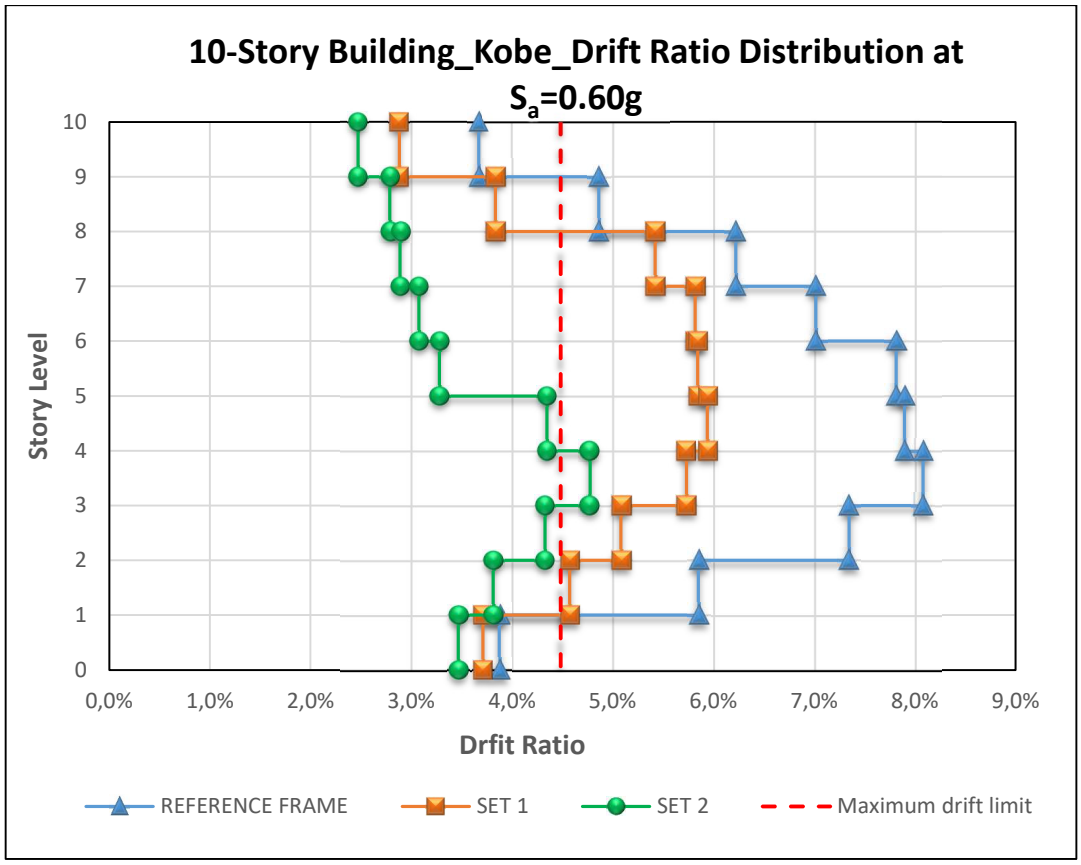


Figure 5.99: Drift ratio distributions along 10-story models' height at S_a=0.60g under the Kobe earthquake.

5.2.5 New Zealand_587 Earthquake

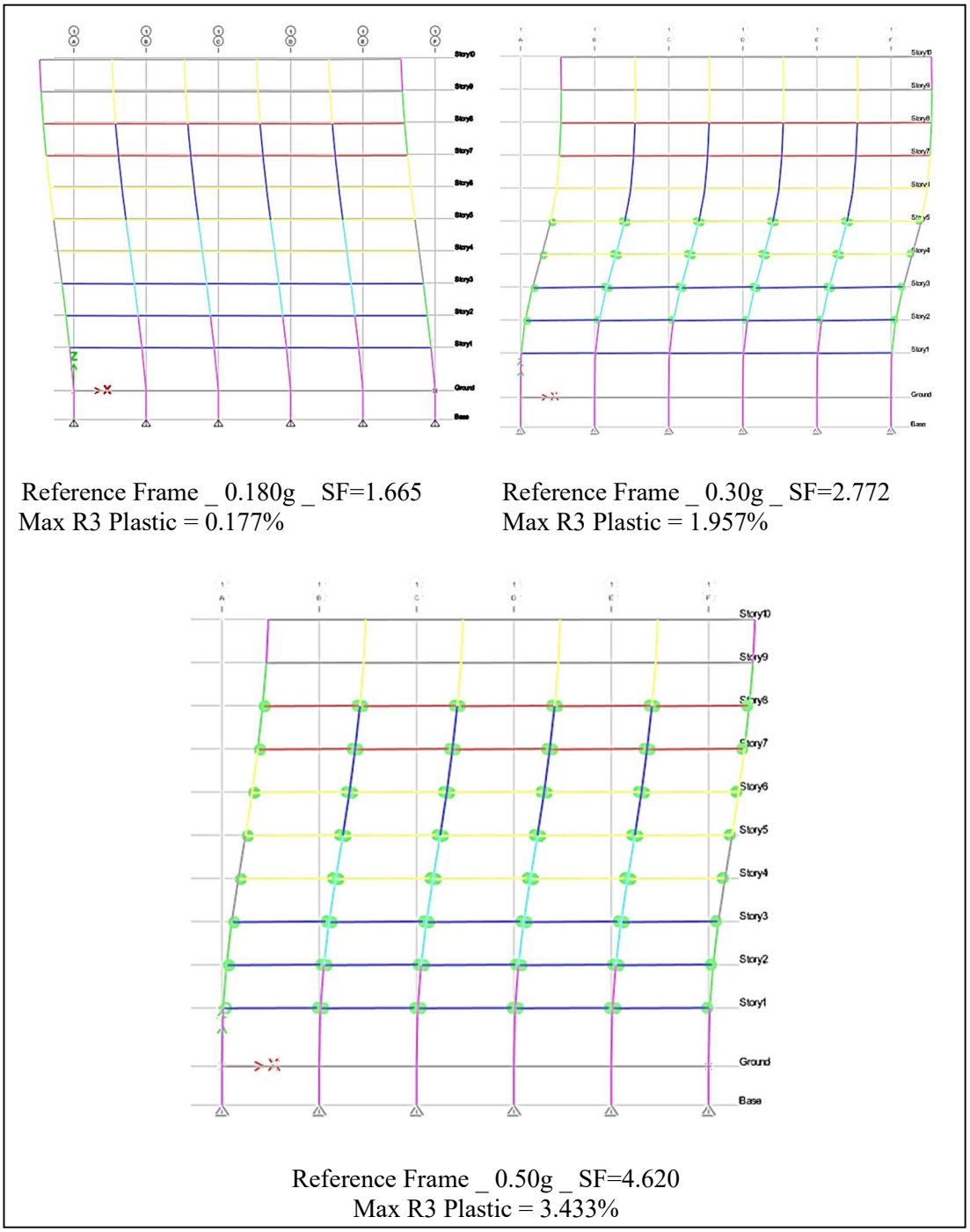
Table 5.23: SFs for 10-story models under the New Zealand earthquake.

10 Story_Reference Frame		
(S_a)	(SF)	Scale
g	unitless	mm/s²
0,100	0,924	9060,561
0,108	1,000	9806,650
0,180	**1,665**	**16323,507**
0,200	1,848	18121,122
0,300	2,772	27181,683
0,400	3,696	36242,244
0,500	4,620	45302,805
0,600	5,544	54363,366
0,700	6,467	63423,927
0,800	7,391	72484,488
0,900	8,315	81545,049

10 Story_Set 1		
(S_a)	(SF)	Scale
g	unitless	mm/s²
0,100	0,978	9592,429
0,102	1,000	9806,650
0,183	**1,790**	**17556,064**
0,200	1,956	19184,858
0,300	2,934	28777,288
0,400	3,913	38369,717
0,500	4,891	47962,146
0,600	5,869	57554,575
0,700	6,847	67147,004
0,800	7,825	76739,433
0,900	8,803	86331,863

10 Story_Set 2		
(S_a)	(SF)	Scale
g	unitless	mm/s²
0,087	1,000	9806,650
0,100	1,154	11320,988
0,189	**2,184**	**21419,309**
0,200	2,309	22641,976
0,300	3,463	33962,964
0,400	4,618	45283,952
0,500	5,772	56604,940
0,600	6,927	67925,927
0,700	8,081	79246,915
0,800	9,235	90567,903
0,900	10,390	101888,891

Application of acceleration intensities to 10-story models under New Zealand earthquake in three stages starting from the acceleration intensities corresponding to the SF obtained from the design spectrum;

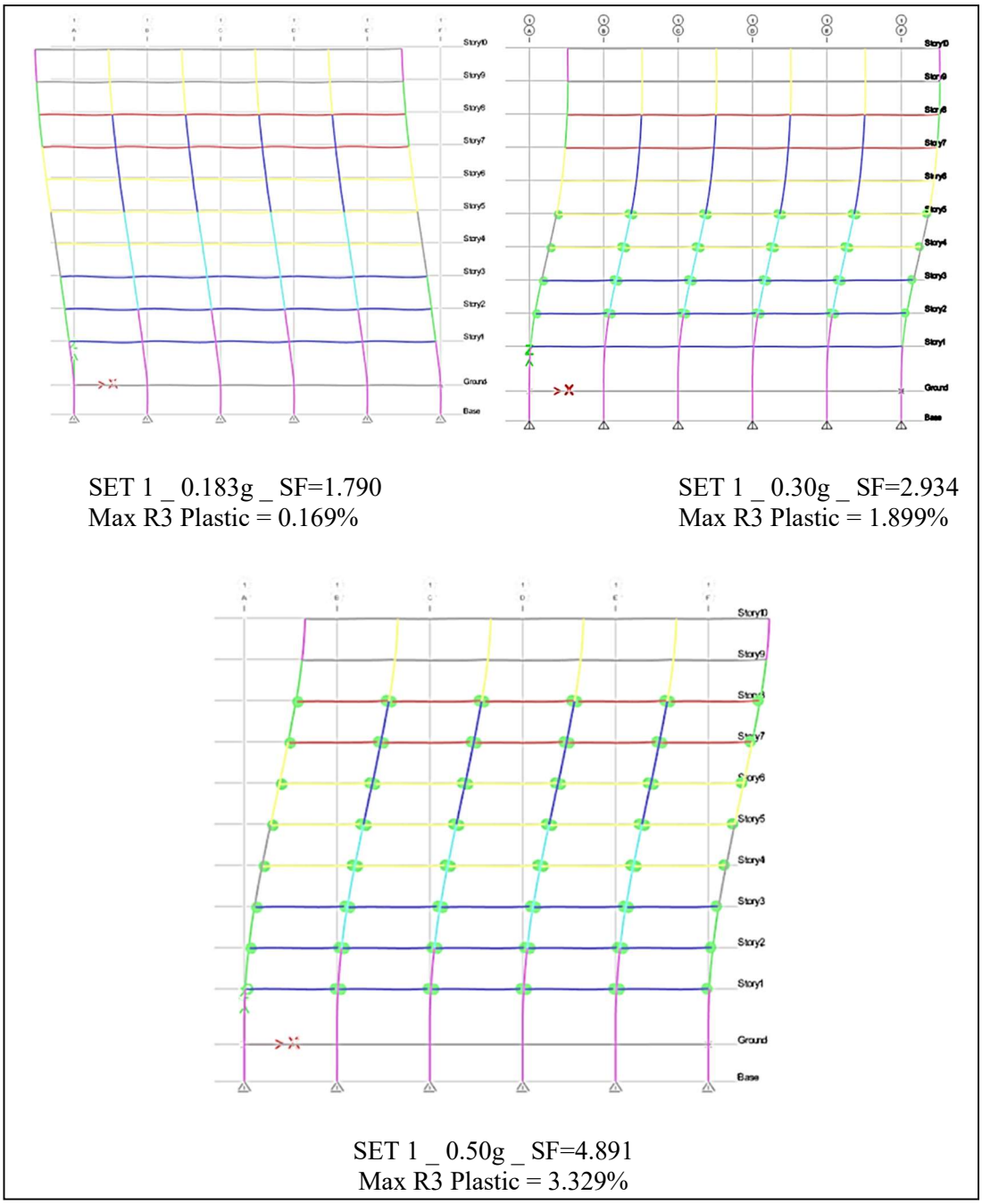


Reference Frame _ 0.180g _ SF=1.665
Max R3 Plastic = 0.177%

Reference Frame _ 0.30g _ SF=2.772
Max R3 Plastic = 1.957%

Reference Frame _ 0.50g _ SF=4.620
Max R3 Plastic = 3.433%

Figure 5.100: Hingings and plastic rotation demands of 10-story RFs under the New Zealamd earthquake.

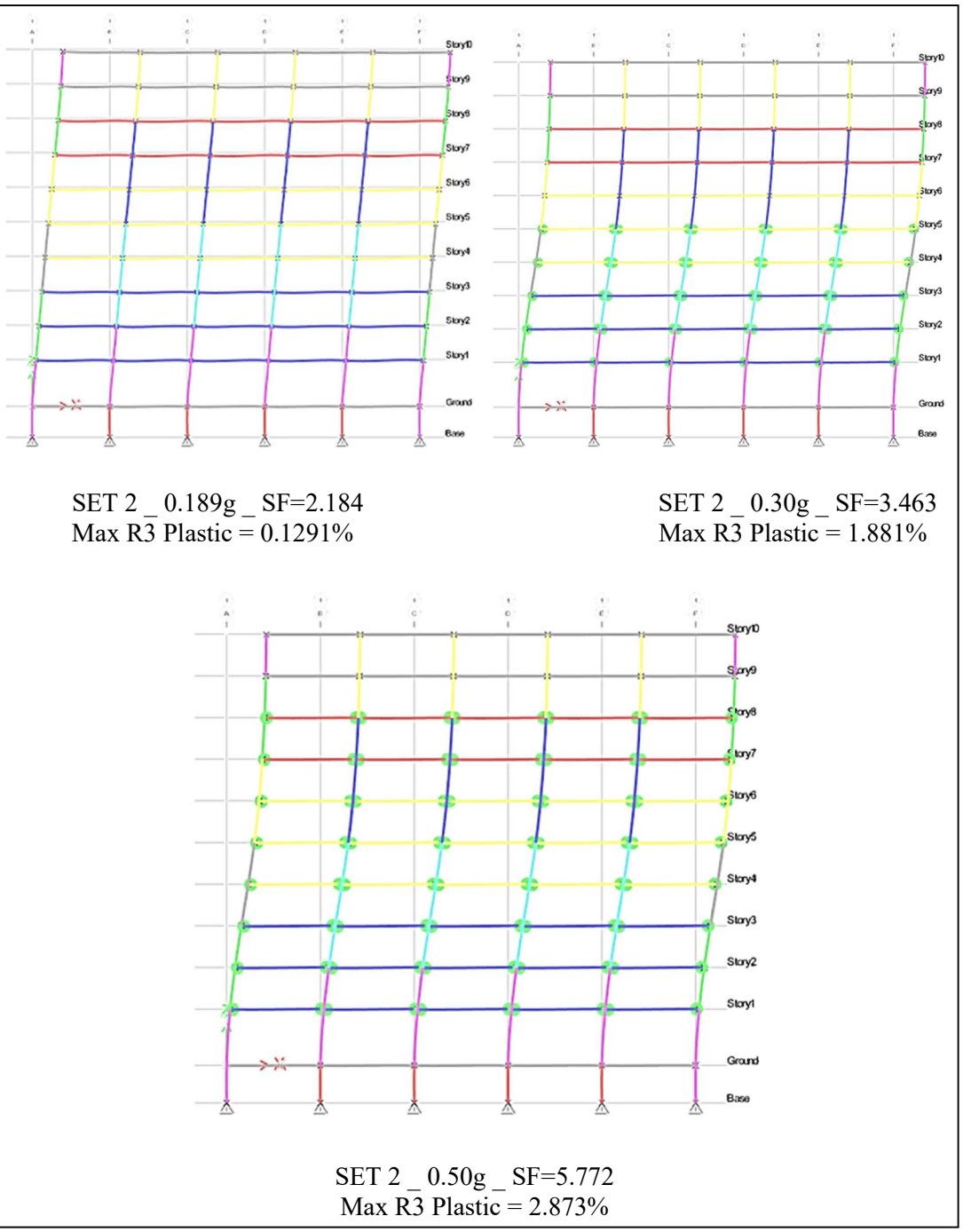


SET 1 _ 0.183g _ SF=1.790
Max R3 Plastic = 0.169%

SET 1 _ 0.30g _ SF=2.934
Max R3 Plastic = 1.899%

SET 1 _ 0.50g _ SF=4.891
Max R3 Plastic = 3.329%

Figure 5.101: Hingings and plastic rotation demands of 10-story Set-1 under the New Zealamd earthquake.



SET 2 _ 0.189g _ SF=2.184
Max R3 Plastic = 0.1291%

SET 2 _ 0.30g _ SF=3.463
Max R3 Plastic = 1.881%

SET 2 _ 0.50g _ SF=5.772
Max R3 Plastic = 2.873%

Figure 5.102: Hingings and plastic rotation demands of 10-story Set-2 under the New Zealamd earthquake.

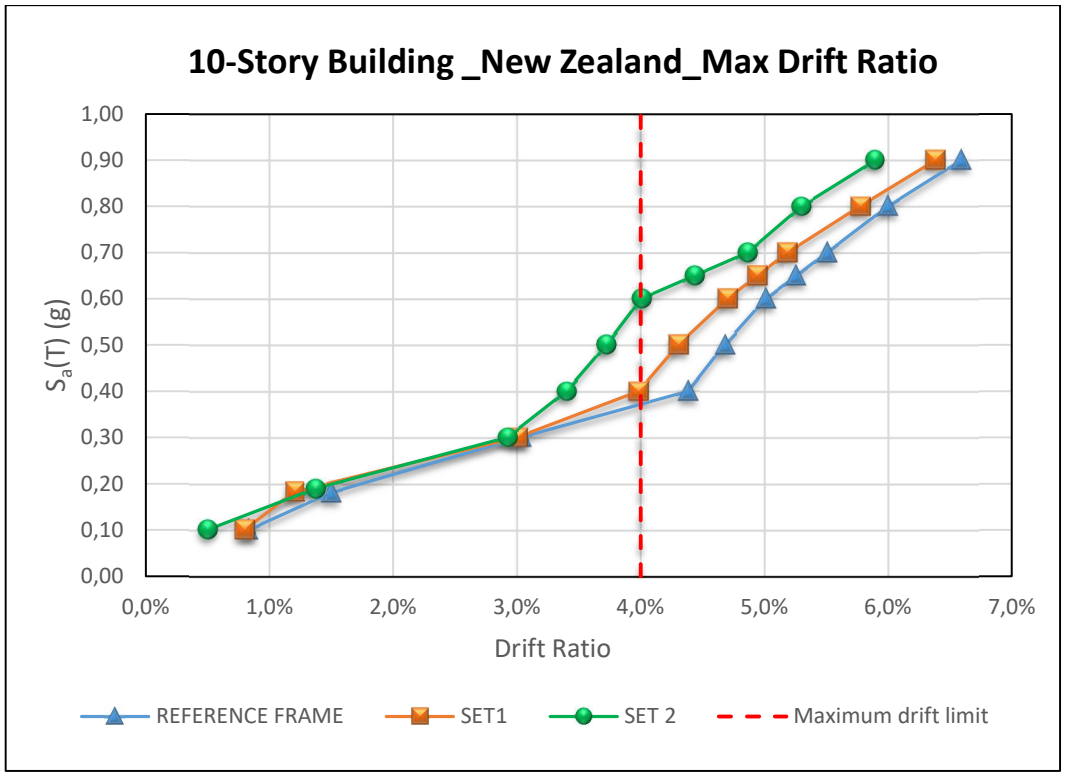


Figure 5.103: Max drift ratios of 10-story models under New Zealand earthquake acceleration intensities.

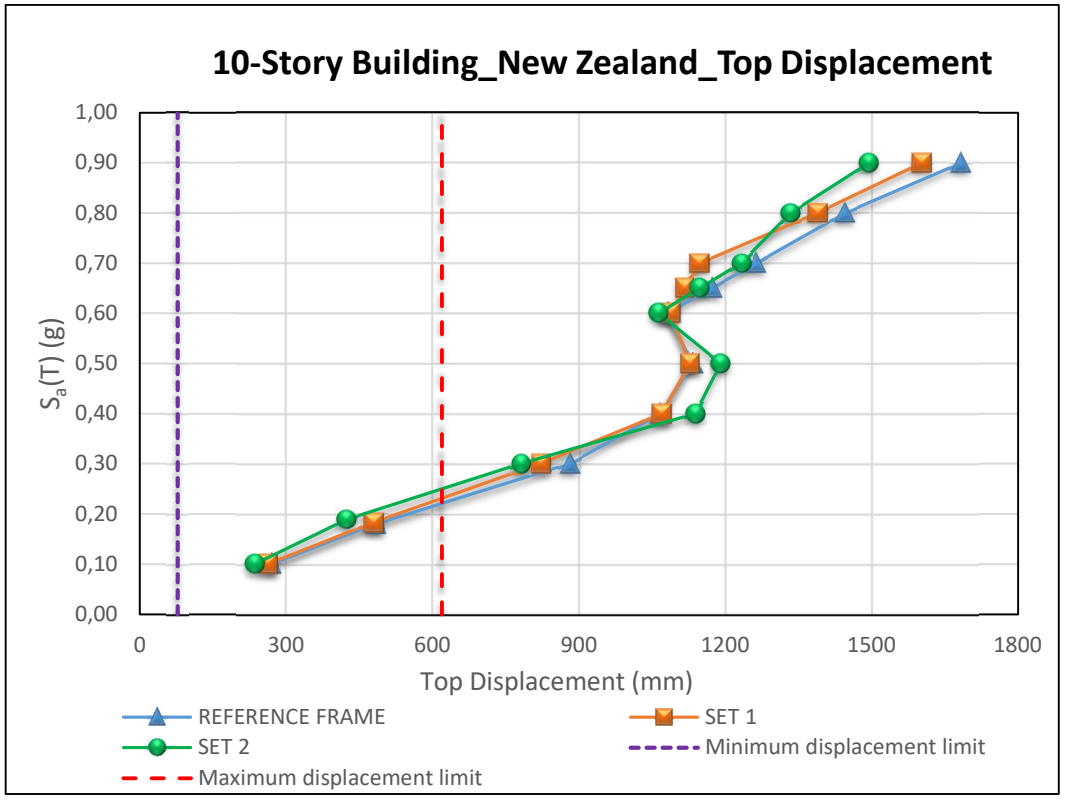


Figure 5.104: Max top displacements of 10-story models under New Zealand earthquake acceleration intensities.

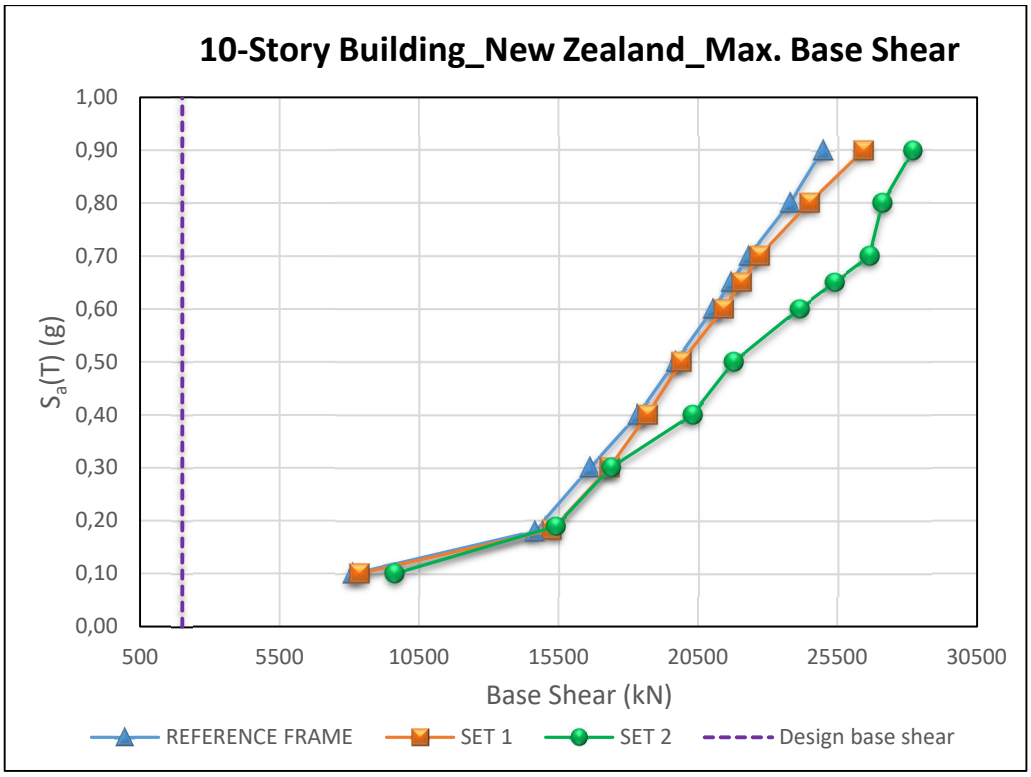


Figure 5.105: Max base shears of 10-story models under New Zealand earthquake acceleration intensities.

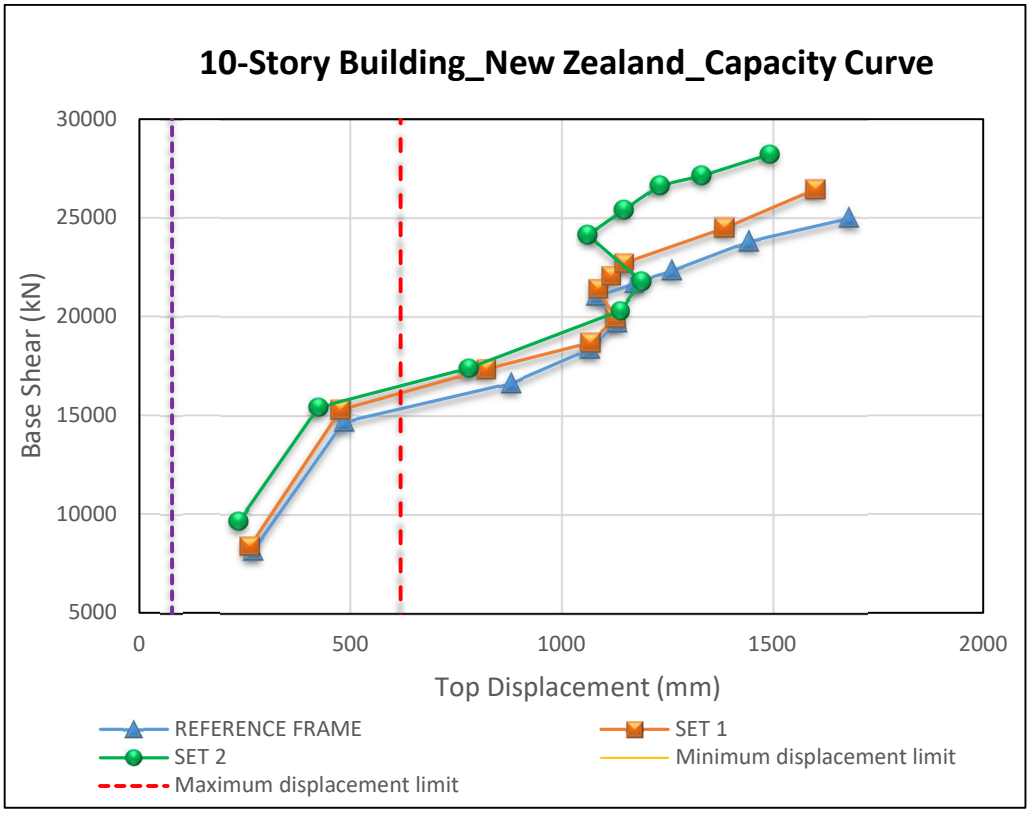
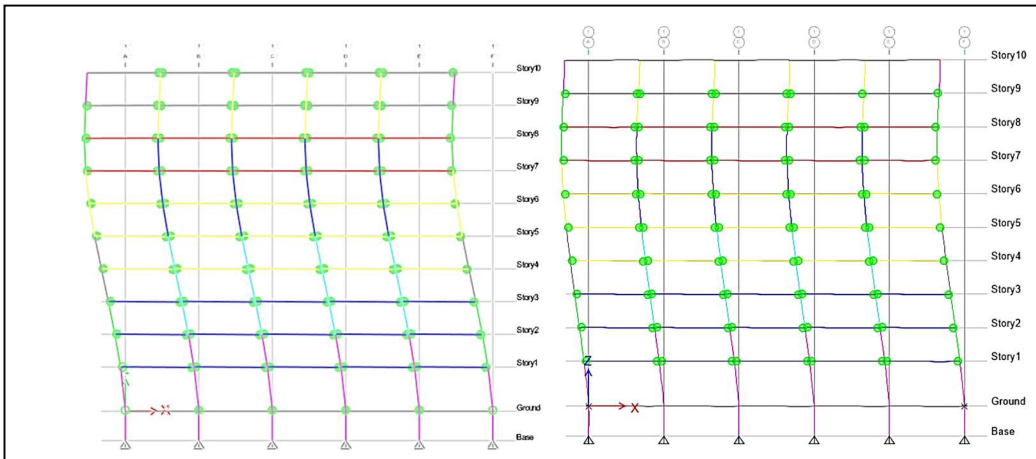


Figure 5.106: Capacity curves of 10-story models under New Zealand earthquake acceleration intensities.

Table 5.24: Responses of 10-story models under New Zealand earthquake.

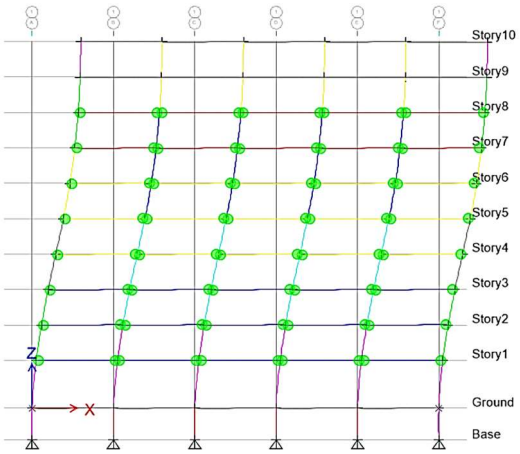
NEW ZEALAND / 10-STORY	$S_a(T)$ values corresponding to drift ratio limit	$S_a(T)$ values corresponding to maximum top displacement limit	The base shears corresponding to maximum top displacement
Reference Frame	0.37 g	0.22 g	15317.10 kN
Set-1	0.40 g	0.23 g	16115.97 kN
Set-2	0.60 g	0.25 g	16477.40 kN

The hinging and plastic rotation demands and drift ratio distributions along the structure height of all models at 0.60g acceleration intensity, where the 10-story Set-2 structure under the New Zealand earthquake reached the 4.00% drift ratio limit;



Reference Frame- Max R3 Plastic = 4.747%

SET 1- Max R3 Plastic = 3.843%



SET 2- Max R3 Plastic = 3.473%

Figure 5.107: Hinging and plastic rotation demands of 10-story models at S_a=0.60g under the New Zealand earthquake.

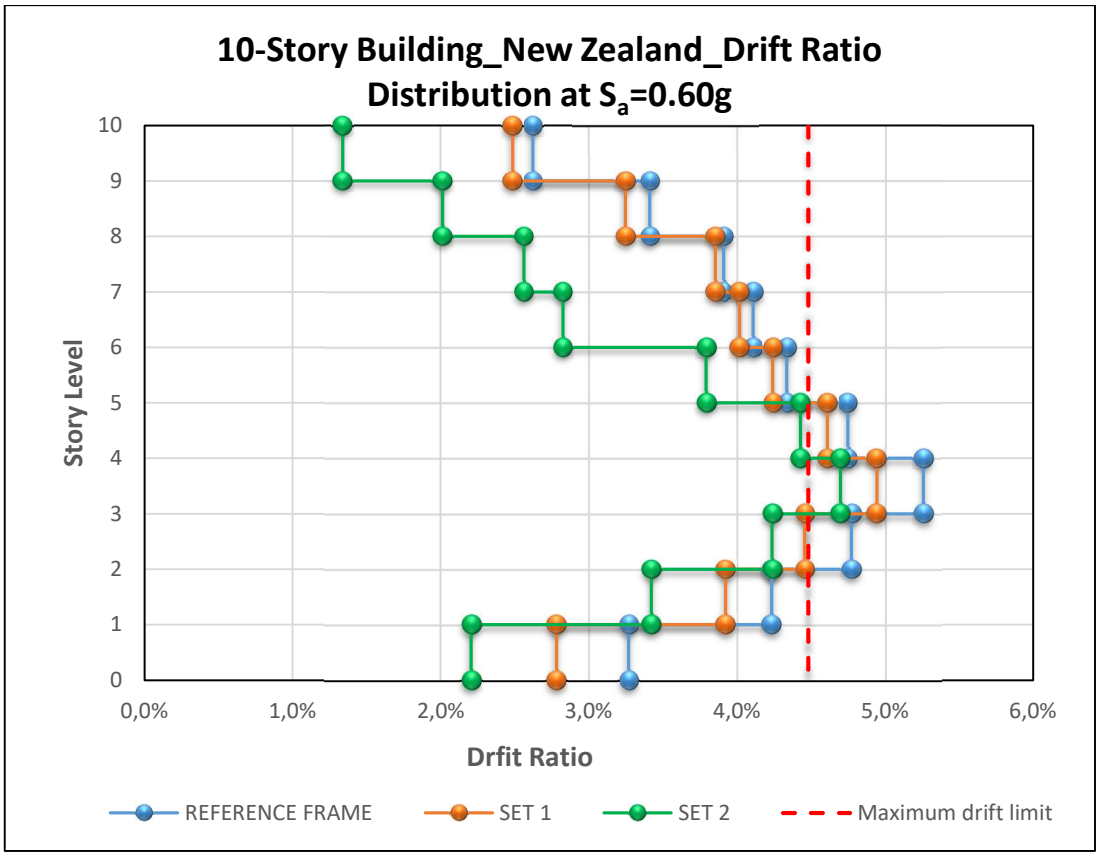


Figure 5.108: Drift ratio distributions along 10-story models' height at S_a=0.60g under the New Zealand earthquake.

5.2.6 Morgan Hill_451 Earthquake

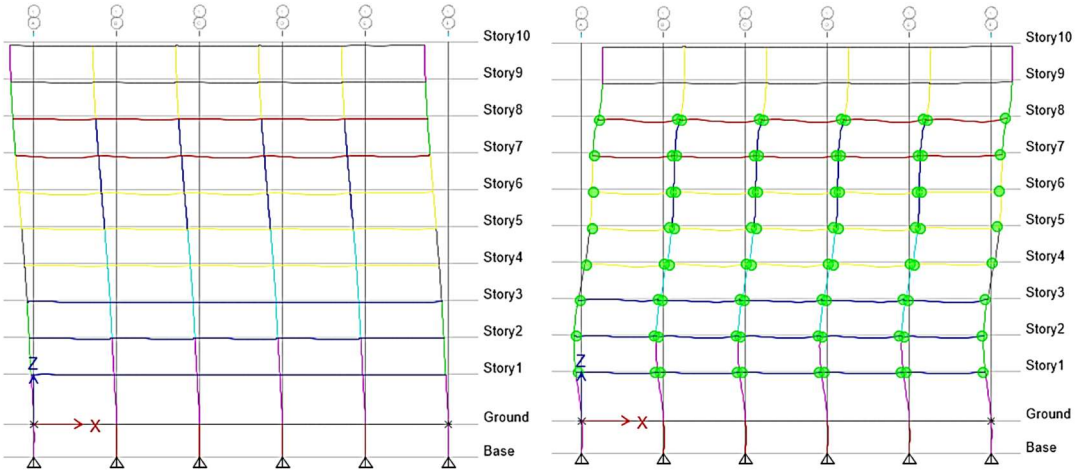
Table 5.25: SFs for 10-story models under the Morgan Hill earthquake.

10 Story_Reference Frame		
(S_a)	(SF)	Scale
g	unitless	mm/s²
0,033	1,000	9806,650
0,100	3,008	29502,019
0,180	**5,420**	**53150,838**
0,200	6,017	59004,039
0,300	9,025	88506,058
0,400	12,033	118008,077
0,500	15,042	147510,097
0,600	18,050	177012,116
0,700	21,059	206514,135
0,800	24,067	236016,154
0,900	27,075	265518,174

10 Story_Set 1		
(S_a)	(SF)	Scale
g	unitless	mm/s²
0,035	1,000	9806,650
0,100	2,871	28156,308
0,183	**5,255**	**51531,675**
0,200	5,742	56312,616
0,300	8,613	84468,924
0,400	11,485	112625,231
0,500	14,356	140781,539
0,600	17,227	168937,847
0,700	20,098	197094,155
0,800	22,969	225250,463
0,900	25,840	253406,771

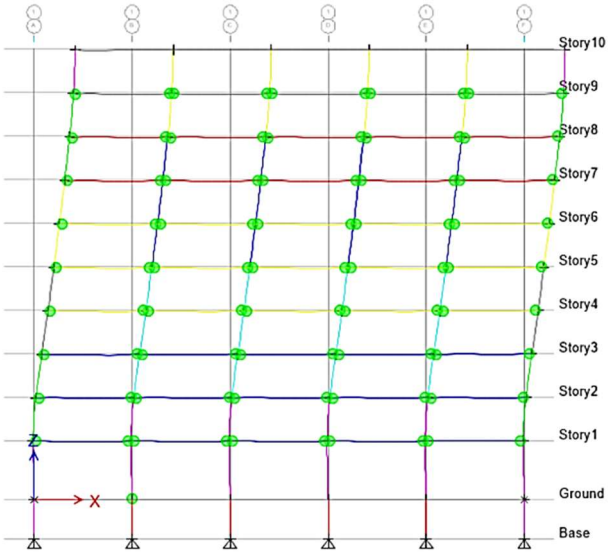
10 Story_Set 2		
(S_a)	(SF)	Scale
g	unitless	mm/s²
0,040	1,000	9806,650
0,100	2,478	24303,832
0,189	**4,689**	**45982,849**
0,200	4,957	48607,663
0,300	7,435	72911,495
0,400	9,913	97215,326
0,500	12,392	121519,158
0,600	14,870	145822,990
0,700	17,348	170126,821
0,800	19,826	194430,653
0,900	22,305	218734,484

Application of acceleration intensities to 10-story models under Morgan Hill earthquake in three stages starting from the acceleration intensities corresponding to the SF obtained from the design spectrum;



Reference Frame _ 0.180g _ SF=5.42
Max R3 Plastic = 0.840%

Reference Frame _ 0.30g _ SF=9.025
Max R3 Plastic = 1.794%



Reference Frame _ 0.50g _ SF=15.042
Max R3 Plastic = 3.925%

Figure 5.109: Hingings and plastic rotation demands of 10-story RFs under the Morgan Hill earthquake.

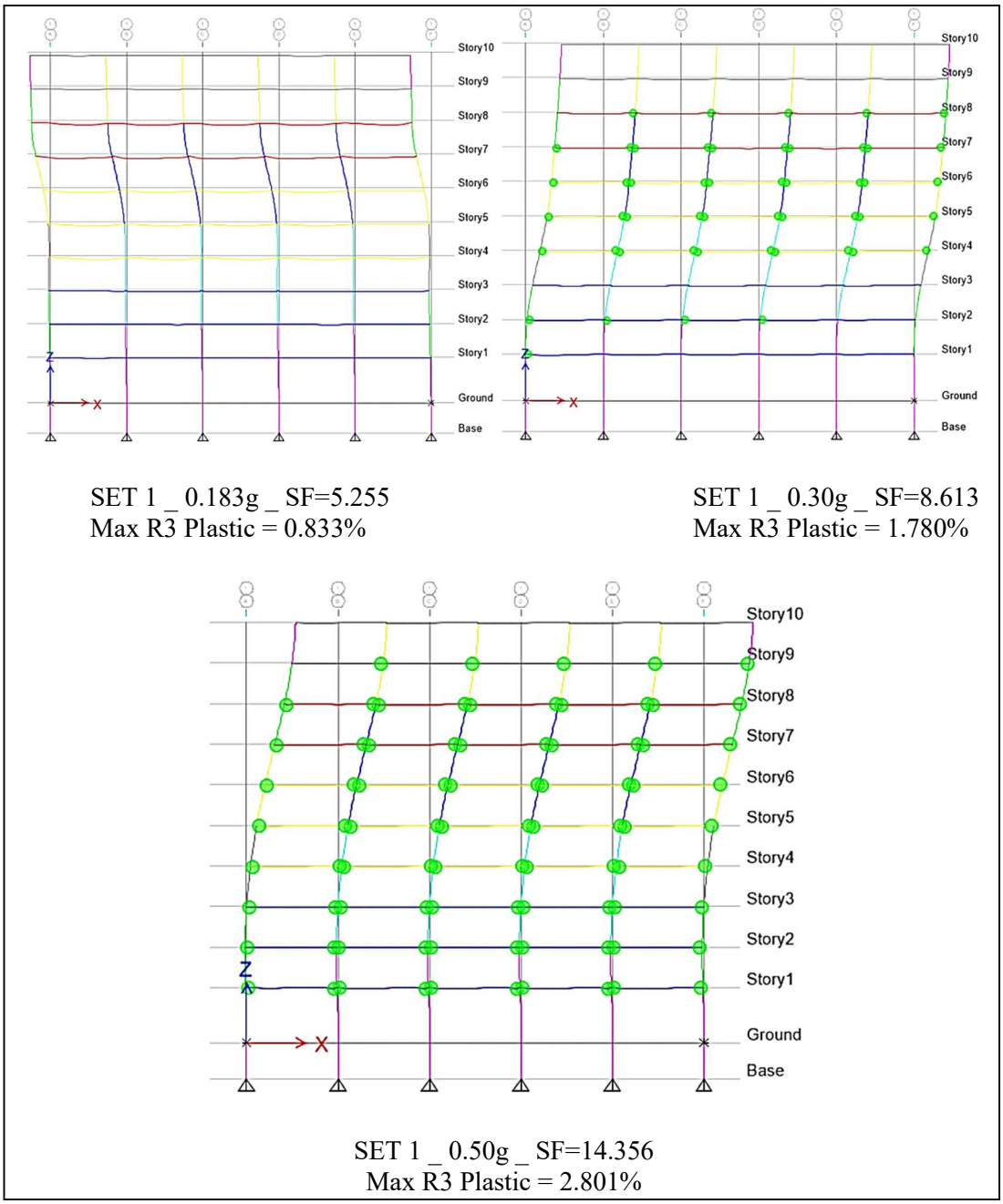


Figure 5.110: Hingings and plastic rotation demands of 10-story Set-1 under the Morgan Hill earthquake.

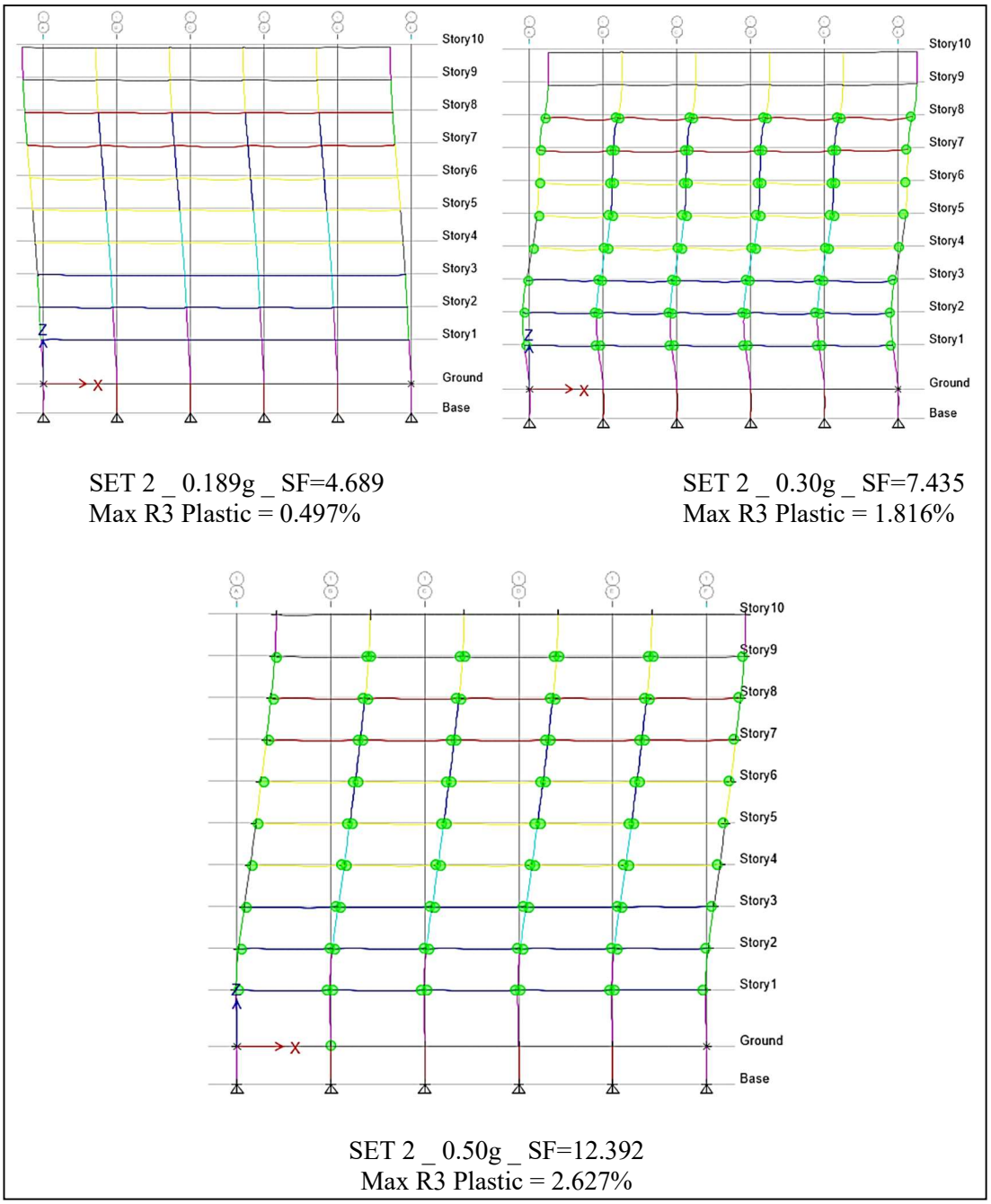


Figure 5.111: Hingings and plastic rotation demands of 10-story Set-2 under the Morgan Hill earthquake.

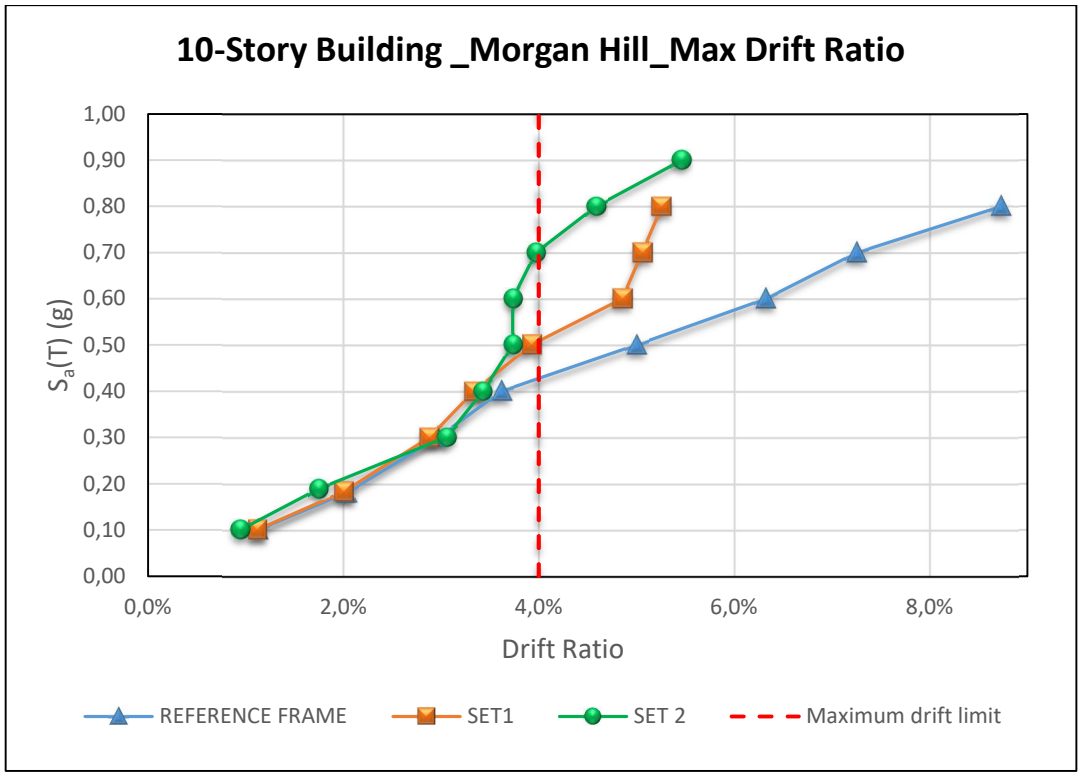


Figure 5.112: Max drift ratios of 10-story models under Morgan Hill earthquake acceleration intensities.

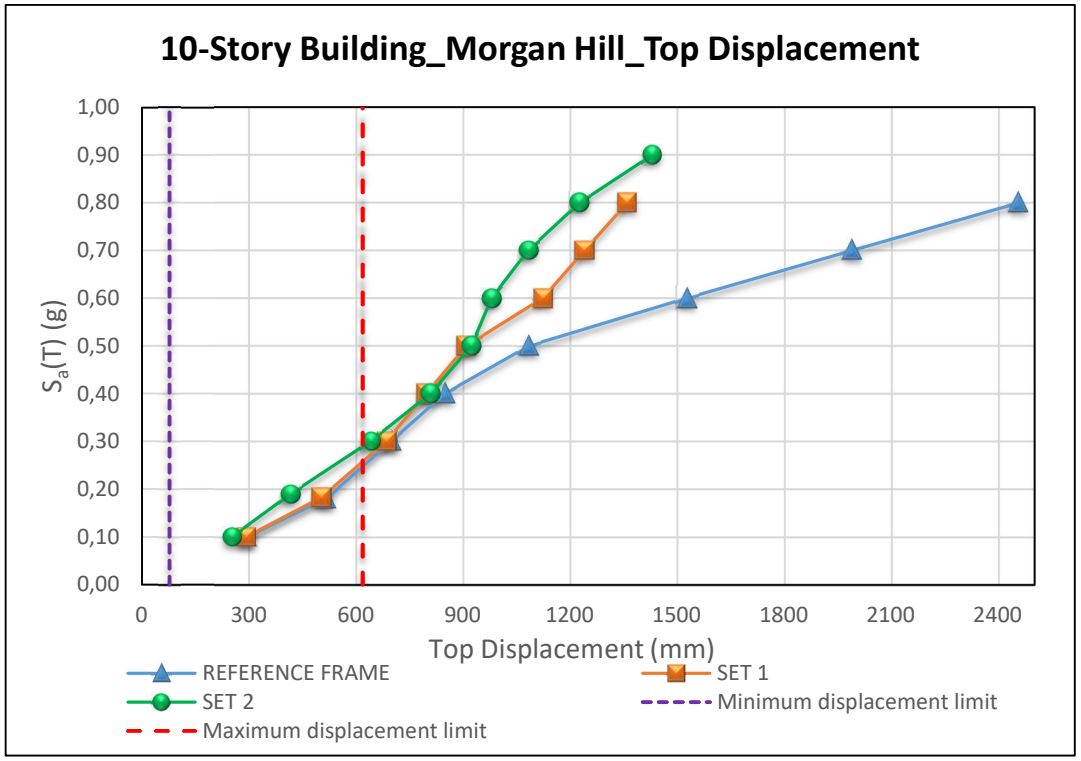


Figure 5.113: Max top displacements of 10-story models under Morgan Hill earthquake acceleration intensities.

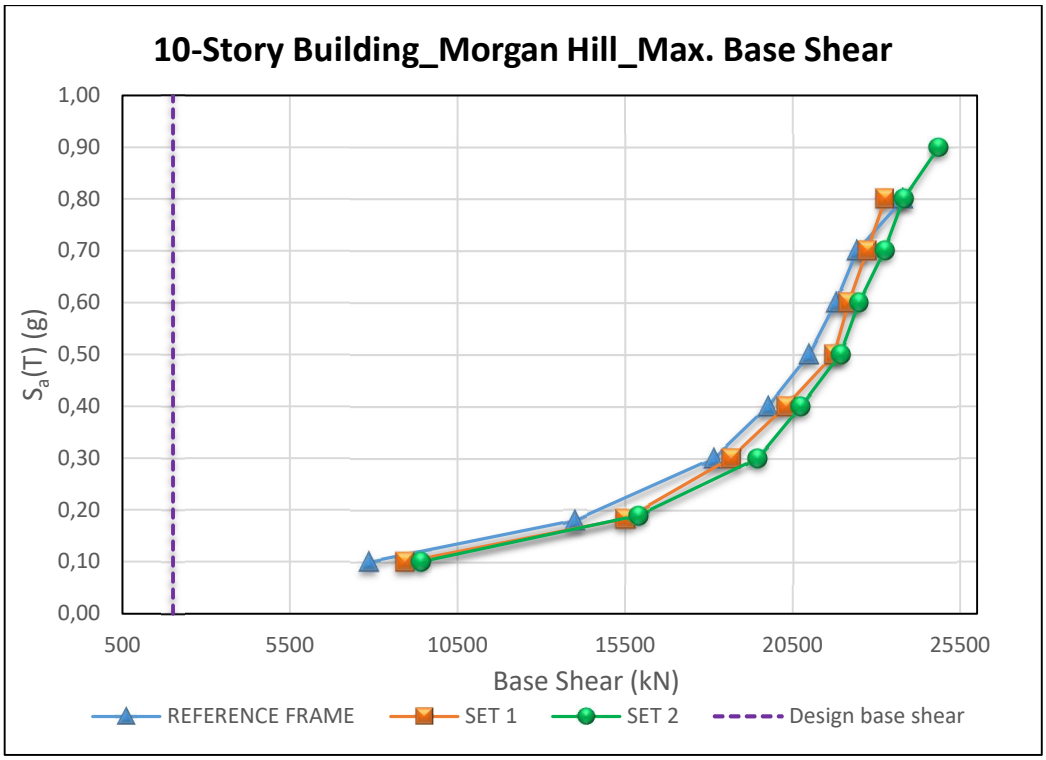


Figure 5.114: Max base shears of 10-story models under Morgan Hill earthquake acceleration intensities.

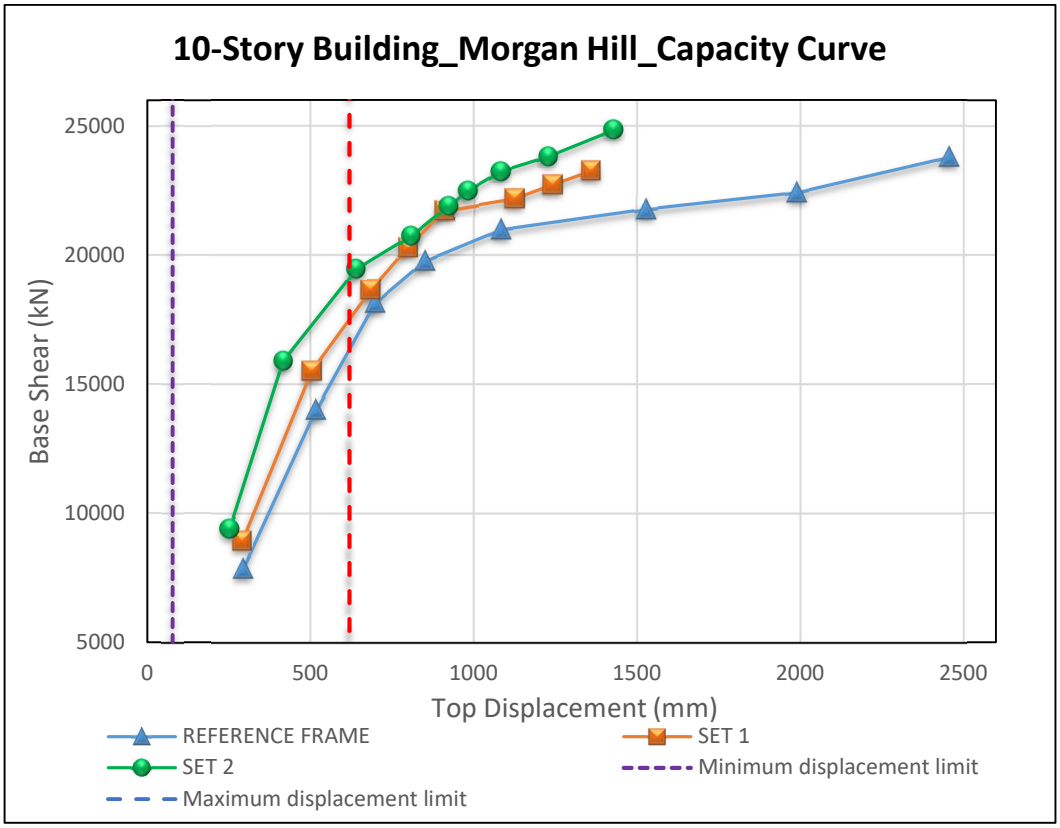
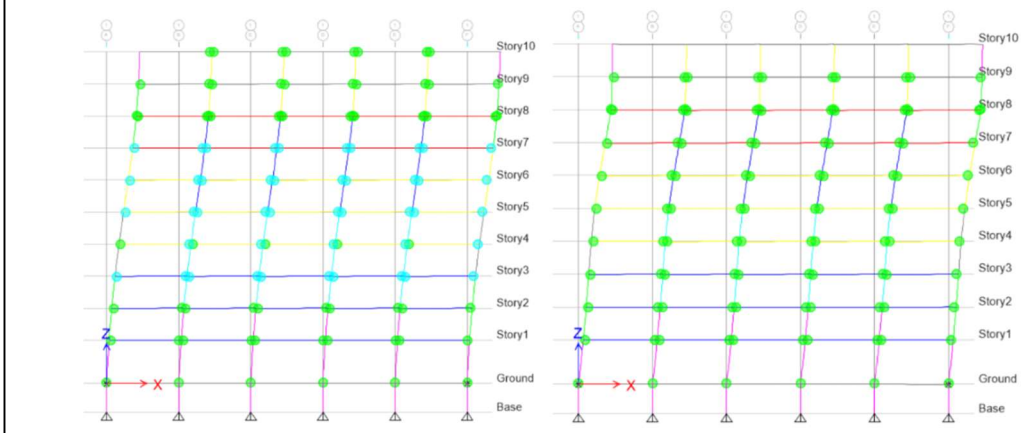


Figure 5.115: Capacity curves of 10-story models under Morgan Hill earthquake acceleration intensities.

Table 5.26: Responses of 10-story models under Morgan Hill earthquake.

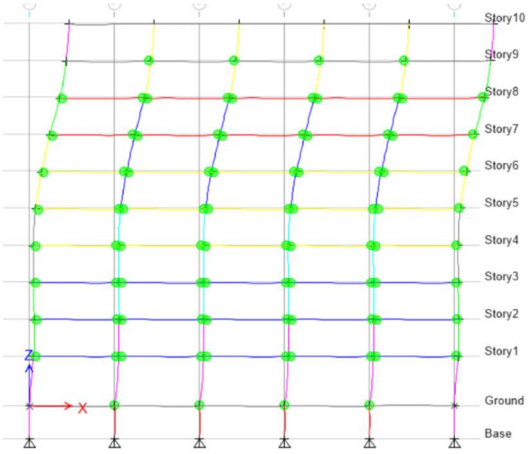
MORGAN HILL / 10-STORY	S_a(T) values corresponding to drift ratio limit	S_a(T) values corresponding to maximum top displacement limit	The base shears corresponding to maximum top displacement
Reference Frame	0.43 g	0.25 g	16326.19 kN
Set-1	0.50 g	0.26 g	17502.26 kN
Set-2	0.70 g	0.29 g	19112.65 kN

The hinging and plastic rotation demands and drift ratio distributions along the structure height of all models at 0.70g acceleration intensity, where the 10-story Set-2 structure under the Morgan Hill earthquake reached the 4.00% drift ratio limit;



Reference Frame- Max R3 Plastic = 4.512%

SET 1- Max R3 Plastic = 4.235%



SET 2- Max R3 Plastic = 3.249%

Figure 5.116: Hinging and plastic rotation demands of 10-story models at S_a=0.70g under the Morgan Hill earthquake.

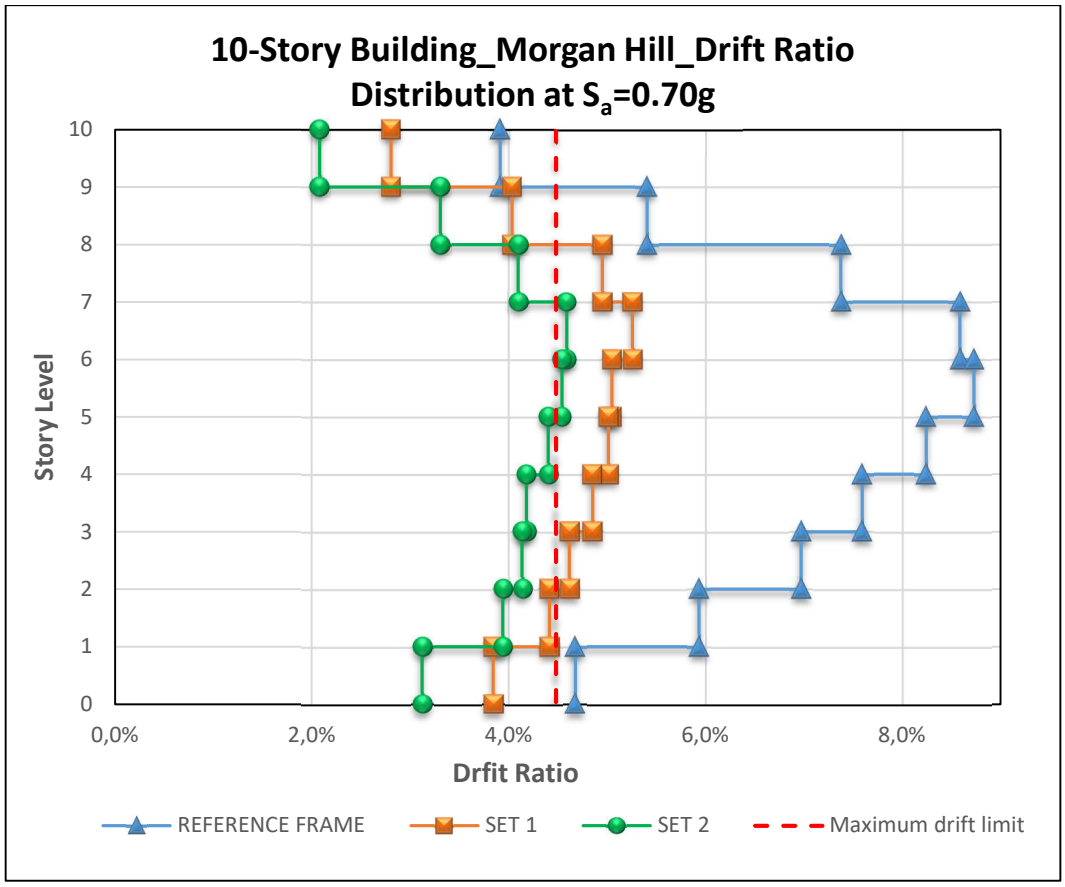


Figure 5.117: Drift ratio distributions along 10-story models' height at S_a=0.70g under the Morgan Hill earthquake.

5.2.7 Chuetsu_4840 Earthquake

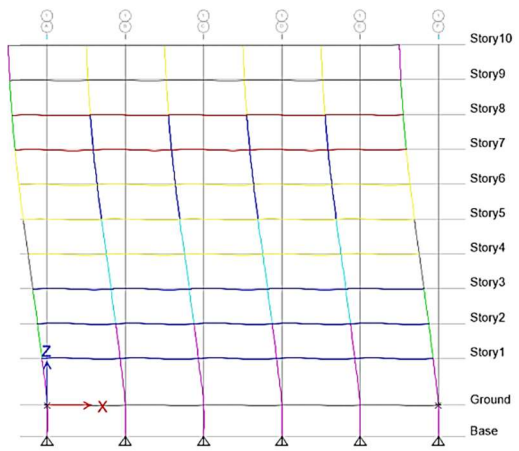
Table 5.27: SFs for 10-story models under the Chuetsu earthquake.

10 Story_Reference Frame		
(S_a)	(SF)	Scale
g	unitless	mm/s²
0,058	1,000	9806,650
0,100	1,727	16937,505
0,180	**3,112**	**30514,609**
0,200	3,454	33875,010
0,300	5,181	50812,515
0,400	6,909	67750,021
0,500	8,636	84687,526
0,600	10,363	101625,031

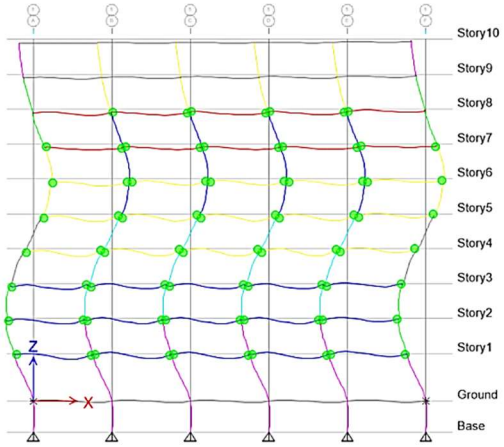
10 Story_Set 1		
(S_a)	(SF)	Scale
g	unitless	mm/s²
0,060	1,000	9806,650
0,100	1,679	16470,154
0,183	**3,074**	**30143,676**
0,200	3,359	32940,308
0,300	5,038	49410,463
0,400	6,718	65880,617
0,500	8,397	82350,771
0,600	10,077	98820,925

10 Story_Set 2		
(S_a)	(SF)	Scale
g	unitless	mm/s²
0,062	1,000	9806,650
0,100	1,622	15909,462
0,189	**3,069**	**30100,702**
0,200	3,245	31818,924
0,300	4,867	47728,386
0,400	6,489	63637,848
0,500	8,112	79547,310
0,600	9,734	95456,772

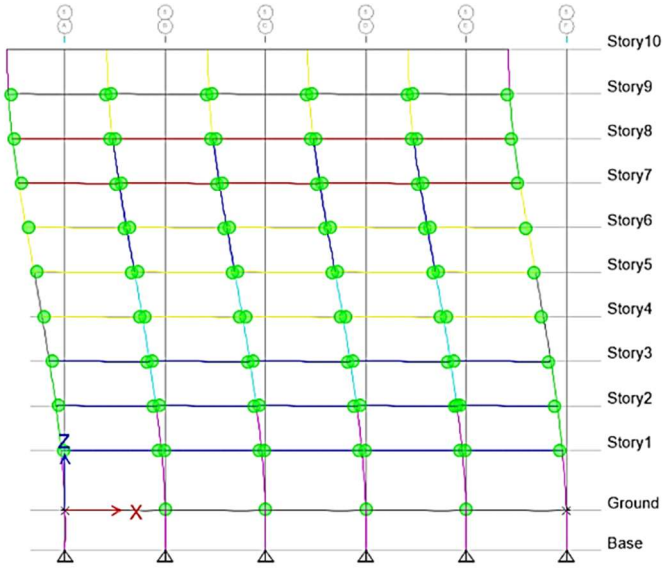
Application of acceleration intensities to 10-story models under Chuetsu earthquake in three stages starting from the acceleration intensities corresponding to the SF obtained from the design spectrum;



Reference Frame _ 0.180g _ SF=3.112
Max R3 Plastic = 0.445%



Reference Frame _ 0.30g _ SF=5.181
Max R3 Plastic = 1.714%



Reference Frame _ 0.50g _ SF=8.636
Max R3 Plastic = 7.292%

Figure 5.118: Hingings and plastic rotation demands of 10-story RFs under the Chuetsu earthquake.

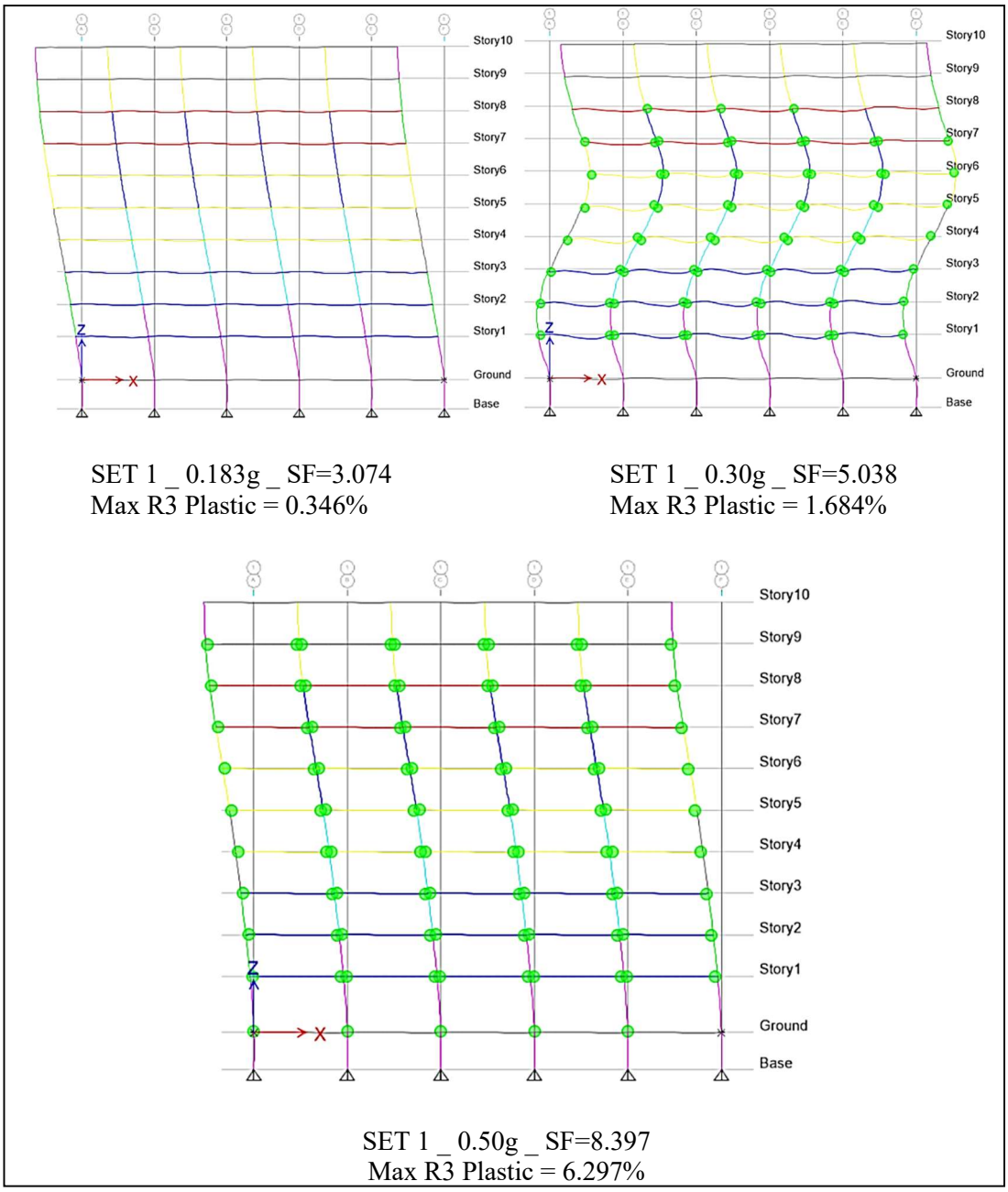
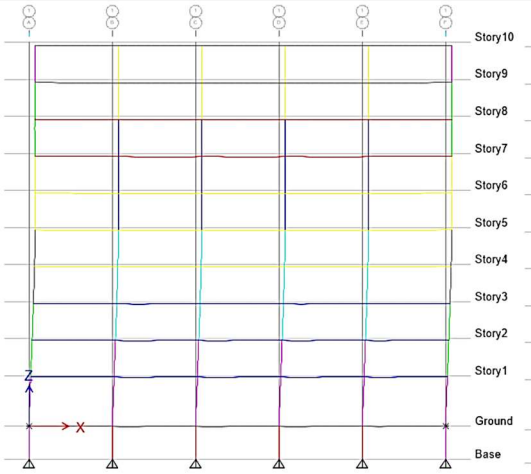
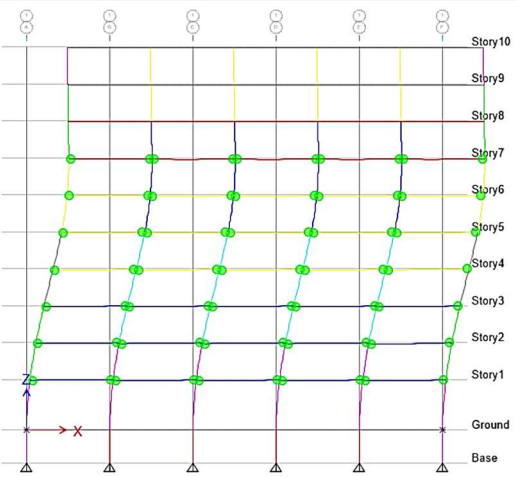


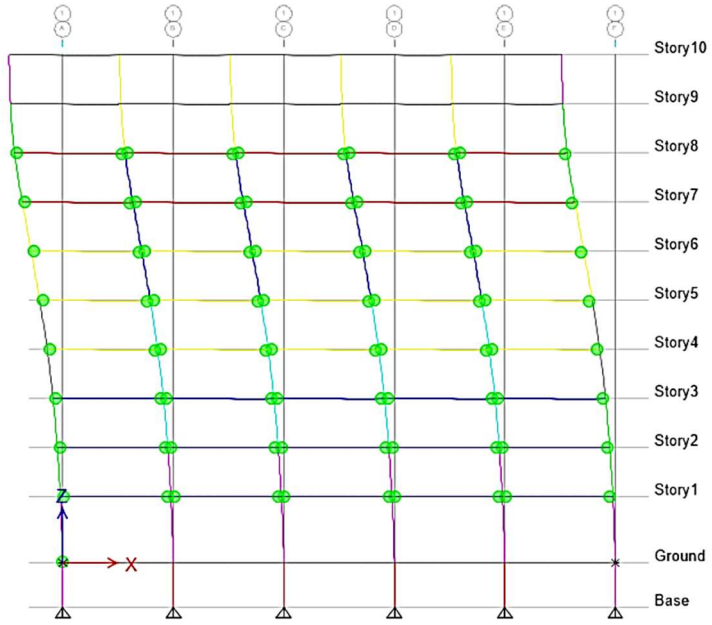
Figure 5.119: Hingings and plastic rotation demands of 10-story Set-1 under the Chuetsu earthquake.



SET 2 _ 0.189g _ SF=3.069
Max R3 Plastic = 0.133%



SET 2 _ 0.30g _ SF=4.867
Max R3 Plastic = 1.466%



SET 2 _ 0.50g _ SF=8.112
Max R3 Plastic = 4.742%

Figure 5.120: Hingings and plastic rotation demands of 10-story Set-2 under the Chuetsu earthquake.

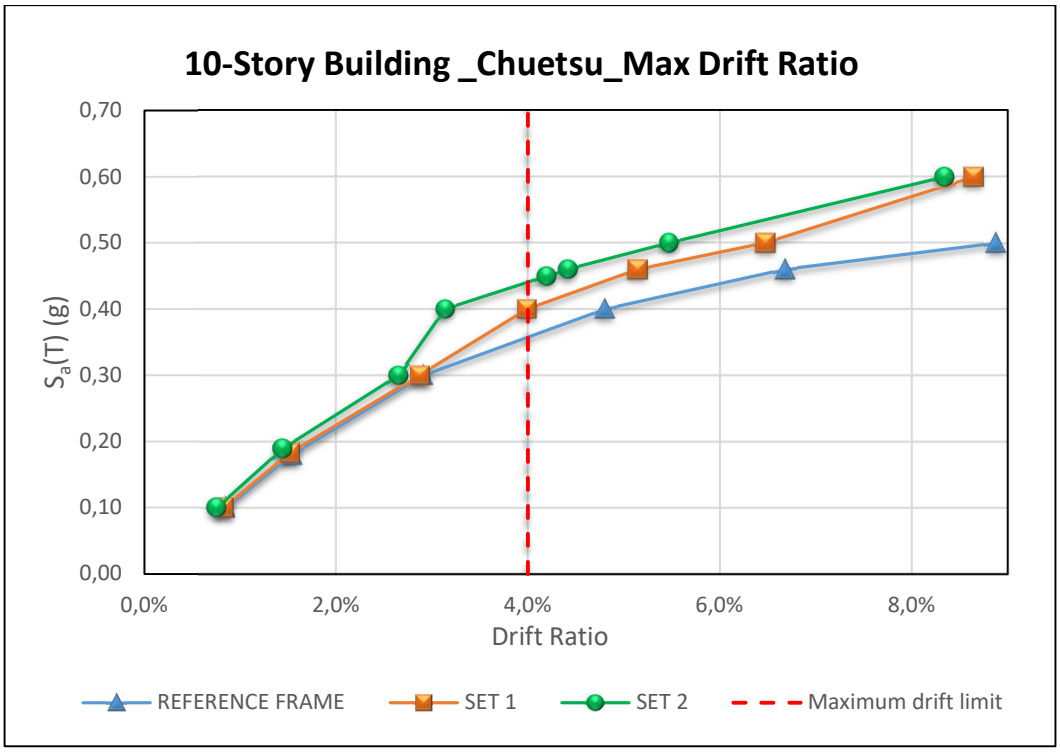


Figure 5.121: Max drift ratios of 10-story models under Chuetsu earthquake acceleration intensities.

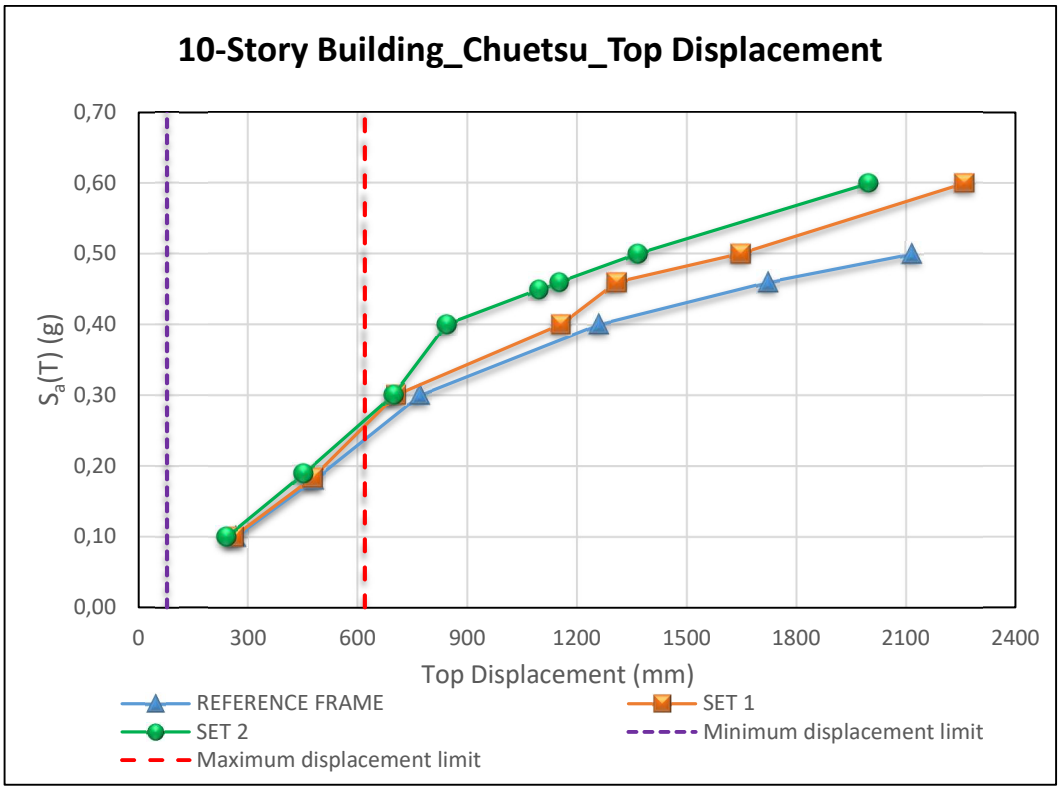


Figure 5.122: Max top displacements of 10-story models under Chuetsu earthquake acceleration intensities.

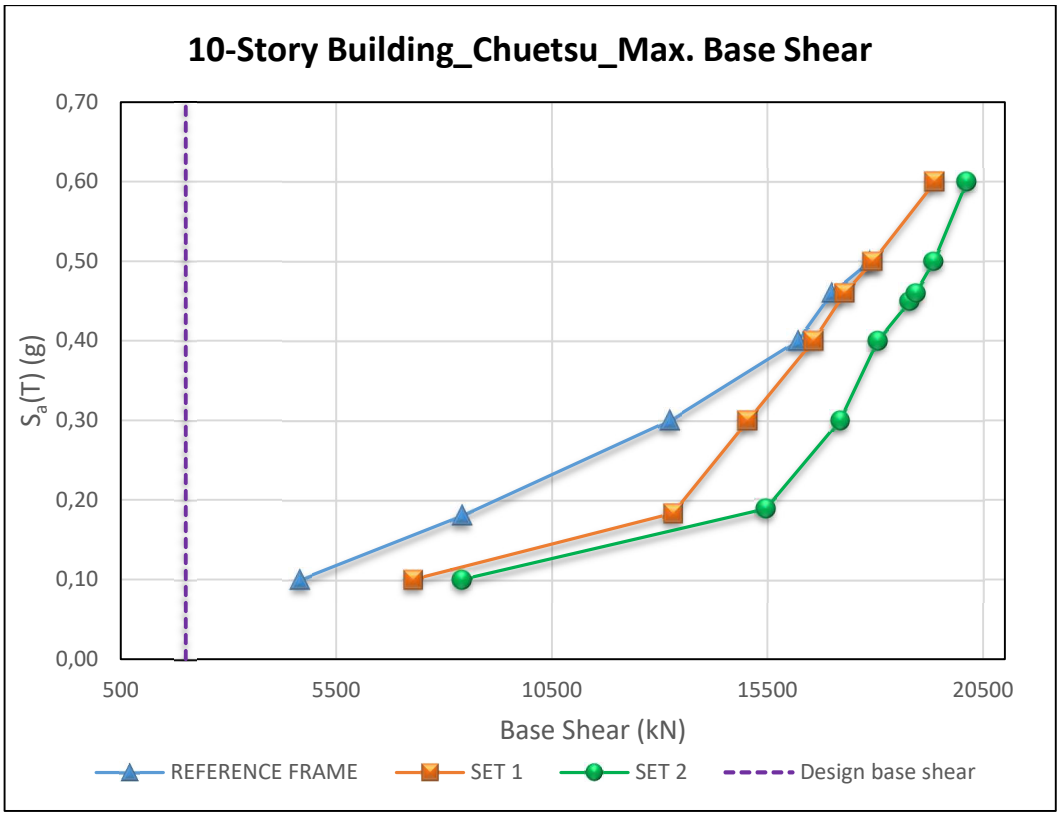


Figure 5.123: Max base shears of 10-story models under Chuetsu earthquake acceleration intensities.

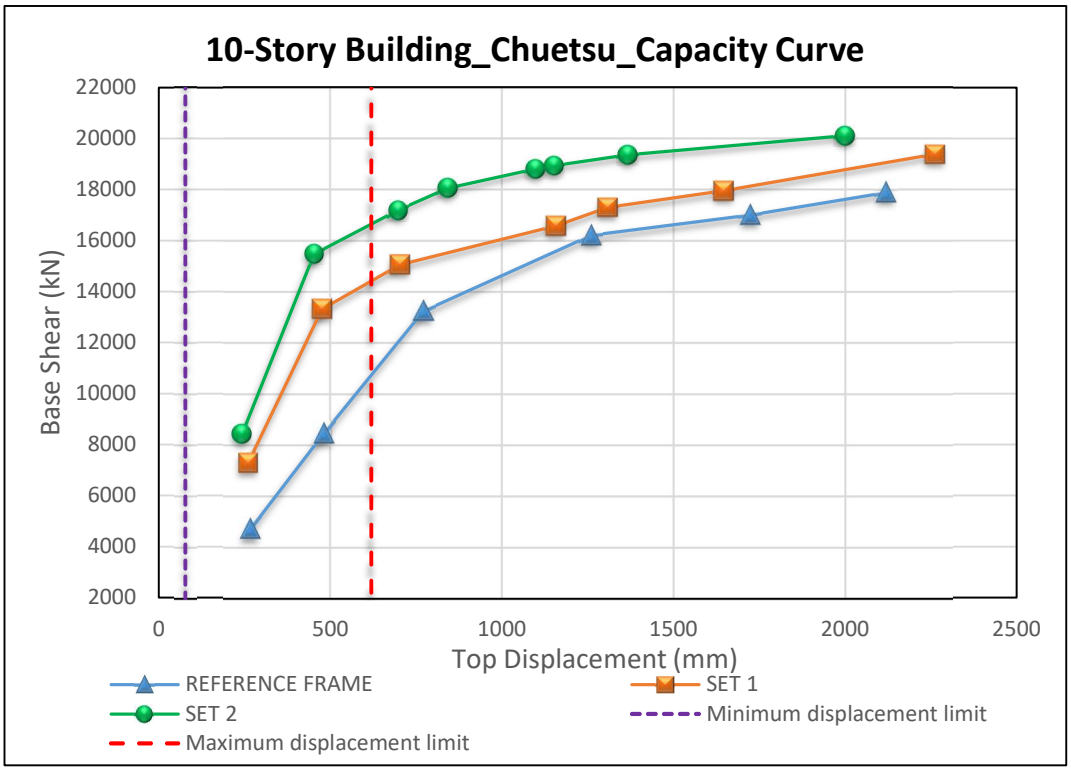
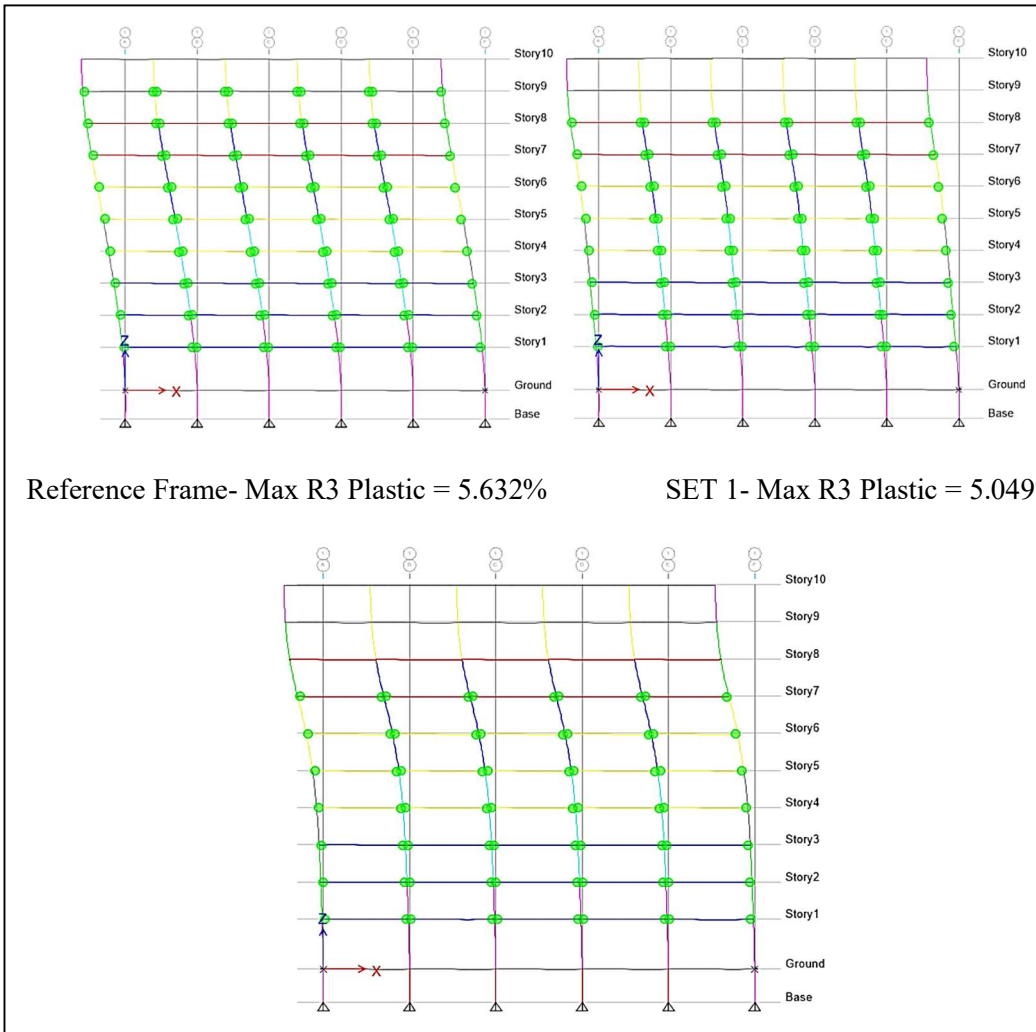


Figure 5.124: Capacity curves of 10-story models under Chuetsu earthquake acceleration intensities.

Table 5.28: Responses of 10-story models under Chuetsu earthquake.

CHUETSU / 10-STORY	S_a(T) values corresponding to drift ratio limit	S_a(T) values corresponding to maximum top displacement limit	The base shears corresponding to maximum top displacement
Reference Frame	0.35 g	0.24 g	10713.45 kN
Set-1	0.40 g	0.25 g	14402.00 kN
Set-2	0.45 g	0.27 g	16634.13 kN

The hinging and plastic rotation demands and drift ratio distributions along the structure height of all models at 0.45g acceleration intensity, where the 10-story Set-2 structure under the Chuetsu earthquake reached the 4.00% drift ratio limit;



Reference Frame- Max R3 Plastic = 5.632%

SET 1- Max R3 Plastic = 5.049%

SET 2- Max R3 Plastic = 3.645%

Figure 5.125: Hinging and plastic rotation demands of 10-story models at S_a=0.45g under the Chuetsu earthquake.

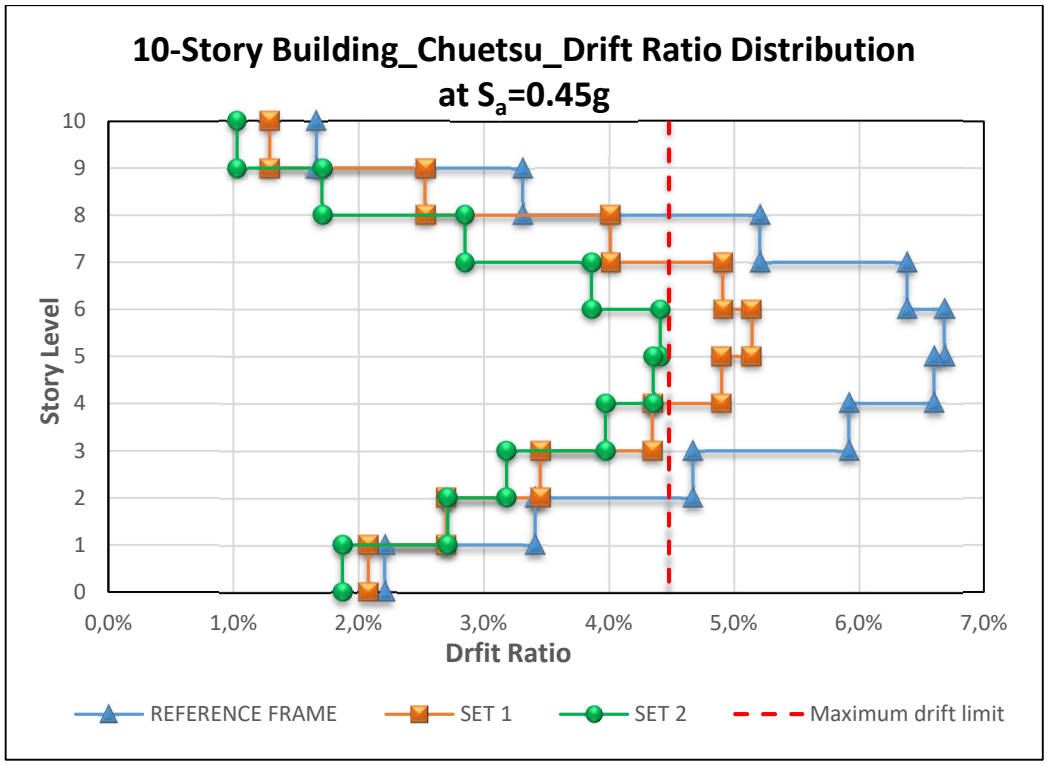


Figure 5.126: Drift ratio distributions along 10-story models' height at S_a=0.45g under the Chuetsu earthquake.

5.3 Average of Results Obtained with IDA

As a result of the analyzes made under the earthquake records defined in (X) and (Y) directions in TBEC-2018, it is stated that the behavior magnitudes such as internal force components, displacement, and relative story drift should be calculated by averaging the largest absolute values. For this reason, IDA curves were plotted according to the increasing first mode spectral acceleration intensities as taking the averages of maximum drift ratio, top displacement, base shears magnitudes obtained as a result of applying the above-mentioned 7 earthquake records to the RF, Set-1 and Set-2 models of 5-story and 10-story buildings. In addition, the averages of the plastic rotation demands and drift ratio distributions of all models were calculated at the acceleration intensity where the Set-2 structures reached the 4.00% relative story drift ratio limit in the IDA curve of the maximum drift ratios whose averages were calculated. As a result of the calculations, the RF, Set-1, and Set-2 models were visualized on the same graphic, so that the results obtained were clearer and more understandable, and comparisons were made between them.

5.3.1 Results for 5-Story Buildings

IDA curves created by plotting under increasing acceleration intensities of maximum drift ratio and their averages of 5-story models obtained from 7 earthquakes;

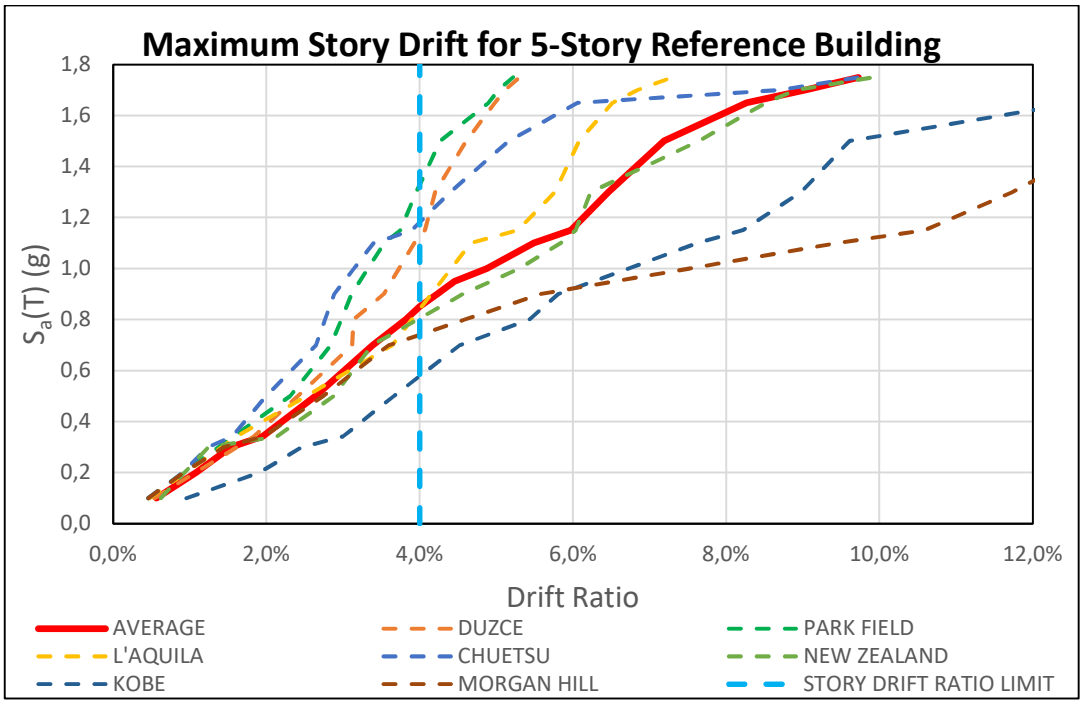


Figure 5.127: The average of the max drift ratios of the 5-story RF model.

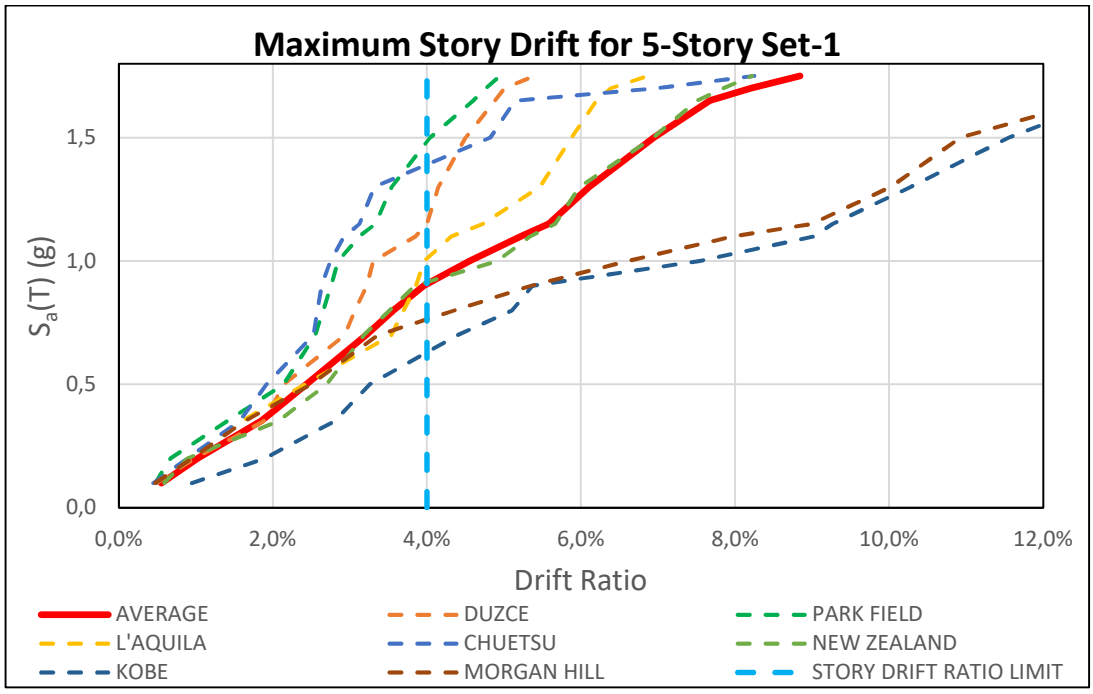


Figure 5.128: The average of the max drift ratios of the 5-story Set-1 model.

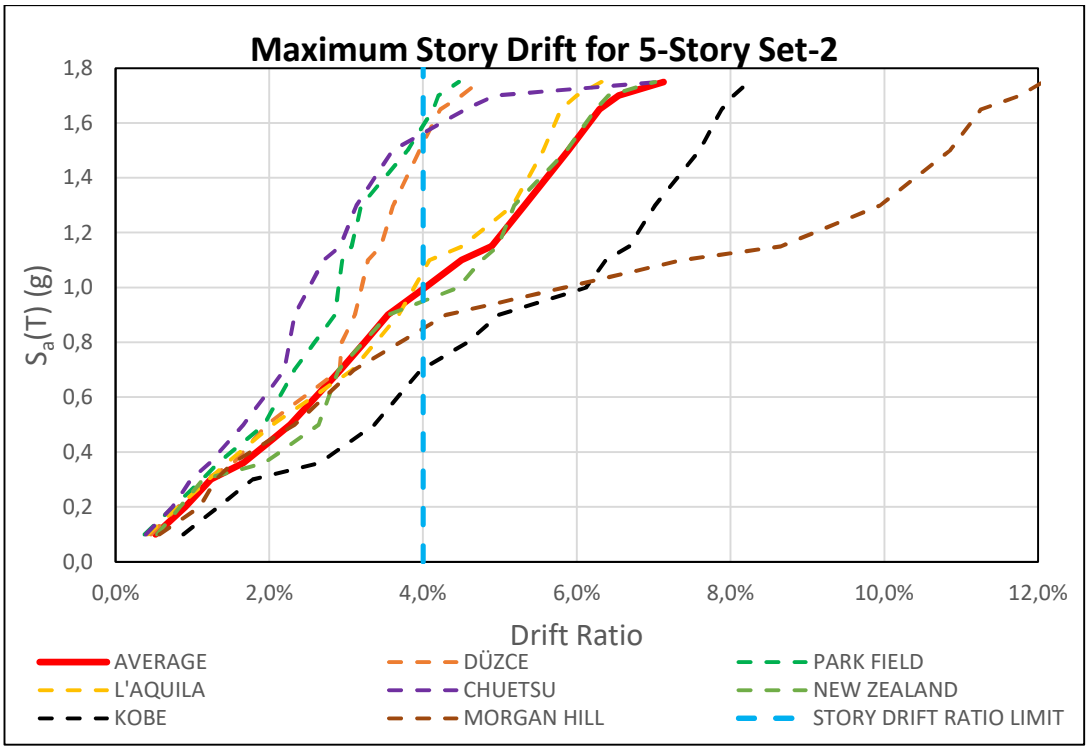


Figure 5.129: The average of the max drift ratios of the 5-story Set-2 model.

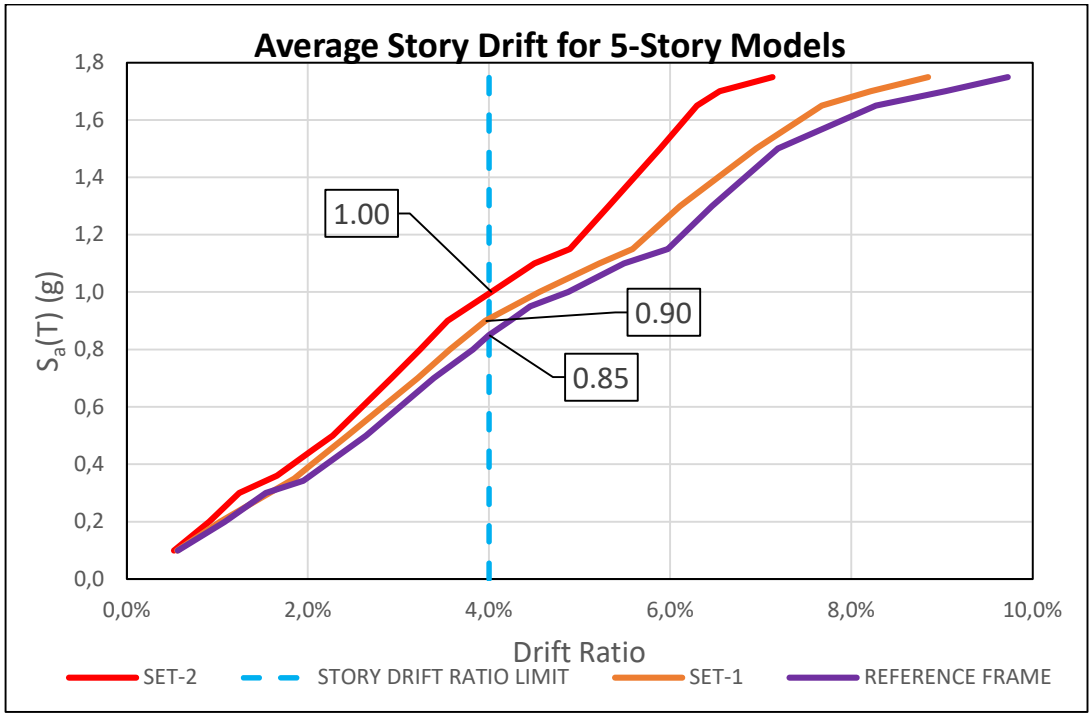


Figure 5.130: Averages of max drift ratios for the 5-story models.

- The 4.00% which is two times of design drift ratio is reached approximately at spectral accelerations, S_a, of 0.85 g / 0.90 g / 1.00 g, respectively, for RF, Set-1, and Set-2 models of the 5-story buildings.

IDA curves created by plotting under increasing acceleration intensities of top displacements and their averages of 5-story models obtained from 7 earthquakes;

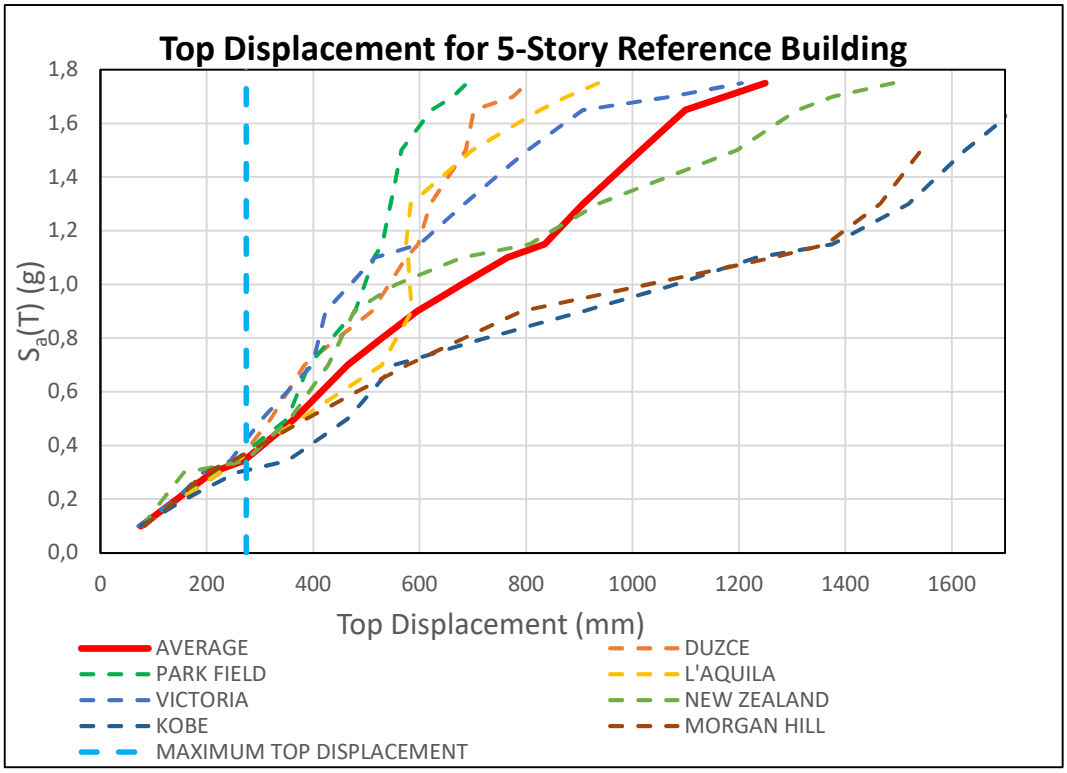


Figure 5.131: The average of the top displacements of the 5-story RF model.

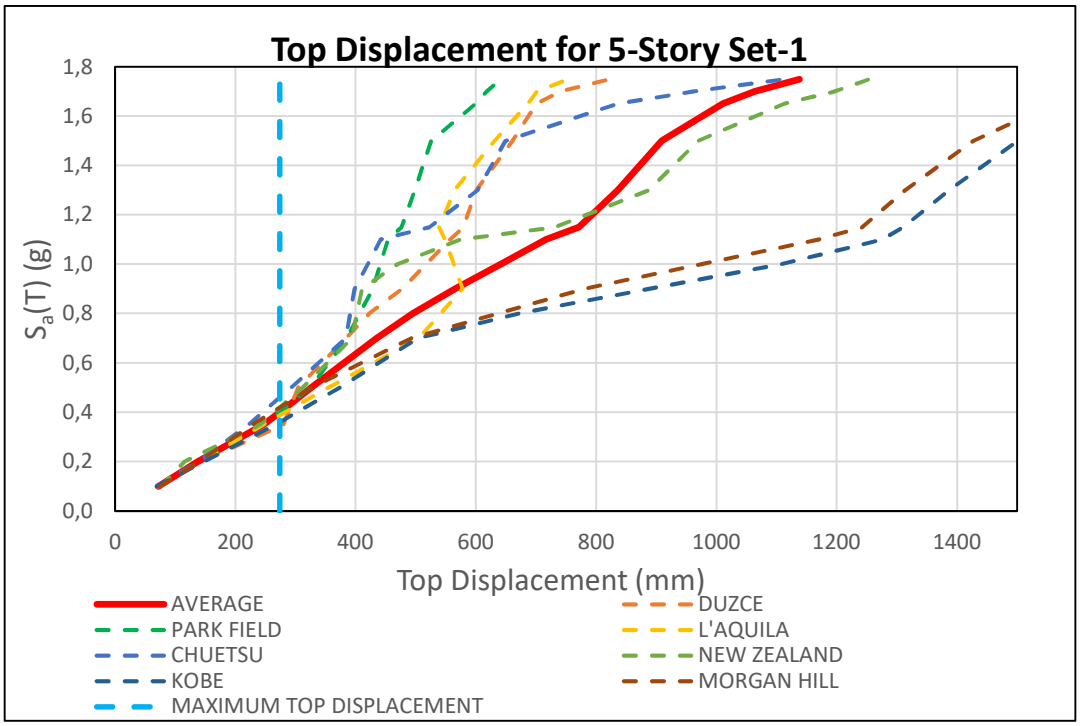


Figure 5.132: The average of the top displacements of the 5-story Set-1 model.

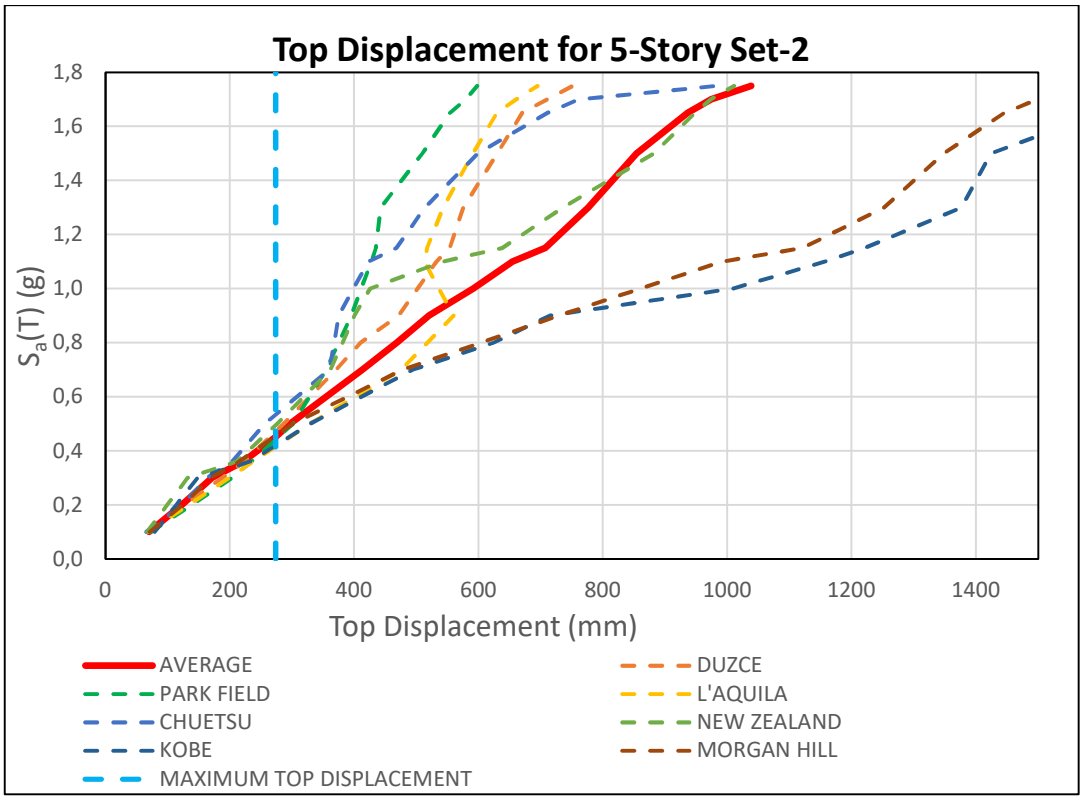


Figure 5.133: The average of the top displacements of the 5-story Set-2 model.

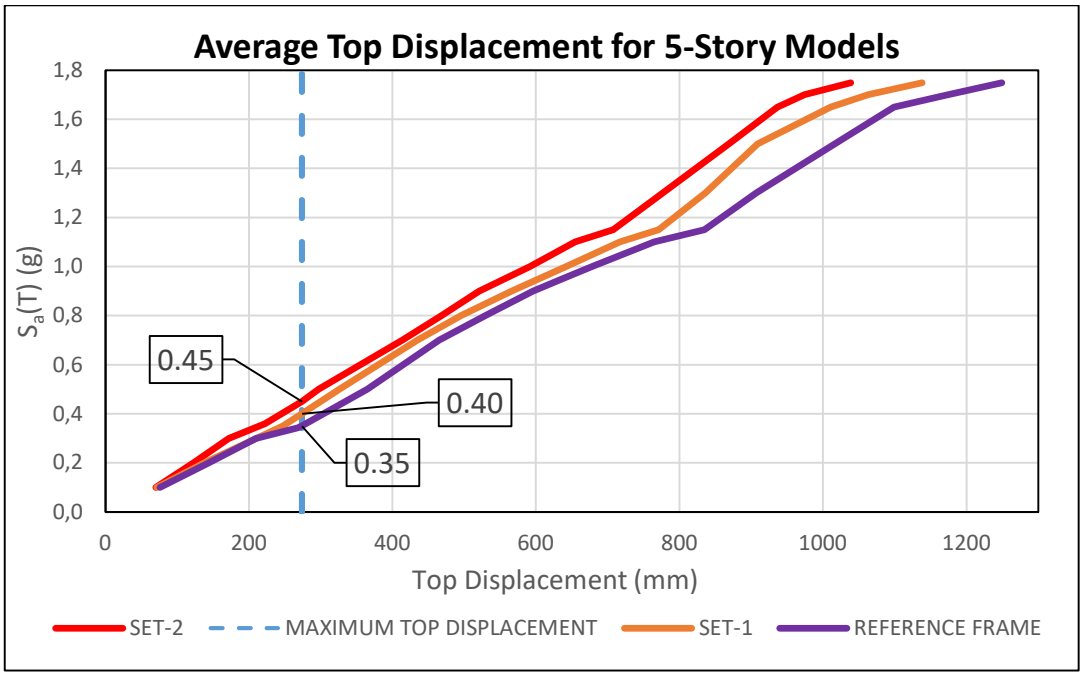


Figure 5.134: Averages of top displacements for the 5-story models.

- The 5-story buildings reach their design roof displacement of 274 mm, approximately at spectral accelerations, S_a, of 0.35 g / 0.40g / 0.45 g, respectively, for RF, Set-1, and Set-2 models.

IDA curves created by plotting under increasing acceleration intensities of maximum base shears and their averages of 5-story models obtained from 7 earthquakes;

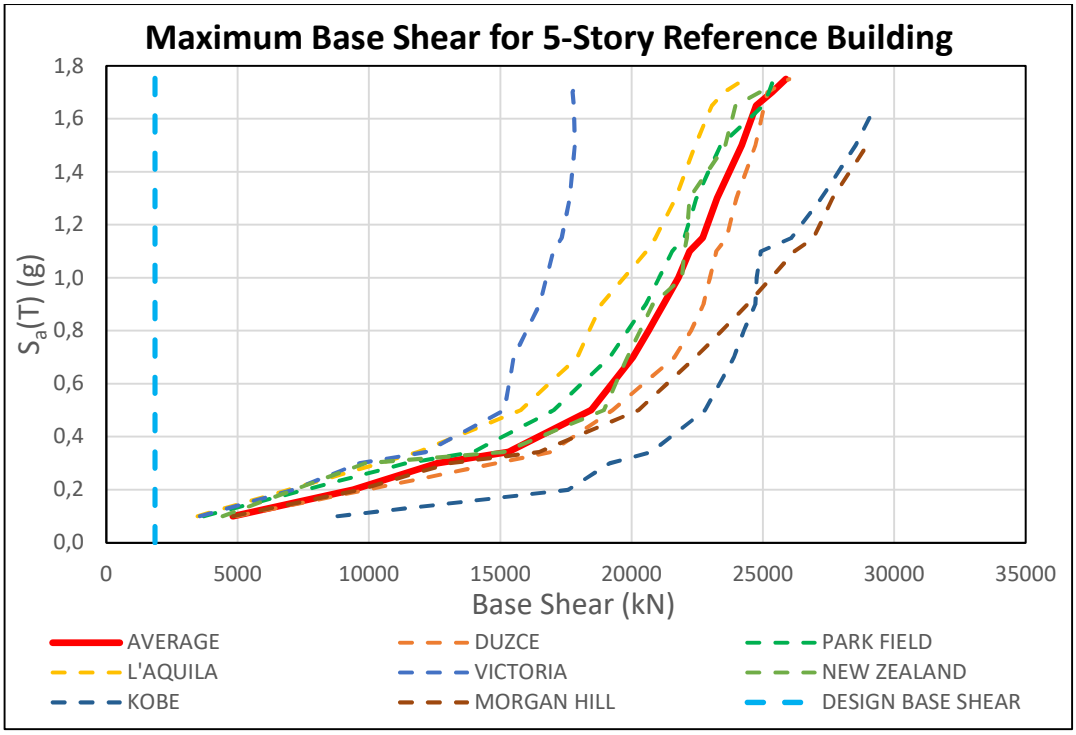


Figure 5.135: The average of the max base shears of the 5-story RF model.

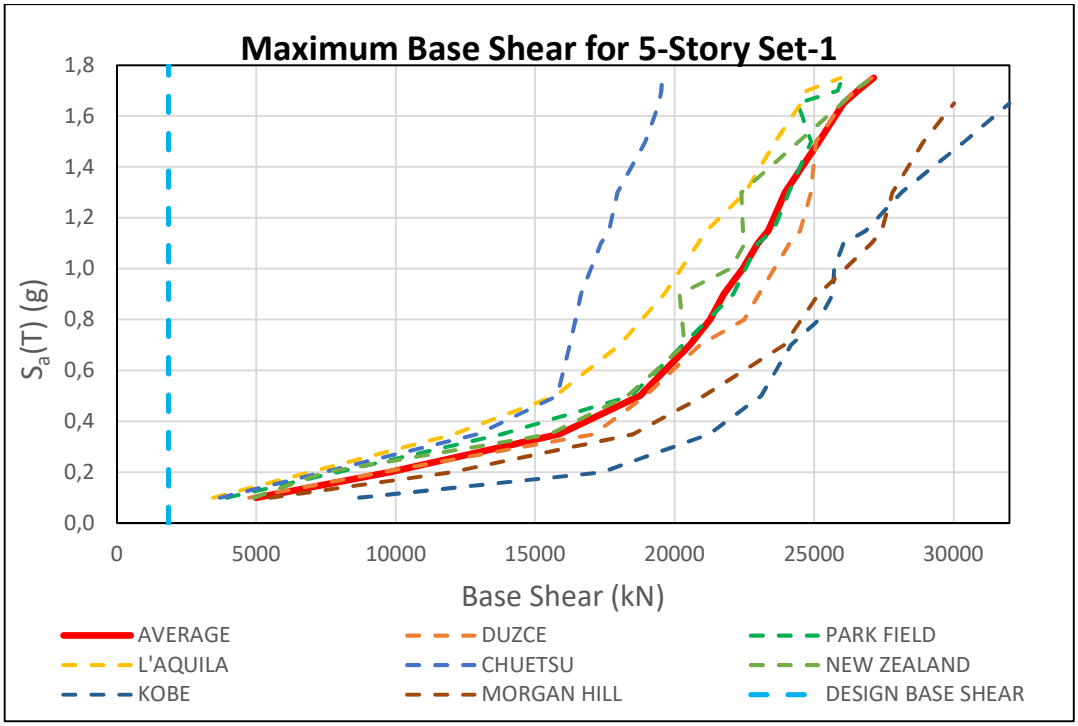


Figure 5.136: The average of the max base shears of the 5-story Set-1 model.

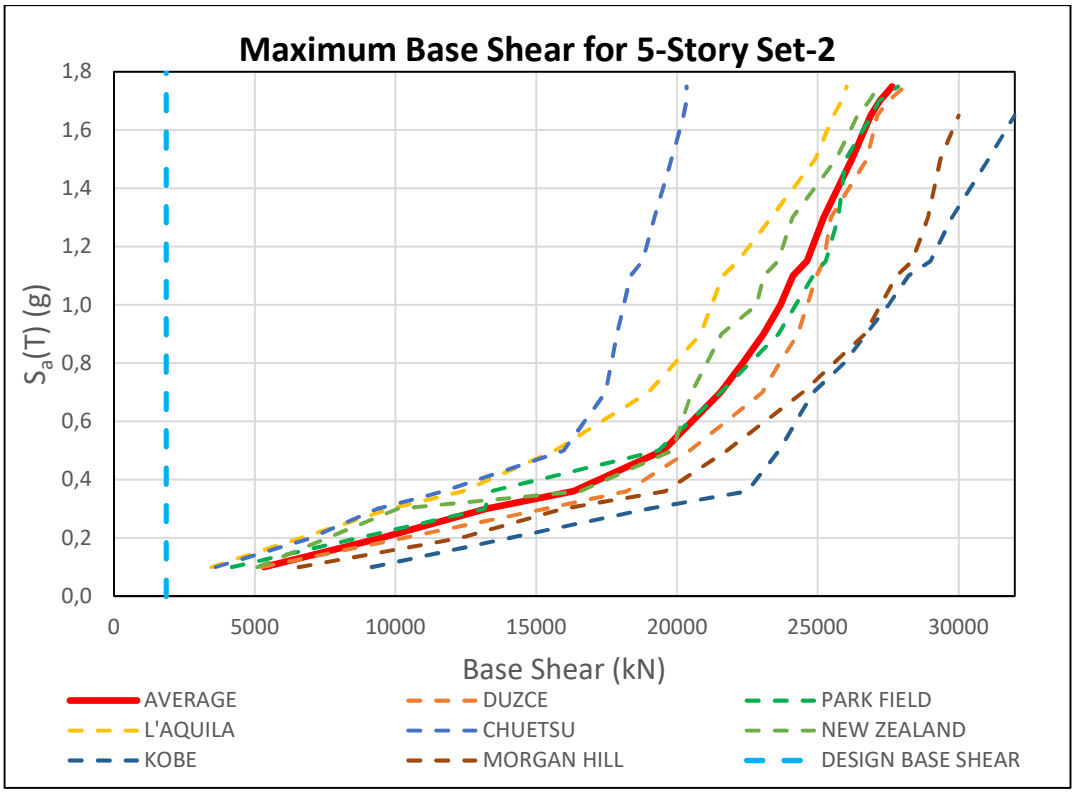


Figure 5.137: The average of the max base shears of the 5-story Set-2 model.

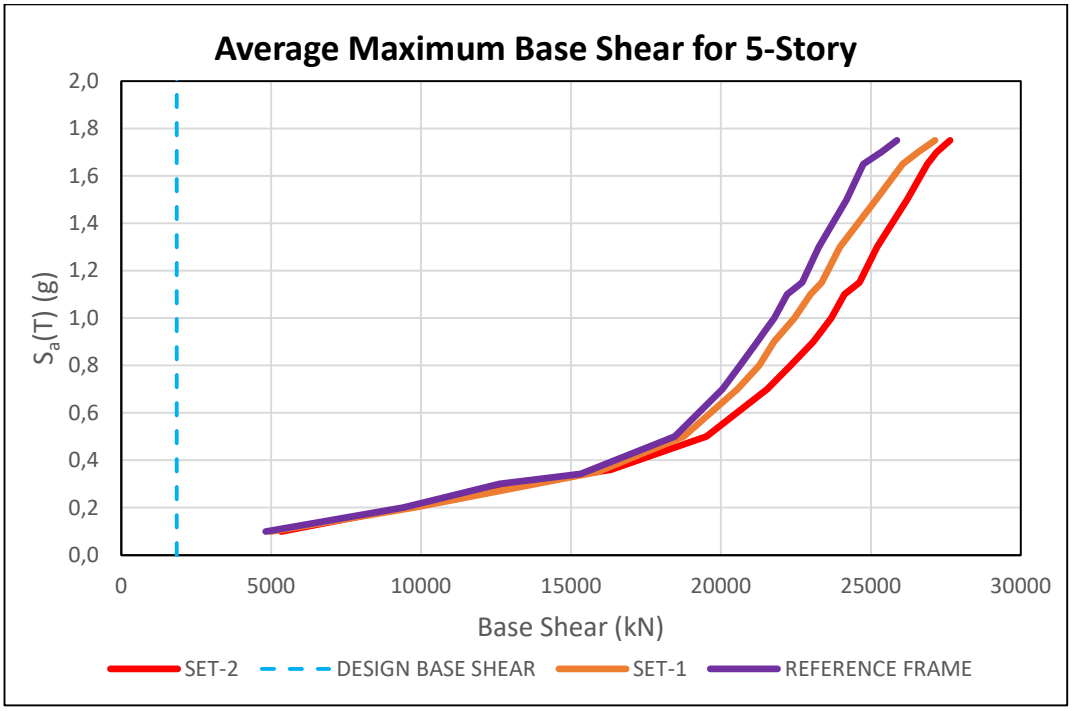


Figure 5.138: Averages of max base shears for the 5-story models.

Curves created by plotting top displacements corresponding to maximum base shears and their averages of 5-story models obtained from 7 earthquakes;

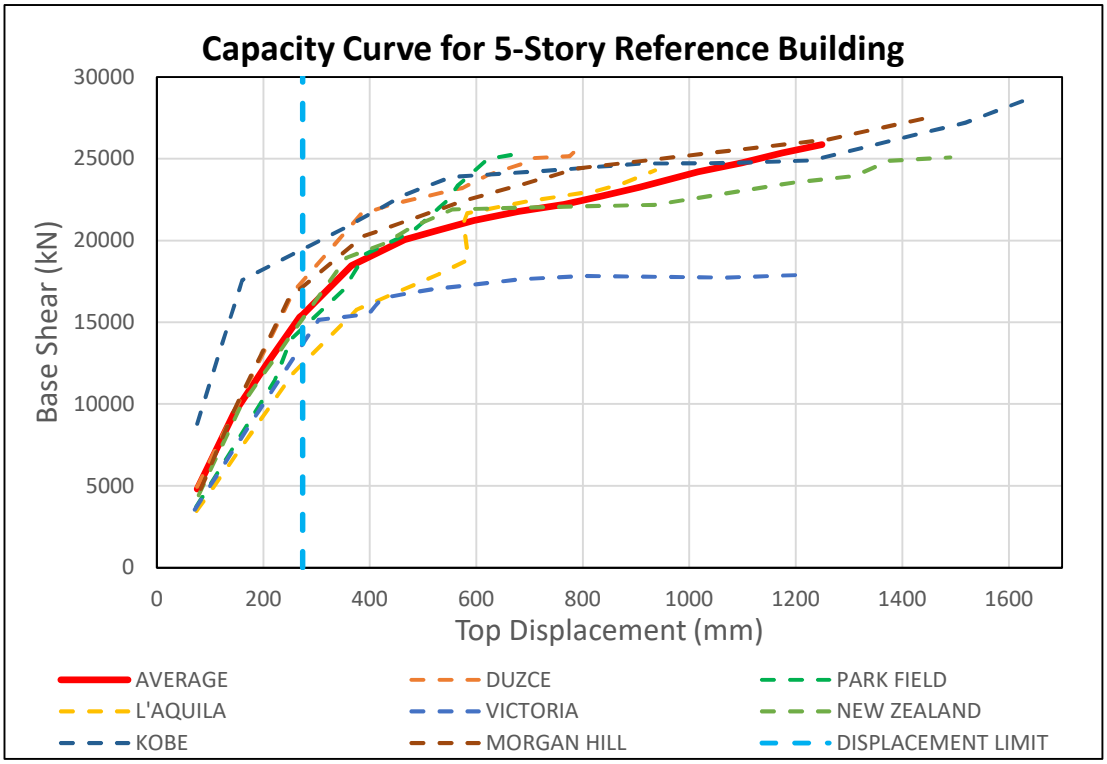


Figure 5.139: The average of the capacity curves of the 5-story RF model.

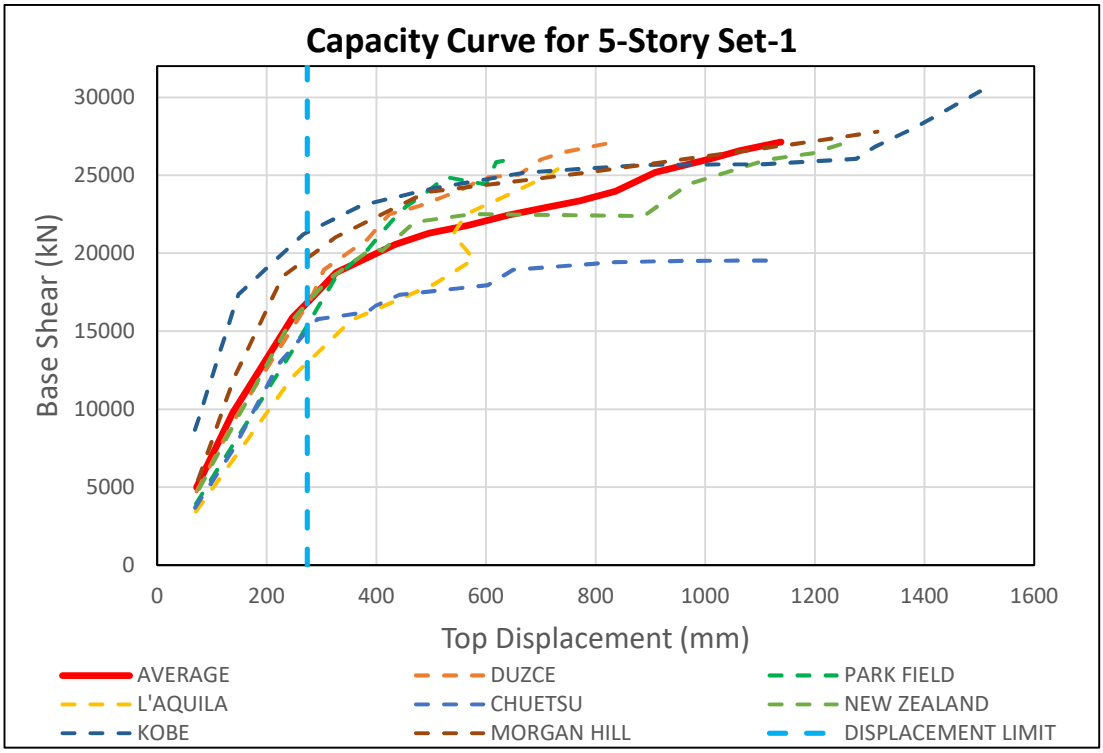


Figure 5.140: The average of the capacity curves of the 5-story Set-1 model.

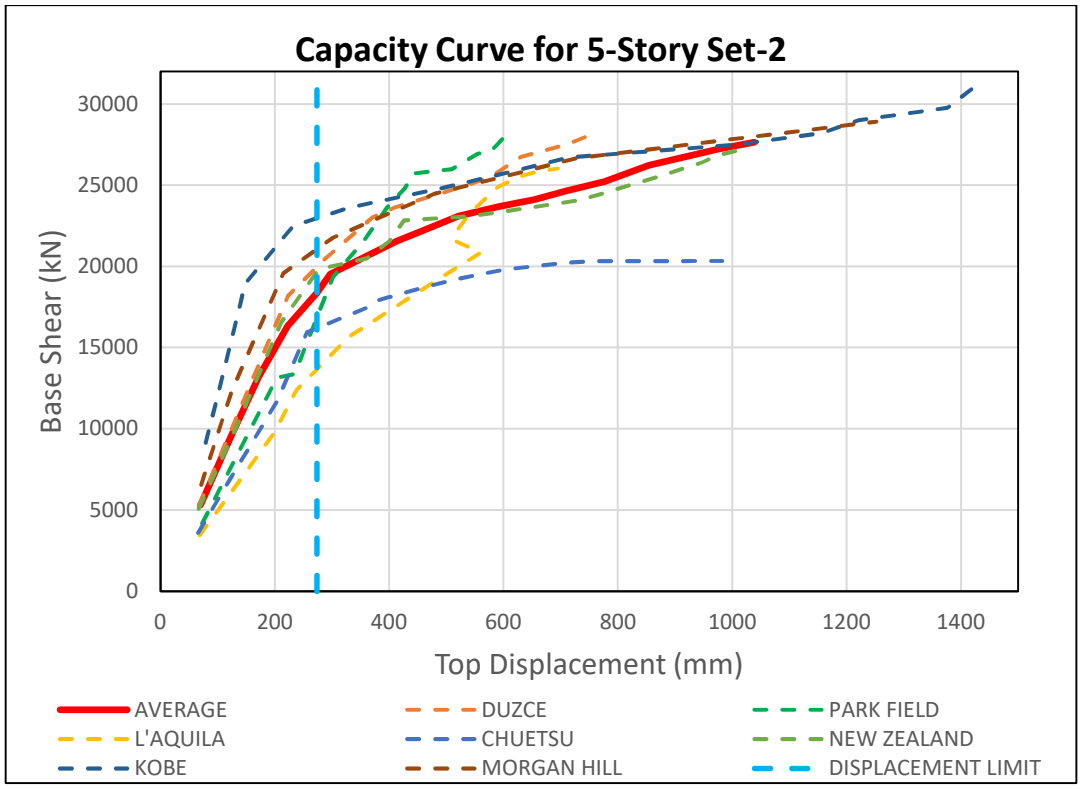


Figure 5.141: The average of the capacity curves of the 5-story Set-2 model.

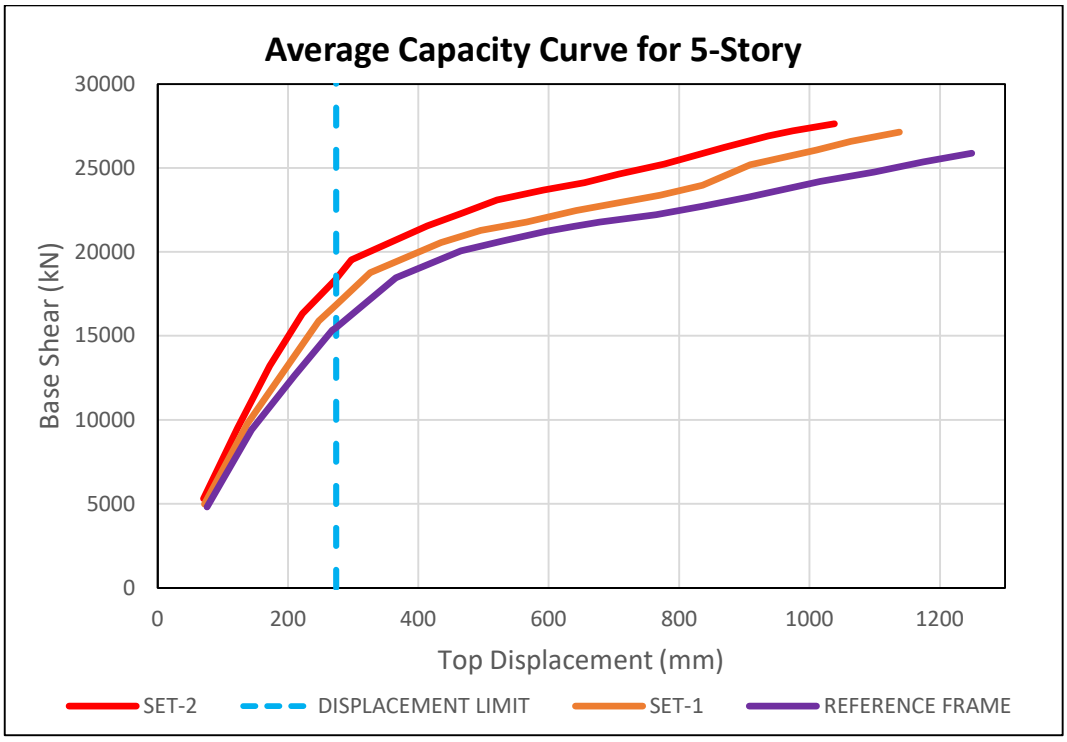


Figure 5.142: Averages of capacity curves for the 5-story models.

- Base shear forces corresponding to design roof displacement 274 mm for 5-story building models, were obtained as 15509.35 kN / 16844.94 kN / 18522.58 kN, respectively.

In the 5-story structure, the Set-2 model reached the 4.00% drift ratio limit at 1.00 g acceleration intensity. For this reason, it has been visualized by taking the average of the distributions of the drift ratios along the structure obtained from all earthquakes at 1.00 g in 5-story models.

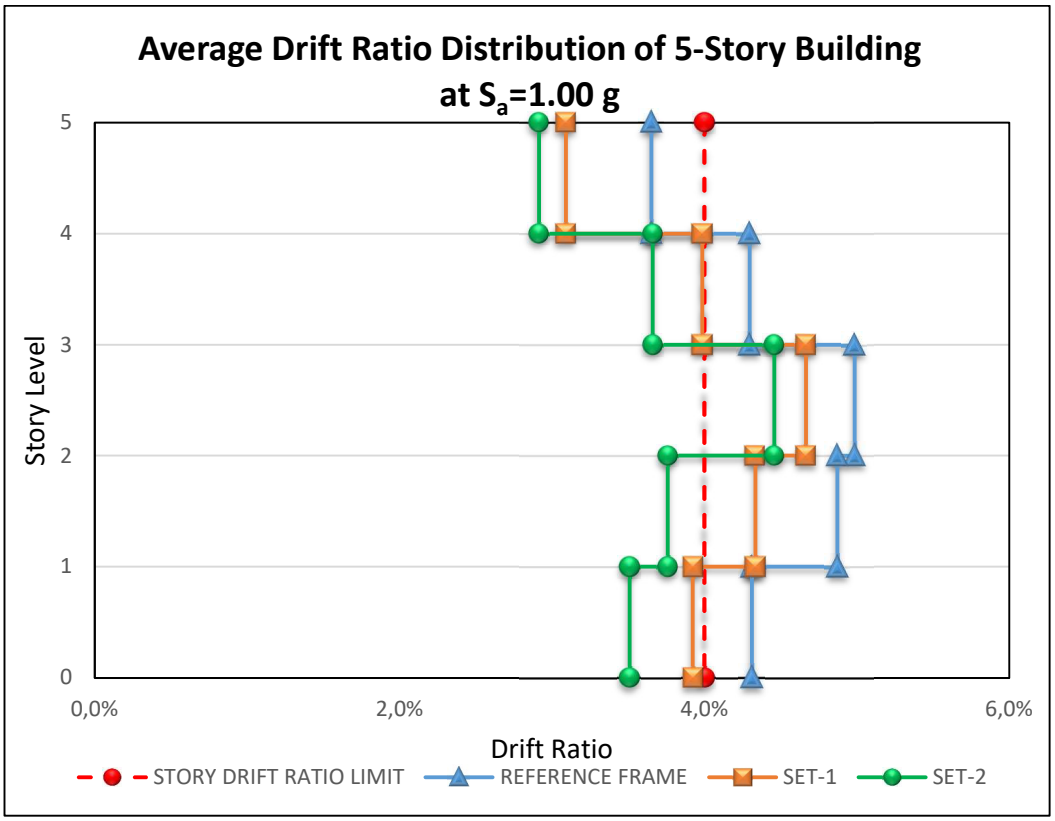


Figure 5.143: Average drift ratio distributions of 5-story models at S_a=1.00 g.

In the Set-2 model of the 5-story building, It is seen that the model that makes the largest drift ratio distribution throughout the building height at 1.00 g acceleration intensity is the Reference Frame. The least distribution was observed in Set-2 models, which were designed to meet 10% of the earthquake forces of gravity load-carrying frames.

5.3.2 Results for 10-Story Buildings

IDA curves created by plotting under increasing acceleration intensities of maximum story drift and their averages of 10-story models obtained from 7 earthquakes;

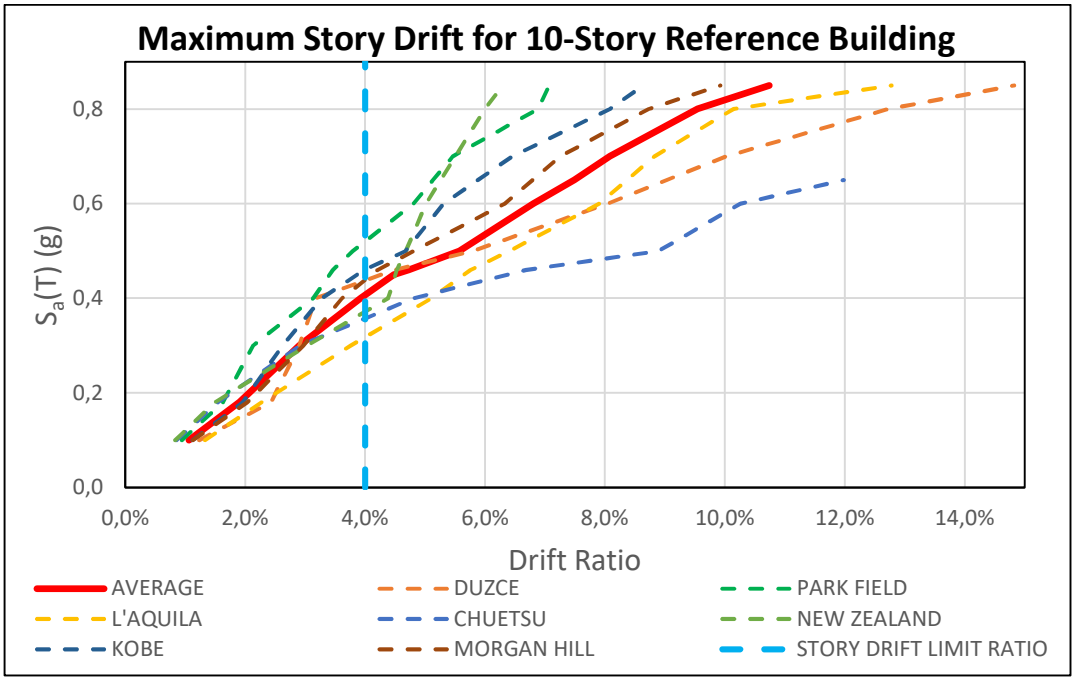


Figure 5.144: The average of the max story drift ratios of the 10-story RF model.

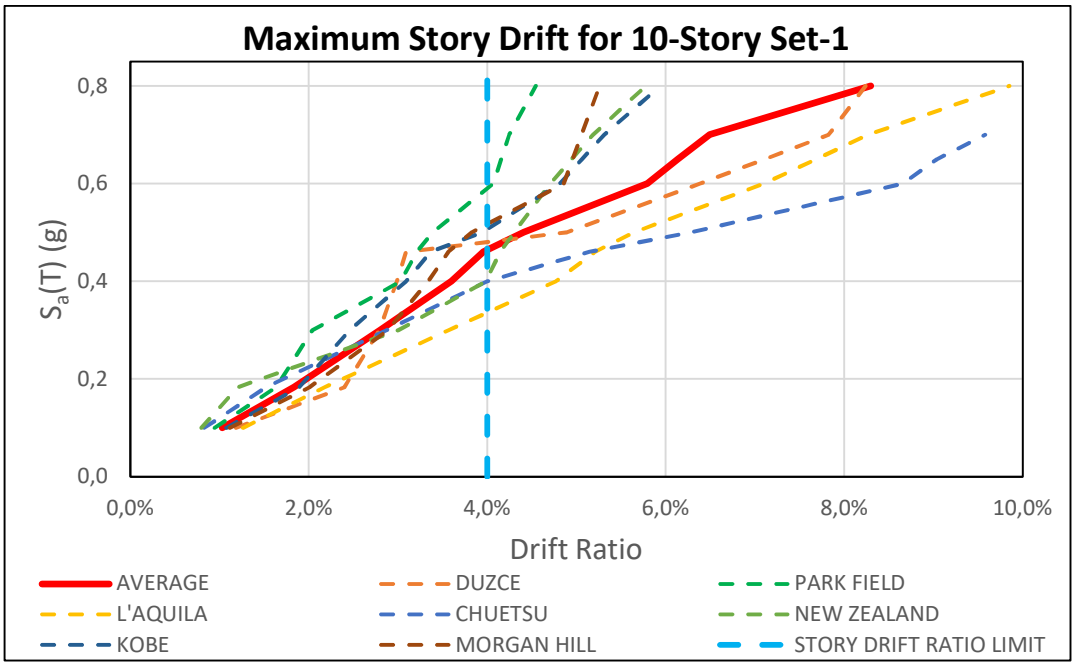


Figure 5.145: The average of the max story drift ratios of the 10-story Set-1 model.

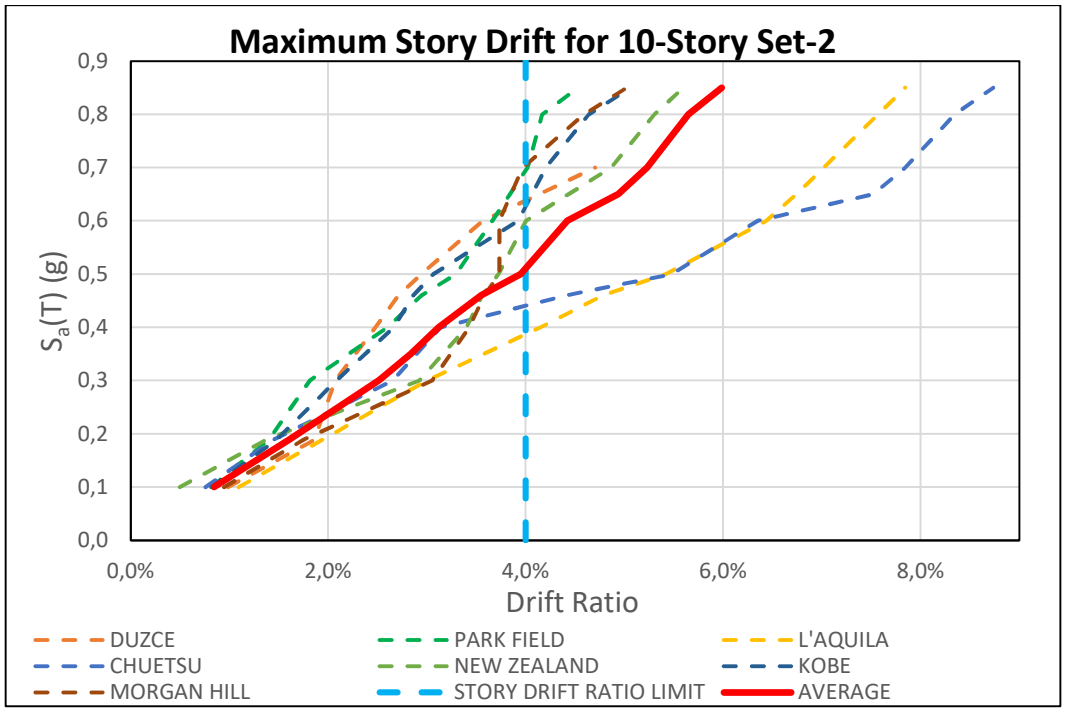


Figure 5.146: The average of the max story drift ratios of the 10-story Set-2 model.

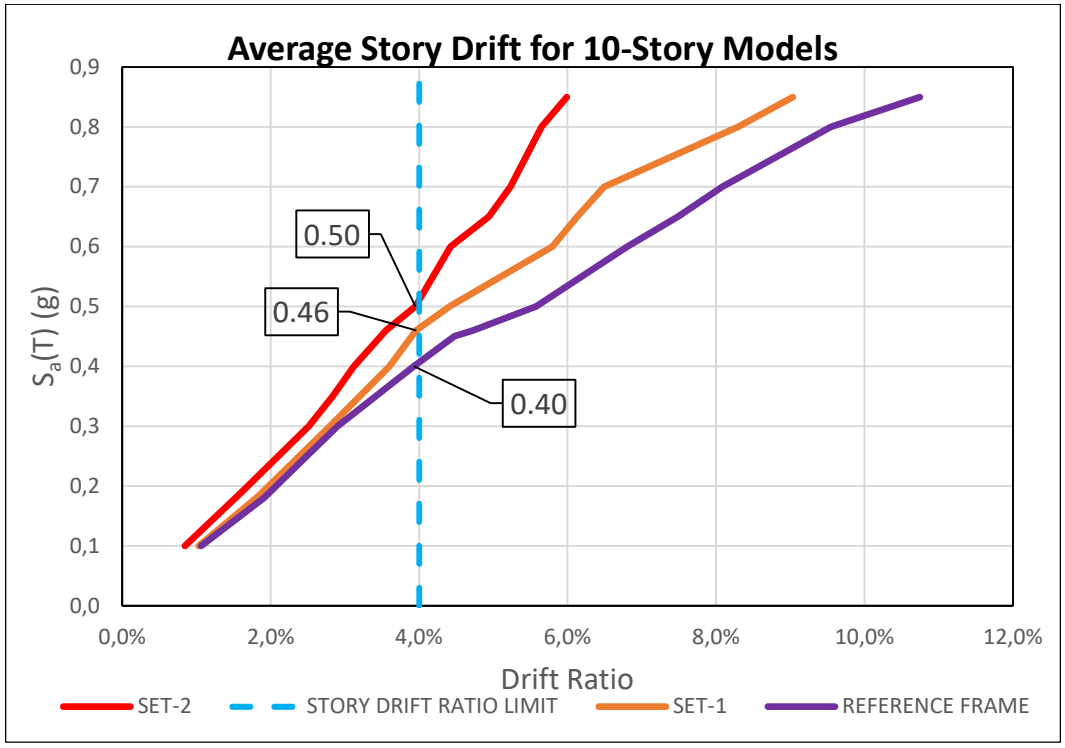


Figure 5.147: Averages of max drift ratios for the 10-story models.

- The 4.00% which is two times of design drift ratio is reached approximately at spectral accelerations, S_a, of 0.40 g / 0.46 g / 0.50 g, respectively, for RF, Set-1, and Set-2 models of the 10-story buildings.

IDA curves created by plotting under increasing acceleration intensities of top displacements and their averages of 10-story models obtained from 7 earthquakes;

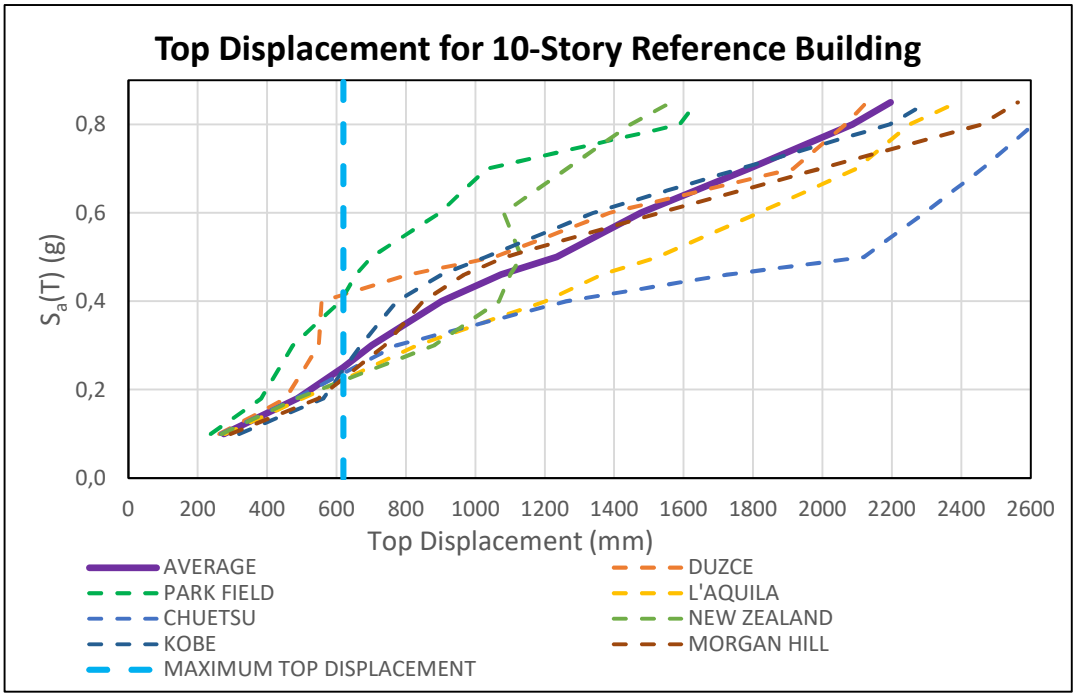


Figure 5.148: The average of the top displacements of the 10-story RF model.

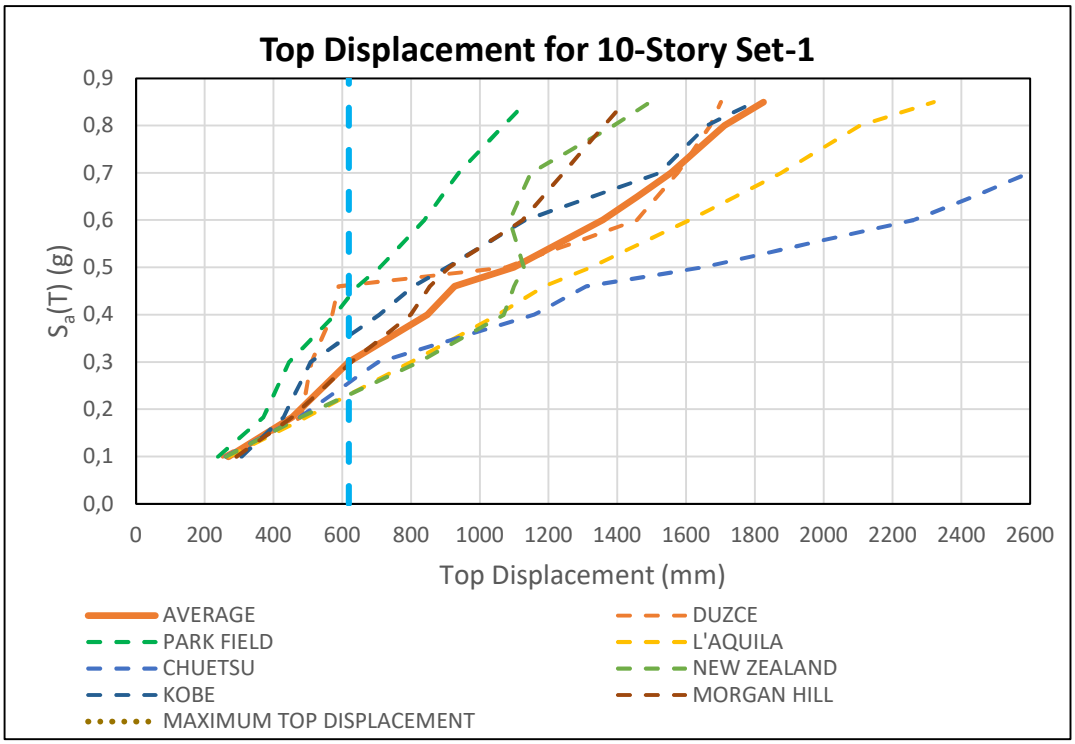


Figure 5.149: The average of the top displacements of the 10-story Set-1 model.

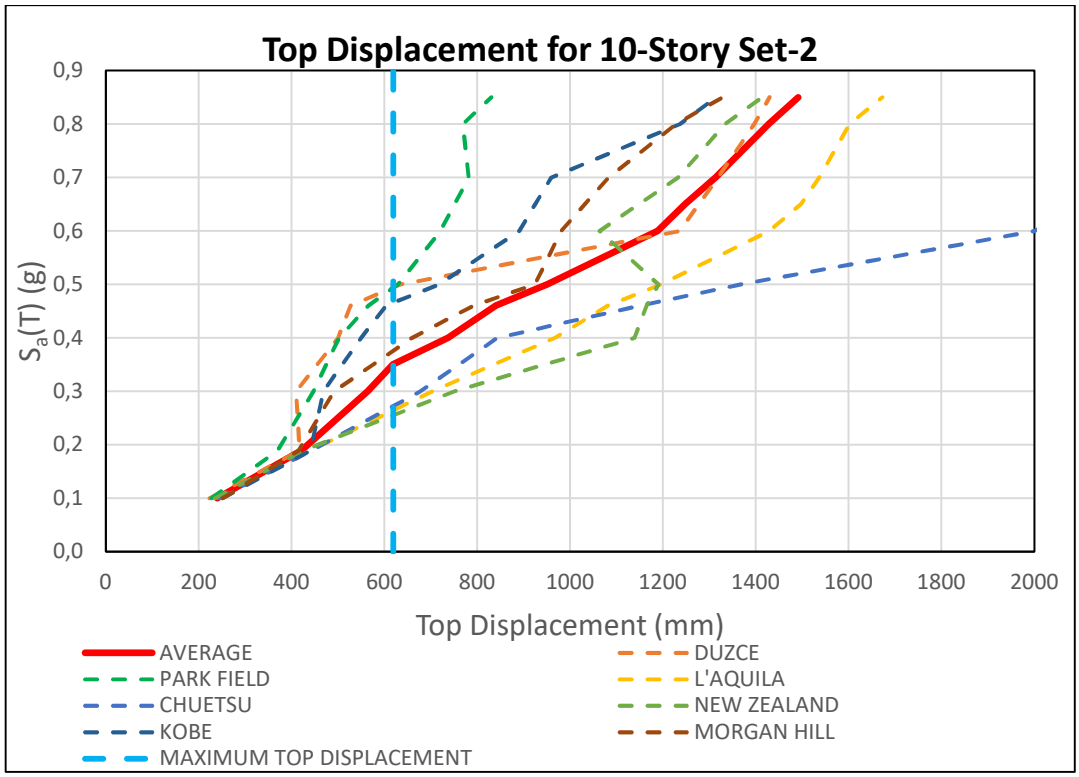


Figure 5.150: The average of the top displacements of the 10-story Set-2 model.

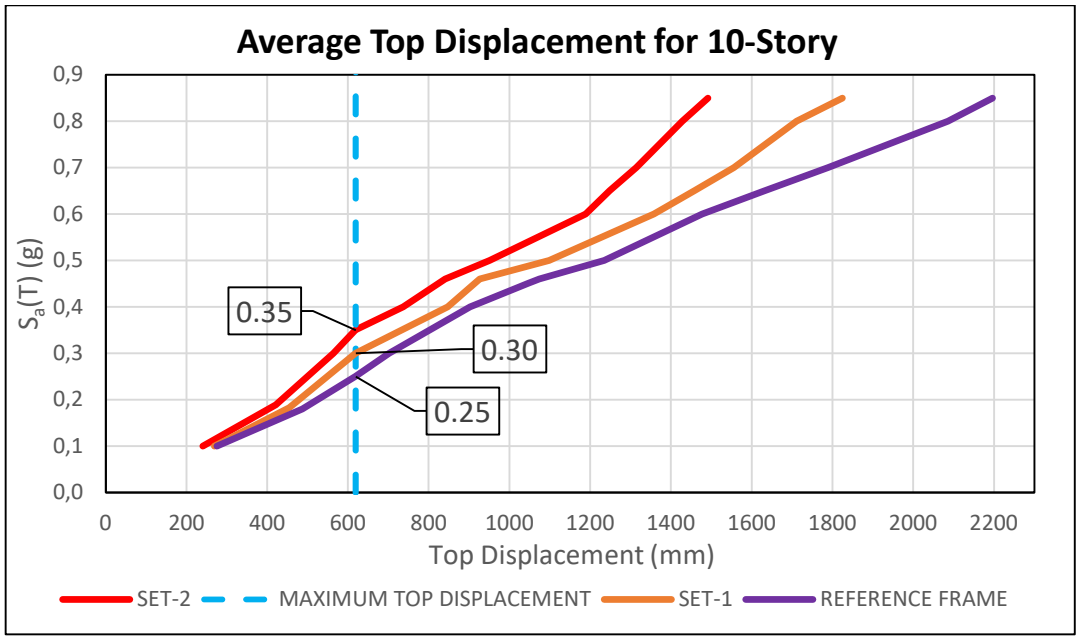


Figure 5.151: Averages of top displacements for the 10-story models.

- The 10-story buildings reach their design roof displacement of 619 mm, approximately at spectral accelerations, S_a, of 0.25 g / 0.30 g / 0.35 g, respectively, for RF, Set-1, and Set-2 models.

IDA curves created by plotting under increasing acceleration intensities of maximum base shears and their averages of 10-story models obtained from 7 earthquakes;

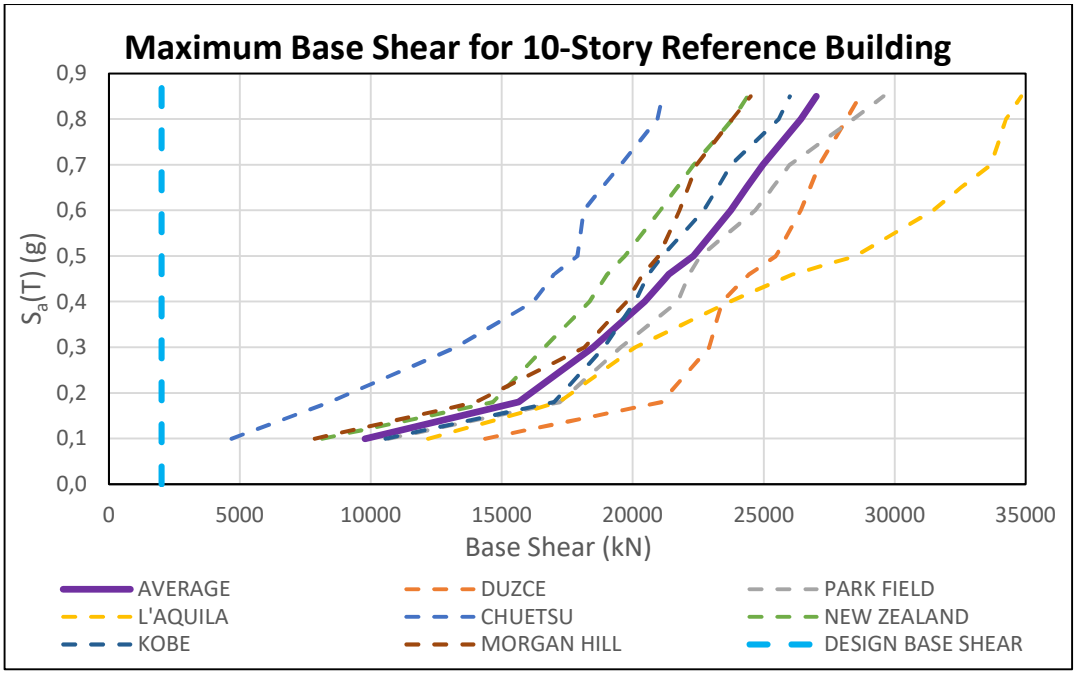


Figure 5.152: The average of the max base shears of the 10-story RF model.

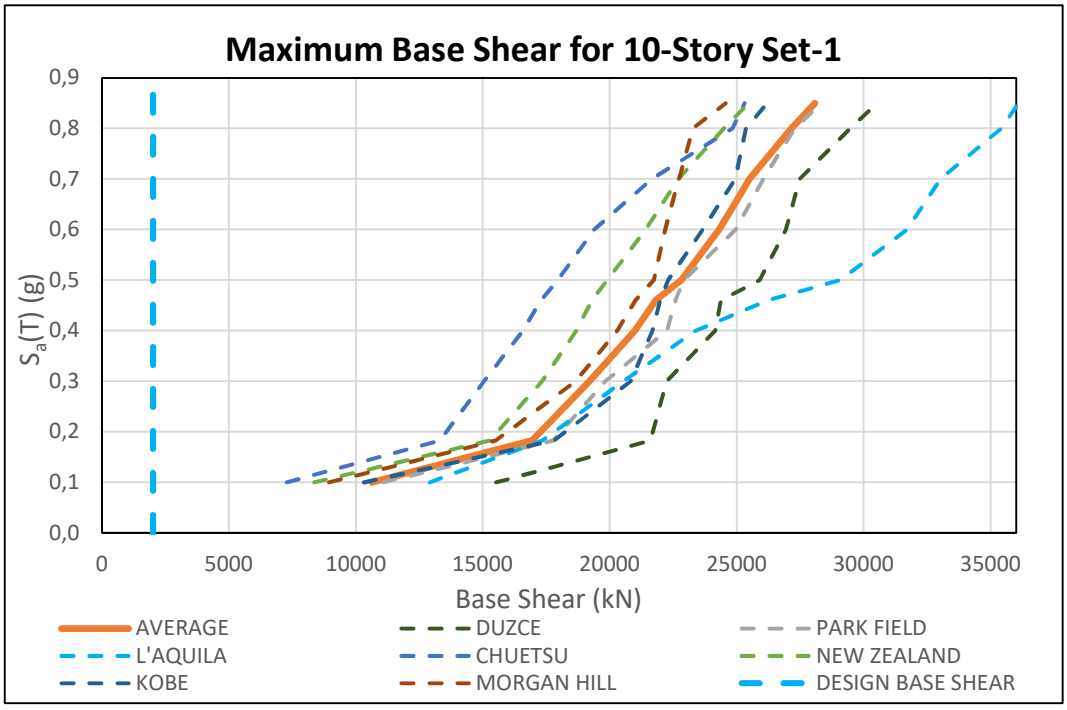


Figure 5.153: The average of the max base shears of the 10-story Set-1 model.

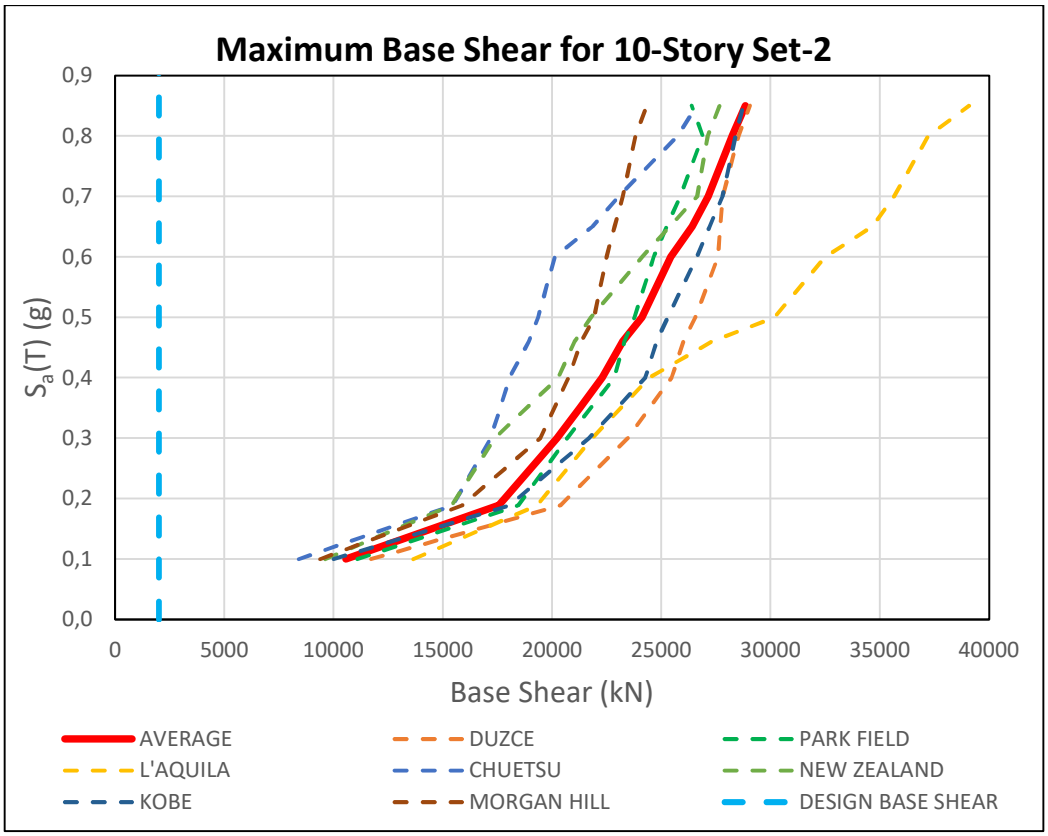


Figure 5.154: The average of the max base shears of the 10-story Set-2 model.

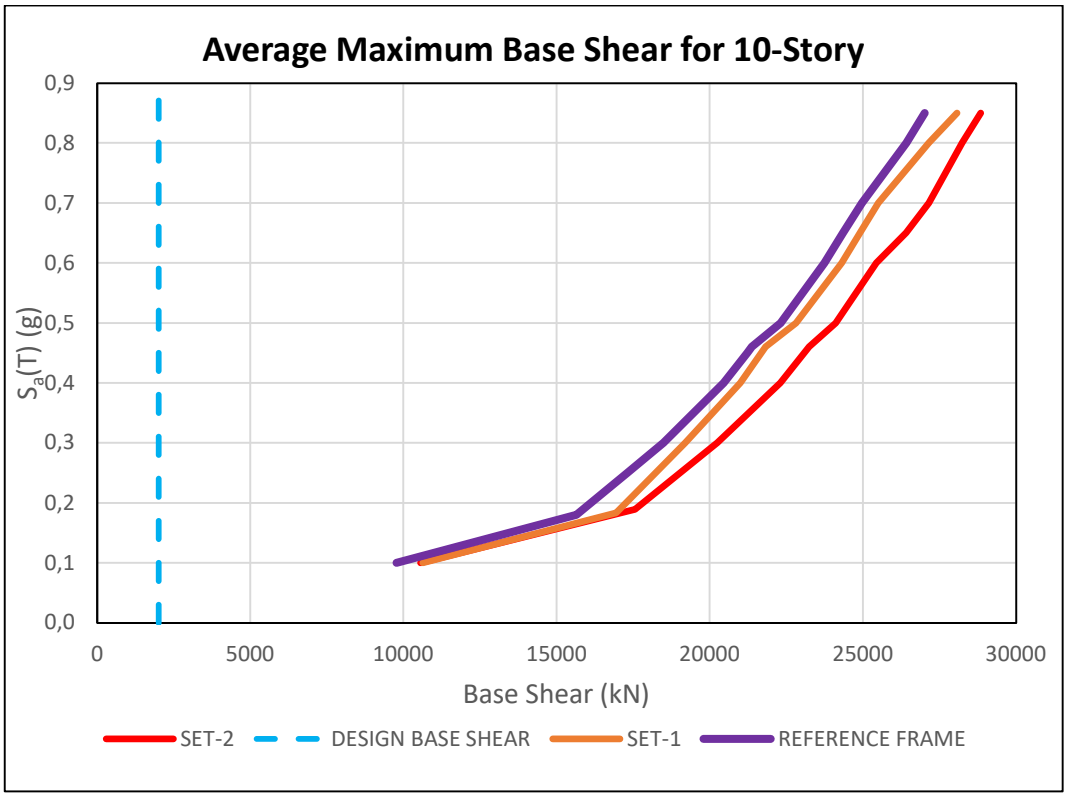


Figure 5.155: Averages of max base shears for the 10-story models.

Curves created by plotting top displacements corresponding to maximum base shears and their averages of 10-story models obtained from 7 earthquakes;

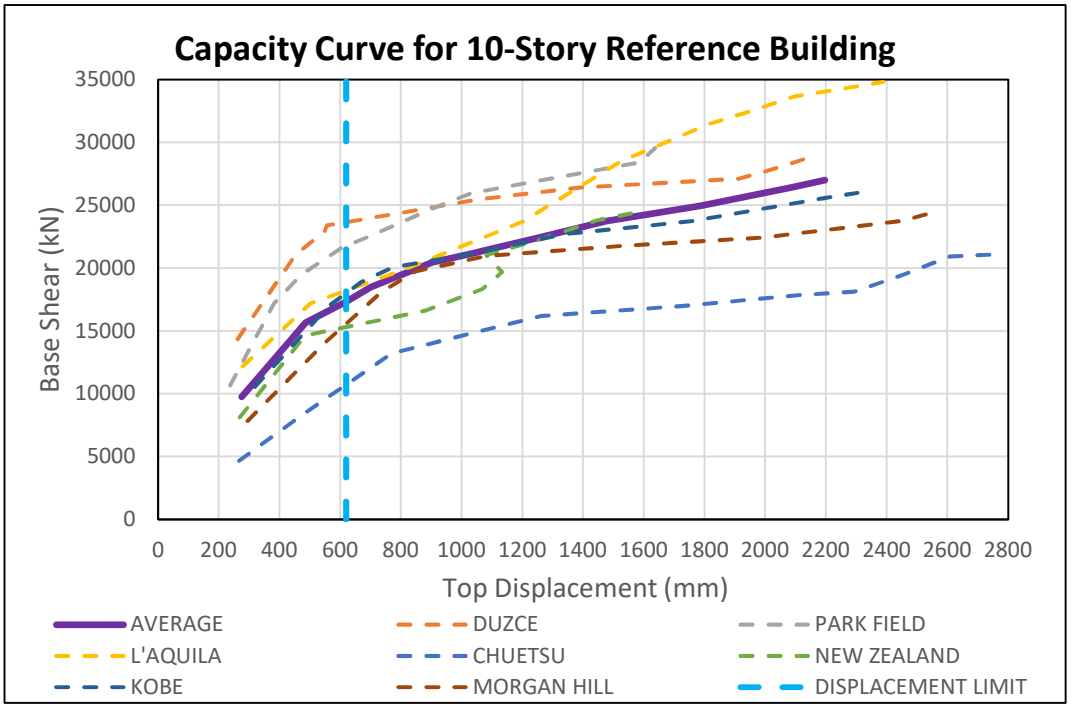


Figure 5.156: The average of the capacity curves of the 10-story RF model.

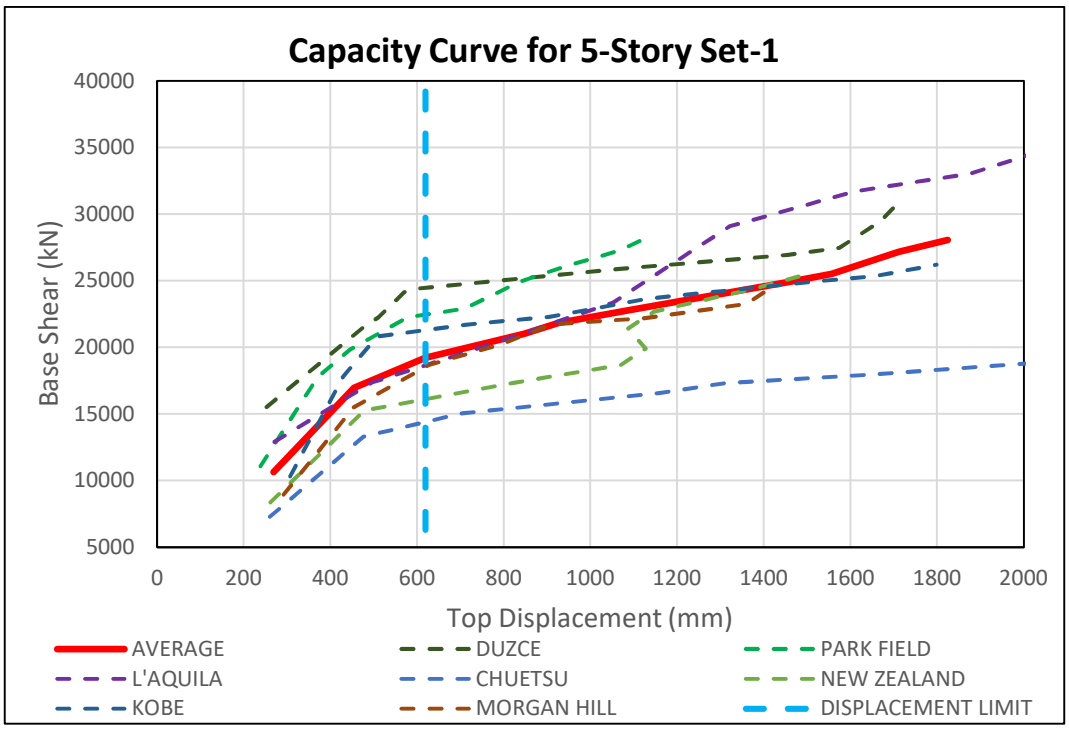


Figure 5.157: The average of the capacity curves of the 10-story Set-1 model.

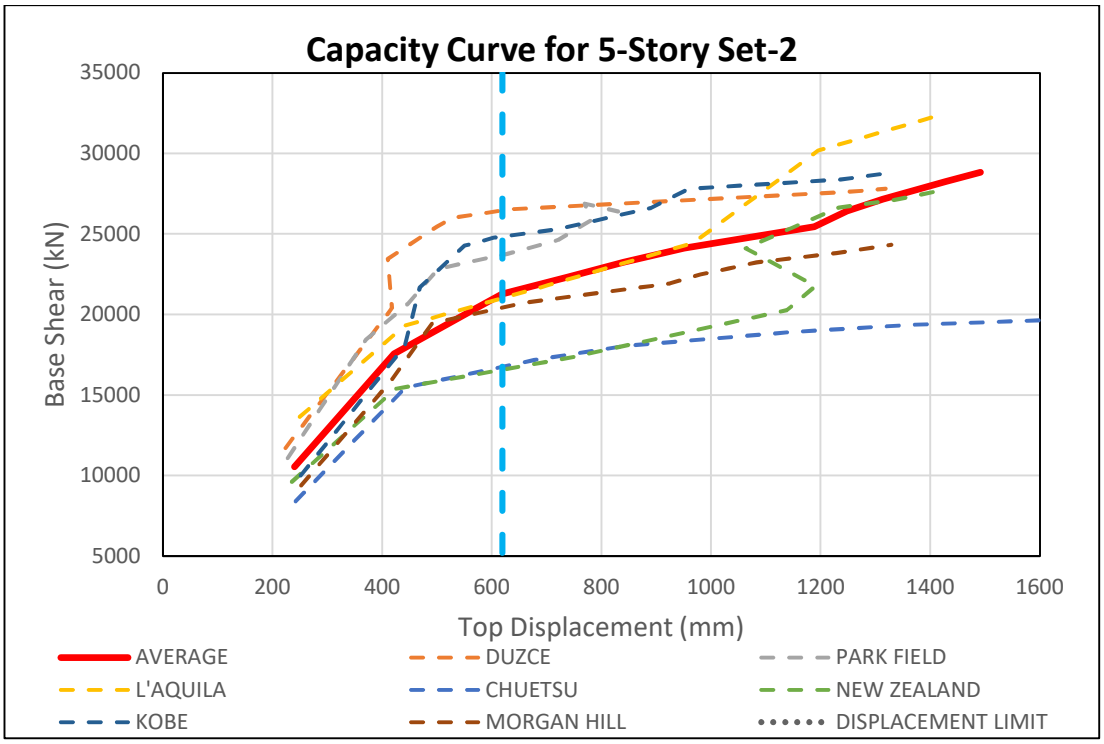


Figure 5.158: The average of the capacity curves of the 10-story Set-2 model.

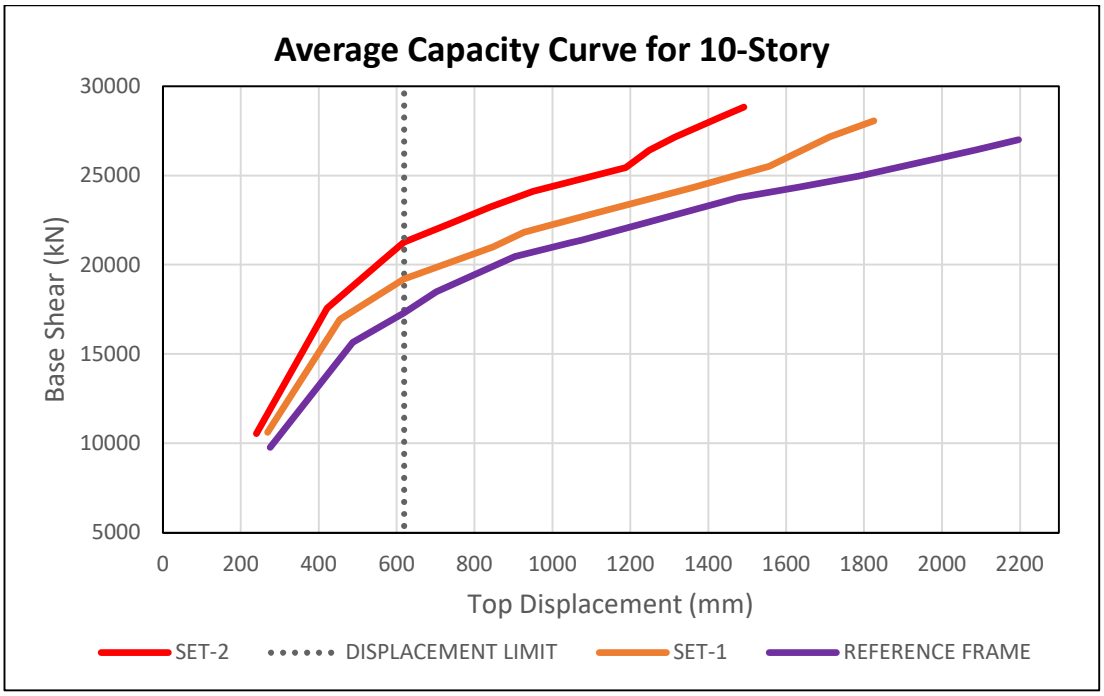


Figure 5.159: Averages of capacity curves obtained for the 10-story models.

- Base shear forces corresponding to design roof displacement 619 mm for 10-story building models, were obtained as 17393.15 kN / 19061.08 kN / 20896.3 kN, respectively.

In the 10-story structure, the Set-2 model reached the 4.00% drift ratio limit at 0.50 g acceleration intensity. For this reason, it has been visualized by taking the average of the distributions of the drift ratios along the structure obtained from all earthquakes at 0.50 g in 10-story models.

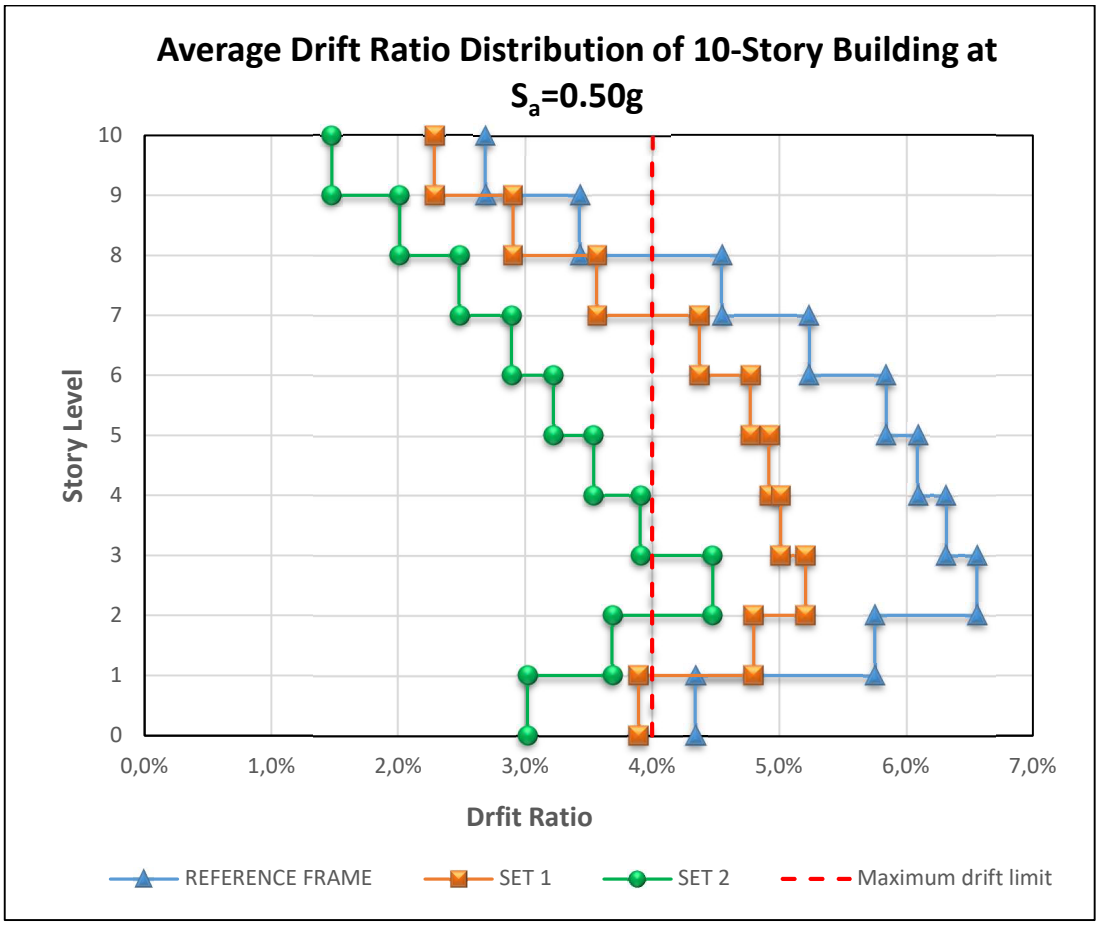


Figure 5.160: Average drift ratio distributions of 10-story models at S_a=0.50 g.

In the Set-2 model of the 10-story building, It is seen that the model that makes the largest drift ratio distribution throughout the building height at 0.50 g acceleration intensity is the Reference Frame. The least distribution was observed in Set-2 models, which were designed to meet 10% of the earthquake forces of gravity load-carrying frames like in 5-story models. However, it should not be overlooked that 10-story building models have more drift ratio distribution than 5-story building models.

6. RESULTS and SUGGESTIONS

Within the scope of this research, the seismic performance of 5 and 10 story structures designed with moment frames with lateral load resistance and the contribution of the additional rigidity and strength created by the semi-rigid design of gravity load-bearing frames to the seismic performance of SMRFs has been investigated. For this purpose, the models designed according to TBEC-2018 were subjected to nonlinear dynamic time-history analyses under different earthquake records. After the structures were modeled, the fundamental periods of the models and the maximum drift ratio, top displacement, base shear, and plastic rotation demand results obtained from the analyzes were noted as explained below.

6.1 Numerical Results

Table 6.1: Fundamental periods of 5 and 10-story models.

Fundamental Period (sec)	Reference Frame	Set 1	Set 2
5-Story	1.459	1.426	1.39
10-Story	2.773	2.733	2.635

Table 6.2: S_a corresponding to max drift ratio limit for 5 and 10-story models.

S_a(T) Values Corresponding to 4.00% Drift Ratio (g)	Reference Frame	Set 1	Set 2
5-Story	0.85 g	0.90 g	1.00 g
10-Story	0.40 g	0.46 g	0.50 g

Table 6.3: S_a corresponding to max design displacement limits for 5 and 10-story models.

S_a(T) Values Corresponding to Maximum Design Top Displacement Limits	Reference Frame	Set 1	Set 2
5-Story (274 mm)	0.35 g	0.40 g	0.45 g
10-Story (619 mm)	0.25 g	0.30 g	0.35 g

Table 6.4: Max base shear forces for 5 and 10-story models.

Base Shears Corresponding to Maximum Design Displacement Limits	Reference Frame	Set 1	Set 2
5-Story (274 mm)	15509.35 kN	16844.94 kN	18522.58 kN
10-Story (619 mm)	17393.15 kN	19061.08 kN	20896.3 kN

Table 6.5: Max plastic rotation demands for 5 and 10-story models.

Maximum Rotational Demand	Reference Frame	Set 1	Set 2
5-Story (1.00 g)	3.28%	3.06%	2.70%
10-Story (0.50 g)	4.92%	3.70%	3.14%

6.2 Theoretical Results and Suggestions

While the structure periods of the 5-story building were 1.459 s, 1.426 s, and 1.390 s for the Reference Frame, Set-1, and Set-2 models, respectively, they were 2.773 s, 2.733 s, and 2.635 s for the 10-story building models, respectively. In Set-1 and Set-2 models, it has been observed that the structure fundamental periods are reduced by the semi-rigid design of the connections of the gravity load-bearing frames.

According to TBEC-2018, the design drift ratio limit was determined as 2.00%. In the study, the drift ratio of 4.00%, which is twice this ratio, was taken as a basis. In the Set-2 models of 5 and 10 story buildings, where gravity frames contribute 10% to the seismic lateral force lateral load-carrying system, the ground motion intensities that meet the design drift ratio were obtained as SF=1.00 g and SF=0.50 g as maximum, respectively.

While the Set-2 models of 5 and 10-story structures reached their maximum design peak displacement limits of 274 mm and 619 mm, respectively, at SF=0.45g and SF=0.35g acceleration intensities, other models have reached their displacement limits under smaller acceleration intensities, without can providing stability up to these accelerations. This is showed the 10% contribution of Set-2 models to the resistance system and the effect of semi-rigid connection with the concrete composite deck.

Base shear forces corresponding to the top displacement examined to be able to evaluate performance and capacity were concluded that the responses of the models in Set-1 and Set-2 were 9% and 17% larger than the Reference Frame, which is the bare moment frame model. Since the periods of Set-2 models are lower than the other models due to semi-rigid connections and gravity frames, their structural rigidities are higher. Therefore, in the results, it is seen that the base shear forces of the Set-2 models are larger than the other models.

In the Set-2 models, in which the contribution of the gravity load-carrying frames is taken into account, the maximum plastic rotation demand for the 5-story structure with the contribution of semi-rigid connections is 2.70%, it reduced approximately 12% compared to the Set-1 structure and 18% compared to the Reference Frame. The rotation demand of the 10-story building in the Set-2 model is 3.14%, it decreased approximately 15% compared to Set-1 and 36% compared to the Reference Frame model. In addition, it is seen that maximum rotational demands on all models are at the controlled damage performance level. In other words, it is expected that repairable damages will occur in the structural elements for life safety.

Story drift ratio distributions observed along the structure height in both mid-rise and low-rise buildings decrease in the Reference Frame, Set-1, and Set-2 models, respectively according to obtained graphics. This situation can be interpreted as follows:

Since the base shear forces increase cumulatively from top to bottom, the least drift distributions are seen on the upper floors. On the lower floor, it is seen that the distributions decrease due to the rigidity of the ground.

In addition, it was concluded that due to the high fundamental periods of mid-rise buildings, they reached the limits determined under smaller earthquake accelerations compared to low-rise buildings and hingings occurred.

As a result of this research, it was observed that the expected overstrength in the structure increased and a secondary reserve capacity was provided by the addition of gravity load-carrying systems designed with moment frames to the numerical models via semi-rigid connections and also taking into account the effects of concrete composite deck.

It has been concluded that moment frames, which are widely used in the world, perform well under lateral seismic forces and gravity load-carrying frames increase seismic performance.

Although these studies for low-rise and mid-rise steel structures are promising for future studies on will be considering the seismic performance of gravity frames, more detailed and systematic research can be done by changing parameters such as building height, building base plan, ductility level, soil type, and material type.

REFERENCES

[1] TBEC, (2018), Turkish Building Earthquake Code, Turkey Environment and Urban Ministry, Ankara.

[2] AISC 360-10, (2010), Specification for Structural Steel Buildings, American Institute of Steel Construction, Chicago, IL, USA.

[3] ETABS, (2016), "Extended 3d Analysis of Building Systems", Computers and Structures Inc., Berkeley, California.

[4] Bruneau M., Uang C., Sabelli R., (2011), "Ductile Design of Steel Structures", 2nd Edition, McGraw-Hill.

[5] Web 1, (2019), http://www.ecs.umass.edu/cee434/tour/Science%20Building/, (Date Accessed: 09/04/2019).

[6] Web 2, (2009), https://www.nehrp.gov/pdf/nistgcr9-917-3.pdf, (Date Accessed: 06/2009).

[7] ANSI/AISC 341 – 16, (2016), Specification for Structural Steel Buildings, American Institute of Steel Construction Inc, Chicago, IL, USA.

[8] Tama Y.S., (2003), "Çelik Yapılarda Moment Dayanımlı Çerçeveler", Pamukkale University Journal of Engineering Sciences, 9 (1), 63-72.

[9] AISC 358 – 16, (2016), Specification for Structural Steel Buildings, American Institute of Steel Construction Inc, Chicago, IL, USA.

[10] FEMA P695, (2009), Quantification of Building Seismic Performance Factors, Federal Emergency Management Agency, Washington, D.C.

[11] PEER Database (2014), Pacific Earthquake Engineering Research Center, 325 Davis Hall, University of California, Berkeley, CA, USA.

[12] ASCE/SEI 41 – 13, (2010), Seismic Evaluation And Retrofit Of Existing Buildings, American Society of Civil Engineers, Reston, VA, USA.

[13] SDCCSS, (2016), Specification for Design, Calculation and Construction of Steel Structures, Ministry of Environment and Urbanization, Ankara, Turkey.

[14] Yenev Ö., (2019), "Merkezi Çaprazlı Çelik Bir Yapıda Yarı-Rijit Kompozit Kolon-Kiriş Birleşim Kullanımının Yapının Deprem Performansına Etkisinin İncelenmesi", Master Thesis, Sakarya University.

[15] Liu J, Astaneh-Asl A., (2004), "Moment-rotation parameters for composite shear tab connections", Journal of Structural Engineering, 130 (9), 1371-1380.

[16] TEC, (2007), Turkish Earthquake Code, Turkey Federal Emergency Management Agency (AFAD), Ankara, Turkey.

[17] TEC, (1997), Turkish Earthquake Code, Turkey Federal Emergency Kandilli Observatory and Earthquake Research Institute, İstanbul, Turkey.

[18] TS – 498, (1997), Turkish Standard: Design Loads for Buildings, Ankara, Turkey.

[19] AISC 360 – 16, (2016), Specification for Structural Steel Buildings, American Institute of Steel Construction Inc, Chicago, IL, USA.

[20] Liu J, Astaneh-Asl A., (2000), "Cyclic testing of simple connections including effects of slab", Journal of Structural Engineering, 126 (1), 32-39.

[21] Wen R, Akbas B, Shen J., (2013) "Practical moment-rotation relations of steel shear tab connections", Journal of Constructional Steel Research, 88, 296-308.

[22] Flores FX, Charney FA, Lopez-Garcia D, (2014) "Influence of the gravity framing system on the collapse performance of special steel moment frames", Journal of Constructional Steel Research, 101(0), 351-362.

[23] Zorlu M, Akbaş B, Shen J, Şeker O., (2018), "Contribution of gravity frames to seismic performance of steel moment resisting frames", Eskişehir Technical University Journal of Science and Technology B – Theoretical Science, 6, 57-66.

[24] Seker O., (2020) "Impact of gravity frames on collapse performance of special steel moment frames", Pamukkale University Journal of Engineering Sciences, 26(6), 1086-1097.

[25] Web 3, (2017), "AFAD", https://tdth.afad.gov.tr.

[26] Shen J, Wen R, Akbas B, Seker O, Uckan E, (2015), "Near-collapse behavior of steel buildings with non-ductile concentrically braced frames", Journal of Constructional Steel Research, 113, 101-114.

[27] Vamvatsikos D, Cornell CA., (2002), "Incremental dynamic analysis", Earthquake Engineering and Structural Dynamics, 31, 491-514.

BIOGRAPHY

Gamze Karakaş completed her high school education at Ülkün Yalçın Anatolian High School. She successfully completed Manisa Celal Bayar University, Faculty of Engineering, Department of Civil Engineering. Later on, in the same year, she started her graduate education at Gebze Technical University Graduate School of Natural and Applied Sciences Department of Earthquake and Structural Engineering Program.

APPENDICES

Appendix A: Publications Based on the Thesis

Akbaş B., Karakaş G., (2021), "Seismic Performance of Steel Moment Frames With Gravity-Only Frames", Gebze Technical University Graduate School of Natural and Applıed Scıences, Graduate Researches Symposium, Kocaeli, Türkiye, 11 June.

Appendix B: Design of 5-Story Building Special Moment Frames

Appendix B1: Calculation of seismic base shear

The total earthquake load value in the Y direction obtained from the Etabs program according to the Modal Response Spectrum Method for the 5-story building is $V_{ty}^{(Y)}$, 1849.288 kN. Calculations for $V_{tE}^{(Y)}$ in order to control $V_{ty}^{(Y)} < \gamma_E V_{tE}^{(Y)}$ are given below.

$$T_{pA} = 0.08 * 20^{3/4} = 0.757\ s$$

$$Max\left(T_p^{(Y)}\right) = 1.4 * 0.757 = 1.059\ s$$

As calculated in Section 3.1. T_A and T_B corner periods were obtained as 0.068 s and 0.340 s, respectively. Since the building period is accepted as the maximum period of 1.059 s; It satisfies the $(T_B \leq T \leq T_L)$ condition. In this case, the horizontal elastic design spectral accelerations $S_{ae}\ (T)$;

$$S_{ae}\ (T) = \frac{S_{D1}}{T} = \frac{0.4995}{1.059} = 0.4716$$

Since $T = 1.059\ s > T_B = 0.340\ s$, $R_a\ (T) = \frac{8}{1} = 8$

$$S_{aR}\left(T_p^{(Y)}\right) = \frac{0.4716}{8} = 0.05895$$

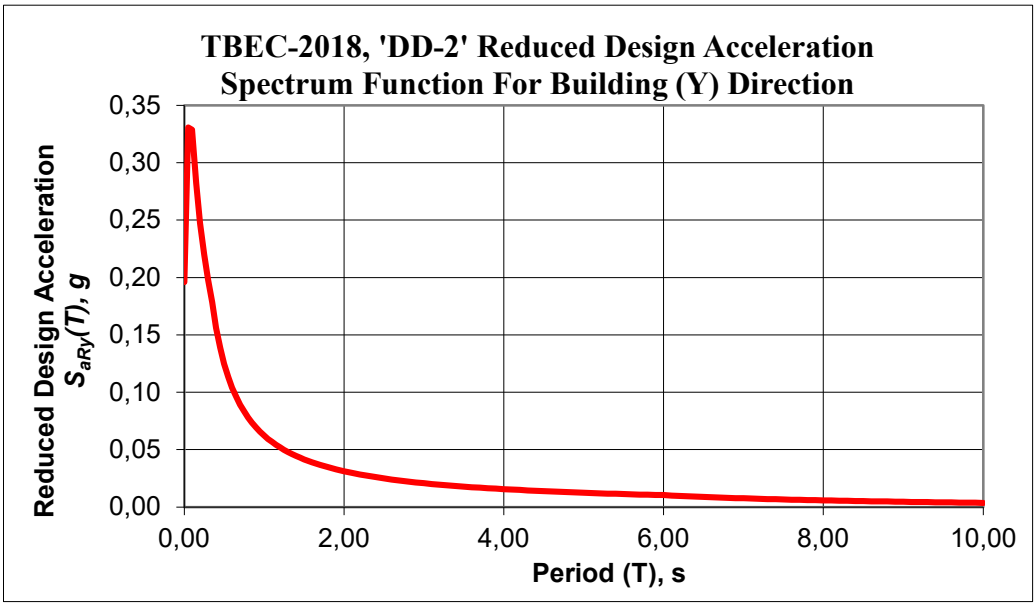


Figure B1.1: Reduced design acceleration spectrum for building (Y) direction.

Table B1.1: Seismic effective weight.

Floor	Dead Load (kN/m²)	Live Load (kN/m²)	n	Area (m²)	Seismic Effective Weight (kN)	ΣMaterial Weight (kN)	ΣStory Weight (kN)	m = W/g
Roof	3.0	1.5	0.3	1620	5589	1273.833	6862.833	699.575
4th	4.4	2.0	0.3	1620	8100	1430.935	9530.935	971.553
3rd	4.4	2.0	0.3	1620	8100	1457.944	9557.944	974.306
2nd	4.4	2.0	0.3	1620	8100	1603.298	9703.298	989.123
1st	4.4	2.0	0.3	1620	8100	1603.298	9703.298	989.123
				TOTAL	**37989**	**7369.308**	**45358.308**	**4623.681**

If the total equivalent seismic load mentioned in Equation (3.4) above is calculated;

$$V_{tE}^{(Y)} = 4623.681 * 0.05895 * 9.81 \geq 0.04 * 4623.681 * 1 * 1.4688 * 9.81$$

$$V_{tE}^{(Y)} = 2673.872\ kN \geq 2664.891\ kN$$

$$V_{tE}^{(Y)} = 2673.872\ kN$$

As the total equivalent seismic load has been obtained;

$$\gamma_E\ V_{tE}^{(Y)} = 0.80 * 2673.872 = 2139.098\ kN$$

Since $V_{ty}^{(Y)} = 1849.288\,kN < \gamma_E\, V_{tE}^{(Y)} = 2139.098\,kN$, the equivalent base shear force amplification coefficient has been included in the calculations.

$$\beta_{tE}^{(Y)} = \frac{0.80 * 2673.872}{1849.288} = 1.157 \geq 1$$

As a result, in the calculations, all reduced internal forces and displacement values calculated with Spec Y loading obtained by Modal Response Spectrum Method were multiplied by 1.157.

Appendix B2: Story drift requirement

Table B2.1: Sections of 5-story building.

Story	SMRFs_Columns		SMRFs_Beam	Gravity Frames_Columns		GFs_Beams
	Exterior	Interior		Exterior (Braced B.)	Interior	
5	HD400×421	HD400×509	HE 500 A	HE 450 B	HE 220 B	IPE O 400
4	HD400×421	HD400×509	HE 500 A	HE 450 B	HE 220 B	IPE O 450
3	HD400×421	HD400×509	HE 500 B	HE 450 B	HE 220 B	IPE O 450
2	HD400×551	HD400×551	HE 550 B	HD 400 X 382	HE 340 B	IPE O 450
1	HD400×551	HD400×551	HE 550 B	HD 400 X 382	HE 340 B	IPE O 450

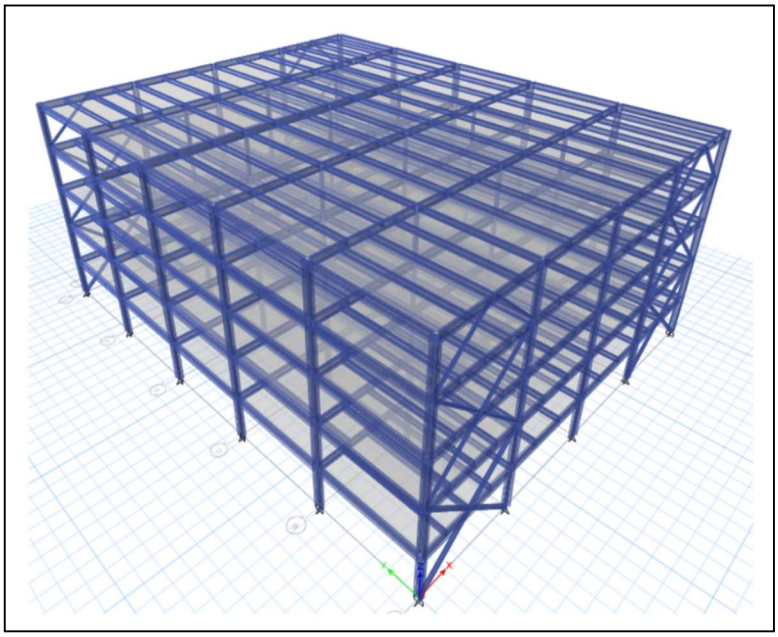


Figure B2.1: 3D model of 5-story building.

Table B2.2: Story drifts of 5-story building for (Y) direction.

Story	Load	Drift_Y	$R^{(Y)}$	I	Story Height	$\lambda^{(Y)}$	$\lambda\delta_i^{(Y)}/h_i$	0.016 κ	Conclusion (Y)
		$\Delta_i^{(Y)}/h_i$	Table 3.3	Table 3.3	h_i (m)	$S_{ae}(T)_{DD-3}$ /$S_{ae}(T)_{DD-2}$			
5	SPECY	0.00160	8	1	4.0	0.357	0.0046	0.008	OK
4	SPECY	0.00208	8	1	4.0	0.357	0.0059	0.008	OK
3	SPECY	0.00228	8	1	4.0	0.357	0.0065	0.008	OK
2	SPECY	0.00219	8	1	4.0	0.357	0.0063	0.008	OK
1	SPECY	0.00148	8	1	4.0	0.357	0.0042	0.008	OK

As a result of the modal analysis made using sections that meet the story drift condition, the first fundamental vibration period of the structure was obtained as $T_1 = 1.432\ s$. Therefore, the assumption $T_1 < 1.4\ T_{pA} = 1.059\ s$ made at the beginning of the design was confirmed. There is no need to recalculate the earthquake loads since the numerically obtained fundamental period of the building exceeds the upper limit based on the design.

Appendix B3: Second order effects

Table B3.1: Second order effects.

Floor	h_i (m)	$\sum w_k$ (kN)	$V_i^{(Y)}$ (kN)	$(\Delta_i^{(Y)})_{ort}$ (m/h_i)	$\theta^{(Y)}_{II,i}$	$\theta^{(Y)}_{II,max}$	D	h	R	0.12*D / (C_h*R)	$\theta^{(Y)}_{II,max} \leq$ 0.12*D / (C_h*R)
5	4.0	6862.83	882.78	0.00160	0.0125		3	1	8	0.045	OK
4	4.0	16393.77	1276.04	0.00208	0.0267		3	1	8	0.045	OK
3	4.0	25951.71	1566.21	0.00228	0.0378	0.04269	3	1	8	0.045	OK
2	4.0	35655.01	1829.03	0.00219	0.0427		3	1	8	0.045	OK
1	4.0	45358.31	2145.17	0.00148	0.0313		3	1	8	0.045	OK

Appendix B4: Strong column-weak beam requirement

Table B4.1: Check of SC/WB for 5-story building.

Axis	Floors	Column Above	Gross Area	Plastic Modulüs	Depth	Top Column Axial Load	Top Column Capacity
			A_g (m^2)	W_{pc} (m^3)	d_c(m)	$P_{r,above}$ (kN)	$\Sigma M_{pc,above}$ (kNm)
Interior Columns	1st	HD400X551	0.07014	0.01205	0.455	1494.474	4021.000
	2nd	HD400X509	0.06490	0.01103	0.446	1087.435	3730.836
	3rd	HD400X509	0.06490	0.01103	0.446	687.749	3798.765
	4th	HD400X509	0.06490	0.01103	0.446	294.987	3865.516
Exterior Columns	1st	HD400X551	0.07014	0.01205	0.455	1543.004	4012.663
	2nd	HD400X421	0.05371	0.00888	0.425	964.911	2992.869
	3rd	HD400X421	0.05371	0.00888	0.425	707.171	3035.482
	4th	HD400X421	0.05371	0.00888	0.425	166.972	3124.794

Table B4.2: Continued.

Axis	Floors	Column Below	Gross Area	Plastic Modülüs	Depth	Bottom Column Axial Load	Bottom Column Capacity
			A_g (m^2)	W_{pc} (m^3)	d_c(m)	$P_{r,below}$ (kN)	$\Sigma M_{pc,below}$ (kNm)
Interior Columns	1st	HD400X551	0.07014	0.01205	0.455	1904.505	3950.557
	2nd	HD400X551	0.07014	0.01205	0.455	1494.474	4021.000
	3rd	HD400X509	0.0649	0.01103	0.446	1087.435	3730.836
	4th	HD400X509	0.0649	0.01103	0.446	687.749	3798.765
Exterior Columns	1st	HD400X551	0.07014	0.01205	0.455	1826.215	3964.008
	2nd	HD400X551	0.07014	0.01205	0.455	1543.004	4012.663
	3rd	HD400X421	0.05371	0.00888	0.425	964.911	2992.869
	4th	HD400X421	0.05371	0.00888	0.425	707.171	3035.482

Table B4.3: Continued.

Axis	Floors	Total Column Capacity	Left Beam	Right Beam	Beam Capacity	Capacity Ratio	Conclusion
		ΣM^*_{pc} (kNm)			**ΣM^*_{pb} (kNm)**	**ΣM^*_{pc} / ΣM^*_{pb} (kNm)**	**ΣM^*_{pc} / $\Sigma M^*_{pb} > 1$**
Interior Columns	**1st**	7971.558	HE 550 B	HE 550 B	7335.031	1.087	OK
	2nd	7751.837	HE 550 B	HE 550 B	7326.989	1.058	OK
	3rd	7529.601	HE 500 B	HE 500 B	6312.537	1.193	OK
	4th	7664.280	HE 500 A	HE 500 A	5180.430	1.479	OK
Exterior Columns	**1st**	7976.671	HE 550 B	HE 550 B	3667.515	2.175	OK
	2nd	7005.532	HE 550 B	HE 550 B	3654.143	1.917	OK
	3rd	6028.351	HE 500 B	HE 500 B	3148.159	1.915	OK
	4th	6160.276	HE 500 A	HE 500 A	2583.492	2.384	OK

Appendix B5: Stability analysis

Table B5.1: Ratio of second-order drifts to first-order drifts (Δ^{2nd} / Δ^{1st}).

Combination	$\Delta_{max}^{2.order}$ (mm)	$\Delta_{max}^{1.order}$ (mm)	$\Delta_{max}^{2.order}$ / $\Delta_{max}^{1.order}$ (mm)	$\Delta_{max}^{2.order}$ / $\Delta_{max}^{1.order} \leq$ 1.7
1.4G ∓**1.4NG**	0.307	0.291	1.055	OK
1.2G + 1.6Q + 0.5Q_r ± **(1.2NG + 1.6NQ + 0.5NQ_r)**	0.883	0.826	1.069	OK
1.2G + 1.0Q + 1.6Q_r ± **(1.2NG + 1.0NQ + 1.6NQ_r)**	0.840	0.792	1.061	OK
(1.2 + 0.2S_{DS}) G ± E + 0.5Q + 0.2S	35.489	32.556	1.090	OK
(0.9- 0.2S_{DS}) G ± E	35.473	32.432	1.094	OK

Table B5.2: τ values for 5-story building.

	Floor	Section	A_g (mm^2)	F_y (N/mm^2)	P_r (kN)	P_{ns} (kN)	P_r / P_{ns}	$P_r / P_{ns} \leq 0.5$	$\tau_b = 1$
INTERIOR COLUMNS	Roof	HD400X509	64900	355	291.41	23039.5	0.013	OK	OK
	4th	HD400X509	64900	355	682.58	23039.5	0.030	OK	OK
	3rd	HD400X509	64900	355	1078.68	23039.5	0.047	OK	OK
	2nd	HD400X551	70140	355	1478.62	24899.7	0.059	OK	OK
	1st	HD400X551	70140	355	1880.23	24899.7	0.076	OK	OK
EXTERIOR COLUMNS	Roof	HD400X421	53710	355	115.06	19067.1	0.006	OK	OK
	4th	HD400X421	53710	355	577.70	19067.1	0.030	OK	OK
	3rd	HD400X421	53710	355	737.46	19067.1	0.039	OK	OK
	2nd	HD400X551	70140	355	1177.03	24899.7	0.047	OK	OK
	1st	HD400X551	70140	355	1349.56	24899.7	0.054	OK	OK

Appendix B6: Strength requirement

Table B6.1: Strength check for columns.

Axis	Floor	Section of Column	P_r (kN)	P_c (ϕP_n) (kN)	P_r / P_c	M_r (kNm)	W_{px} (cm^3)	M_c(ϕM_n)	P-M Ratio	P-M Ratio ≤ 1
Interior Column	**5th**	HD400X509	291.41	18694.13	0.0156	172.38	12050	3849.98	0.053	OK
	4th	HD400X509	682.58	18694.13	0.0365	243.51	12050	3849.98	0.082	OK
	3rd	HD400X509	1078.68	18694.13	0.0577	283.34	12050	3849.98	0.102	OK
	2nd	HD400X551	1478.62	20230.43	0.0731	366.62	14220	4543.29	0.117	OK
	1st	HD400X551	1880.23	20230.43	0.0929	571.19	14220	4543.29	0.172	OK
Exterior Column	**5th**	HD400X421	115.06	15416.08	0.0075	137.75	8880	2837.16	0.052	OK
	4th	HD400X421	577.70	15416.08	0.0375	178.46	8880	2837.16	0.082	OK
	3rd	HD400X421	737.46	15416.08	0.0478	191.09	8880	2837160	0.091	OK
	2nd	HD400X551	1177.03	20230.43	0.0582	266.18	12050	3849.98	0.098	OK
	1st	HD400X551	1349.56	20230.43	0.0667	484.19	12050	3849.98	0.159	OK

Table B6.2: Strength check for columns under extreme axial loads.

Axis	Floor	Section of Column	P_r (kN)	r (cm)	L/r (cm)	$4.71\sqrt{(E/Fy)}$	F_e (Mpa)	F_{cr} (Mpa)	ϕP_n (kN)	$P_r \leq \phi P_n$
Interior Column	5th	HD400X509	294.99	10.78	37.11	111.80	1433.66	320.05	18694.13	OK
	4th	HD400X509	687.75	10.78	37.11	111.80	1433.66	320.05	18694.13	OK
	3rd	HD400X509	1087.44	10.78	37.11	111.80	1433.66	320.05	18694.13	OK
	2nd	HD400X551	1494.48	10.85	36.87	111.80	1452.34	320.48	20230.43	OK
	1st	HD400X551	1903.59	10.85	36.87	111.80	1452.34	320.48	20230.43	OK
Exterior Column	5th	HD400X421	166.97	10.60	37.74	111.80	1386.19	318.92	15416.0	OK
	4th	HD400X421	707.17	10.60	37.74	111.80	1386.19	318.92	15416.08	OK
	3rd	HD400X421	964.91	10.60	37.74	111.80	1386.19	318.92	15416.08	OK
	2nd	HD400X551	1543.00	10.85	36.87	111.80	1452.34	320.48	20230.43	OK
	1st	HD400X551	1826.22	10.85	36.87	111.80	1452.34	320.48	20230.43	OK

Table B6.3: Spacing of lateral bracing.

Section of Beams	i_y (m)	$L_{b,\,max}$ (m)	Choosen L_b (L/3) (m)	L_p (m)	$L_b < L_p$
HE 500 A	0.0724	3.51	3.0	3.02	OK
HE 500 B	0.0727	3.52	3.0	3.04	OK
HE 550 B	0.0717	3.47	3.0	2.995	NOT OK

Table B6.4: Moment strength checks for girders.

Floors	Section of Beam	M_r (kNm)	W_{px} mm^3	Design Flexural Strength $\phi_f M_n$ (kNm)	$M_r \leq \phi_f M_n$	Ratio of M_r / $\phi_f M_n$ (%)
5th	HE500 A	129.21	3949000	1261.70	OK	10.24
4th	HE500 A	183.61	3949000	1261.70	OK	14.55
3rd	HE500 B	255.81	4815000	1538.40	OK	16.63
2nd	HE550 B	317.96	5591000	1786.30	OK	17.80
1st	HE550 B	299.65	5591000	1786.30	OK	16.77

Table B6.5: Shear strength checks for girders.

Floors	Section of Beam	V_r (kN)	Web Thickness (mm)	Height (mm)	Design Shear Strength $\phi_v V_n$ (kN)	$V_r \leq \phi_v V_n$
5th	HE500 A	36.31	12.0	490	1252.440	OK
4th	HE500 A	49.10	12.0	490	1252.440	OK
3rd	HE500 B	66.96	14.5	500	1544.250	OK
2nd	HE550 B	81.48	15.0	550	1757.250	OK
1st	HE550 B	76.89	15.0	550	1757.250	OK

Table B6.6: Axial strength of gravity columns under gravity loads ($1.2G + 1.6Q_r$).

Floors	Section Columns	Axial Loading	r (cm)	A (cm^2)	(KL/r) cm	$4.71\sqrt{(E/Fy)}$	F_e (Mpa)	F_{cr} (Mpa)	ϕP_n (kN)	$P_u \leq \phi P_n$
5th	HE220B	536.56	5.59	91.04	71.56	111.795	385.51	241.46	1978.4	OK
4th	HE220B	1023.47	5.59	91.04	71.56	111.795	385.51	241.46	1978.40	OK
3rd	HE220B	1510.39	5.59	1.04	1.56	111.795	385.51	241.46	1978.40	OK
2nd	HE340B	1999.98	7.53	70.9	3.12	111.795	699.52	287.07	4415.34	OK
1st	HE340B	2489.57	7.53	70.9	3.12	111.795	699.52	287.07	4415.34	OK

Pinned girders parallel to moment frame beams;

Table B6.7: Moment strength for GF girders parallel to SMF beams ($1.2G + 1.6Q_r$).

Floors	M_u (kNm)	$W_{px,\,req}$ (cm^3)	Selected Section	$W_{px,\,sel}$ (cm^3)	$Ø_b M_n$ (kNm)	M_u (kNm) $< Ø_b M_n$ (kNm)
5th	195.2796	550.083	IPEO400	2691.00	859.7745	OK
4th-1st	175.4296	494.168	IPEO450	3410.00	1089.495	OK

Table B6.8: Shear strength for GF girders parallel to SMF beams (1.2G + 1.6Q_r).

Floors	Selected Section	V_u (kN)	$Ø_vV_n$ (kN)	V_u (kN) <$Ø_vV_n$ (kN)
5th	IPEO400	86.791	681.191	OK
4th-1st	IPEO450	77.969	837.346	OK

Table B6.9: Deflection for GF girders parallel to SMF beams (G+Q).

Floors	Selected Section	δ (cm)	$δ_{lmt}$ (cm)	δ (cm) <$δ_{lmt}$ (cm)
5th	IPE O 400	2.321	2.5	OK
4th-1st	IPE O 450	2.128	2.5	OK

Pinned girders perpendicular to moment frame beams

Table B6.10: Moment strength for GF girders perpendicular to SMF beams (1.2G + 1.6Q_r).

	Floor	M_u (kNm)	$W_{px, req}$ (cm^3)	Selected Section	$W_{px, sel}$ (cm^3)	$Ø_bM_n$ (kNm)	M_u <$Ø_bM_n$ (kNm)
Interior Girder	**5th**	515.536	1452.215	IPEO550	4805.00	1535.20	OK
	4th-1st	468.193	1318.855	IPEO600	6401.00	2045.12	OK

Table B6.11: Shear strength for GF girders perpendicular to SMF beams (1.2G + 1.6Q_r).

	Floors	Selected Section	V_u (kN)	$Ø_vV_n$ (Kn)	V_u (kN) <ØvVn (Kn)
Interior Girders	**5th**	IPEO550	179.908	1173.119	OK
	4th-1st	IPEO600	163.926	1795.590	OK

Table B6.12: Deflection for GF girders perpendicular to SMF beams (G+Q).

	Floors	Selected Section	δ (cm)	$δ_{lmt}$ (cm)	δ (cm) <$δ_{lmt}$ (cm)
Interior Girders	**5th**	IPE O 550	2.104	2.5	OK
	4th-1st	IPE O 600	1.979	2.5	OK

Appendix B7: Member requirement

Table B7.1: Limiting width-to-thickness ratios for SMF girders.

Floors	Section of Beam	b (mm)	t_f (mm)	$b/2t_f$	$\lambda_{hd} = 0.30*\sqrt{(E/Fy)}$	$b/2t_f \leq \lambda_{hd}$
4th-5th	HE 500 A	300	23	6.522	7.121	OK
3rd	HE 500 B	300	28	5.357	7.121	OK
1st-2nd	HE 550 B	300	29	5.172	7.121	OK

Table B7.2: Limiting depth-to-thickness ratios for SMF girders.

Floor	Section of Beams	h (mm)	t_w (mm)	h/t_w	A_g (mm^2)	$C_a < 0.125$	$1.49\sqrt{(E/Fy)}$	Max Limit	$h/t_w <$ Max Limit
4th-5th	HE500A	490	12	40.833	19750	58.152	35.366	58.152	OK
3rd	HE500B	500	14.5	34.483	23860	58.152	35.366	58.152	OK
1st-2nd	HE550B	550	15	36.667	25410	58.152	35.366	58.152	OK

Table B7.3: Limiting width-to-thickness ratios for SMF columns.

Section of Columns	b (mm)	t_f (mm)	$b/2t_f$	$\lambda_{hd} = 0.30*\sqrt{(E/Fy)}$	$b/2t_f \leq \lambda_{hd}$
HD 400×421	409	52.6	3.888	7.121	OK
HD 400×551	418	67.6	3.092	7.121	OK
HD 400×509	416	62.7	3.317	7.121	OK

Table B7.4: Limiting depth-to-thickness ratios for SMF columns.

	Floor	Section of Column	h (mm)	t_w (mm)	h/t_w	P_u (kN)	C_a	$C_a < 0.125$	$1.49\sqrt{(E/Fy)}$	Max Limit	$h/t_w <$Max Limit
Interior Columns	**1st-2nd**	HD400×551	455	42	10.83	1904.51	0.085	53.56	35.37	53.56	OK
	3rd-5th	HD400×509	446	39.1	11.41	4087.44	0.197	47.49	35.37	47.49	OK
Exterior Columns	**1st-2nd**	HD400×551	455	42	10.83	1826.22	0.082	53.75	35.37	53.75	OK
	3rd-5th	HD400×421	425	32.8	12.96	964.9	0.056	55.11	35.37	55.11	OK

Appendix C: Design of 5-Story Building Special Concentrically Braced Frames

Appendix C1: Calculation of seismic base shear

The total earthquake load value in the X-direction obtained from the Etabs program according to the Modal Response Spectrum Method for the 5-story building is $V_{tX}^{(X)}$, 6743.989 kN. Calculations for $V_{tE}^{(X)}$ in order to control $V_{tX}^{(X)} < \gamma_E V_{tE}^{(X)}$ are given below.

$$T_{pA} = 0.08 * 20^{3/4} = 0.757\ s$$

$$T_A = 0.068\ \text{s and}\ T_B = 0.340\ s$$

$$(T_B \leq T \leq T_L) \rightarrow S_{ae}(T) = \frac{S_{D1}}{T} = \frac{0.4995}{0.757} = 0.6598$$

$$\text{Since } T = 0.757\ s > T_B = 0.340\ s\ ,\ R_a(T) = \frac{5}{1} = 5$$

$$S_{aR}\left(T_p^{(X)}\right) = \frac{0.6598}{5} = 0.132$$

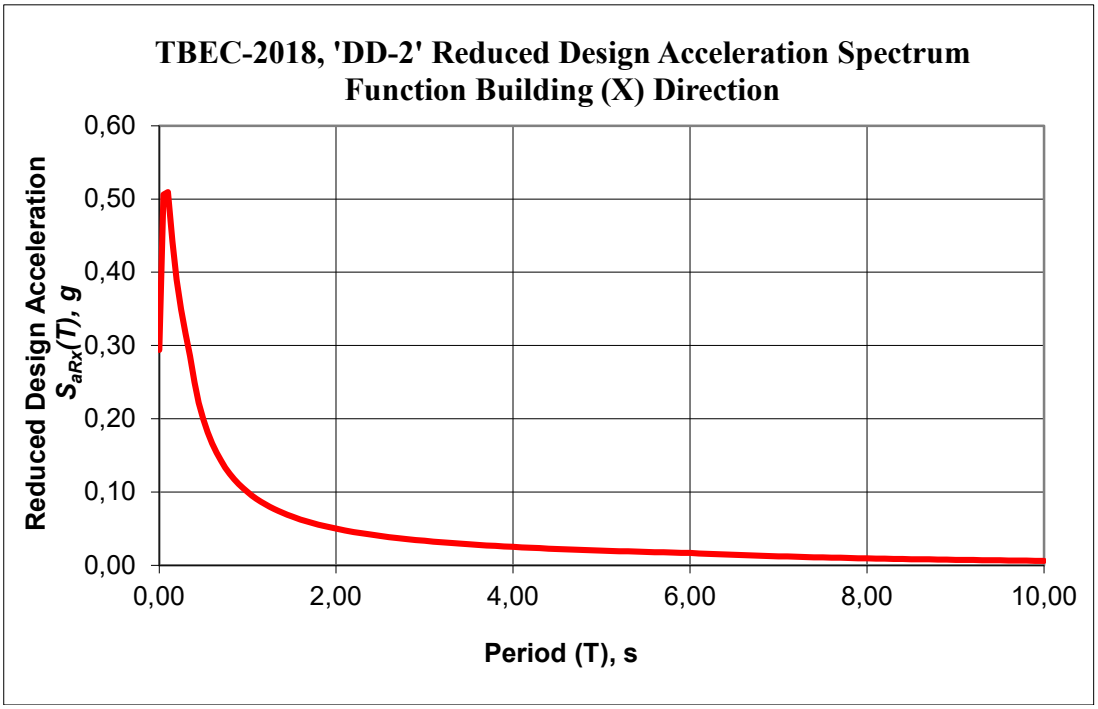


Figure C1.1: Reduced design acceleration spectrum for building (X) direction.

If the total equivalent seismic load mentioned in Equation (3.4) above is calculated;

$$m_t = 4623.681\ (Table\ B1.1)$$

$$V_{tE}^{(X)} = 4623.681 * 0.132 * 9.81 \geq 0.04 * 4623.681 * 1 * 1.4688 * 9.81$$

$$V_{tE}^{(X)} = 5989.076\ kN \geq 2664.891\ kN$$

$$V_{tE}^{(X)} = 5989.076\ kN$$

As the total equivalent seismic load has been obtained;

$$\gamma_E\ V_{tE}^{(X)} = 0.80 * 5989.076 = 4791.261\ kN$$

Since $V_{tx}^{(X)} = 6743.989\ kN < \gamma_E\ V_{tE}^{(X)} = 4791.261\ kN$, the equivalent base shear amplification coefficient was not included in the calculations.

Appendix C2: Brace design

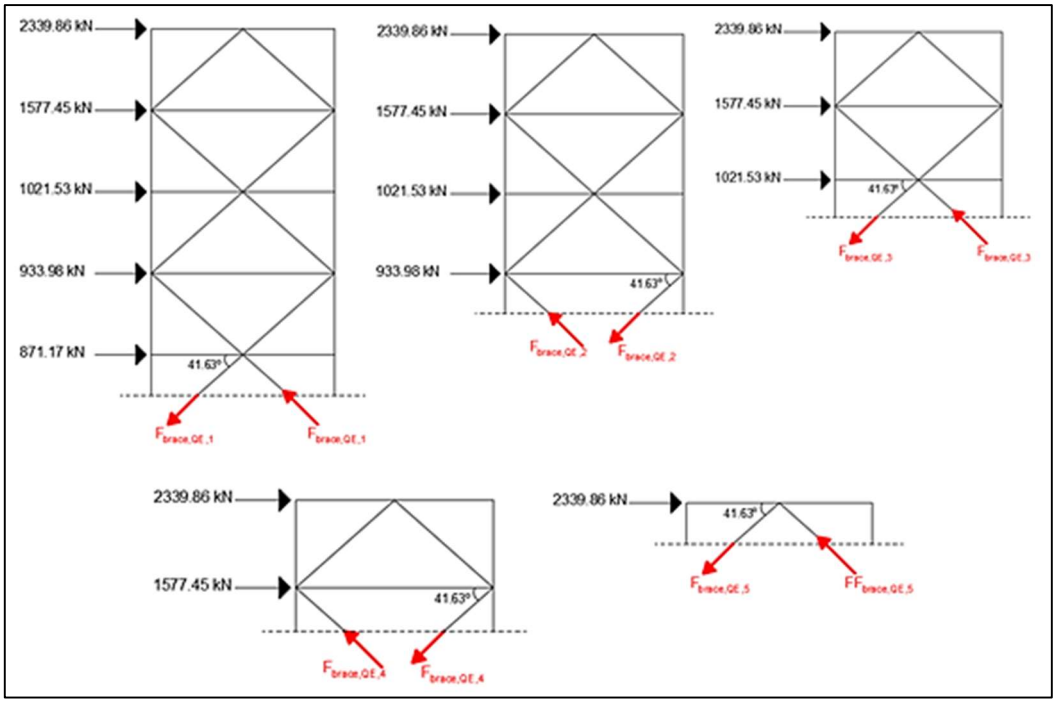


Figure C2.1: Forces caused by earthquake loads on the braces.

Table C2.1: Control of local buckling (width-to-thickness ratio) of brace sections.

Floors	Section of Braces	$b/2t_f$	$\lambda_{hd} = 0.55*\sqrt{(E/Fy)}$	$b/2t_f \leq \lambda_{hd}$
1st Floor	Tubo200x200x20	7.800	14.832	OK
2nd Floor	Tubo200x200x20	7.800	14.832	OK
3rd Floor	Tubo160x160x12.5	10.800	14.832	OK
4th Floor	Tubo160x160x12.5	10.800	14.832	OK
5th Floors	Tubo140x140x12.5	9.000	14.832	OK

Table C2.2: Control of slenderness ratio of brace sections.

Floor	Brace Section	Gross Section Area	i (mm)	$L_{b,c}$ (m)	Slenderness Ratio	Slenderness Limit	$4.71*\sqrt{(E/Fy)}$
		A_g (mm^2)			L_c/r (KL/r)	KL/r ≤ 200	
5th	Tubo140x140x12.5	6375	52.3	6.021	115.120	OK	127.02
4th	Tubo160x160x12.5	7375	60.4	6.021	99.682	OK	127.02
3rd	Tubo160x160x12.5	7375	60.4	6.021	99.682	OK	127.02
2nd	Tubo200x200x20	14400	73.9	6.021	81.472	OK	127.02
1st	Tubo200x200x20	14400	73.9	6.021	81.472	OK	127.02

Table C2.3: Characteristic axial compressive strength.

Floor	Brace Section	Dead Load	Live Load	Brace Dead Load	Brace Live Load	Cum. Earthquake Loads	Earthquake Loads	Axial Load
		P_{DL} (kN)	P_{LL} (kN)	$F_{b,DL}$ (kN)	$F_{b,LL}$ (kN)	Q_e (kN)	$F_{b,E}$ (kN)	P_r (kN)
5th	Tubo140x140x12.5	30.38	15.19	54.18	27.09	2339.86	1565.333	418.34
4th	Tubo160x160x12.5	44.55	20.25	39.73	18.06	3917.31	2620.625	674.51
3rd	Tubo160x160x12.5	44.55	20.25	39.73	18.06	4938.84	3304.011	845.35
2nd	Tubo200x200x20	44.55	20.25	39.73	18.06	5872.82	3928.833	1001.5
1st	Tubo200x200x20	44.55	20.25	39.73	18.06	6743.99	4511.633	1147.26

Table C2.4: Brace design for 5-Story SCBF.

Floor	Brace Section	Elastic Buckling Stress	Critical Stress	Compressive Strength	Design Compressive Strength	
		F_e	F_{cr}	P_n (kN)	P_c (kN)	$P_r \leq P_c$ (kN)
5th	Tubo140x140x12.5	148.945	126.975	809.467	728.520	OK
4th	Tubo160x160x12.5	198.653	154.063	1136.216	1022.594	OK
3rd	Tubo160x160x12.5	198.653	154.063	1136.216	1022.594	OK
2nd	Tubo200x200x20	297.379	186.740	2689.060	2420.154	OK
1st	Tubo200x200x20	297.379	186.740	2689.060	2420.154	OK

Appendix C3: Girder design

Table C3.1: Expected brace strength in analysis Case II.

Floor	Brace Section	A_g (mm^2)	$L_{b,c}$ (m)	i (mm)	0.80* (L_c/r)	$4.71*\sqrt{(E/R_yF_y)}$	T (kN)	F_e (MPa)	F_{cr} (Mpa)	C_{EPB} (kN)
5th	TUBO140x140x12.5	6375	6.02	52.3	92.096	107.351	2454.38	232.73	137.60	300.01
4th	TUBO160x160x12.5	7375	6.02	60.4	79.746	107.351	2839.38	310.40	163.63	412.72
3rd	TUBO160x160x12.5	7375	6.02	60.4	79.746	107.351	2839.38	310.40	163.63	412.72
2nd	TUBO200x200x20	14400	6.02	73.9	65.178	107.351	5544.00	464.66	194.41	957.43
1st	TUBO200x200x20	14400	6.02	73.9	65.178	107.351	5544.00	464.66	194.41	957.43

Table C3.2: Selection girder sections according to required W_{px} for Case II.

	Floor	Braced Section	$(1.2+0.2S_{DS})$ G + E + Q	$W_{px,\ min\ req}$ (mm^3)	Selected Beam	W_{px} (mm^3)	$W_{px>}$ $W_{px,min}$	i_x	i_y	A_g
Intersected Girders	5th	Tubo140x140x12.5	53.847	168536.46	IPE600	3512000	OK	243.0	46.6	15600
	3rd	Tubo160x160x12.5	70.471	220565.88	IPEO600	4471000	OK	245.2	47.9	19680
	1st	Tubo200x200x20	67.222	210397.50	IPO600	4471000	OK	245.2	47.9	19680
Not Intersected Girders	4th	Tubo160x160x12.5	373.595	1169311.42	IPEO600	4471000	OK	245.2	47.9	19680
	2nd	Tubo200x200x20	374.451	1171989.36	IPEO600	4471000	OK	245.2	47.9	19680

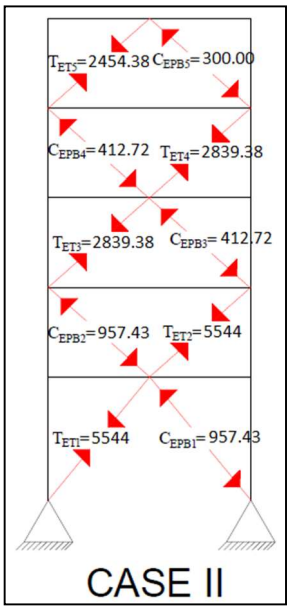
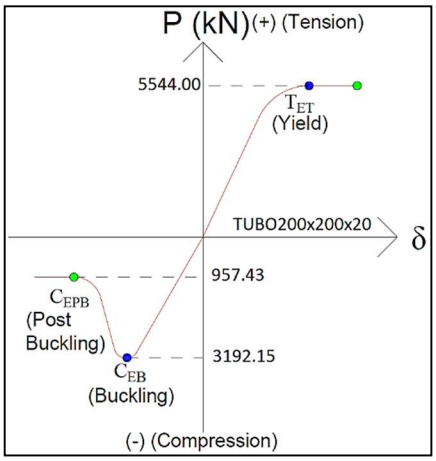
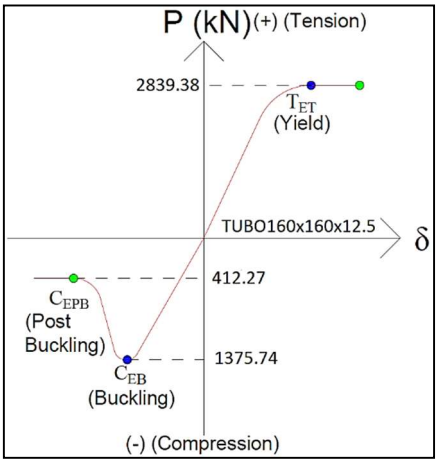


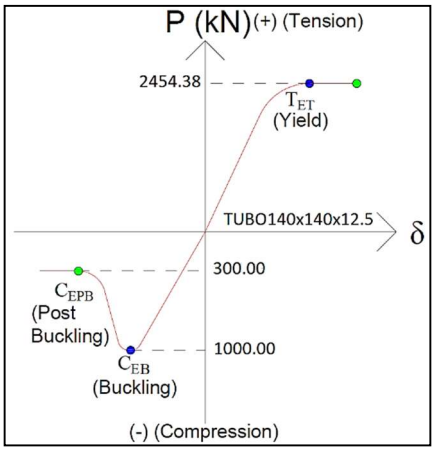
Figure C3.1: T_{ET}, C_{EPB} values for Case II.



(a) 1st and 2nd Floors



(b) 3rd and 4th Floors



(c) 5th Floor

Figure C3.2: Tension-compression graphs for floors.

Table C3.3: Control of maximum spacing in the girder sections for Case II.

	Floor	Selected Beam	$L_{b,max}$ (m)	$L_{b,x}$ (m)	$L_{b,y}$ (m)	$L_{b,y} < L_{b,max}$	L_p (m)	$L_b \leq L_p$	L_r (m)
Intersected Girders	**5th**	IPE600	2.26	9.00	2.25	OK	1.947	NOT OK	5.31
	3rd	IPEO600	2.32	9.00	2.25	OK	2.001	NOT OK	5.75
	1st	IPEO600	2.32	9.00	2.25	OK	2.001	NOT OK	5.75
Not Intersected Girders	**4th**	IPEO600	2.32	9.00	2.25	OK	2.001	NOT OK	5.75
	2nd	IPEO600	2.32	9.00	2.25	OK	2.001	NOT OK	5.75

Table C3.4: Control of moment strength in the girder sections for Case II.

	Floor	Selected Beam	M_p	C_b	W_{ex}	M_n	M_n (min (M_p;M_n))	$0.9*M_n$	$0.9M_n > M_u$
			(kNm)		(mm^3)	(kNm)	(kNm)	(kNm)	
Intersected Girders	**5th**	IPE 600	1246.70	1.11	307900	1265.04	1246.760	1122.08	OK
	3rd	IPEO600	1587.21	1.11	403600	1650.51	1587.205	1428.49	OK
	1st	IPEO600	1587.21	1.11	403600	1650.51	1587.205	1428.49	OK
Not Intersected Girders	**4th**	IPEO600	1587.21	1.11	403600	1650.51	1587.205	1428.49	OK
	2nd	IPEO600	1587.21	1.11	403600	1650.51	1587.205	1428.49	OK

Table C3.5: Control of member requirements for girders.

Selected Beam	$b/2t_f$	$0.3*\sqrt{(E/F_y)}$	$b/2t_f < 0.3\sqrt{(E/Fy)}$	$C_a \leq$ or > 0.125	$1.49\sqrt{(E/Fy)}$	Max Limit	h/tw	$h/t_w \leq$ Max Limit
IPE600	5.789	7.121	OK	58.152	35.366	58.152	42.8	OK
IPEO600	4.667	7.121	OK	58.152	35.366	58.152	34.3	OK

Appendix C4: Column design

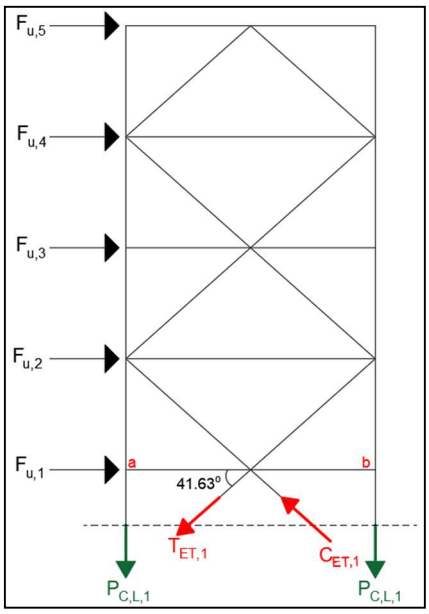


Figure C4.1: Tension and compression in 1st floor column according to Case I.

Table C4.1: Column forces for structural analysis Case I.

Floors	Brace Section	T (kN)	F_{cre} (N/mm^2)	C_{EB} (kN)	F_u (kN)	$P_{C,L,1}$ (kN)	$P_{C,R,1}$ (kN)	$P_{QE,1}$ (kN)
5th	Tubo140x140x12.5	2454.38	137.60	1000.24	2581.98	0.00	0.00	0.00
4th	Tubo160x160x12.5	2839.38	163.63	1376.04	568.62	661.46	1633.64	1633.64
3rd	Tubo160x160x12.5	2839.38	163.63	1376.04	0.00	2061.72	3033.90	3033.90
2nd	Tubo200x200x20	5544.00	194.41	3192.15	3378.79	3166.84	4729.32	4729.32
1st	Tubo200x200x20	5544.00	194.41	3192.15	0.00	6068.80	7631.27	7631.27

Table C4.2: Required axial strength for SCBF columns.

Floor	$P_{DL,COL}$ (kN)	$PL_{L,COL}$ (kN)	$P_{DL,BEAMS\_SPAN}$ (kN)	$PL_{L,BEAM\_SPAN}$ (kN)	P_G (kN)	P_Q (kN)	$P_{QE,1}$ (kN)	P_U (kN)
5th	75.94	37.97	30.38	15.19	121.5	60.75	0.00	242.24
4th	111.38	50.63	44.55	20.25	299.7	141.75	1633.64	2223.07
3rd	111.38	50.63	44.55	20.25	477.9	222.75	3033.90	3970.52
2nd	111.38	50.63	44.55	20.25	656.1	303.75	4729.32	6013.13
1st	111.38	50.63	44.55	20.25	834.3	384.75	7631.27	9262.27

Table C4.3: Axial strength capacity for SCBF columns.

Column Section	r (m)	A (m^2)	KL/r (m)	4.71√(E/Fy)	F_e (Kpa)	F_{cr} (Kpa)	$\phi_c * P_n$	$P_U < P_c$
HE450B	0.1914	0.0218	20.90	111.80	4519533.66	343518.69	6739.84	OK
HE450B	0.1914	0.0218	20.90	111.80	4519533.66	343518.69	6739.84	OK
HE450B	0.1914	0.0218	20.90	111.80	4519533.66	343518.69	6739.84	OK
HD4000×382	0.1049	0.04871	38.13	111.80	1357565.32	318196.11	13949.40	OK
HD4000×382	0.1049	0.04871	38.13	111.80	1357565.32	318196.11	13949.40	OK

Table C4.4: Limiting depth-to-thickness ratios for SCBF columns.

Floor	Column	h (mm)	t_w (mm)	h/t_w	P_u (kN)	C_a	Ca < 0.125	1.49√(E/Fy)	Max Limit	$h/t_w <$ Max Limit
1^{st}-2^{nd}	HD400X382	416	29.8	13.96	1728.70	0.111	52.15	35.37	52.15	OK
3^{rd}-5^{th}	HE450B	450	14	32.14	981.75	0.141	50.53	35.37	50.53	OK

Table C4.5: Limiting width-to-thickness ratios for SCBF columns.

Section of Columns	b (mm)	t_f (mm)	$b/2t_f$	$\lambda_{hd} = 0.30*\sqrt{(E/Fy)}$	$b/2t_f \leq \lambda_{hd}$
HD400X382	406	48	4.229	7.121	OK
HE450B	300	26	5.769	7.121	OK

Appendix C5: Story drift requirement

Table C5.1: Story drifts of 5-story building for (X) direction.

Floor	Load	DriftX	$R^{(X)}$	I	Story Height	$\lambda^{(X)}$	$\lambda\delta_i^{(X)}/h_i$	0.016 κ	Conclusion (X)
		$\Delta_i^{(X)}/h_i$			h_i (m)	$S_{ae}(T)_{DD-3}$ /$S_{ae}(T)_{DD-2}$			
5	SPECX	0.00113	5	1	4.0	0.357	0.0020	0.008	OK
4	SPECX	0.00143	5	1	4.0	0.357	0.0026	0.008	OK
3	SPECX	0.00147	5	1	4.0	0.357	0.0026	0.008	OK
2	SPECX	0.00103	5	1	4.0	0.357	0.0018	0.008	OK
1	SPECX	0.00086	5	1	4.0	0.357	0.0015	0.008	OK

Table C5.2: Final sections of 5-story building.

Floor	SMRFs_Columns		SMRFs_Beam	Gravity Frames_Column		GFs_Beam
	Exterior	Interior		Exterior (Braced B.)	Interior	
5	HD400×421	HD400×509	HE500A	H450B	HE220B	IPEO400
4	HD400×421	HD400×509	HE500A	HE450B	HE220B	IPEO450
3	HD400×421	HD400×509	HE500B	HE450B	HE220B	IPEO450
2	HD400×551	HD400×551	HE550B	HD400X382	HE340B	IPEO450
1	HD400×551	HD400×551	HE550B	HD400X382	HE340B	IPEO450

Appendix D: Design of 10-Story Building Special Moment Frames

Appendix D1: Calculation of seismic base shear

The total earthquake load value in the X direction obtained from the Etabs program according to the Modal Response Spectrum Method for the 10-story building is $V_{tx}^{(X)}$, 2007.115 kN. Calculations for $V_{tE}^{(X)}$ in order to control $V_{tx}^{(X)} < \gamma_E V_{tE}^{(X)}$ are given below.

$$T_{pA} = 0.08 * 41.4^{3/4} = 1.306\ s$$

$$Max\left(T_p^{(X)}\right) = 1.4 * 1.306 = 1.828\ s$$

As calculated in Section 3.1. T_A and T_B corner periods were obtained as 0.068 s and 0.340 s, respectively. Since the building period is accepted as the maximum period of 1.828 s; It satisfies the $(T_B \leq T \leq T_L)$ condition. In this case, the horizontal elastic design spectral accelerations $S_{ae}\ (T)$;

$$S_{ae}\ (T) = \frac{S_{D1}}{T} = \frac{0.4995}{1.828} = 0.273$$

Since $T = 1.828\ s > T_B = 0.340\ s$, $R_a\ (T) = \frac{8}{1} = 8$

$$S_{aR}\left(T_p^{(Y)}\right) = \frac{0.273}{8} = 0.0341$$

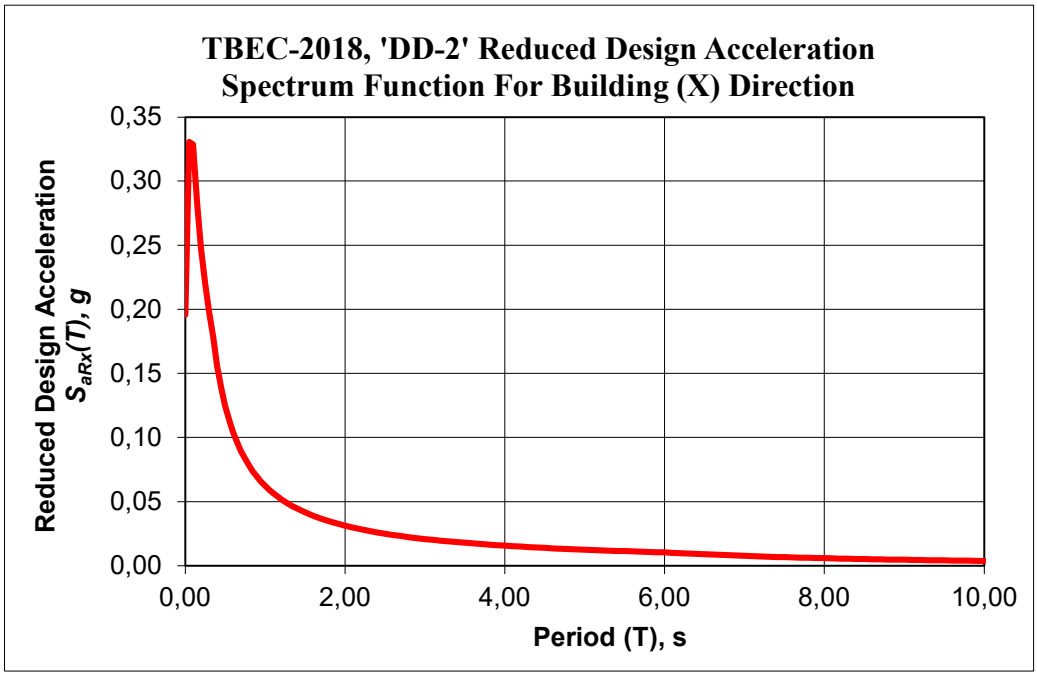


Figure D1.1: Reduced design acceleration spectrum for building (X) direction.

Table D1.1: Seismic effective weight.

Floor	Dead Load (kN/m^2)	Live Load (kN/m^2)	n	Area (m^2)	Seismic Effective Weight (kN)	ΣMaterial Weight (kN)	ΣStory Weight (kN)	m = W/g
Roof	3.0	1.5	0.3	1620	5589	1214.65	6803.65	693.54
9th	4.4	2.0	0.3	1620	8100	1372.22	9472.22	965.57
8th	4.4	2.0	0.3	1620	8100	1427.36	9527.36	971.19
7th	4.4	2.0	0.3	1620	8100	1475.490	9575.49	976.10
6th	4.4	2.0	0.3	1620	8100	1503.30	9603.31	978.93
5th	4.4	2.0	0.3	1620	8100	1579.34	9679.34	986.68
4th	4.4	2.0	0.3	1620	8100	1579.34	9679.34	986.68
3rd	4.4	2.0	0.3	1620	8100	1660.42	9760.42	994.95
2nd	4.4	2.0	0.3	1620	8100	1720.45	9820.45	1001.07
1st	4.4	2.0	0.3	1620	8100	2029.21	10129.21	1032.54
				TOTAL	**78489**	**15561.788**	**94050.79**	**9587.24**

If the total equivalent seismic load mentioned in Equation (3.4) above is calculated;

$$V_{tE}^{(X)} = 3212.474\ kN$$

As the total equivalent seismic load has been obtained;

$$\gamma_E\ V_{tE}^{(X)} = 0.80 * 3212.474 = 2569.979\ kN$$

Since $V_{tx}^{(X)} = 2007.1\ kN < \gamma_E\ V_{tE}^{(X)} = 2569.979\ kN$, the equivalent base shear force amplification coefficient has been included in the calculations.

$$\beta_{tE}^{(X)} = \frac{0.80 * 3212.474}{2007.1} = 1.28 \geq 1$$

As a result, in the calculations, all reduced internal forces and displacement values calculated with Spec X loading obtained by Modal Response Spectrum Method were multiplied by 1.28.

Appendix D2: Story drift requirement

Table D2.1: Sections of 10-story building.

Floor	SMRFs_Column		SMRFs_Beam	Gravity Frames_Column		GFs_Beam
	Exterior	Interior		Exterior (Braced B.)	Interior	
Roof	HD400 ×216	HD400×463	HE500A	HE200B	HE240C	IPEO400
9	HD400 ×314	HD400×463	HE500A	HE240B	HE240C	IPEO450
8	HD400 ×314	HD400×592	HE550A	HE240B	HE260C	IPEO450
7	HD400 ×463	HD400×592	HE550A	HD320×158	HE260C	IPEO450
6	HD400 ×463	HD400×592	HE550B	HD320×158	HE260C	IPEO450
5	HD400 ×509	HD400×677	HE550B	HD400×262	HD320 ×158	IPEO450
4	HD400 ×509	HD400×677	HE550B	HD400×262	HD320 ×158	IPEO450
3	HD400 ×634	HD400×677	HE650B	HD400×382	HD320 ×158	IPEO450
2	HD400 ×634	HD400×818	HE650B	HD400382	HD360 ×196	IPEO450
1	HD400 ×818	HD400×818	HE650B	HD400×592	HD360 ×196	IPEO450

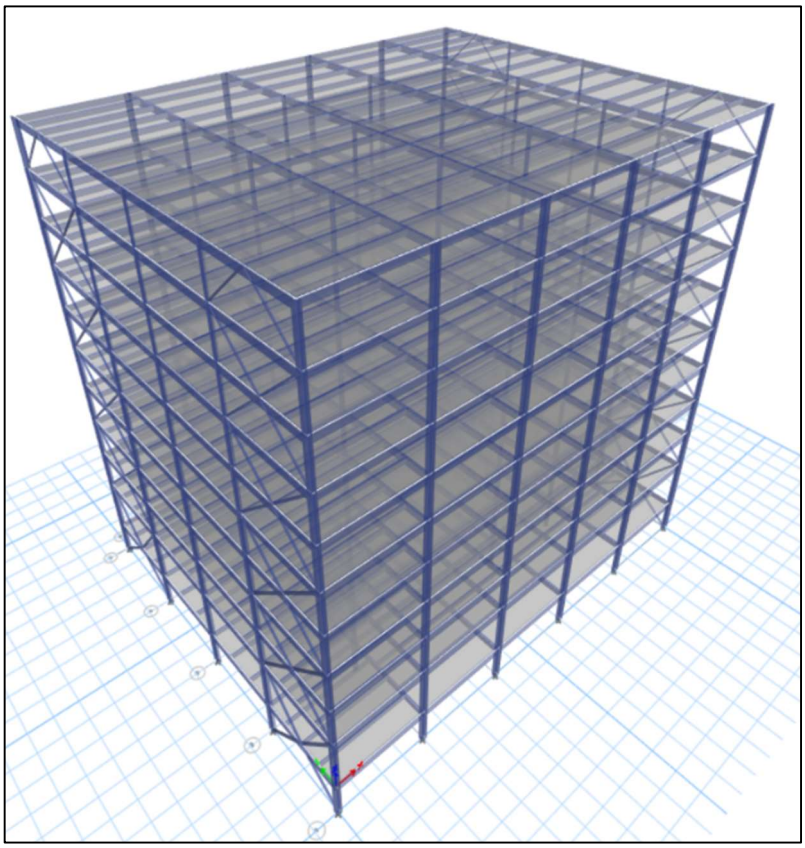


Figure D2.1: 3D model of 10-story building.

Table D2.2: Story drifts of 10-story building for (X) direction.

Floor	**Load**	**Drift_Y**	**$R^{(X)}$**	**I**	**Story Height**	**$\lambda^{(X)}$**	**$\lambda\delta_i^{(X)}/h_i$**	**0.016 κ**	**Conclusion (X)**
		$\Delta_i^{(X)}/h_i$	Table 3.4	Table 3.4	h_i (m)	$S_{ae}(T)_{DD-3}$ /$S_{ae}(T)_{DD-2}$			
10	SPECX	0.00150	8	1.0	4.0	0.357	0.0043	0.008	OK
9	SPECX	0.00183	8	1.0	4.0	0.357	0.0052	0.008	OK
8	SPECX	0.00212	8	1.0	4.0	0.357	0.0061	0.008	OK
7	SPECX	0.00220	8	1.0	4.0	0.357	0.0063	0.008	OK
6	SPECX	0.00236	8	1.0	4.0	0.357	0.0067	0.008	OK
5	SPECX	0.00237	8	1.0	4.0	0.357	0.0068	0.008	OK
4	SPECX	0.00230	8	1.0	4.0	0.357	0.0066	0.008	OK
3	SPECX	0.00211	8	1.0	4.0	0.357	0.0060	0.008	OK
2	SPECX	0.00207	8	1.0	4.0	0.357	0.0059	0.008	OK
1	SPECX	0.00182	8	1.0	5.4	0.357	0.0052	0.008	OK

As a result of the modal analysis made using sections that meet the story drift condition, the first fundamental vibration period of the structure was obtained as $T_1 = 2.678\ s$. Therefore, the assumption $T_1 < 1.4\ T_{pA} = 1.828\ s$ made at the beginning of the design was confirmed. There is no need to recalculate the earthquake loads since the numerically obtained fundamental period of the building exceeds the upper limit based on the design.

Appendix D3: Second order effects

Table D3.1: Second order effects.

Floor	h_i (m)	$\sum w_k$ (kN)	$V_i^{(X)}$ (kN)	$(\Delta_i^{(X)})_{ort}$ (m/h_i)	$\theta^{(X)}_{II,i}$	$\theta^{(X)}_{II,max}$	D	C_h	R	0.12*D / (C_h*R)	$\theta^{(X)}_{II,max} \leq$ 0.12*D / (C_h*R)	$\beta_{II}^{(X)}$
10	4.0	6803.65	662.96	0.00150	0.0154		3	1	8	0.045	NOT OK	1.075
9	4.0	16275.88	1049.70	0.00183	0.0283		3	1	8	0.045	NOT OK	1.075
8	4.0	25803.23	1321.34	0.00212	0.0413		3	1	8	0.045	NOT OK	1.075
7	4.0	35378.72	1538.95	0.00220	0.0506		3	1	8	0.045	NOT OK	1.075
6	4.0	44982.03	1730.55	0.00236	0.0613	0.07304	3	1	8	0.045	NOT OK	1.075
5	4.0	54661.37	1904.34	0.00237	0.0681		3	1	8	0.045	NOT OK	1.075
4	4.0	64340.71	2066.66	0.00230	0.0715		3	1	8	0.045	NOT OK	1.075
3	4.0	74101.13	2226.28	0.00211	0.0703		3	1	8	0.045	NOT OK	1.075
2	4.0	83921.58	2381.86	0.00207	0.0730		3	1	8	0.045	NOT OK	1.075
1	5.4	94050.79	2569.11	0.00182	0.0665		3	1	8	0.045	NOT OK	1.075

Appendix D4: Strong column-weak beam requirement

Table D4.1: Check of SC/WB for 10-story building.

Axis	Floor	Column Above	Gross Area	Plastic Modulüs	Depth	Top Column Factored Axial Load	Top Column Capacity
			A_g (m^2)	W_{pc} (m^3)	d_c(m)	$\beta_{II}^{(x)}$ x $P_{r,\ above}$ (kN)	$\Sigma M_{pc,above}$ (kNm)
Interior Columns	1st	HD 400X818	0.1043	0.01926	0.514	3784.589	6138.439
	2nd	HD 400×677	0.08634	0.01535	0.483	3340.057	4855.436
	3rd	HD 400×677	0.08634	0.01535	0.483	2908.856	4932.098
	4th	HD 400×677	0.08634	0.01535	0.483	2471.904	5009.781
	5th	HD 400×592	0.07549	0.01314	0.465	2035.762	4310.350
	6th	HD 400×592	0.07549	0.01314	0.465	1605.524	4385.238
	7th	HD 400×592	0.07549	0.01314	0.465	1175.235	4460.135
	8th	HD 400×463	0.05895	0.009878	0.435	739.863	3382.714
	9th	HD 400X463	0.05890	0.009878	0.435	319.094	3453.175
Exterior Columns	1st	HD 400X634	0.08080	0.014220	0.474	4298.873	4291.541
	2nd	HD 400×634	0.0808	0.00888	0.474	3881.449	4365.003
	3rd	HD 400×509	0.0649	0.01422	0.446	3129.651	3383.754
	4th	HD 400×509	0.0649	0.01103	0.446	2791.129	3441.287
	5th	HD 400×463	0.05895	0.01103	0.435	2073.708	3159.208
	6th	HD 400×463	0.05895	0.009878	0.435	1756.077	3212.432
	7th	HD 400×314	0.03992	0.009878	0.399	1034.410	2097.606
	8th	HD 400×314	0.03992	0.00888	0.399	787.786	2136.985
	9th	HD 400X216	0.02755	0.004262	0.375	143.378	1490.829

Table D4.2: Continued.

Axis	Floor	Column Below	Gross Area	Plastic Modülüs	Depth of Columns	Bottom Column Factored Axial Load	Bottom Column Capacity
			A_g (m^2)	W_{pc} (m^3)	d_c(m)	$\beta_{ll}^{(x)}$ x $P_{r,\ below}$ (kN)	$\Sigma M_{pc,\ below}$ (kNm)
Interior Columns	1st	HD 400X818	0.1043	0.01926	0.514	4251.456	6052.228
	2nd	HD 400×818	0.1043	0.01926	0.514	3784.589	6138.439
	3rd	HD 400×677	0.08634	0.01535	0.483	3340.057	4855.436
	4th	HD 400×677	0.08634	0.01535	0.483	2908.856	4932.098
	5th	HD 400×677	0.08634	0.01535	0.483	2471.904	5009.781
	6th	HD 400×592	0.07549	0.01314	0.465	2035.762	4310.350
	7th	HD 400×592	0.07549	0.01314	0.465	1605.524	4385.238
	8th	HD 400×592	0.07549	0.01314	0.465	1175.235	4460.135
	9th	HD 400X463	0.0589	0.00988	0.435	739.863	3382.609
Exterior Columns	1st	HD 400X818	0.1043	0.01926	0.514	5149.651	5886.367
	2nd	HD 400×634	0.0808	0.01422	0.474	4298.873	4291.541
	3rd	HD 400×634	0.0808	0.01422	0.474	3881.449	4365.003
	4th	HD 400×509	0.0649	0.01103	0.446	3129.651	3383.754
	5th	HD 400×509	0.0649	0.01103	0.446	2791.129	3441.287
	6th	HD 400×463	0.05895	0.00988	0.435	2073.708	3159.208
	7th	HD 400×463	0.05895	0.00988	0.435	1756.077	3212.432
	8th	HD 400×382	0.04871	0.00797	0.416	1034.410	2658.429
	9th	HD 400X382	0.04871	0.00797	0.416	787.786	2698.757

Table D4.3: Continued.

Axis	Floors	Total Column Capacity	Left Beam	Right Beam	Beam Capacity	Capacity Ratio	Conclusion
		ΣM^*_{pc} (kNm)			ΣM^*_{pb} (kNm)	$\Sigma M^*_{pc} / \Sigma M^*_{pb}$ (kNm)	$\Sigma M^*_{pc} / \Sigma M^*_{pb} > 1$
Interior Columns	1st	12190.667	HE 650 B	HE 650 B	9666.537	1.261	OK
	2nd	10993.875	HE 650 B	HE 650 B	9630.260	1.142	OK
	3rd	9787.534	HE 650 B	HE 650 B	9630.260	1.016	OK
	4th	9941.879	HE 550 B	HE 550 B	7360.148	1.351	OK
	5th	9320.131	HE 550 B	HE 550 B	7343.984	1.269	OK
	6th	8695.588	HE 550 B	HE 550 B	7343.984	1.184	OK
	7th	8845.373	HE 550 A	HE 550 A	6074.406	1.456	OK
	8th	7842.850	HE 550 A	HE 550 A	6052.051	1.296	OK
	9th	6835.784	HE 500 A	HE 500 A	5173.379	1.321	OK
Exterior Columns	1st	10177.908	HE 650 B	HE 650 B	4809.887	2.116	OK
	2nd	8656.544	HE 650 B	HE 650 B	4809.887	1.800	OK
	3rd	7748.757	HE 650 B	HE 650 B	4793.641	1.616	OK
	4th	6825.041	HE 550 B	HE 550 B	3663.495	1.863	OK
	5th	6600.495	HE 550 B	HE 550 B	3658.591	1.804	OK
	6th	6371.639	HE 550 B	HE 550 B	3658.591	1.742	OK
	7th	5310.038	HE 550 A	HE 550 A	3012.704	1.763	OK
	8th	4795.414	HE 550 A	HE 550 A	3012.704	1.592	OK
	9th	4189.587	HE 500 A	HE 500 A	2567.599	1.632	OK

Appendix D5: Stability analysis

Table D5.1: τ values for 10-story building.

	Floor	Section	A_g (mm^2)	F_y (N/mm^2)	$\beta_{II}^{(X)} x P_r$ (kN)	P_{ns} (kN)	$\beta_{II}^{(X)} x P_r / P_{ns}$	$\beta_{II}^{(X)} x P_r / P_{ns} \leq 0.5$	$\tau_b = 1$
Interior Column	10th	HD400x463	58950	355	307.63	20927.25	0.015	OK	OK
	9th	HD400×463	58950	355	722.51	20927.25	0.035	OK	OK
	8th	HD400×592	75490	355	1159.97	26798.95	0.043	OK	OK
	7th	HD400×592	75490	355	1586.50	26798.95	0.059	OK	OK
	6th	HD400×592	75490	355	2015.62	26798.95	0.075	OK	OK
	5th	HD400×677	86340	355	2449.98	30650.70	0.080	OK	OK
	4th	HD400×677	86340	355	2884.48	30650.70	0.094	OK	OK
	3rd	HD400×677	86340	355	3318.64	30650.70	0.108	OK	OK
	2nd	HD400x818	104300	355	3762.84	37026.50	0.102	OK	OK
	1st	HD400x818	104300	355	4226.73	37026.50	0.114	OK	OK
Exterior Column	10th	HD400×216	27550	355	103.73	9780.25	0.011	OK	OK
	9th	HD400×314	39920	355	690.78	14171.60	0.049	OK	OK
	8th	HD400×314	39920	355	847.30	14171.60	0.060	OK	OK
	7th	HD400×463	58950	355	1464.95	20927.25	0.070	OK	OK
	6th	HD400×463	58950	355	1653.20	20927.25	0.079	OK	OK
	5th	HD400×509	64900	355	2239.16	23039.50	0.097	OK	OK
	4th	HD400×509	64900	355	2436.15	23039.50	0.106	OK	OK
	3rd	HD400×634	80800	355	3005.84	28684.00	0.105	OK	OK
	2nd	HD400×634	80800	355	3235.35	28684.00	0.113	OK	OK
	1st	HD400×818	104300	355	3829.180	37026.50	0.103	OK	OK

Table D5.2: Ratio of second-order drifts to first-order drifts (Δ^{2nd} / Δ^{1st}).

Combination	**$\Delta_{max}^{2.order}$ (mm)**	**$\Delta_{max}^{1.order}$ (mm)**	**$\Delta_{max}^{2.order}$ / $\Delta_{max}^{1.order}$ (mm)**	**$\Delta_{max}^{2.order}$ / $\Delta_{max}^{1.order}$ ≤ 1.7**
1.4G ∓**1.4NG**	5.321	4.828	1.102	OK
1.2G + 1.6Q + 0.5Q_r ± **(1.2NG + 1.6NQ + 0.5NQ_r)**	7.205	6.396	1.126	OK
1.2G + 1.0Q + 1.6Q_r ± **(1.2NG + 1.0NQ + 1.6NQ_r)**	6.555	5.887	1.113	OK
(1.2 + 0.2S_{DS})G ± E + 0.5Q + 0.2S	79.874	75.172	1.063	OK
(0.9- 0.2S_{DS}) G ± E	79.529	75.026	1.060	OK

Appendix D6: Strength requirement

Table D6.1: Strength check for columns.

Axis	**Floors**	**Section of Column**	**$\beta_{II}^{(X)}$xP_r (kN)**	**ϕP_n (kN)**	**P_r / P_c**	**$\beta_{II}^{(X)}$x M_r (kNm)**	**W_{px} (cm^3)**	**ϕM_n (kNm)**	**P-M Ratio**	**P-M Ratio ≤ 1**
Interior Column	**1^{st}-2^{nd}**	HD400×818	4319.38	30374.38	0.142	707.11	19260	6153.57	0.186	OK
	3^{rd}-5^{th}	HD400×677	3374.38	25029.88	0.135	438.49	15350	4904.33	0.157	OK
	6^{th}-7^{th}-8^{th}	HD400×592	2029.20	21806.04	0.093	358.87	13140	4198.23	0.132	OK
	9^{th}-10^{th}	HD400×463	726.21	16940.46	0.043	197.01	9878	3156.02	0.084	OK
Exterior Column	**1^{st}**	HD400×818	3718.25	30374.38	0.122	26.82	19260	6153.57	0.066	OK
	2^{nd}-3^{th}	HD400×634	3171.45	23382.40	0.136	22.15	14220	4543.29	0.073	OK
	4^{th}-5^{th}	HD400×509	2395.78	18694.12	0.128	13.79	11030	3524.09	0.068	OK
	6^{th}-7^{th}	HD400×463	1620.70	16940.46	0.096	13.76	9878	3156.02	0.052	OK
	8^{th}-9^{th}	HD400×314	839.15	11393.16	0.074	12.88	6374	2036.49	0.043	OK
	10^{th}	HD400×216	113.27	7827.45	0.015	114.09	4262	1361.71	0.091	OK

Table D6.2: Strength check for columns under extreme axial loads.

Axis	Floors	Section of Column	$\beta_{II}^{(X)}xP_r$ (kN)	r (cm)	L/r (cm)	$4.71\sqrt{(E/Fy)}$	F_e (Mpa)	F_{cr} (Mpa)	ϕP_n (kN)	$P_r \leq \phi P$
Interior Column	1st-2nd	HD400×818	4446.91	11.4	35.09	111.80	1603.32	323.58	30374.38	OK
	3rd-5th	HD400×677	3469.05	11.13	35.94	111.80	1528.27	322.11	25029.88	OK
	6th-7th-8th	HD400×592	2072.73	10.93	36.60	111.80	1473.84	320.96	21806.04	OK
	9th-10th	HD400×463	731.61	10.66	37.52	111.80	1401.92	319.30	16940.46	OK
Exterior Column	1st	HD400×818	4809.79	11.4	35.09	111.80	1603.32	323.58	30374.38	OK
	2nd-3th	HD400×634	4091.86	11.03	36.26	111.80	1500.93	321.54	23382.40	OK
	4th-5th	HD400×509	3004.81	10.78	37.11	111.80	1433.66	320.05	18694.12	OK
	6th-7th	HD400×463	1992.27	10.66	37.52	111.80	1401.92	319.30	16940.46	OK
	8th-9th	HD400×314	1013.45	10.33	38.72	111.80	1316.47	317.11	11393.16	OK
	10th	HD400×216	156.59	10.13	39.49	111.80	1265.99	315.69	7827.45	OK

Table D6.3: Spacing of lateral bracing.

Section of Beam	i_y (m)	$L_{b,\,max}$ (m)	Choosen L_b (L/3)	L_p (m)	$L_b < L_p$
HE 500 A	0.0724	3.51	3.0	3.020	OK
HE 550 A	0.0715	3.46	3.0	2.990	NOT OK
HE 550 B	0.0717	3.47	3.0	2.995	NOT OK
HE 650 B	0.0699	3.39	3.0	2.920	NOT OK

Table D6.4: Moment strength checks for girders.

Floors	Section of Beam	$\beta_{II}^{(X)}xM_r$ (kNm)	W_{px} mm^3	Design Flexural Strength $\phi_f M_n$ (kNm)	$M_r \leq \phi_f M_n$	Ratio of $M_r / \phi_f M_n$ (%)
1st-2nd-3rd	HE650B	599.74	6480000	2070.360	OK	28.97
4rd-5th-6th	HE550B	494.67	4971000	1588.235	OK	31.15
7th-8th	HE550A	344.98	4146000	1324.647	OK	26.04
9th-10th	HE500A	247.68	3530000	1127.835	OK	21.96

Table D6.5: Shear strength checks for girders.

Floors	Section of Beam	$\beta_{II}^{(X)}xV_r$ (kN)	Web Thickness (mm)	Height (mm)	Design Shear Strength $\phi_v V_n$ (kN)	$V_r \leq \phi_v V_n$
1st-2nd-3rd	HE650B	190.830	16.0	650	2215.200	OK
4rd-5th-6th	HE550B	162.594	15.0	550	1757.250	OK
7th-8th	HE550A	124.490	12.5	540	1437.750	OK
9th-10th	HE500A	101.083	12.0	490	1252.440	OK

Table D6.6: Axial strength of gravity columns under gravity loads ($1.2G + 1.6Q_r$).

Floors	Section	$\beta_{II}^{(X)}xP_u$ (kN)	r (cm)	A (cm^2)	(KL/r) cm	$4.71\sqrt{(E/F_y)}$	F_e (Mpa)	ϕP_n (kN)	$\beta_{II}^{(X)}xP_u \leq \phi P_n$
1st - 2nd	HD360x196	5337.90	9.56	250.3	56.49	111.795	618.67	6289.66	OK
3th-4th-5th	HD320×158	4272.55	7.67	201.2	52.15	111.795	725.77	5238.26	OK
6th-7th-8th	HE260C	2687.39	6.75	168.4	59.26	111.795	562.11	4130.60	OK
9th-10th	HE240C	1105.98	6.24	152.2	64.10	111.795	480.37	3569.05	OK

Pinned girders parallel to moment frame beams;

Table D6.7: Moment strength for GF girders parallel to SMF beams ($1.2G + 1.6Q_r$).

Floors	$\beta_{II}^{(X)}xM_u$ (kNm)	$W_{px,req}$ (cm^3)	Selected Section	$W_{px,sel}$ (cm^3)	$\emptyset_b M_n$ (kNm)	$\beta_{II}^{(X)}xM_u$ (kNm) $<\emptyset_b M_n$ (kNm)
10th	209.881	591.214	IPEO400	2691.00	859.7745	OK
9th-1st	188.543	531.106	IPEO450	3410.00	1089.495	OK

Table D6.8: Shear strength for GF girders parallel to SMF beams ($1.2G + 1.6Q_r$).

Floors	Selected Section	$\beta_{II}^{(X)}xV_u$ (kN)	$\emptyset_v V_n$ (kN)	$\beta_{II}^{(X)}xV_u$ (kN) $<\emptyset_v V_n$ (kN)
10th	IPE O 400	93.280	681.191	OK
9th-1st	IPE O 450	165.933	837.346	OK

Table D6.9: Deflection for GF girders parallel to SMF beams (G+Q).

Floors	Selected Section	$\beta_{II}^{(X)}x\delta$ (cm)	δ_{lmt} (cm)	$\beta_{II}^{(X)}x\delta$ (cm) $<\delta_{lmt}$ (cm)
10th	IPE O 400	2.399	2.5	OK
9th-1st	IPE O 450	2.287	2.5	OK

Pinned girders perpendicular to moment frame beams

Table D6.10: Moment strength for GF girders perpendicular to SMF beams (1.2G + 1.6Q_r).

	Floors	$\beta_{II}^{(X)}xM_u$ (kNm)	$W_{px,\ req}$ (cm^3)	Selected Section	$W_{px,\ sel}$ (cm^3)	ϕM_n (kNm)	$\beta_{II}^{(X)}xM_u$ $<\phi M_n$
Interior Girder	**10th**	551.76	1554.26	IPEO550	4805.00	1535.20	OK
	9th-1st	528.93	1489.94	IPEO600	6401.00	2045.12	OK

Table D6.11: Shear strength for GF girders perpendicular to SMF beams (1.2G + 1.6Q_r).

	Floors	Selected Section	$\beta_{II}^{(X)}xV_u$ (kN)	$\emptyset_v V_n$ (Kn)	$\beta_{II}^{(X)}xV_u$ (kN) $< \emptyset_v V_n$
Interior Girders	**10th**	IPEO550	193.341	1173.119	OK
	9th-1st	IPEO600	190.273	1795.590	OK

Table D6.12: Deflection for GF girders perpendicular to SMF beams (G+Q).

	Floors	Selected Section	δ (cm)	δ_{lmt} (cm)	δ (cm) $<\delta_{lmt}$ (cm)
Interior Girders	**5th**	IPE O 550	2.104	2.5	OK
	4th-1st	IPE O 600	1.979	2.5	OK

Appendix D7: Member requirement

Table D7.1: Limiting width-to-thickness ratios for SMF girders.

Floors	Section of Beam	b (mm)	t_f (mm)	$b/2t_f$	$\lambda_{hd} = 0.30*\sqrt{(E/Fy)}$	$b/2t_f \leq \lambda_{hd}$
1st-2nd-3rd	HE 650 B	300	31	4.839	7.121	OK
4rd-5th-6th	HE 550 B	300	29	5.172	7.121	OK
7th-8th	HE 550A	300	24	6.250	7.121	OK
9th-10th	HE 500A	300	23	6.522	7.121	OK

Table D7.2: Limiting depth-to-thickness ratios for SMF girders.

Floors	Section of Beam	h (mm)	t_w (mm)	h/t_w	A_g (mm^2)	$C_a <$ 0.125	$1.49\sqrt{(E/Fy)}$	Max Limit	$h/t_w <$ Max Limit
1st-2nd-3rd	HE650B	650	16	40.63	28630	58.15	35.37	58.15	OK
4rd-5th-6th	HE550B	550	15	36.67	25410	58.152	35.37	58.15	OK
7th-8th	HE550A	540	24	22.50	21180	58.1	35.37	58.15	OK
9th-10th	HE500A	490	23	21.30	19750	58.15	35.37	58.15	OK

Table D7.3: Limiting width-to-thickness ratios for SMF columns.

Section of Column	b (mm)	t_f (mm)	$b/2t_f$	$\lambda_{hd} = 0.30*\sqrt{(E/Fy)}$	$b/2t_f \leq \lambda_{hd}$
HD 400×818	437	97	2.253	7.121	OK
HD 400×677	428	81.5	2.626	7.121	OK
HD 400×634	424	77.1	2.750	7.121	OK
HD 400×592	421	72.3	2.911	7.121	OK
HD 400×509	416	62.7	3.317	7.121	OK
HD 400×463	412	57.4	3.589	7.121	OK
HD 400×314	401	39.6	5.063	7.121	OK
HD 400×216	394	27.7	7.112	7.121	OK

Table D7.4: Limiting depth-to-thickness ratios for SMF columns.

	Floors	Section of Column	h (mm)	t_w (mm)	h/t_w	$\beta_{II}^{(X)} x P_u$ (kN)	C_a	$C_a <$ 0.125	$1.49\sqrt{(E/Fy)}$	Max Limit	h/t_w <Max Limit
Interior Column	1^{st}-2^{nd}	HD400×818	14	60.5	8.50	4226.73	0.13	51.29	35.37	51.30	OK
	3^{rd}-5^{th}	HD400×677	483	51.2	9.43	3318.64	0.12	51.65	35.37	51.65	OK
	6^{th}-7^{th}-8^{th}	HD400×592	465	45	10.33	2015.62	0.08	53.63	35.37	53.63	OK
	9^{th}-10^{th}	HD400×463	435	35.8	12.15	731.19	0.04	56.05	35.37	56.05	OK
Exterior Column	1^{st}	HD400×818	514	60.5	8.50	3829.18	0.12	51.94	35.37	51.94	OK
	2^{nd}-3^{th}	HD400×634	474	47.6	9.96	3235.35	0.13	51.37	35.37	51.37	OK
	4^{th}-5^{th}	HD400×509	446	39.1	11.41	2436.15	0.12	51.80	35.37	51.80	OK
	6^{th}-7^{th}	HD400×463	435	35.8	12.15	1653.20	0.09	53.41	35.37	53.41	OK
	8^{th}-9^{th}	HD400×314	399	24.9	16.02	847.30	0.07	54.56	35.37	54.56	OK
	10^{th}	HD400×216	375	17.3	21.68	103.73	0.01	57.52	35.37	57.52	OK

Appendix E: Design of 10-Story Building Special Concentrically Braced Frames

Appendix E1: Calculation of seismic base shear

The total earthquake load value in the Y direction obtained from the Etabs program according to the Modal Response Spectrum Method for the 10-story building is $V_{ty}^{(Y)}$, 5787.3 kN. Calculations for $V_{tE}^{(Y)}$ in order to control $V_{ty}^{(Y)} < \gamma_E V_{tE}^{(Y)}$ are given below.

$T_{pA} = 0.08 * 41.4^{3/4} = 1.306\ s$

$T_A = 0.068$ s and $T_B = 0.340\ s$

$(T_B \leq T \leq T_L) \rightarrow S_{ae}(T) = \frac{S_{D1}}{T} = \frac{0.4995}{1.306} = 0.383$

Since $T = 1.306\ s > T_B = 0.340\ s$, $R_a(T) = \frac{5}{1} = 5$

$S_{aR}\left(T_p^{(Y)}\right) = \frac{0.383}{5} = 0.0765$

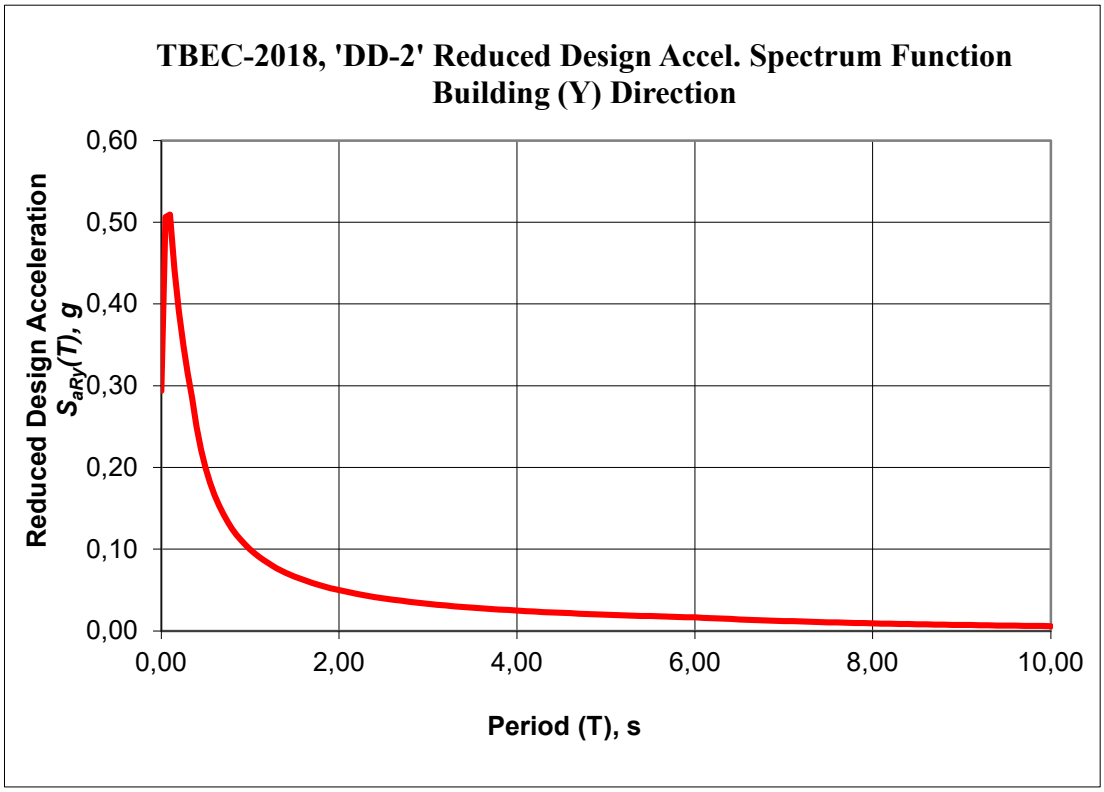


Figure E1.1: Reduced design acceleration spectrum for building (Y) direction.

If the total equivalent seismic load mentioned in Equation (3.4) above is calculated;

$$V_{tE}^{(Y)} = 7195.94\ kN$$

As the total equivalent seismic load has been obtained;

$$\gamma_E\ V_{tE}^{(X)} = 0.80 * 7195.94\ = 5756.754\ kN$$

Since $V_{ty}^{(Y)} = 5787.295\ kN < \gamma_E\ V_{tE}^{(Y)} = 5756.754\ kN$, the equivalent base shear amplification coefficient was not included in the calculations.

Appendix E2: Brace design

Table E2.1: Control of local buckling (width-to-thickness ratio) of brace sections.

Floors	Section of Brace	$b/2t_f$	$\lambda_{hd} = 0.55*\sqrt{(E/F_y)}$	$b/2t_f \leq \lambda_{hd}$
Base- 1st	Tubo200x200x20	7.80	14.832	OK
2nd-3th	Tubo180x180x20	6.70	14.832	OK
4th-5th	Tubo180x180x14.2	10.60	14.832	OK
6th-7th	Tubo160x160x12.5	10.80	14.832	OK
8th-9th	Tubo140x140x10	12.00	14.832	OK
10th	Tubo120x120x8	13.00	14.832	OK

Table E2.2: Control of slenderness ratio of brace sections.

Floor	Brace Section	A_g (mm^2)	i (mm)	$L_{b,c}$ (m)	L_c/r (KL/r)	KL/r ≤ 200	$4.71*\sqrt{(E/F_y)}$
10th	Tubo120x120x8	3580	45.8	6.02	131.46	OK	127.02
9th	Tubo140x140x10	5200	53.2	6.02	113.17	OK	127.02
8th	Tubo140x140x10	5200	53.2	6.02	113.17	OK	127.02
7th	Tubo160x160x125	7375	60.4	6.02	99.68	OK	127.02
6th	Tubo160x160x125	7375	60.4	6.02	99.68	OK	127.02
5th	Tubo180x180x14.2	9417	67.9	6.02	88.672	OK	127.02
4th	Tubo180x180x14.2	9417	67.9	6.02	88.6	OK	127.02
3rd	Tubo180x180x20	12800	65.8	6.02	91.50	OK	127.02
2nd	Tubo180x180x20	12800	65.8	6.02	91.50	OK	127.02
1st	Tubo200x200x20	14400	73.9	6.02	81.47	OK	127.02
Base	Tubo200x200x20	14400	73.9	7.03	95.12	OK	127.02

Table E2.3: Characteristic axial compressive strength.

Floors	Brace Section	Dead Load	Live Load	Brace Dead Load	Brace Live Load	Cum. Earthquake Loads	Earthquake Loads	Axial Load
		P_{DL} (kN)	P_{LL} (kN)	$F_{b,DL}$ (kN)	$F_{b,LL}$ (kN)	Q_e (kN)	$F_{b,E}$ (kN)	P_r (kN)
10th	Tubo120x120x8	30.38	15.19	54.18	27.09	1537.48	1028.55	284.14
9th	Tubo140x140x10	44.55	20.25	39.73	18.06	2488.62	1664.85	435.57
8th	Tubo140x140x10	44.55	20.25	39.73	18.06	2940.67	1967.27	511.17
7th	Tubo160x160x12.5	44.55	20.25	39.73	18.06	3200.47	2141.07	554.62
6th	Tubo160x160x12.5	44.55	20.25	39.73	18.06	3485.53	2331.77	602.29
5th	Tubo180x180x14.2	44.55	20.25	39.731	18.06	3801.25	2542.98	655.10
4th	Tubo180x180x14.2	44.55	20.25	39.7	18.06	4210.39	2816.69	723.52
3rd	Tubo180x180x20	44.55	20.25	39.73	18.06	4693.22	3139.70	804.28
2nd	Tubo180x180x20	44.55	20.25	39.73	18.06	5258.64	3517.95	898.84
1st	Tubo200x200x20	44.55	20.25	39.73	18.06	5787.30	3871.62	987.26
Base	Tubo200x200x20	44.55	20.25	34.36	15.62	898.85	702.03	192.24

Table E2.4: Brace design for 5-Story SCBF.

Floor	Brace Section	F_e (N/mm^2)	F_{cr} (N/mm^2)	P_n (kN)	P_c (kN)	$P_r \leq P_c$ (kN)
10th	Tubo120x120x8	114.22	311.34	1114.58	1003.12	OK
9th	Tubo140x140x10	154.12	135.37	703.91	633.52	OK
8th	Tubo140x140x10	154.12	135.37	703.91	633.52	OK
7th	Tubo160x160x12.5	198.65	168.03	1239.24	1115.31	OK
6th	Tubo160x160x12.5	198.65	168.03	1239.24	1115.31	OK
5th	Tubo180x180x14.2	251.05	196.42	1849.70	1664.73	OK
4th	Tubo180x180x14.2	251.05	196.42	1849.70	1664.73	OK
3rd	Tubo180x180x20	235.76	189.03	2419.53	2177.58	OK
2nd	Tubo180x180x20	235.76	189.03	2419.53	2177.58	OK
1st	Tubo200x200x20	297.38	215.39	3101.67	2791.50	OK
Base	Tubo200x200x20	218.17	179.66	2587.14	2328.42	OK

Appendix E3: Girder design

Table E3.1: Expected brace strength in analysis Case II.

Floor	Brace Section	A_g (mm^2)	$L_{b,c}$ (m)	i (mm)	0.80* (L_c/r)	4.71*√(E/$R_y F_y$)	T (kN)	F_e (MPa)	F_{cr} (Mpa)	C_{EPB} (kN)
10th	Tubo120x120x8	3580	6.02	45.8	105.17	107.351	1378.30	178.47	156.08	191.14
9th	Tubo140x140x10	5200	6.02	53.2	90.54	107.351	2002.00	240.81	197.17	350.72
8th	Tubo140x140x10	5200	6.02	53.2	90.54	107.351	2002.00	240.81	197.17	350.72
7th	Tubo160x160x12.5	7375	6.02	60.4	79.75	107.351	2839.38	310.40	229.09	577.94
6th	Tubo160x160x12.5	7375	6.02	60.4	79.75	107.351	2839.38	310.40	229.09	577.94
5th	Tubo180x180x14.2	9417	6.02	67.9	70.94	107.351	3625.55	392.27	255.30	822.41
4th	Tubo180x180x14.2	9417	6.02	67.9	70.94	107.351	3625.55	392.27	255.30	822.41
3rd	Tubo180x180x20	12800	6.02	65.8	73.20	107.351	4928.00	368.38	248.59	1088.47
2nd	Tubo180x180x20	12800	6.02	65.8	73.20	107.351	4928.00	368.38	248.59	1088.47
1st	Tubo200x200x20	14400	6.02	73.9	65.18	107.351	5544.00	464.66	272.17	1340.70
Base	Tubo200x200x20	14400	7.03	73.9	76.09	107.351	5544.00	340.90	239.98	1182.10

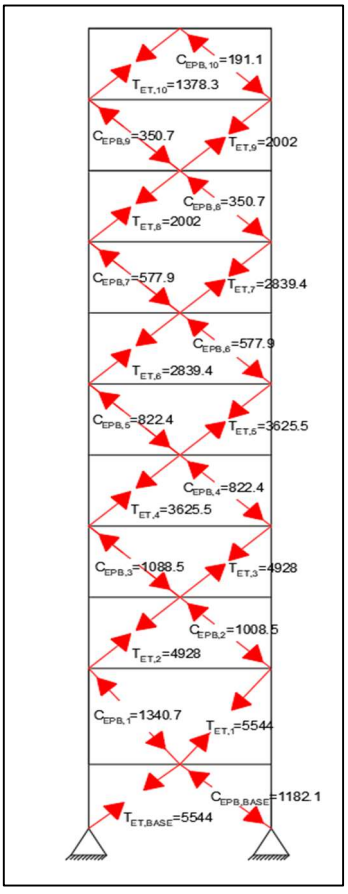


Figure E3.1: T_{ET}, C_{EPB} values for Case II.

Table E3.2: Selection girder sections according to required W_{px} for Case II.

	Floor	Braced Section	$(1.2+0.2S_{DS})$ G + E + Q	$W_{px,\ min\ req}$ (mm^3)	Selected Beam	W_{px} (mm^3)	$W_{px>}$ $W_{px,\ min}$	i_x (mm)	i_y (mm)	Am^2)
Intersected Girders	10th	Tubo120x120x8	60.81	190315.18	IPE600	3512000	OK	243	46.6	15600
	8th	Tubo140x140x10	70.69	221244.13	IPE600	3512000	OK	243	46.6	15600
	6th	Tubo160x160x12.5	69.03	216059.78	IPE600	3512000	OK	243	46.6	15600
	4th	Tubo180x180x14.2	67.48	211209.39	IPE600	3512000	OK	243	46.6	15600
	2rd	Tubo180x180x20	66.14	207001.57	IPE600	3512000	OK	243	46.6	15600
	Base	Tubo200x200x20	68.86	215521.75	IP 600	3512000	OK	243	46.6	15600
Not Intersected Girders	9th	Tubo140x140x10	376.54	1178519.88	IPE600	3512000	OK	243	46.6	15600
	7th	Tubo160x160x12.5	373.18	1168008.76	IPE600	3512000	OK	243	46.6	15600
	5th	Tubo180x180x14.2	371.14	1161629.101	IPE600	3512000	OK	243	46.6	15600
	3th	Tubo180x180x20	369.90	1157743.6	IPE600	3512000	OK	243	46.6	15600
	1st	Tubo200x200x20	367.82	1151221.91	IPE600	3512000	OK	243	46.6	15600

Table E3.3: Control of maximum spacing in the girder sections for Case II.

	Floor	Selected Beam	$L_{b,\ max}$ (m)	$L_{b,\ x}$ (m)	$L_{b,\ y}$ (m)	$L_{b,\ y}$ $<L_{b,max}$	L_p (m)	$L_b \leq L_p$	L_r (m)
Intersected Girders	10th	IPE 600	2.26	9.00	2.25	OK	1.947	NOT OK	7.65
	8th	IPE 600	2.26	9.00	2.25	OK	1.947	NOT OK	7.65
	6th	IPE 600	2.26	9.00	2.25	OK	1.947	NOT OK	7.65
	4th	IPE 600	2.26	9.00	2.25	OK	1.947	NOT OK	7.65
	2rd	IPE 600	2.26	9.00	2.25	OK	1.947	NOT OK	7.65
	Base	IPE 600	2.26	9.00	2.25	OK	1.947	NOT OK	7.65
Not Intersected Girders	9th	IPE 600	2.26	9.00	2.25	OK	1.947	NOT OK	7.65
	7th	IPE 600	2.26	9.00	2.25	OK	1.947	NOT OK	7.65
	5th	IPE 600	2.26	9.00	2.25	OK	1.947	NOT OK	7.65
	3th	IPE 600	2.26	9.00	2.25	OK	1.947	NOT OK	7.65
	1st	IPE 600	2.26	9.00	2.25	OK	1.947	NOT OK	7.65

Table E3.4: Control of moment strength in the girder sections for Case II.

	Floor	Selected Beam	M_p (kNm)	C_b	W_{ex} (mm^3)	M_n (kNm)	M_n (min (M_p; Mn))	$0.9*M_n$	$0.9M_n > M_u$
Intersected Girders	10th	IPE600	1246.76	1.11	3069	1310.34	1246.76	1122.08	OK
	8th	IPE600	1246.76	1.11	3069	1310.34	1246.76	1122.08	OK
	6th	IPE600	1246.76	1.11	3069	1310.34	1246.76	1122.08	OK
	4th	IPE600	1246.76	1.11	3069	1310.34	1246.76	1122.08	OK
	2rd	IPE600	1246.76	1.11	3069	1310.34	1246.76	1122.08	OK
	Base	IPE600	1246.76	1.11	3069	1310.34	1246.76	1122.08	OK
Not Intersected Girders	9th	IPE600	1246.76	1.11	3069	1310.34	1246.76	1122.08	OK
	7th	IPE600	1246.76	1.11	3069	1310.34	1246.76	1122.08	OK
	5th	IPE600	1246.76	1.11	3069	1310.34	1246.76	1122.08	OK
	3th	IPE600	1246.76	1.11	3069	1310.34	1246.76	1122.08	OK
	1st	IPE600	1246.76	1.11	3069	1310.34	1246.76	1122.08	OK

Table E3.5: Control of member requirements for girders.

Selected Beam	$b/2t_f$	$0.3\sqrt{(E/F_y)}$	$b/2t_f < 0.3\sqrt{(E/Fy)}$	$C_a \leq$ or> 0.125	$1.49\sqrt{(E/F_y)}$	Max Limit	h/tw	$h/t_w \leq$ Max Limit
IPE 600	5.79	7.121	OK	58.15	35.37	58.15	42.8	OK

Appendix E4: Column design

Table E4.1: Column forces for structural analysis Case I.

STORY	Brace Section	T_{ET} (kN)	F_{cre} (N/mm^2)	C_{EB} (kN)	F_u (kN)	$P_{C,L,1}$ (kN)	$P_{C,R,1}$ (kN)	$P_{QE,1}$ (kN)
10th	Tubo120x120x8	1378.30	156.08	637.12	1506.33	0.00	0.00	0.00
9th	Tubo140x140x10	2002.00	197.17	1169.08	863.74	627.12	1180.48	1180.48
8th	Tubo140x140x10	2002.00	197.17	1169.08	0.00	1145.36	1698.72	1698.72
7th	Tubo160x160x12.5	2839.38	229.09	1926.46	1191.92	2841.62	3448.13	3448.13
6th	Tubo160x160x12.5	2839.38	229.09	1926.46	0.00	3940.66	4547.17	4547.17
5th	Tubo180x180x14.2	3625.55	255.30	2741.37	1196.65	6202.79	6790.20	6790.20
4th	Tubo180x180x14.2	3625.55	255.30	2741.37	0.00	8503.88	9091.29	9091.29
3rd	Tubo180x180x20	4928.00	248.59	3628.23	1636.30	10480.77	11344.29	11344.29
2nd	Tubo180x180x20	4928.00	248.59	3628.23	0.00	13577.50	14441.01	14441.01
1st	Tubo200x200x20	5544.00	272.17	4469.00	1088.79	16438.53	17264.36	17264.36
Base	Tubo200x200x20	5544.00	239.98	3940.33	395.13	20090.52	21322.49	21322.49

Table E4.2: Required axial strength for SCBF columns.

STORY	$P_{DL,COL}$ (kN)	$PL_{L,COL}$ (kN)	$P_{DL,BEAMS\_SPAN}$ (kN)	$PL_{L,BEAM\_SPAN}$ (kN)	P_G (kN)	P_Q (kN)	$P_{QE,1}$ (kN)	P_U (kN)
10th	75.94	37.9688	30.375	15.188	121.5	60.75	0.000	242.24
9th	111.38	50.625	44.55	20.25	178.2	81.00	1180.477	1527.66
8th	111.38	50.625	44.55	20.25	178.2	81.00	1698.718	2045.91
7th	111.38	50.625	44.55	20.25	178.2	81.00	3448.131	3795.32
6th	111.38	50.625	44.55	20.25	178.2	81.00	4547.165	4894.35
5th	111.38	50.625	44.55	20.25	178.2	81.00	6790.201	7137.39
4th	111.38	50.625	44.55	20.25	178.2	81.00	9091.292	9438.48
3rd	111.38	50.625	44.55	20.25	178.2	81.00	11344.288	11691.48
2nd	111.38	50.625	44.55	20.25	178.2	81.00	14441.013	14788.20
1st	111.38	50.63	44.55	20.25	178.2	81.00	17264.362	17611.55

Table E4.3: Axial strength capacity for SCBF columns.

Floors	Column Section	r (m)	A (m^2)	KL/r (m)	$4.71\sqrt{(E/Fy)}$	F_e (Kpa)	F_{cr} (Kpa)	$\phi_c * P_n$	$P_U < P_c$
10th	HE200B	0.0507	0.00781	78.895	111.795	317121.49	222199.09	1561.44	OK
9th	HE240B	0.0608	0.0106	65.789	111.795	456054.68	256290.55	2445.01	OK
8th	HE240B	0.0608	0.0106	65.789	111.795	456054.68	256290.55	2445.01	OK
7th	HD320×158	0.0767	0.02012	52.151	111.795	725772.46	289278.70	5238.26	OK
6th	HD320×158	0.0767	0.02012	52.151	111.795	725772.46	289278.70	5238.26	OK
5th	HD400×262	0.1023	0.03346	39.101	111.795	1291103.40	316408.39	9528.32	OK
4th	HD400×262	0.1023	0.03346	39.101	111.795	1291103.40	316408.39	9528.32	OK
3rd	HD400×382	0.1049	0.04871	38.132	111.795	1357565.32	318196.11	13949.40	OK
2nd	HD400×382	0.1049	0.04871	13.346	111.795	11082165.87	350272.06	15355.58	OK
1st	HD400×592	0.1093	0.07549	32.937	111.795	1819554.48	327162.66	22227.76	OK

Table E4.4: Limiting depth-to-thickness ratios for SCBF columns.

Floors	Column	h (mm)	t_w (mm)	h/t_w	P_u (kN)	A_g (mm^2)	C_a	Ca < 0.125	$1.49\sqrt{(E/F_y)}$	Max Limit	$h/t_w <$ Max Limit
Base- 1st	HD400×592	465	45	10.33	3073.48	75490	0.13	51.26	35.37	51.26	OK
2nd-3th	HD400×382	320	29.8	10.74	2561.11	48710	0.17	49.25	35.37	49.25	OK
4th-5th	HD400×262	320.4	21.4	14.97	1871.52	33460	0.18	48.6	35.37	48.69	OK
6th-7th	HD320×158	279	14.5	19.24	1243.82	20120	0.19	47.689	35.37	47.69	OK
8rd-9th	HE240 B	240	10	24.00	701.77	10600	0.21	46.95	35.37	46.95	OK
10th	HE200 B	200	9	22.22	201.79	7808	0.08	53.78	35.37	53.78	OK

Table E4.5: Limiting width-to-thickness ratios for SCBF columns.

Section of Column	b (mm)	t_f (mm)	$b/2t_f$	$\lambda_{hd} = 0.30*\sqrt{(E/Fy)}$	$b/2t_f \leq \lambda_{hd}$
HD 400×592	421	72.3	2.911	7.121	OK
HD 400×382	406	48	4.229	7.121	OK
HD 400×262	398	33.3	5.976	7.121	OK
HD 320×158	303	25.5	5.941	7.121	OK
HE 240 B	240	17	7.059	7.121	OK
HE 200 B	200	15	6.667	7.121	OK

Appendix E5: Story drift requirement

Table E5.1: Story drifts of 5-story building for (Y) direction.

Floors	Load	DriftY	$R^{(Y)}$	I	Story Height	$\lambda^{(Y)}$	$\lambda\delta_i^{(Y)}/h_i$	0.016 κ	Conclusion (Y)
		$\Delta_i^{(Y)}/h_i$			h_i (m)	$S_{ae}(T)_{DD-3}$ /$S_{ae}(T)_{DD-2}$			
10	SPECY	0.002138	5	1.0	4.0	0.357	0.0038	0.008	OK
9	SPECY	0.00229	5	1.0	4.0	0.357	0.0041	0.008	OK
8	SPECY	0.00229	5	1.0	4.0	0.357	0.0041	0.008	OK
7	SPECY	0.00211	5	1.0	4.0	0.357	0.0038	0.008	OK
6	SPECY	0.00193	5	1.0	4.0	0.357	0.0034	0.008	OK
5	SPECY	0.00179	5	1.0	4.0	0.357	0.0032	0.008	OK
4	SPECY	0.00157	5	1.0	4.0	0.357	0.0028	0.008	OK
3	SPECY	0.00138	5	1.0	4.0	0.357	0.0025	0.008	OK
2	SPECY	0.00118	5	1.0	4.0	0.357	0.0021	0.008	OK
1	SPECY	0.00113	5	1.0	5.4	0.357	0.0020	0.008	OK

Table E5.2: Final sections of 10-story building.

Floor	SMRFs_Columns		SMRFs_Beam	Gravity Frames_Column		GFs_Beam
	Exterior	Interior		Exterior (Braced B.)	Interior	
10	HD 400 × 216	HD 400 × 463	HE 500 A	HE 200 B	HE 240 C	IPE O 400
9	HD 400 × 314	HD 400 × 463	HE 500 A	HE 240 B	HE 240 C	IPE O 450
8	HD 400 × 314	HD 400 × 592	HE 550 A	HE 240 B	HE 260 C	IPE O 450
7	HD 400 × 463	HD 400 × 592	HE 550 A	HD 320 × 158	HE 260 C	IPE O 450
6	HD 400 × 463	HD 400 × 592	HE 550 B	HD 320 × 158	HE 260 C	IPE O 450
5	HD 400 × 509	HD 400 × 677	HE 550 B	HD 400 × 262	HD 320 × 158	IPE O 450
4	HD 400 × 509	HD 400 × 677	HE 550 B	HD 400 × 262	HD 320 × 158	IPE O 450
3	HD 400 × 634	HD 400 × 677	HE 650 B	HD 400 × 382	HD 320 × 158	IPE O 450
2	HD 400 × 634	HD 400 × 818	HE 650 B	HD 400 × 382	HD 360 × 196	IPE O 450
1	HD 400 × 818	HD 400 × 818	HE 650 B	HD 400 × 592	HD 360 × 196	IPE O 450
Baement	HD 400 × 818	HD 400 × 818	HE 500 A	HD 400 × 592	HD 360 × 196	IPE O 450